

**SOLVENT EXTRACTION AND SELECTIVE
SEPARATION OF BASE METAL IONS BY MEANS OF
PYRAZOLE- AND IMIDAZOLE-PYRIDINYL LIGANDS**

by

Brendan Harold Pearce



*Dissertation presented for the degree of Doctor of Philosophy
in the Faculty of Science at Stellenbosch University*

Supervisor: Dr Robert C. Luckay

December 2020

DECLARATION

By submitting this thesis electronically, I declare that the entirety of the work contained therein is my own, original work, that I am the sole author thereof (save to the extent explicitly otherwise stated), that reproduction and publication thereof by Stellenbosch University will not infringe any third party rights and that I have not previously in its entirety or in part submitted it for obtaining any qualification.

December 2020

Copyright © 2020 Stellenbosch University

All rights reserved

ACKNOWLEDGEMENTS

Writing the acknowledgements section of a PhD dissertation is an incredibly daunting task. The sudden realisation that this study is nearing its end, coupled with the fact that so many incredible people contributed to its success, is an overwhelming thought. My mind cannot fathom why I have been blessed in this manner, yet I will do my best in recognising all who have contributed to the fulfilment of this remarkable journey.

Firstly, I must express my deep sense of gratitude to Dr Robert Luckay. It has been a tremendous privilege and honour to have had you as my supervisor. You have undoubtedly played an important role in my successes. You deserve all the accolades in the world for graciously and patiently nurturing my academic growth. Thank you for leading with immense humility and kindness. I have always felt at home in your research group. I will remember our time in beautiful Dresden with great fondness and nostalgia. Thank you for your continued support, encouragement and drive that enabled me to deliver high-quality work!

A special thanks is extended to Elsa Malherbe/Dr Jaco Brand (NMR analyses), Dr Marietjie Stander (MS analyses), Dr Leigh Loots (crystal structure elucidations) and all staff members at the Central Analytical Facilities (CAF) of Stellenbosch University. Without your sound technical advice and guidance this dissertation would not have been up to an appreciable standard. Special mention should also be given to the Mass Spectrometry Unit at the University of KwaZulu-Natal (Pietermaritzburg) for all elemental analyses done.

Without doubt, I must thank our technical officers, Peta Steyn and Ayanda Nxopo, for ensuring that we work safely and securely in a potentially dangerous environment. I commend you for maintaining impeccable safety standards and for having our best interests at heart. Thanks to all our technical staff members for making my studies as bump-free as possible and for swiftly sourcing solvents and glassware whenever I needed it. You have certainly spared me many a headache regarding broken glassware and faulty instruments. Thank you for always putting a smile on my face when I entered the inorganic chemistry building.

To my group members, past and present: You have welcomed me as one would welcome a family member. Thank you for helping me throughout my studies and for your continued practical advice. I appreciate it very much! I would especially like to thank Laura, Annick, Cassiem, Emile, Jacquin, Ené, Claire, Hezron and Hillary for their kind friendship and countless hours spent talking and laughing. Without you, my studies would most certainly not have been as fun. You made the hard times more bearable by cracking a few “flou” jokes!

I am incredibly honoured for all the academic advice that has been given to me by the following phenomenal academics: Dr Rehana Malgas-Enus, Dr Prinessa Chellan, Dr Paul Verhoeven and Prof. Selwyn Mapolie. Of course, I cannot forget the invaluable contributions all my chemistry lecturers have made throughout my undergraduate and postgraduate studies at Stellenbosch University. I will forever hold a dear place in my heart for this institution—my *alma mater*—and the people that roam its corridors.

My time spent in Germany at Technische Universität Dresden has truly been some of the best times of my life! I am profoundly humbled that I was able to experience this picturesque city during my 3-month PhD internship in 2019. For this, I thank Prof. Jan Weigand and Dr Marco Wenzel. You have been superb hosts and I cannot wait to visit Dresden and greater Saxony again. Special thanks should also be extended to the Leonardo-Büro Sachsen Office for funding this academic exchange program. Vielen Dank!

To Prof. Peter Tasker at the University of Edinburgh—I am incredibly excited to be collaborating with you and your colleagues on current and future solvent extraction endeavours. Thank you for considering me as a “co-worker”. I look forward to contributing to future high-quality publications.

I am deeply grateful for the financial support from the National Research Foundation (NRF) of South Africa, the SASOL-Stellenbosch 2020 committee and the Department of Chemistry and Polymer Science at Stellenbosch University. This study would not have been possible if it were not for your assistance.

Dankie Ma en Pa vir julle ondersteuning en oorvloed liefde. Julle seun is nou uiteindelik klaar met sy studies! Hierdie proefskrif is die bewys dat ek die beste ouers op aarde het. Julle het keer op keer bonatuurlike geduld en insig getoon en my soveel kere aangemoedig en hoop gegee. Daar was tye wat ek net nie meer lus was nie, maar as ek aan julle gedink het het ek weer nuwe krag gekry. Aan my sussies Grizelda, Lindi en Melissa—julle boetie is nou uiteindelik ‘n Doktor! Ek sou hierdie dekadellange reis nie sonder julle kon aanpak nie.

To my extended family members (uncles, aunts and cousins) and dear friends Deodonne, Emma, Shano, Sarah-Lee, Michael, Tanya, Ewald, Lodewiek and Yolanda: Thank you for your continued love and support. You were the ones that believed in my dreams when I had lost all motivation. This dissertation is testament to your loyalty and never-ceasing encouragements.

Lastly, I want to thank the most important person of all—my Heavenly Father. You, Lord Jesus, are the king of my heart. It is far too wonderful for me to comprehend that the King of kings has bestowed this incredible honour upon me. Who am I, a mere sinful mortal, to be loved by you? What have I done to deserve such boundless grace and favour? The one who flung the stars into existence, the unchanging one who gives without measure has greatly blessed me. I deem it the highest possible honour that I have been able to study the mechanics of your creation, albeit on the minutest of scales. Thank you, Lord, for granting me the title of “Doctor of Philosophy”. I strive to make it my lifelong mission to make you proud!

“To the one who showed me cobalt blue skies and silver clouds...”

Gerbrandt Kotzé (01.06.1991—28.05.2018)

ABSTRACT

In this dissertation, tridentate aromatic *N*-donor pyrazole- and imidazole-pyridinyl ligands, in a solvent extraction context, were investigated as potential base metal ion extractants.

The syntheses of pyrazolyl ligands 2,6-bis(5-methyl-1*H*-pyrazol-3-yl)pyridine (**1**), 2,6-bis(5-ethyl-1*H*-pyrazol-3-yl)pyridine (**2**), 2,6-bis(5-propyl-1*H*-pyrazol-3-yl)pyridine (**3**), 2,6-bis(5-butyl-1*H*-pyrazol-3-yl)pyridine (**4**), 2,6-bis(5-pentyl-1*H*-pyrazol-3-yl)pyridine (**5**), 2,6-bis(5-hexyl-1*H*-pyrazol-3-yl)pyridine (**6**), 2,6-bis(5-heptyl-1*H*-pyrazol-3-yl)pyridine (**7**), 2,6-bis(5-octyl-1*H*-pyrazol-3-yl)pyridine (**8**), 2,6-bis(5-(*tert*-butyl)-1*H*-pyrazol-3-yl)pyridine (**9**) and 2,6-bis(5-phenyl-1*H*-pyrazol-3-yl)pyridine (**10**) followed the Claisen-Schmidt condensation of diethyl pyridine-2,6-dicarboxylate with the appropriate alkyl ketone, yielding a crude symmetrical bis(1,3-dicarbonyl) intermediary species. This crude product was used without purification in the classic Knorr synthesis for pyrazoles, with hydrazine acting as the heterocyclic initiator. The imidazole-pyridinyl ligands 2,6-bis(1-butylimidazol-2-yl)pyridine (**11**) and 2,6-bis(1-octylimidazol-2-yl)pyridine (**12**) were synthesised via the nucleophilic substitution of an appropriate imidate with diethylacetal-protected aminoacetaldehyde, followed by the deprotection-cyclisation step under acidic conditions. Pyrazolyl ligands **1–10** were obtained in yields of 33–80%, generally increasing as the number of C-atoms of the alkyl-tethered arms increased, while imidazolyl ligands **11** and **12** were obtained in moderate yields of 60–65%. All ligands were characterised via ¹H and ¹³C NMR, IR, MS and EA.

Competitive extraction studies were performed with ligands **1–12** and these showed copper(II) to be effectively separated (%*E* > 90%) from a cobalt(II), nickel(II), zinc(II), cadmium(II) and lead(II) mixture. Subsequent experiments revealed nickel(II) to be the predominant second-most extractable species in solution (60% < %*E* < 70%). Selectivity experiments, where $[Cu^{2+}] = \frac{[M^{2+}]}{60}$, showed that copper(II) was extracted at ~85% whilst competing with other base metal ions present at much higher concentrations. In the presence of 1 M HNO₃ pyrazolyl ligands **6–8** remarkably released ~90% of their extracted nickel(II) ions, while merely releasing 29 (± 0.2), 19 (± 1.8) and 9.1 (± 0.7)% of their extracted copper(II) in the presence of 10 M HNO₃, respectively.

Ligand-to-metal stoichiometric ratios were determined by implementing the method of continuous variance (Job plots) via UV/Vis experiments. L:Cu²⁺ stoichiometric ratios for ligands **2–12** were 1:1, while ligand **1** surprisingly exhibited a 2:1 ratio. Both pyrazolyl ligand **2** and imidazolyl ligand **12** displayed 2:1 L:M²⁺ (M = Co, Ni, Zn and Cd) ratios. Slope analyses of log *D* vs log [ligand] plots corroborated these results once investigated via ICP-OES.

Evaluation of various synergists revealed the optimum synergist-to-nickel(II) ratio to be 1:1 due to emulsions forming at >1×10⁻² M. Pyrazolyl ligands **6–8**, in conjunction with dodecylbenzenesulfonic acid (DBSA), exhibited synergistic gains of >10%, while *p*-toluenesulfonic acid (*p*TSA), in conjunction with pyrazolyl

ligand **7**, exhibited remarkable synergistic gains of ~17% (4:1 *p*TSA:Ni²⁺ ratio). No real synergistic gains were observed for imidazolyl ligand **12** in the presence of *p*TSA.

Nickel(II) was also extracted by means of aromatic oxime ligands (**13** and **14**) and bidentate pyrazolyl ligands (**15** and **16**) in the presence of sulfonic-, carboxylic- and phosphinic acid synergists. Only the sulfonic acid synergist, dinonylnaphthalenesulfonic acid (DNNSA), appeared to combine well in solution with ligands **13–16**, resulting in nickel(II) extractions of ~83, ~44, ~92 and ~80%, respectively.

Finally, single crystals of [Cu(L**2**)₂](NO₃)₂, [Cu(H₂O)₂(L**2**)]SO₄ and [Ni₂(H₂O)₂(L**15**)₄(SO₄)·(naphth-SO₃)₂] were grown and analysed via X-ray diffraction analyses. Coordination around the copper(II) centres was octahedral (L:Cu²⁺ = 2:1) and square pyramidal (L:Cu²⁺ = 1:1), respectively, while the interesting sulfate-bridged complex contained two nickel(II) “subcomplexes”. Each nickel(II) “subcomplex” consisted of two ligand **15** molecules, a water molecule, a centralised sulfate anion and a peripheral naphtha-SO₃ molecule stabilising the assembly via H-bonds.

OPSOMMING

In hierdie proefskrif word drieledige aromatiese *N*-skenker pirasool- en imidasoolpiridienligande ondersoek aangaande die selektiewe ekstraksie van basismetaalione binne die konteks van vloeistofekstraksies.

Die sintese van pirasoolligande 2,6-bis(5-metiel-1*H*-pirasol-3-iel)piridien (**1**), 2,6-bis(5-etiel-1*H*-pirasol-3-iel)piridien (**2**), 2,6-bis(5-propiel-1*H*-pirasol-3-iel)piridien (**3**), 2,6-bis(5-butiel-1*H*-pirasol-3-iel)piridien (**4**), 2,6-bis(5-pentiel-1*H*-pirasol-3-iel)piridien (**5**), 2,6-bis(5-heksiel-1*H*-pirasol-3-iel)piridien (**6**), 2,6-bis(5-heptiel-1*H*-pirasol-3-iel)piridien (**7**), 2,6-bis(5-oktiel-1*H*-pirasol-3-iel)piridien (**8**), 2,6-bis(5-(*ters*-butiel)-1*H*-pirasol-3-iel)piridien (**9**) en 2,6-bis(5-feniel-1*H*-pirasol-3-iel)piridien (**10**) het die Claisen-Schmidt kondensasiemetode gevolg waar diëtielpiridien-2,6-dikarboksilaat met 'n gepaste alkielketoon gereageer is om 'n simmetriese bis(1,3-dikarboniel) intermediêre ru-produk te lewer. Hierdie ru-produk is sonder addisionele suiweringsmetodes in die klassieke Knorr-pirasoolsintese gebruik, met hidrasien wat as heterosikliese inisieerder intree. Die imidasoolpiridienligande, 2,6-bis(1-butielimidazol-2-iel)piridien (**11**) en 2,6-bis(1-oktielimidazol-2-iel)piridien (**12**), is gesintetiseer deur die nukleofiliese substitusie van 'n toepaslike imidaat met diëtielasetaal-beskernde aminoasetaldehyd, gevolg deur die sikliseringstap wat onder lae pH-toestand plaasvind. Pirasolielligande **1–10** het opbrengste van 33–80% opgelewer. Dit kan hoofsaaklik toegeskryf word aan die toename in C-atome van die alkielarms, terwyl imidasolielligande **11** and **12** in hul beurt weer gematigde opbrengste van 60–65% opgelewer het. Alle ligande is deur middel van ¹H en ¹³C KMR, IR, MS and EA ontleed.

Mededingingsekstraksies is uitgevoer met ligande **1–12** en toon dat koper(II) effektief vanuit 'n kobalt(II)-, nikkell(II)-, sink(II)-, kadmium(II)- en lood(II)-mengsel geskei kan word (%*E* > 90%). Daaropvolgende eksperimente het getoon dat nikkell(II) die tweede effektiefste geëkstraëer word (60% < %*E* < 70%). Selektiwiteitseksperimente, waar $[Cu^{2+}] = \frac{[M^{2+}]}{60}$, het merkwaardig getoon dat koper(II) teen ~85% geëkstraëer word, te midde van ander basismetaalione wat teen veel hoër konsentrasies teenwoordig was. Vêrder het nikkell(II)-herwinningsstudies bewys dat pirasolielligande **6–8** ongeveer 90% van die geëkstraëerde nikkell(II)-ione vrygelaat het in die teenwoordigheid van 1 M HNO₃. Terseldertyd, het hierdie ligande onderskeidelik slegs 29 (± 0.2), 19 (± 1.8) en 9.1 (± 0.7)% van die geëkstraëerde koper(II)-ione in die teenwoordigheid van 10 M HNO₃ vrygelaat.

Ligand-tot-metaal stoichiometriese verhoudings is vasgestel deur middel van die deurlopende afwykingsmetode (Job-plotte), wat op sigself van UV/Vis eksperimente afhanklik is. Die L:Cu²⁺ stoichiometriese verhoudings vir ligande **2–12** was hoofsaaklik 1:1, terwyl ligand **1** 'n verhouding van 2:1 getoon het. Beide die pirasolielligand **2** en imidasolielligand **12** het L:M²⁺ (M = Co, Ni, Zn and Cd) verhoudings van 2:1 getoon. Gradiëntanalises van log *D* vs. log [ligand] plotte wat deur middel van IGP-OES bepaal is het dergelik ook die bevindinge van die Job-plotte onderskraag.

Evaluering van verskeie sinergiste het bewys dat the optimale sinergis-tot-nikkel(II) verhouding 1:1 is as gevolg van emulsies wat vorm teen $>1 \times 10^{-2}$ M. Pirasolielligande **6–8**, in samewerking met dodesielbenseensulfoniese suur (DBSS), het sinergistiese winste van $>10\%$ getoon, terwyl *p*-tolueensulfoniese suur (*p*TSS) in samerwerking met ligand **7** uitsonderlike sinergistiese winste van $\sim 17\%$ (4:1 *p*TSS: Ni^{2+} verhouding) getoon het. Geen winste is opgelet vir ligand **12** met *p*TSS nie.

Vêrder is nikkell(II) ook geëkstraëer deur middel van aromatiese oksiemligande (**13** en **14**) en tweeledige pirasolielligande (**15** en **16**) in die teenwoordigheid van sulfoniese-, karboksiel- en fosfoniese suursinergiste. Slegs die sulfoniese suursinergis, dinonielnaftaleensulfoniese suur (DNNSS), het oënskynlik effektief met ligande **13–16** in toluen gemeng. Gevolglik is nikkell(II)-ekstraksies van ~ 83 , ~ 44 , ~ 92 en $\sim 80\%$ onderskeidelik verkry.

Ten einde was hoë-gehalte enkelkristalle van die $[\text{Cu}(\text{L}2)_2](\text{NO}_3)_2$, $[\text{Cu}(\text{H}_2\text{O})_2(\text{L}2)]\text{SO}_4$ en $[\text{Ni}_2(\text{H}_2\text{O})_2(\text{L}15)_4(\text{SO}_4) \cdot (\text{naphth-SO}_3)_2]$ komplekse gekweek en deur middel van X-straaldiffraksieanalises ontleed. Koördinering rondom die koper(II)-sentrum was onderskeidelik oktahedraal (L: $\text{Cu}^{2+} = 2:1$) en vierkantig piramidaal (L: $\text{Cu}^{2+} = 1:1$), terwyl die interessante sulfaat-gekoppelde kompleks twee nikkell(II) “subkomplekse” bevat. Elke nikkell(II)-subkompleks bestaan uit twee ligand **15** molekules, ‘n water molekule, ‘n sentrale sulfaatanioon en ‘n eksterne nafta- SO_3 molekule wat die algehele samestelling via H-bindings stabiliseer.

TABLE OF CONTENTS

DECLARATION	i
ACKNOWLEDGEMENTS	ii
DEDICATION	iv
ABSTRACT	v
OPSOMMING	vii
TABLE OF CONTENTS	ix
LIST OF TABLES	xv
LIST OF FIGURES	xvii
LIST OF SCHEMES	xxii
LIST OF ABBREVIATIONS	xxv

CHAPTER 1: LITERARY BACKGROUND REGARDING SOLVENT EXTRACTION SYSTEMS AND THE VARIOUS EXTRACTANTS INVOLVED

1.1	Synoptic history of extractive metallurgy	1
1.2	General introduction to base metals	3
1.2.1	Properties and applications of cobalt	3
1.2.2	Properties and applications of nickel	4
1.2.3	Properties and applications of copper	5
1.2.4	Properties and applications of zinc	6
1.2.5	Properties and applications of cadmium	7
1.2.6	Properties and applications of lead	8
1.3	Hydrometallurgical processes for the separation of base metals	8
1.3.1	Crystallisation	9
1.3.2	Ionic precipitation	9
1.3.3	Electrochemical reduction	10
1.3.4	Reduction with gas	10

1.3.5	Carbon adsorption	10
1.3.6	Ion exchange	11
1.3.7	Electrolytic process	11
1.3.8	Solvent extraction	12
1.4	Types of extractants and additives commonly used in solvent extraction systems	14
1.4.1	Cationic extractants	15
1.4.2	Anionic extractants	17
1.4.3	Solvating extractants	19
1.4.4	Additives	20
1.5	Synergism and how its related to solvent extraction	21
1.6	Ligand-metal compatibility	22
1.6.1	Choosing the correct donor atoms	23
1.7	Chelating ligands	26
1.7.1	The chelate effect	26
1.7.2	The standard reference state and the chelate effect	27
1.8	Metal ion selectivity of <i>N</i> -donor ligands	29
1.8.1	The chelate ring geometry and preferred metal ion sizes	29
1.9	Steric- and inductive effects in <i>N</i> -donor chelating ligands	31
1.10	Factors to consider in ligand design: A concise summary	32
1.11	Literary background on pyrazole- and imidazole-pyridinyl ligands	33
1.11.1	Relevant literature on various pyrazole- and imidazole-pyridinyl ligands	33
1.11.2	Relevant literature on tridentate pyrazole- and imidazole-pyridinyl ligands as utilised in solvent extraction systems	34
1.12	Problem statement	34
1.13	Aim of this dissertation	35
1.12.1	Minor expounded objectives	35
1.14	References	36

**CHAPTER 2: SYNTHESIS AND CHARACTERISATION OF TRIDENTATE
PYRAZOLE- AND IMIDAZOLE-PYRIDINYL LIGANDS**

2.1	Introduction	46
2.2	Materials and methods	48
2.2.1	Chemicals and reagents	48
2.2.2	Instrumentation	49
2.3	Experimental	50
2.3.1	Synthesis of diethyl pyridine-2,6-dicarboxylate	50
2.3.2	Synthesis of 2,6-bis(5-methyl-1 <i>H</i> -pyrazol-3-yl)pyridine (1)	51
2.3.3	Synthesis of 2,6-bis(5-ethyl-1 <i>H</i> -pyrazol-3-yl)pyridine (2)	54
2.3.4	Synthesis of 2,6-bis(5-propyl-1 <i>H</i> -pyrazol-3-yl)pyridine (3)	55
2.3.5	Synthesis of 2,6-bis(5-butyl-1 <i>H</i> -pyrazol-3-yl)pyridine (4)	57
2.3.6	Synthesis of 2,6-bis(5-pentyl-1 <i>H</i> -pyrazol-3-yl)pyridine (5)	58
2.3.7	Synthesis of 2,6-bis(5-hexyl-1 <i>H</i> -pyrazol-3-yl)pyridine (6)	60
2.3.8	Synthesis of 2,6-bis(5-heptyl-1 <i>H</i> -pyrazol-3-yl)pyridine (7)	61
2.3.9	Synthesis of 2,6-bis(5-octyl-1 <i>H</i> -pyrazol-3-yl)pyridine (8)	63
2.3.10	Synthesis of 2,6-bis(5-(<i>tert</i> -butyl)-1 <i>H</i> -pyrazol-3-yl)pyridine (9)	64
2.3.11	Synthesis of 2,6-bis(5-phenyl-1 <i>H</i> -pyrazol-3-yl)pyridine (10)	66
2.3.12	Synthesis of 2,6-bis(1 <i>H</i> -imidazol-2-yl)pyridine	67
2.3.13	Synthesis of 2,6-bis(1-butylimidazol-2-yl)pyridine (11)	68
2.3.14	Synthesis of 2,6-bis(1-octylimidazol-2-yl)pyridine (12)	69
2.4	Results and discussion	71
2.4.1	Pyrazole-pyridinyl ligands	71
2.4.2	Imidazole-pyridinyl ligands	82
2.5	Conclusions	88
2.6	References	89

CHAPTER 3: SOLVENT EXTRACTION OF SIX DIVALENT BASE METAL IONS BY MEANS OF TRIDENTATE PYRAZOLE- AND IMIDAZOLE-PYRIDINYL LIGANDS

3.1	Introduction	94
	3.1.1 Synergism and synergistic additives	95
3.2	Materials and methods	99
	3.2.1 Chemicals and reagents	99
	3.2.2 Instrumentation	100
	3.2.3 Preparation of buffered solutions	100
	3.2.4 General solvent extraction procedure and conditions	101
3.3	Results and discussion	102
	3.3.1 Competitive extraction studies	102
	3.3.2 Selectivity studies	108
	3.3.3 Extraction and metal ion recovery of copper(II) and nickel(II)	110
	3.3.4 Time-dependent extraction study of copper(II) and nickel(II)	116
	3.3.5 pH isotherm studies	118
	3.3.6 Determining the ligand-to-metal (L:M ²⁺) ratio by means of Job's method	120
	3.3.7 Slope analyses via ICP-OES	130
	3.3.8 Synergistic extraction of nickel(II)	135
3.4	Conclusions	142
3.5	References	144

CHAPTER 4: SYNTHESIS AND CHARACTERISATION OF VARIOUS BASE METAL COMPLEXES IN ADDITION TO CRYSTAL AND MOLECULAR STRUCTURES OF TWO COPPER(II) COMPLEXES

4.1	Introduction	150
4.2	Materials and methods	151

4.2.1	Chemicals and reagents	151
4.2.2	Instrumentation	151
4.3	Experimental	152
4.3.1	General syntheses of various divalent base metal complexes	152
4.4	Crystal and molecular structures of two copper(II) complexes	154
4.4.1	Techniques for growing quality crystals	154
4.4.2	Instrumentation and determination of crystal structures	155
4.4.3	Preparation of the crystalline $[\text{Cu}(\text{L}2)_2](\text{NO}_3)_2$ complex	156
4.4.4	Preparation of the crystalline $[\text{Cu}(\text{H}_2\text{O})_2(\text{L}2)]\text{SO}_4$ complex	156
4.5	Results and discussion	156
4.5.1	Crystal and molecular structure of the $[\text{Cu}(\text{L}2)_2](\text{NO}_3)_2$ complex	157
4.5.2	Crystal and molecular structure of the $[\text{Cu}(\text{H}_2\text{O})_2(\text{L}2)]\text{SO}_4$ complex	162
4.6	Concluding remarks and making sense of seemingly contradictory results	167
4.7	References	168
 CHAPTER 5: EXTRACTION OF NICKEL(II) BY MEANS OF AROMATIC OXIMES AND BIDENTATE PYRAZOLYL LIGANDS IN THE PRESENCE OF SULFONIC-, CARBOXYLIC- AND PHOSPHINIC ACID SYNERGISTS		
5.1	Introduction	169
5.2	Materials and methods	172
5.2.1	Chemicals and reagents	172
5.2.2	Instrumentation	173
5.3	Experimental	173
5.3.1	Synthesis of (1-hydroxycyclohexyl)-phenyl ketone oxime (13)	173
5.3.2	Phenyl 2-pyridyl ketoxime (14)	174
5.3.3	Synthesis of 2-(5-(<i>tert</i> -butyl)-1 <i>H</i> -pyrazol-3-yl)pyridine (15)	174
5.3.4	Synthesis of 5,5'-di- <i>tert</i> -butyl-1 <i>H</i> ,1' <i>H</i> -3,3'-bipyrazole (16)	175

5.4	Synthetic results and discussion	176
5.4.1	(1-Hydroxycyclohexyl)-phenyl ketone oxime	176
5.4.2	2-(5-(<i>Tert</i> -butyl)-1 <i>H</i> -pyrazol-3-yl)pyridine	176
5.4.3	5,5'-Di- <i>tert</i> -butyl-1 <i>H</i> ,1' <i>H</i> -3,3'-bipyrazole	177
5.5	Solvent extraction of nickel(II)	181
5.5.1	General solvent extraction procedure, conditions and synergists	181
5.6	Solvent extraction results and discussion	182
5.6.1	Nickel(II) extractive ability of ligands and synergists	182
5.6.2	Combinative (synergistic) extraction of nickel(II)	183
5.6.3	pH isotherm studies	184
5.7	Crystallographic results and discussion	186
5.7.1	Preparation of free ligand 5,5'-di- <i>tert</i> -butyl-1 <i>H</i> ,1' <i>H</i> -3,3'-bipyrazole (16)	186
5.7.2	Crystal and molecular structure of free 5,5'-di- <i>tert</i> -butyl-1 <i>H</i> ,1' <i>H</i> -3,3'-bipyrazole	186
5.7.3	Preparation of the crystalline $[\text{Ni}_2(\text{H}_2\text{O})_2(\text{C}_{12}\text{H}_{15}\text{N}_3)_4(\text{SO}_4)\cdot(\text{naphth-SO}_3)_2]$ assembly	190
5.7.4	Crystal and molecular structure of the $[\text{Ni}_2(\text{H}_2\text{O})_2(\text{C}_{12}\text{H}_{15}\text{N}_3)_4(\text{SO}_4)\cdot(\text{naphth-SO}_3)_2]$ assembly	191
5.8	Conclusions	197
5.9	References	199

CHAPTER 6: CHAPTER SUMMARIES, CONCLUDING REMARKS AND FUTURE WORK

6.1	Chapter summaries	201
6.2	Suggested future work	203
6.2.1	Structural modifications to enhance metal ion extractability	203
6.2.2	Extraction of base metal ions using pyrazolyl- and imidazolyl ligands on resin, silica-based and nanofibrous polymeric supports	205
6.2.3	Computational modelling and calculations	206
6.3	References	206

LIST OF TABLES

CHAPTER 1

Table 1.1	Commercial cationic extractants and their uses in industry	16
Table 1.2	Commercial anionic extractants and their uses in industry	18
Table 1.3	Commercial solvating extractants and their uses in industry	20
Table 1.4	Examples of commercial diluents	21
Table 1.5	Examples of commercial modifiers	21
Table 1.6	The hard- and soft metal ions as reported by Pearson	23
Table 1.7	The hard- and soft organic bases as reported by Pearson and Songstad	23
Table 1.8	The formation constants of polyamine nickel(II) complexes compared to analogous NH ₃ complexes	26
Table 1.9	A comparison of the observed formation constant, log K ₁ , with the calculated formation constant derived from Eqs. 37 and 38	28
Table 1.10	Examples of steric effects outweighing inductive effects by systematically methylating the <i>N</i> -donor atoms of ethylenediamine	31
Table 1.11	Examples of inductive effects outweighing steric effects in <i>N</i> -alkyl ligands	31

CHAPTER 2

Table 2.1	List of chemicals used in alphanumeric order	48
Table 2.2	Percentage yields of ligands 1–10 compared to their corresponding ketone reagent's boiling point	79

CHAPTER 3

Table 3.1	Extraction of Ni ²⁺ by means of DNNSA by increasing the equilibrium pH	96
Table 3.2	List of chemicals used in alphanumeric order	99
Table 3.3	The synergistic gains (synergism) of pyrazolyl ligands 6–8 and synergistic losses (antisynergism) of imidazolyl ligands 11–12 in the presence of ~1×10 ⁻² M DBSA	127
Table 3.4	Extraction of nickel(II) by means of the synergist, <i>p</i> TSA, at various synergist to Ni ²⁺ (S:Ni ²⁺) ratios	128
Table 3.5	Extraction of nickel(II) by means of imidazolyl ligand 12 at increasing <i>p</i> TSA:Ni ²⁺ ratios	138

CHAPTER 4

Table 4.1	List of chemicals used in alphanumeric order	151
Table 4.2	Selected bond lengths and angles of the $[\text{Cu}(\text{L}2)_2](\text{NO}_3)_2$ complex	159
Table 4.3	Symmetry elements and operators of the crystalline $[\text{Cu}(\text{L}2)_2](\text{NO}_3)_2$ complex	160
Table 4.4	Crystallographic data and structure refinement of the $[\text{Cu}(\text{L}2)_2](\text{NO}_3)_2$ complex	162
Table 4.5	Selected bond lengths and angles of the $[\text{Cu}(\text{H}_2\text{O})_2(\text{L}2)]\text{SO}_4$ complex	164
Table 4.6	Symmetry elements and operators of the crystalline $[\text{Cu}(\text{H}_2\text{O})_2(\text{L}2)]\text{SO}_4$ complex	165
Table 4.7	Crystallographic data and structure refinement of the $[\text{Cu}(\text{H}_2\text{O})_2(\text{L}2)]\text{SO}_4$ complex	166

CHAPTER 5

Table 5.1	List of chemicals used in alphanumeric order	172
Table 5.2	Crystallographic symmetry elements and operators of free 5,5'-di- <i>tert</i> -butyl-1 <i>H</i> ,1' <i>H</i> -3,3'-bipyrazole (16)	188
Table 5.3	Crystallographic data and structure refinement of 5,5'-di- <i>tert</i> -butyl-1 <i>H</i> ,1' <i>H</i> -3,3'-bipyrazole (16)	190
Table 5.4	Selected bond lengths and angles for the $[\text{Ni}_2(\text{H}_2\text{O})_2(\text{L}15)_4(\text{SO}_4)\cdot(\text{naphth-SO}_3)_2]$ complex	193
Table 5.5	Crystallographic symmetry elements and operators of the complex, $[\text{Ni}_2(\text{H}_2\text{O})_2(\text{L}15)_4(\text{SO}_4)\cdot(\text{naphth-SO}_3)_2]$	195
Table 5.6	Crystallographic data and structure refinement of the $[\text{Ni}_2(\text{H}_2\text{O})_2(\text{L}15)_4(\text{SO}_4)\cdot(\text{naphth-SO}_3)_2]$ complex	196

LIST OF FIGURES

CHAPTER 1

Figure 1.1	A step-wise portrayal of the global hydrometallurgical process	9
Figure 1.2	A simplified depiction of the solvent extraction process	12
Figure 1.3	The HSAB trend for non-metals based on electronegativity	24
Figure 1.4	An illustration of Schwarzenbach's model of the chelate effect	27
Figure 1.5	Cyclohexane in its chair conformation	29
Figure 1.6	The idealised bond lengths and angles of a) 6-membered (1,3-diaminopropane) and b) 5-membered (ethylenediamine) chelate rings	30
Figure 1.7	The idealised bond lengths and angles of a) 6-membered (1,3-propanediol) and b) 5-membered (1,2-ethanediol) chelate rings	30
Figure 1.8	Chemical structures and pK _a values of a) pyridine, b) imidazole and c) pyrazole	33

CHAPTER 2

Figure 2.1	Schematic overview of ligands 1–12	75
Figure 2.2	¹ H NMR spectrum of 2,6-bis(5-butyl-1 <i>H</i> -pyrazol-3-yl)pyridine (4)	80
Figure 2.3	¹³ C{ ¹ H} NMR spectrum of 2,6-bis(5-butyl-1 <i>H</i> -pyrazol-3-yl)pyridine (4)	81
Figure 2.4	¹ H NMR spectrum of 2,6-bis(1 <i>H</i> -imidazol-2-yl)pyridine	84
Figure 2.5	¹³ C{ ¹ H} NMR spectrum of 2,6-bis(1 <i>H</i> -imidazol-2-yl)pyridine	85
Figure 2.6	¹ H NMR spectrum of 2,6-bis(1-octylimidazol-2-yl)pyridine (12)	87
Figure 2.7	¹³ C{ ¹ H} NMR spectrum of 2,6-bis(1-octylimidazol-2-yl)pyridine (12)	88

CHAPTER 3

Figure 3.1	General experimental setup and execution of the solvent extraction process	101
Figure 3.2	Photos of duplicate samples immediately after competitive solvent extraction studies of extractants 1–8	103
Figure 3.3	Photos of duplicate samples immediately after competitive extraction studies by means of ligands 11 and 12	105
Figure 3.4	Competitive 1:1 (L:M ²⁺) extraction of six base metal ions using ligands 1–12	106
Figure 3.5	Competitive 2:1 (L:M ²⁺) extraction of six base metal ions using ligands 1–12	106
Figure 3.6	Competitive 2:1 (L:M ²⁺) extraction of five base metal ions using ligands 1–12 (Cu ²⁺ excluded)	108

Figure 3.7	Copper(II) selectivity study using pyrazolyl ligands 3–10 [Copper(II) concentration decreased tenfold]	109
Figure 3.8	Copper(II) selectivity study using pyrazolyl ligands 3–10 [Copper(II) concentration decreased sixtyfold]	110
Figure 3.9	Typical experimental setup and execution of the metal ion recovery process	111
Figure 3.10	Copper(II) extraction (loading) by means of ligands, 1–12 , in a 2:1 (L:Cu ²⁺) ratio	111
Figure 3.11	Copper(II) recovery from loaded organic phases containing ligands 1–12	113
Figure 3.12	Nickel(II) extraction (loading) by means of pyrazolyl ligands, 1–10 , in a 2:1 (L:Ni ²⁺) ratio	114
Figure 3.13	Nickel(II) extraction via imidazolyl ligands 11 and 12 with varying L:Ni ²⁺ ratios	115
Figure 3.14	Nickel(II) recovery from loaded organic phases containing ligands 1–12	116
Figure 3.15	Extraction of copper(II) over a 24-hour period using A) pyrazolyl ligands 2, 5 and 7 as well as B) imidazolyl ligands 11 and 12	117
Figure 3.16	Extraction of nickel(II) over a 24-hour period using C) pyrazolyl ligands 2, 5 and 7 as well as D) imidazolyl ligands 11 and 12	118
Figure 3.17	Extraction of cadmium(II), copper(II) and nickel(II) at varying pH values by means of pyrazolyl ligands A) 3 , B) 5 and C) 8	120
Figure 3.18	An idealised Job plot of the simplest form, where a 0.5 mole fraction of A (f_A) indicates a 1:1 (ligand:M ²⁺) complexation ratio	122
Figure 3.19	A <i>Heidolph Reax 2</i> overhead shaker/rotator equipped with a universal adapter	123
Figure 3.20	Stacked UV/Vis spectrum depicting increasing mole fractions of a ligand 6 and Cu(NO ₃) ₂ ·3H ₂ O complex	124
Figure 3.21	Uncorrected Job plot for the ligand 6 -Cu ²⁺ complex	124
Figure 3.22	Graphically corrected Job plot for the ligand 6 -Cu ²⁺ complex	125
Figure 3.23	Copper(II) coordination Job plots of pyrazolyl ligands 1–5 & 7–9 in addition to imidazolyl ligands 11 and 12	127
Figure 3.24	Job plots of pyrazolyl ligand 2 coordinating to Co(II), Ni(II), Zn(II), Pb(II) and Cd(II)	129
Figure 3.25	Job plots of imidazolyl ligand 12 coordinating to Co(II), Ni(II), Zn(II) and Cd(II)	130
Figure 3.26	Plots for the variable ligand concentration experiments of ligands 5 and 7 with copper(II)	132
Figure 3.27	Plots for the variable ligand concentration experiments of ligands 5 and 7 with copper(II)	133
Figure 3.28	Theorised micellar-like structure capable of extracting copper(II) under extreme pH conditions	133

Figure 3.29	Plots for the variable ligand concentration experiments of ligands 5 and 7 with nickel(II)	134
Figure 3.30	Plots for the variable ligand concentration experiments of ligands 5 and 7 with cobalt(II)	135
Figure 3.31	Extraction of nickel(II) by means of the synergist, DBSA, at various synergist to Ni ²⁺ (S:Ni ²⁺) ratios	136
Figure 3.32	Extraction of nickel(II) by means of pyrazolyl ligands 6–8 and imidazolyl ligands 11–12 in the presence of DBSA	137
Figure 3.33	Extraction of nickel(II) by means of ligand 7 and <i>p</i> TSA with increasing (<i>p</i> TSA:Ni ²⁺) ratios	140

CHAPTER 4

Figure 4.1	Schematic diagram representing various crystal growth techniques: a) slow evaporation, b) slow cooling, c) vapour diffusion and d) liquid-liquid diffusion	154
Figure 4.2	Asymmetric unit cell diagram of the [Cu(L2) ₂](NO ₃) ₂ complex	157
Figure 4.3	ORTEP diagrams of the full [Cu(L2) ₂](NO ₃) ₂ complexing unit	158
Figure 4.4	ORTEP diagram with selected labels of the [Cu(L2) ₂](NO ₃) ₂ complex	159
Figure 4.5	Symmetry elements present in an asymmetric unit cell of the [Cu(L2) ₂](NO ₃) ₂ complex along the b-axis	160
Figure 4.6	ORTEP diagram of the [Cu(L2) ₂](NO ₃) ₂ complex revealing H-bonding from pyrazolyl NH atoms to neighbouring NO ₃ ⁻ ions	161
Figure 4.7	Packing diagram of the [Cu(L2) ₂](NO ₃) ₂ complex along the c-axis	161
Figure 4.8	The a) asymmetric unit cell diagram along the a-axis and the b) full representation of the [Cu(H ₂ O) ₂ (L2)]SO ₄ complex	163
Figure 4.9	ORTEP diagram with selected labels of the [Cu(H ₂ O) ₂ (L2)]SO ₄ complex	164
Figure 4.10	Symmetry elements present in an asymmetric unit cell of the [Cu(H ₂ O) ₂ (L2)]SO ₄ complex along the a*-axis	165
Figure 4.11	ORTEP diagram of the [Cu(H ₂ O) ₂ (L2)]SO ₄ complex revealing H-bonding from pyrazolyl NH atoms and coordinated H ₂ O molecules to neighbouring SO ₄ ²⁻ counter ions	165
Figure 4.12	Packing diagram of the [Cu(H ₂ O) ₂ (L2)]SO ₄ complex along the b*-axis	166

CHAPTER 5

Figure 5.1	X-ray crystal structure of three bipyrazolyl ligands coordinated to nickel (octahedral geometry) with H-bonded sulfonic acid moieties acting as stabilisers	171
Figure 5.2	X-ray crystal structure of three bidentate pyrazole-pyridinyl ligands coordinated to nickel (octahedral geometry) with H-bonded naphthalenesulfonic acid acting as stabilisers on the periphery (outer coordination sphere)	171
Figure 5.3	FT-IR (KBr pellet) spectrum of 5,5'-di- <i>tert</i> -butyl-1 <i>H</i> ,1' <i>H</i> -3,3'-bipyrazole (16)	178
Figure 5.4	¹ H NMR spectrum of 5,5'-di- <i>tert</i> -butyl-1 <i>H</i> ,1' <i>H</i> -3,3'-bipyrazole (16)	179
Figure 5.5	¹³ C NMR spectrum of 5,5'-di- <i>tert</i> -butyl-1 <i>H</i> ,1' <i>H</i> -3,3'-bipyrazole (16)	180
Figure 5.6	Zoomed-in ¹³ C NMR spectrum of 5,5'-di- <i>tert</i> -butyl-1 <i>H</i> ,1' <i>H</i> -3,3'-bipyrazole (16), indicating the presence of two broadened resonances	180
Figure 5.7	General experimental setup and execution of the nickel(II) solvent extraction process	181
Figure 5.8	Nickel(II) extraction by means of ligands 13–15 in the presence of SA , CA and PA synergists	183
Figure 5.9	Extraction of nickel(II) at increasing sulfonic acid synergist ratios	184
Figure 5.10	Nickel(II) extraction by means of ligands 13–15 in combination with SA , CA and PA at various pH values	185
Figure 5.11	Nickel(II) extraction by means of ligand 16 in combination with SA , CA and PA at various pH values	186
Figure 5.12	Asymmetric unit cell diagram of free 5,5'-di- <i>tert</i> -butyl-1 <i>H</i> ,1' <i>H</i> -3,3'-bipyrazole	187
Figure 5.13	ORTEP diagram of free 5,5'-di- <i>tert</i> -butyl-1 <i>H</i> ,1' <i>H</i> -3,3'-bipyrazole	187
Figure 5.14	Symmetry elements present in the asymmetric unit cell along the b-axis	188
Figure 5.15	ORTEP diagram of free 5,5'-di- <i>tert</i> -butyl-1 <i>H</i> ,1' <i>H</i> -3,3'-bipyrazole (16) revealing a network of intermolecular hydrogen bonds	189
Figure 5.16	Packing diagram of free 5,5'-di- <i>tert</i> -butyl-1 <i>H</i> ,1' <i>H</i> -3,3'-bipyrazole (16) along the c-axis	189
Figure 5.17	Asymmetric unit cell diagram of the [Ni ₂ (H ₂ O) ₂ (L 15) ₄ (SO ₄)·(naphth-SO ₃) ₂] complex	191
Figure 5.18	ORTEP diagram of the [Ni ₂ (H ₂ O) ₂ (L 15) ₄ (SO ₄)·(naphth-SO ₃) ₂] complex in “depth cue” mode	192
Figure 5.19	ORTEP diagram with selected labels of one half of the [Ni ₂ (H ₂ O) ₂ (L 15) ₄ (SO ₄)·(naphth-SO ₃) ₂] complex in “depth cue” mode	192

Figure 5.20	Bond lengths and angles of the 5-membered chelate ring present in a) $[\text{Ni}_2(\text{H}_2\text{O})_2(\text{L15})_4(\text{SO}_4)\cdot(\text{naphth-SO}_3)_2]$ and b) the minimum strain conformation of ethylenediamine (EN)	193
Figure 5.21	Symmetry elements present in an asymmetric unit cell along the a-axis	194
Figure 5.22	ORTEP diagram of the $[\text{Ni}_2(\text{H}_2\text{O})_2(\text{L15})_4(\text{SO}_4)\cdot(\text{naphth-SO}_3)_2]$ complex revealing intermolecular hydrogen bonds	195
Figure 5.23	Packing diagram of the $[\text{Ni}_2(\text{H}_2\text{O})_2(\text{L15})_4(\text{SO}_4)\cdot(\text{naphth-SO}_3)_2]$ complex along the a-axis in “depth cue” mode	196

LIST OF SCHEMES

CHAPTER 1

Scheme 1.1	The reaction of copper(II) and two hydroxyoxime reagents	25
-------------------	--	----

CHAPTER 2

Scheme 2.1	Synthetic route to diethyl pyridine-2,6-dicarboxylate	50
Scheme 2.2	Synthetic route to 2,6-bis(5-methyl-1 <i>H</i> -pyrazol-3-yl)pyridine (1)	51
Scheme 2.3	Synthetic route to 2,6-bis(5-ethyl-1 <i>H</i> -pyrazol-3-yl)pyridine (2)	54
Scheme 2.4	Synthetic route to 2,6-bis(5-propyl-1 <i>H</i> -pyrazol-3-yl)pyridine (3)	55
Scheme 2.5	Synthetic route to 2,6-bis(5-butyl-1 <i>H</i> -pyrazol-3-yl)pyridine (4)	57
Scheme 2.6	Synthetic route to 2,6-bis(5-pentyl-1 <i>H</i> -pyrazol-3-yl)pyridine (5)	58
Scheme 2.7	Synthetic route to 2,6-bis(5-hexyl-1 <i>H</i> -pyrazol-3-yl)pyridine (6)	60
Scheme 2.8	Synthetic route to 2,6-bis(5-heptyl-1 <i>H</i> -pyrazol-3-yl)pyridine (7)	61
Scheme 2.9	Synthetic route to 2,6-bis(5-octyl-1 <i>H</i> -pyrazol-3-yl)pyridine (8)	63
Scheme 2.10	Synthetic route to 2,6-bis(5-(<i>tert</i> -butyl)-1 <i>H</i> -pyrazol-3-yl)pyridine (9)	64
Scheme 2.11	Synthetic route to 2,6-bis(5-phenyl-1 <i>H</i> -pyrazol-3-yl)pyridine (10)	66
Scheme 2.12	Synthetic route to 2,6-bis(1 <i>H</i> -imidazol-2-yl)pyridine	67
Scheme 2.13	Synthetic route to 2,6-bis(1-butylimidazol-2-yl)pyridine (11)	68
Scheme 2.14	Synthetic route to 2,6-bis(1-octylimidazol-2-yl)pyridine (12)	69
Scheme 2.15	A general framework of the synthesis of ligands 1–10	71
Scheme 2.16	Kinetic- and thermodynamic enolate formation	72
Scheme 2.17	General Claisen-Schmidt condensation reaction mechanism using dimethyl 2,6-pyridinedicarboxylate and the appropriate alkyl ketone to form the tetraketone species as the major intermediary product	73
Scheme 2.18	Claisen-Schmidt condensation reaction mechanism for the attack of the “thermodynamic” enolate on dimethyl 2,6-pyridinedicarboxylate, yielding the unwanted minor tetraketone species	73
Scheme 2.19	Keto- and enol tautomers of 1,1'-(pyridine-2,6-diyl)bis(3-hydroxybut-2-en-1-one), the precursor intermediate to 2,6-bis(5-methyl-1 <i>H</i> -pyrazol-3-yl)pyridine (1)	76
Scheme 2.20	Enol forms of 1,1'-(pyridine-2,6-diyl)bis(3-hydroxybut-2-en-1-one), the precursor to 2,6-bis(5-methyl-1 <i>H</i> -pyrazol-3-yl)pyridine (1), stabilised via conjugation and intramolecular H-bonding	76

Scheme 2.21	Synthesis of possible phenyl substituted bispyrazolyl ligands using “unsymmetrical” phenylhydrazine	77
Scheme 2.22	A 12-step mechanism for the pyrazole cyclisation reaction with a 1,3-dicarbonyl species and hydrazine as reagents in the presence of a catalytic amount of acid	78
Scheme 2.23	Tautomeric forms of 2,6-bis(5-butyl-1 <i>H</i> -pyrazol-3-yl)pyridine (4) in solution	81
Scheme 2.24	Stepwise synthesis of 2,6-bis(1 <i>H</i> -imidazol-2-yl)pyridine from pyridine-2,6-dicarbonitrile and aminoacetaldehyde diethylacetal via an imidate- and acetal-protected imidamide intermediate	82
Scheme 2.25	Expected tautomerism in 2,6-bis(1 <i>H</i> -imidazol-2-yl)pyridine with averaged proton distribution	83
Scheme 2.26	Possible modes of hydrogen bonding of 2,6-bis(1 <i>H</i> -imidazol-2-yl)pyridine in DMSO- <i>d</i> ₆	84
Scheme 2.27	Nucleophilic substitution (S _N 2) mechanism by which ligands 11 and 12 were formed	86

CHAPTER 3

Scheme 3.1	The addition of D2EHPA to [UO ₂ (NO ₃) ₂ (TBP) ₂] to form the neutral species, [UO ₂ (D2EHPA) ₂ (TBP) ₂]	95
Scheme 3.2	Schematic representation of sulfonic acid/sulfonate extractants i) DNNSA, ii) DDNSA and iii) DEHSS	96
Scheme 3.3	Schematic representation of the sulfonic acid synergist (DBSA) used in this study	98
Scheme 3.4	A schematic diagram representing unofficial ligand/synergist conventions 1 and 2	98
Scheme 3.5	Theorised coordination of two tridentate pyrazolyl ligands to nickel(II) with four <i>p</i> TSA molecules stabilising the assembly via hydrogen bonding on the periphery	140

CHAPTER 4

Scheme 4.1	Synthetic route to a variety of base metal complexes by using either 2,6-bis(5-ethyl-1 <i>H</i> -pyrazol-3-yl)pyridine (2) or 2,6-bis(5-(<i>tert</i> -butyl)-1 <i>H</i> -pyrazol-3-yl)pyridine (9) as ligand	152
-------------------	---	-----

CHAPTER 5

Scheme 5.1	Nickel synergist complex with two naphthalenesulfonic acid molecules providing stabilisation via hydrogen bonds	169
Scheme 5.2	Nickel synergist complex with two naphthalenesulfonic acid molecules and two water molecules providing ample stabilisation through hydrogen bonds	170
Scheme 5.3	Nickel synergist complex with two naphthalenesulfonic acid molecules coordinated directly to the copper centre	170

Scheme 5.4	Synthetic route to (1-hydroxycyclohexyl)-phenyl ketone oxime (13)	173
Scheme 5.5	Chemical structure of phenyl 2-pyridyl ketoxime (14)	174
Scheme 5.6	Synthetic route to 2-(5-(<i>tert</i> -butyl)-1 <i>H</i> -pyrazol-3-yl)pyridine (15)	174
Scheme 5.7	Synthetic route to 5,5'-di- <i>tert</i> -butyl-1 <i>H</i> ,1' <i>H</i> -3,3'-bipyrazole (16)	175
Scheme 5.8	Three common acid synergists implemented for the extraction of nickel(II)	182

CHAPTER 6

Scheme 6.1	Modification of tridentate imidazolyl ligands 11 and 12 to include acidic protons to strengthen the overall coordination assembly in solution via hydrogen bonds	203
Scheme 6.2	Suggested methylpyrazolyl tripodal extractant with various electron donating R-groups	204
Scheme 6.3	Proposed “3-pocket” pyrazolyl ligands for the simultaneous extraction of three base metal ions	204
Scheme 6.4	Proposed anchoring of tridentate pyrazole- and imidazole-pyridinyl ligands onto PAN	205

LIST OF ABBREVIATIONS

% <i>E</i>	percentage extraction
(M)Hz	(mega) Hertz
(m)mol	(milli)mole
∫	integral
°C	degrees Celsius
1°, 2°, 3°, 4°	primary, secondary, tertiary, quaternary
¹³ C NMR	carbon 13 nuclear magnetic resonance
¹ H NMR	proton nuclear magnetic resonance
Å	Ångström
<i>aq</i>	aqueous
ATR	attenuated total reflectance
CDCl ₃	deuterated chloroform
cm ⁻¹	reciprocal centimetres (or wavenumber)
CMC	critical micelle concentration
<i>D</i>	distribution coefficient
d	doublet (NMR)
DDNSA	didodecyl-naphthalene sulfonic acid
DEHSS	di-2-ethylhexyl sodium sulfosuccinate
DEPHA	di-2-ethylhexyl phosphoric acid
DFT	density functional theory
dien	diethylenetriamine
DMF	<i>N,N</i> -dimethylformamide
DNNSA	dinonyl-naphthalene disulfonic acid

DNNSA	dinonylnaphthalene sulfonic acid
EA	elemental analysis
EMF	electromotive force
en	ethylenediamine
ESI+	positive electrospray ionisation
F	ratio of molar activity coefficient
ICP-OES	inductively coupled plasma optical emission spectroscopy
<i>in vacuo</i>	in a vacuum
IR	infrared
<i>J</i>	coupling constant
K_{ex}°	thermodynamic extractive equilibrium constant
L	ligand
M	molar/metal
m	multiplet (NMR)
m.p.	melting point
<i>m/z</i>	mass-to-charge ratio
MIBK	methyl isobutyl ketone
MS	mass spectrometry
OPIM	1-octyl-2-(2'-pyridyl)imidazole
<i>org</i>	organic
p	pentet (NMR)
penten	pentaethylenhexamine
PGMs	platinum group metals
pimH	2-(2'pyridyl)imidazole
pimMe	2-(2'pyridyl)-1-methylimidazole

pK_a	acid dissociation constant
$pTSA$	<i>p</i> -Toluenesulfonic acid
q	quartet (NMR)
r^+	metal ion radius
R_f	ratio of the distance moved by the solvent and solute
rpm	revolutions per minute
s	singlet (NMR)
SDBA	sodium dodecylbenzenesulfonic acid
SDBS	sodium dodecylbenzenesulfonate
S_N2	nucleophilic substitution
t	triplet (NMR)
TBAOH	tetrabutylammonium hydroxide
TBP	tributylphosphate
tetren	tetraethylenepentamine
THF	tetrahydrofuran
TOPO	trioctylphosphine oxide
trien	triethylenetetramine
β_n	formation constant
δ	chemical shift (ppm)

CHAPTER 1

LITERARY BACKGROUND REGARDING SOLVENT EXTRACTION SYSTEMS AND THE VARIOUS EXTRACTANTS INVOLVED

1.1 Synoptic history of extractive metallurgy

The purification of metals from their ores can generally be divided into three metallurgical classes: pyro-, hydro- and to a much lesser extent, electrometallurgy. Pyrometallurgy refers to the treatment of metal ores by means of thermal processes and can be dated back thousands of years to the ancient Egyptians and other Near-Eastern cultures of the period. These civilisations managed to develop furnaces in which they melted rocks and obtained pure liquid metals, such as copper and iron.¹ The hardened hand-worked lumps of metal were typically forged into simple weapons and tools, which became far more superior than their stone antecedents. Over the past couple of centuries, however, techniques like high-temperature roasting, smelting, converting and refining were developed and are currently integrated into modern large-scale thermal plants. Hydrometallurgy, on the other hand, is a much more recent development and in many cases replaced the well-known dry and high-temperature processing of ores.² “Hydro” refers to water, while “metallurgy” refers to the study of metal production and purification. Therefore, the composite word “hydrometallurgy” describes the study of metal purification by means of aqueous processes.¹

The genesis of hydrometallurgy can accurately be linked to early alchemists who tried to “convert” inexpensive base metals into pure gold.¹ This sort of alchemy can be traced back to the “conversion” of iron into copper, when an iron plate was serendipitously submerged into a solution of copper sulfate (known as blue vitriol) and found to be coated with metallic copper once removed.¹ At the time, alchemists did not understand that blue vitriol contained copper and were perplexed by the apparent “conversion”. Today we know this chemical reaction to be:



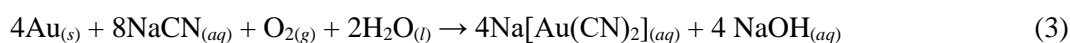
Still, a major question remained, however: How can inexpensive base metals be “converted” into gold—the most sought-after and precious metal of the time? It was well-known that mercury dissolved gold, forming an amalgam, yet gold remained insoluble in all known acids and bases of the time.¹ It was not until Abū Mūsā Jābir ibn Hayyān Al-Azdi (721–815 CE), the Arab alchemist, dissolved gold by means of *aqua regia* (royal water in Latin), which we now know consists of one part nitric acid and three parts hydrochloric acid.¹ It readily dissolves gold, but separately, these acids do not. This “mysterious” and “magical” solution is widely considered to be the most pivotal milestone in the evolution of hydrometallurgical processes.¹ Later, in the

1890s, *aqua regia* was extensively used for gold refining purposes, with chlorine being the crucial ingredient that allowed the formation of chloroauric acid:



In the 1500s, the extraction of copper gained significant appeal as it was previously done by relatively underdeveloped wet methods. Heap leaching was practiced in the Rio Tinto mines of Spain as well as the Harz mountains of Germany. This was an operation where chalcopyrite (CuFeS_2) was mounded in open air, allowing months of rain to instigate both the oxidation and dissolution processes.¹ The copper-containing solution was subsequently drained from the heap and collected. This led to the next phase known as the “cementation process”, whereby scrap iron was used to precipitate metallic copper.¹ This crude and highly inefficient process is still in operation today. The optimised cementation of gold by zinc in the Merrill-Crowe process is an enormously active industry and accounts for a considerable portion of the world’s gold production.³

Modern hydrometallurgy, however, can be traced back to 1887, a year in which two famous processes were invented—the cyanidation- and Bayer processes.¹ The cyanidation process, a process for treating gold ore, in reality had its origins during the 1700s with Swedish chemist, Carl Wilhelm Scheele (1742–1786).⁴ He first observed the dissolution of gold by means of a cyanide solution and later, in 1846, Franz Carl Leonhard Elsner (1802–1874) studied this reaction and noted the important role oxygen plays during the dissolution of gold.⁵ Today, this well-known reaction is described by the famous Elsner equation:

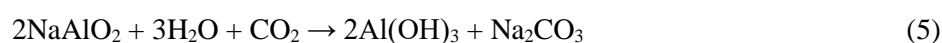


In 1887, Scottish chemists John Stewart MacArthur, Robert Forrest and William Forrest used this knowledge for the extraction of gold from its ores and filed a patent in England.⁵ Today, this patented process is known as the “cyanidation process”. This development was directly responsible for the exponential production of gold during the early 1900s.¹

Another important hydrometallurgical invention by Austrian chemist, Karl Josef Bayer (1847–1904), was the efficient production of pure alumina (Al_2O_3). Today this process is commonly referred to as “Bayer’s process”.⁶ This process involves the leaching of aluminium ore (bauxite) with boiling sodium hydroxide solution in a pressure reactor:¹



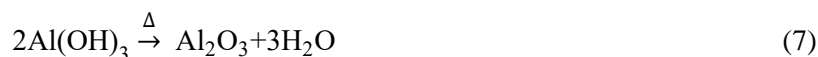
The remaining solid waste material was removed and the solution was slowly cooled whilst bubbling carbon dioxide through it to yield pure crystalline aluminium hydroxide:



This method was later replaced by seeding the supersaturated solution with pure aluminium hydroxide, which eliminated the need for cooling and resulted in a much more economically feasible endeavour:



Pure alumina was subsequently obtained after heating aluminium hydroxide to a temperature of ~1470 K:



Solvent extraction is an often-employed sub-process that is covered under the umbrella of hydrometallurgy. It is an interfacial transport technique whereby metal(s) are purified. For solvent extraction studies, the nineteenth century was a period of great importance. Peligot⁷ was the first to report the extraction of uranyl nitrate into diethyl ether in 1842, while Rothe⁸ and Pomeranz⁹ reported the extraction of iron in hydrochloric acid into diethyl ether in 1892. In 1900, Langmuir¹⁰ used the method proposed by Rothe and Pomeranz to separate iron from various other metal ions. The first general understanding of liquid-liquid distribution equilibria was experimentally introduced in 1872 by French scientists Berthelot and Jungfleisch,¹¹ and subsequently described from a thermodynamic point of view in 1891 by the German scientist, Nernst.¹²

1.2 General introduction to base metals

Before the various sources and characteristics of base metals are delved into, one must first establish what is meant by the term “base metals”. The Oxford dictionary defines it as follows:

“Base metals are common metals that are not considered precious, such as copper, tin or zinc.”

For the purposes of this dissertation, the Oxford dictionary’s definition seemed far too broad and did not contain enough chemical gravitas. Upon researching various scientific disciplines’ view on this matter, it appeared as though the term differs tremendously from one discipline to another. In electrochemistry, base metals are defined as any of the metals in the lower end of the electrochemical series. In geological and mining circles, “base metals” is a non-specific term referring to the high-volume, low-value metallic elements and is commonly restricted to the three elements: copper, lead and zinc. In metallurgy, base metals are the substrates upon which other elements are plated.¹³ These three definitions, in our view, were inadequately phrased as well. Therefore, whenever this study refers to “base metals”, it permanently includes the following set of metals to avoid confusion and/or misinterpretation: cobalt, nickel, copper, zinc, cadmium and lead.

1.2.1 Properties and applications of cobalt

Cobalt is a lustrous first-row transition metal and like iron, can be magnetised. It is stable in air and unaffected by water, but is slowly corroded by dilute acids. According to Pearson’s¹⁴ hard/soft acids and bases (HSAB) theory, cobalt can be classified as a “borderline” metal ion. Theoretically speaking, this means that both oxygen (harder) and nitrogen (softer) donor atoms could coordinate to cobalt(II). This, however, is covered in greater detail in **Section 1.5**.

Cobalt(II) has an electron configuration of $[\text{Ar}]4s^03d^7$ and is paramagnetic in nature due to its three unpaired electrons in its valence shell. Its main applications are found in the superalloy and battery industry and was listed as a critical metal by the U.S. Department of Energy in 2011 and the U.S. Department of the Interior in

2018.^{15,16} Recently, it has enjoyed a tremendous increase in demand, especially in the production of batteries for electric vehicles (4%), computers (9%) and smartphones (18%), which led to an exponential surge in its market price.¹⁷ Therefore, Banza Lubaba Nkulu *et al.*¹⁸ dubbed cobalt as the “*hottest commodity of 2017*”. Additionally, cobalt is widely used in turbine blades of aircraft engines (16%), catalysts (5%) and pigments (5%).¹⁷ Cobalt(II) aluminate, or more commonly known as cobalt blue (CoAl_2O_4), is an important part of any artist’s palette and is frequently used by craft workers in the porcelain, pottery, stained glass, tile and enamel jewellery industries.

1.2.1.1 Sources of cobalt

Cobalt is widely distributed in nature, but it can only be found in the earth’s crust at a mere 0.0025% (crustal abundance), significantly less than common metal resources such as aluminium and iron.^{19,20} According to the 2019 U.S. geological survey (USGS),²¹ the world’s cobalt deposits sit at nearly 7 million tonnes, but is somewhat irregularly distributed throughout the earth’s crust. According to Liu *et al.*,²⁰ 90% of the world’s cobalt reserves can primarily be found, in decreasing order, in the Democratic Republic of the Congo (DRC), Australia, Cuba, Zambia, Russia, New Caledonia (French overseas territory), Canada and China. Remarkably, a mammoth 48.57% of all the known reserves can be found in the DRC alone. The only operating mine with cobalt as its main product is the Bou Azzer mine in Morocco, with its main mineral being cobaltite (CoAsS).¹⁷ Additionally, cobalt reserves are also found in deep-sea manganese nodules, but only exist in marginal abundances of 0.3–2%, making it an extremely expensive venture for any interested investor.

1.2.2 Properties and applications of nickel

Nickel is a first-row transition element and is ferromagnetic under ambient conditions along with iron, cobalt and gadolinium. It displays remarkable resistance to corrosion and mechanical strain. Nickel(II), according to Pearson’s¹⁴ HSAB theory, can be classified as a “borderline” metal ion.

Nickel(II) has an electron configuration of $[\text{Ar}]4s^03d^8$ and is known to form a large number of complexes with coordination numbers of 4, 5 and 6. Typical geometries include octahedral, trigonal bipyramidal, square planar, square pyramidal and tetrahedral arrangements. Nickel(II) is paramagnetic due to two unpaired electrons in its valence shell.

By far, the majority of uses of nickel arises from its alloys—most notably stainless steel.²² However, other nickel containing alloys have special high-end applications, such as a nickel alloy synthesised by Kim *et al.*²³ that exhibits a thermal expansion coefficient of zero. Miller *et al.*,²⁴ on the other hand, synthesised a nickel-titanium alloy that displays shape memory characteristics, while other modern applications include materials for aviation,²⁵ rechargeable batteries,²⁶ electroplating²² and catalysis.²⁷

1.2.2.1 Sources of nickel

Nickel is considered to be one of the most abundant elements in the universe, but forms a mere 0.016% of the earth’s crust, making it the 23rd most abundant element known to man.²⁸ The total amount of nickel in the earth’s crust is more than copper, zinc and lead combined, but large nickel deposits are extremely rare and in

most cases economically impracticable to mine.²⁸ Nickel is mostly found amidst magnesium- and iron-rich ore deposits. This is due to nickel's similar ionic radius (0.69 Å) to that of magnesium (0.65 Å) and iron (0.75 Å), and often displaces these ions in their crystal lattices, especially silicate lattices.²⁸ In nickel-rich peridotite rock, nickel is mostly found in olivine, an orthosilicate mineral with the general formula of M_2SiO_4 ($M = Mg^{2+}, Fe^{2+}$ or Mn^{2+}).²⁸ The feasibility of nickel mining rests largely on the concentration of the nickel in the ores, as in the case of silicate ores or where the nickel in the magma have been precipitated as sulphides.²⁸ Silicate ores were formed by the continuous weathering of peridotite rocks under unique chemical conditions, which solely occurs in the tropics.²⁸ The metal continually dissolves and precipitates in a process known as “laterisation”.²⁸ From this process, laterite ores have their origin of which bauxite is an important example.

The largest deposits of nickel sulphide ores are found in Canada, Russia, South Africa and more recently, Australia.²⁸ The South African deposits are particularly rich in platinum group metals (PGMs—Ru, Rh, Pd, Os, Ir and Pt) and the production of these are the principal reason for treating these ores.²⁸ The combined world nickel reserves are estimated to be ~54 million tonnes, of which 45% are found in sulphide ores and 55% in laterite ores.²⁹ Today, Canada accounts for 20–30% of the world's nickel production.²⁸

1.2.3 Properties and applications of copper

Copper is a shiny red-brown first-row transition metal. It is softer than zinc and therefore highly malleable, in addition to being an effective conductor of both electricity and heat. In moist air, copper's shiny surface oxidises and takes on a light green patina. According to Pearson's¹⁴ HSAB theory, copper(II) can be classified as a “borderline” metal ion.

Copper(II) has an electron configuration of $[Ar]4s^03d^9$ and is weakly paramagnetic due to its solitary unpaired electron in its 3d valence shell. This cupric ion can commonly be found in a tetragonal coordination environment, with four short equatorial bonds and another one or two extended axial bonds.³⁰ Other known geometries include tetrahedral, square planar and trigonal bipyramidal geometries. Most copper(II) complexes are either blue or green, or a combination thereof, due to d–d absorptions in the 600–900 nm range.³⁰ In exceptional circumstances copper(II) complexes might appear red-brown as a result of charge-transfer bands bleeding into the visible region.³⁰

Just shy of 90% of the global copper output is used in electrical devices and communication systems.³¹ After silver, copper has the highest electrical conductivity and is therefore often used in the generation of electricity and electric distribution systems (40%), both for industrial and residential purposes. About 12.5% of copper is used for the construction of electric and electronic equipment, while another 12.5% is used in the transportation industry—conducting current from batteries to various control devices, lighting, on-board computers or satellite navigation systems.^{32,33} A further 20% of the copper output is designated for the building industry (roofing, facade panels and sewage systems).³¹ The remaining 10% is specifically designated for high-end purposes, such as musical instruments, sculptures, jewellery, kitchen utensils and coins.³³ Nowadays, the anti-microbial properties of copper are being exploited as well, with an exclusive application as touch surfaces for hospitals and public facilities.³¹

1.2.3.1 Sources of copper

The mining of pure metallic copper is an extremely rare occurrence, with only about 1% of all mining ventures managing to do just that. The remaining copper resources are obtained from sulphide- (90%) and oxide ores (9%).³¹ Generally though, sulphide deposits tend to be much deeper than oxide deposits and are therefore more expensive to extract and treat, which explains why most companies prefer to mine for copper oxide ores before the sulphide ores.³⁴ In 2015, the largest copper-producing country, Chile, produced around one-third (5.5 Mt) of the world's copper, while Peru (2.5 Mt) and China (1.7 Mt) rounded out the podium in second and third position, respectively.³⁵ From an African perspective, however, the Copperbelt—localised across Zambia and the Democratic Republic of Congo—holds approximately one-tenth of the world's reserves, but several socio-environmental issues of these mines prevent them from taking full advantage of these vast copper reserves.

Low-grade oxides and some sulphide ores are subjected to the hydrometallurgical process, which consists of numerous step-wise processes. The first process, however, known as “leaching” commonly implements sulfuric^{-36,37} or hydrochloric acid³⁸⁻⁴⁰ as leaching agents. Once the leaching process is completed, ion exchange techniques are used to recover copper selectively from solution. Solvent extraction is the most popular technique, while ion exchange resins are also applied. In niche cases, biohydrometallurgical processes are also implemented.⁴¹

1.2.4 Properties and applications of zinc

Zinc is a first-row transition metal with a silver-white hue and a blue tinge. It is a brittle solid at room temperature, but becomes malleable and pliable when heated to 110 °C. According to Pearson's¹⁴ HSAB theory, zinc(II) is classed as a “borderline” metal ion.

Zinc(II) has an electron configuration of $[\text{Ar}]4s^03d^{10}$ and is diamagnetic, since it has a filled valence 3d orbital (all electrons paired). Because of this, complexation usually give rise to complexes with a coordination number of 4 (tetrahedral geometry) and form stable 18-electron complexes with its ligands.⁴² For this reason, 5-coordinate zinc(II) complexes are relatively rare and expected to be unstable, although a handful of literature sources do report the successful synthesis of such complexes.⁴²⁻⁴⁷ Similar to 4-coordinate zinc complexes, 5-coordinate zinc complexes have an oxidation state of +2 as well.⁴²

Zinc has many modern-day applications in the automotive industry, such as automobile casting, galvanising iron and in the preparation of brass (zinc and copper alloy). It enjoys a tremendous demand in the construction industry for both roofing shingles and gutters. Zinc oxide is commonly used as a white pigment in watercolours, paints, plastics, cosmetics, wallpaper and printing inks. Interestingly, zinc oxide is also implemented as a catalyst in the production of rubber and acts as a heat disperser in the final product.⁴⁸

1.2.4.1 Sources of zinc

Zinc is the 24th most abundant element in the earth's crust, with an average concentration of 65 g/t (0.0065%).⁴⁹ Presently, zinc is one of the major non-ferrous metals and the fourth most expended metal, after iron, aluminium and copper.⁴⁹ Over the past few decades, companies mainly opt to mine zinc sulphide deposits,

which currently accounts for ~85% of the world's zinc production.^{50–52} Today, we know of 55 zinc minerals, however, only a handful have economic value, with sphalerite (ZnS) being the most common.⁵³ Zinc sulphides are anticipated to last for around 70 years at the current rate of extraction, thereby rendering zinc non-sulphide ores (often referred to as “zinc oxides”) as important sources to meet future demands.⁴⁹ With current technology, however, it solely makes monetary sense to extract zinc from non-sulphides, such as smithsonite, hydrozincite, zinc silicates hemimorphite and willemite.^{54–56} The current major zinc-producing regions are Asia (54%), Europe (23%) and America (17%).⁴⁹

1.2.5 Properties and applications of cadmium

Cadmium is a lustrous silver-white second-row transition metal and is reasonably pliable under ambient conditions, making it soft enough to cut with a sharp knife. According to Pearson's¹⁴ HSAB theory, cadmium(II) is classed as a “soft” metal ion, primarily due to its large ionic radius. Uniquely, cadmium has eight stable isotopes of abundance (¹⁰⁶Cd, 1.22%; ¹⁰⁸Cd, 0.88%; ¹¹⁰Cd, 12.39%; ¹¹¹Cd, 12.75%; ¹¹²Cd, 24.07%; ¹¹³Cd, 12.26%; ¹¹⁴Cd, 28.86%; ¹¹⁶Cd, 7.58%).⁵⁷

Cadmium(II) has an electron configuration of [Kr]5s⁰4d¹⁰ and is diamagnetic due to the absence of unpaired electrons in its valence shell. Its main coordination number is 6, although coordination numbers 4 and 5 have also been reported.⁵⁸ Due to its larger size, cadmium(II) displays coordination number 6 more easily than zinc(II), which allows monodentate ligands (and larger multidentate ligands) to coordinate in an octahedral manner (generally distorted).⁵⁸

Many years ago, cadmium was identified as a highly toxic element, and the need for precautions in industrial settings in which workers were exposed to micro dust particles of the element—or its corresponding compounds—had long been known.⁵⁷ Its serious impact on human health only became clear in the late 1940s and early 1950s with the outbreak of the itai-itai disease in Japan. Workers were exposed to cadmium, which originated from smelter wastes that were concentrated by the rice plant to levels far above those of the normal environment.⁵⁷

The principal uses of cadmium are as alloys, plating metals, pigments, stabilising materials for polyvinyl plastics and batteries. Additional minor uses include cadmium as a key ingredient in fungicides, nuclear control rods, ceramics and photographic products.⁵⁷

1.2.5.1 Sources of cadmium

Cadmium is a rare metal, and according to Sadegh Safarzadeh *et al.*,⁵⁹ is distributed in the earth's crust at an average of 0.08–0.5 ppm. Fleischer *et al.*,⁵⁷ on the other hand, reported a distribution of 0.15–0.2 ppm. Either way, this makes cadmium a highly sought-after commodity. Cadmium is nearly always divalent and closely resembles the chemical properties of zinc. It often displaces zinc (isomorphous replacement) in almost all zinc ores as a result of their shared chemical properties.⁶⁰ Cadmium is largely produced as a by-product from mining, smelting and refining of sulphide ore deposits of zinc, although it is also present in the metallurgical processing of other metals, such as copper and lead.⁵⁹

Not only are the main producers of cadmium China, Japan and South Korea, but these countries are the largest consumers of the metal as well. This is mainly a result of the booming Ni-Cd battery industry that supplies long-lasting batteries for modern electric vehicles and other rechargeable electronic devices.⁵⁹

1.2.6 Properties and applications of lead

Lead is a blue-white dull metal that is highly malleable and a relatively poor conductor of electricity. According to Pearson's¹⁴ HSAB theory, lead(II) can be classified as a "borderline" metal ion, although many sources prefer to cite lead(II) as a "soft" metal ion due to its large ionic radius.

Lead(II) has an electron configuration of $[\text{Xe}]6s^24f^{14}5d^{10}6p^0$ and is diamagnetic in nature due to the absence of unpaired electrons in its valence shell. Interestingly, three stable lead nuclides are the end-products of radioactive decay of uranium (decays to ^{206}Pb), thorium (decays to ^{208}Pb) and actinium (decays to ^{207}Pb), which is of particular interest to nuclear physicists. Lead's most common oxidation states are +2 and +4, resulting in the formation of numerous lead oxide compounds, such as PbO , PbO_2 and Pb_3O_4 .

The main uses of lead include the production of the alloys, pewter and solder, while lead tetraethyl (PbEt_4) is still used in certain grades of fuel today. This, however, is slowly being phased out due to strict environmental regulations worldwide. Other notable uses are related to the glass of computer and television screens (shields the user from radiation), while it is also used for various types of ammunition, bearings, cables and sheeting. Furthermore, lead oxides are important constituents in ceramic glazes as well.

1.2.6.1 Sources of lead

Lead is the 36th most abundant element in the earth's crust, with an approximate distribution of 10–14 ppm.⁶¹ In general, two types of lead resources exist: primary- and secondary resources. Worldwide, lead ores amount to approximately 85 million tonnes, most of which can be found in Australia (36 Mt), China (18 Mt) and Russia (6.4 Mt). Most of the primary lead resources are in the form of minerals such as, galena (PbS), cerussite (PbCO_3) and sulfuric acid galena (PbSO_4),⁶² while secondary lead resources are primarily produced through the recycling of spent lead-acid batteries.⁶³

1.3 Hydrometallurgical processes for the separation of base metals

To understand the various techniques for the separation of metals in solution, the global hydrometallurgical process requires some detailing. It is imperative to appreciate the whole process from start to finish, *i.e.*, from raw materials (ore) to the eventual pure metal (**Figure 1.1**). The hydrometallurgical process, which includes solvent extraction, starts off with the mining of the ore from metal-rich sources. The metals in the ore are leached (dissolved) by typically introducing an appropriate strong acid—and in some cases bases—for a specific metal ion or combination of metal ions. The metal-rich leach solution (sometimes referred to as the "pregnant leach solution") is brought into contact with an extractant that carries the metal(s) from the aqueous phase to the organic, water-immiscible phase. Numerous conditions, such as temperature, type of extractant, concentration, solvent and pH can be tailored to effect the maximum extraction of the desired metal, whilst maintaining good selectivity too. After extraction, the pH is drastically lowered to strip (recover) the metal ion

from the extractant to afford a fresh metal-rich aqueous solution. Thereafter, a reducing agent is employed to deliver pure metal. Each process is cyclical in nature, meaning that extractants, acids, solvents, *etc.* can be reused to ensure the most efficient use of all resources in the overall hydrometallurgical process. The metals that were not extracted during the solvent extraction process (raffinate) is recycled back into the leaching process.⁶⁴

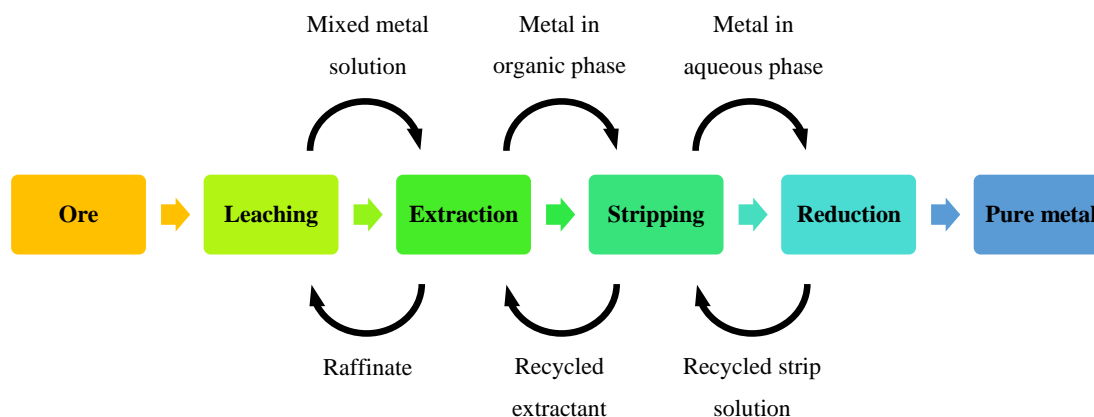


Figure 1.1: A step-wise portrayal of the global hydrometallurgical process. [Adapted from Wilson *et al.*⁶⁴]

Besides solvent extraction, other techniques for the separation of metals are often employed as well. These techniques include crystallisation, ionic precipitation, electrochemical reduction, reduction with gas, carbon adsorption, ion exchange and the electrolytic process.

1.3.1 Crystallisation

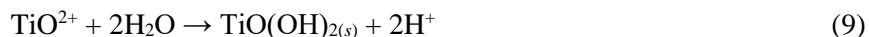
Crystallisation is a centuries-old technique that is still extensively used to purify compounds. It is, however, a technique that is seldom used in the recovery of metals. Crystallisation of a metal salt out of an aqueous solution occurs when the solution is evaporated and the solute goes beyond the point of saturation. Knowing that the solubility of metal salts decreases considerably beyond 200 °C, industry can force crystallisation by implementing high temperatures and pressures. An important aspect of crystallisation within hydrometallurgy is the separation of two or more chemically akin metals. This, of course, is dependent on their relative solubilities in the same aqueous solution.²

1.3.2 Ionic precipitation

Similar to crystallisation, metals can be recovered as insoluble compounds via the ionic precipitation technique. Hydroxides and sulphides are compounds that are readily precipitated and has found extensive application in industry. In this process, an anionic reagent is added to the solution to form a metal salt which is insoluble in the present solution. This is a rapid process, due to the metal salt's poor solubility.² An example of this is the precipitation of copper, as CuS, from an acidic solution by passing H₂S gas through it, as shown below:

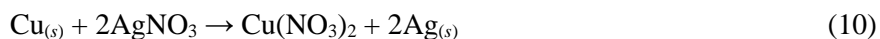


Hydrolytic reactions are also used for ionic precipitation. The precipitation of titanium hydroxide is a prime example of this:



1.3.3 Electrochemical reduction

As mentioned in **Section 1.1**, a common method for the precipitation of metals can be achieved by a process known as “cementation”, which is an electrochemical reduction process. This process involves the fact that a higher metal in the electromotive force (EMF) series, *i.e.*, a less noble metal, can be added to displace a lower metal (more noble metal) from solution.² An example of this was already shown where metallic iron is added to a copper solution (Eq. 1). The copper precipitates while the iron goes into solution. Similarly, copper can displace silver from a solution of silver nitrate too, a reaction often used to determine the metallic copper content of ore samples:²



In another familiar example, zinc can displace cadmium from cadmium sulfate solutions, which is currently the standard procedure for recovering cadmium from leach solutions:²



1.3.4 Reduction with hydrogen gas

In modern hydrometallurgy, hydrogen gas plays a very important role in the recovery of metals. Interestingly, H_2 appears to have a dual function. At times it behaves as a metal (formation at the cathode in the hydrolysis of water) and in other instances more like a non-metal (formation of metal hydrides).² It can be liberated by sodium with water or reaction of zinc with dilute acid. Most notably, however, it reduces copper and nickel ions present in sulfate solutions.² The simplified reduction of nickel(II) can be seen below:



1.3.5 Carbon adsorption

The use of activated carbon in the recovery of gold from cyanide leach solutions can be flagged as a major advancement in hydrometallurgy.² The gold cyanide anion present in the leach liquor is adsorbed onto pseudo-cationic sites on the activated carbon according to the following chemical reaction:



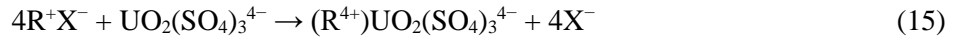
Furthermore, the loaded carbon can be stripped of its gold by reversing Eq. 13 with the help of a hot caustic solution:⁶⁵



Adsorption on activated carbon can also be used for turbid solutions or pulps, thereby saving on expensive filtration processes.¹

1.3.6 Ion exchange

Ion exchange is mainly used as a purification process in the recovery of uranium from low-grade uranium ores.² For the removal of uranium, one must add an anionic exchanger because of its complex anions, $\text{UO}_2(\text{SO}_4)_2^{2-}$ and $\text{UO}_2(\text{SO}_4)_3^{4-}$.² This is a significant advantage, since cationic impurities in leach solutions (Al^{3+} , Co^{2+} , Ni^{2+} , etc.) cannot participate in the following ion exchange reaction:²



where R represents the fixed ion exchange sites of the resin and $\text{X}^- = \text{NO}_3^-$, Cl^- or HSO_4^- .

1.3.7 Electrolytic process

Both the electrowinning and electrorefining processes have been at the forefront of metal recovery industries over the past few decades.² Electrolysis can broadly be described as two equivalent reactions that occur simultaneously, *i.e.*, oxidation and reduction reactions. Oxidation takes place at the anode and reduction at the cathode.

In electrorefining, the oxidation of a metal at the anode, proportional to the current passing through, is directly accompanied by the reduction of the same equivalent amount of metal ion at the reductive cathode.² The electrolyte composition remains unchanged and the net cell reaction is equal to the simultaneous corrosion of the metal at the anode and metal deposition at the cathode.² The voltage required is only needed to overcome the ohmic resistance of the electrolyte, since no decomposition potential is involved.²

In electrowinning, the net cell reactions are also equivalent oxidation and reduction reactions, but the presence of insoluble anodes prevent the oxidation and reduction of equivalent amounts of the same metal.² The electrowinning of nickel can be used as a good example to illustrate this phenomenon. Nickel from an acidic sulfate solution undergoes the oxidation-reduction reaction, where NiSO_4 is oxidised at the anode into Ni^{2+} ions.² The simple reduction reaction at the cathode is shown below:



This reaction is similar to the electrorefining process, but the oxidation reaction at the anode discharges the sulfate ion. The sulfate radical formed, however, is extremely unstable and reacts with water instantaneously to form sulfuric acid according to the following reaction:²



1.3.8 Solvent extraction

Solvent extraction is a two-phase system whereby metal ions are efficiently and selectively transported from a metal-rich aqueous phase to a metal-receiving organic phase. The metal ion of interest is often present at low concentrations and mixed with various other metal ions. The aim of the organic extractant is to coordinate to the appropriate metal ion in a selective fashion. Once the organic extractant coordinates to the metal ion, the resulting complex partitions into the organic phase due to its poor aqueous solubility (**Figure 1.2**).

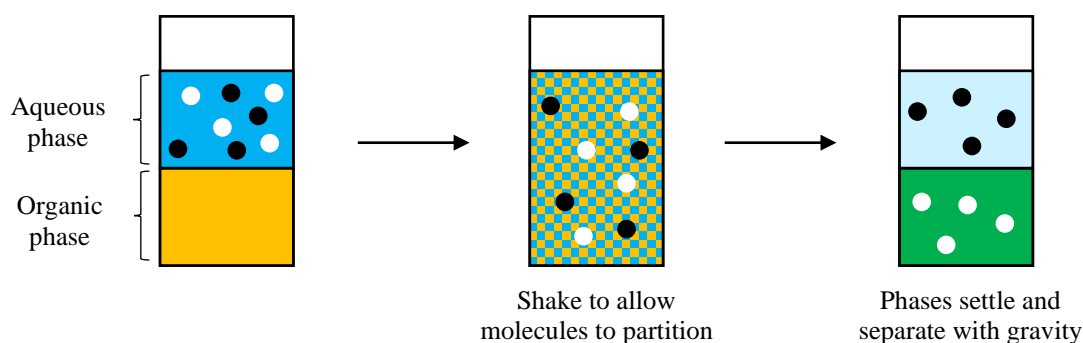


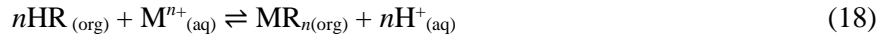
Figure 1.2: A simplified depiction of the solvent extraction process. Black and white dots represent two distinct metal ions—first combined in the aqueous phase, and later separated into two phases.

After the metal is extracted into the organic layer, the metal-rich organic layer often becomes brightly coloured. This is due to the complexation of the metal ion with the organic extractant. Conversely, the aqueous phase loses its bright colour due to the depletion of metal ions in solution. At the end of the extraction procedure the organic phase is physically separated from the aqueous phase and brought into contact with a fresh aqueous solution. This process, known as scrubbing, removes most unwanted impurities that were co-extracted with the metal ion of interest.⁶⁵ This process is usually done either by a solution of acid or alkali salt that has a pH favouring the extraction procedure.⁶⁵ In industry, a solution of the metal itself is used to rid the organic phase of impurities.⁶⁵

In order to recover the extracted metal species, the scrubbed organic phase is mixed with a highly acidic aqueous solution ($\text{pH} < 2$) to release the metal into the aqueous phase. The high concentration of protons competes for binding sites (donor sites) on the extractant. Alternatively, the organic extractant can be reacted with another reagent that will dissociate the extractant from the metal and release the metal back into the fresh aqueous phase. The release of the metal into the aqueous phase is colloquially termed “stripping”.⁶⁵ Once the metal has been retrieved, the extractant-rich organic phase can be recycled, either immediately or after it has been rid of impurities or decomposed extractants.²

In solvent extraction, net electrical neutrality is preserved. This is done by the transfer of neutral molecules from one phase to another, the transfer of ion pairs or by the exchange of ions between the two liquid phases.² The driving force for the transfer process depends heavily on the manner in which the metal is associated with the extractant in solution. The extractant could form a chemically neutral complex with the metal via

coordination, including chelate formation or ion association.² A reversible chemical reaction is shown below to illustrate the overall solvent extraction procedure:



The thermodynamic derivations of solvent extraction are explained in great detail by Sekine and Hasegawa.⁶⁶ They derived a set of equations to determine the optimum extractant concentration as well as the optimum pH for solvent extractions. For a chelating reagent, HR, the extraction reaction for a metal ion, M^{n+} , is represented by Eq. 18 above. The thermodynamic extractive equilibrium constant (K_{ex}°) can be expressed as follows:

$$K_{ex}^{\circ} = \frac{[\text{MR}_n]_{\text{org}} [\text{H}^{+}]_{\text{aq}}^n}{[\text{M}^{n+}]_{\text{aq}} [\text{HR}]_{\text{org}}^n} \cdot F \quad (19)$$

where F is the ratio of molar activity coefficient. Usually, F is unknown and is combined with K_{ex}° to give the extraction constant, K, as seen below:

$$K = \frac{K_{ex}^{\circ}}{F} = \frac{[\text{MR}_n]_{\text{org}} [\text{H}^{+}]_{\text{aq}}^n}{[\text{M}^{n+}]_{\text{aq}} [\text{HR}]_{\text{org}}^n} \quad (20)$$

At this stage, the distribution ratio, D , can be introduced. It is defined as the ratio of total analytical concentration of the solute in the solvent to that in the aqueous phase:

$$D = \frac{[\text{MR}_n]_{\text{org}}}{[\text{M}^{n+}]_{\text{aq}}} \quad (21)$$

Now, the expression for K can be expressed as follows:

$$K = \frac{D [\text{H}^{+}]_{\text{aq}}^n}{[\text{HR}]_{\text{org}}^n} \quad (22)$$

From Eq. 22 we can now derive the following:

$$\log D = \log K + n\text{pH} + n \log [\text{HR}]_{\text{org}} \quad (23)$$

It is quite obvious that for any solvent extraction system, a high value for D is extremely desirable for achieving satisfactory extraction results. This, according to Eq. 23, is achieved at a high concentration of extractant and at a high pH of the aqueous solution containing the metal ion mix.⁶⁶

In the hydrometallurgical application of solvent extraction systems, the purpose is to transfer the metal ions from the aqueous phase to the extractant-rich organic phase. Therefore, in industry the term, percentage extraction ($\%E$), is used to determine the amount of metal extracted from the aqueous phase.⁶⁵ $\%E$ can be determined by means of the following simple equation:

$$\%E = \left(\frac{C_i - C_s}{C_i} \right) \times 100 \quad (24)$$

where C_i represents the initial stock concentration of the metal-rich aqueous solution and C_s represents the concentration of the aqueous solution after extraction.

1.3.8.1 IUPAC terminology applicable to solvent extraction systems

In general, the International Union of Pure and Applied Chemistry (IUPAC) prefers to use the term “liquid-liquid distribution” or “liquid-liquid extraction”, instead of “solvent extraction”. I am of the opinion that the use of “solvent extraction” is justified by its far more common usage in both the academic fraternity and in industry.⁶⁷

To avoid confusion and misuse, I thought it imperative to define specific terms related to solvent extraction systems in alphabetic order, according to IUPAC:⁶⁷

Diluent is “an inert (organic) solvent used to improve the physical properties (density, viscosity, etc.) or the extractive properties (e.g., selectivity) of the extractant. The diluent has negligible extractant properties for the substance to be extracted.”

Distribuend is “the substance that is distributed between two immiscible liquids or liquid phases.”

Extract is “the separated phase (usually organic) containing the substance extracted from the other phase.”

Extractant is “the reagent which forms a complex or other adduct in the solvent with the substance which partitions across the phase boundary of the extraction system. The extractant (extracting agent) may also partition.”

Solvent is “a liquid phase (usually an organic liquid) or the solution of an extractant in an organic diluent which is used to extract a substance from another liquid (usually aqueous).”

Stripping is “the process of back-extraction of the distribuend from the extract (usually into the aqueous phase).”

1.4 Types of extractants and additives commonly used in solvent extraction systems

For analytical small-scale laboratory solvent extraction systems, the rate of extraction and stripping is of relatively low importance. This, however, is certainly not the case in industry, where large-scale solvent extraction processes are performed on a day-to-day basis. For an extractant to be successfully integrated into an industrial setting, it has to meet six key criteria: (1) be relatively inexpensive; (2) be highly soluble in the organic phase and highly insoluble in the aqueous phase; (3) be able to selectively form a metal complex with the desired metal ion of interest and have good complex solubility in the organic phase; (4) be easy to recover the metal from; (5) be regenerated and reused without significant decomposition; (6) have suitable physical properties, such as low viscosity, low flash point, non-toxicity and non-volatility.⁶⁵ As previously mentioned,

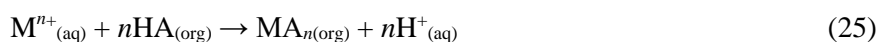
these factors are of less importance in small-scale analytical environments, therefore, only a limited number of extractants ever make it out of the laboratory and into a real-world setting. Only a few extractants that have been synthesised in such a manner have been found to be commercially viable.⁶⁵

Most metal salts are ionic in nature and easily dissolve in water due to water's high dielectric constant and the well-known tendency of water to solvate ions.⁶⁵ The coordination number of the metal primarily dictates the number of water molecules that are bonded to the metal ion. Such metal ions, are generally not expected to be carried into the organic phase, which is mostly non-polar with an extremely low dielectric constant.⁶⁵ Therein lies the challenge of solvent extraction researchers the world over—to ensure that these metal ions are efficiently transferred from the aqueous phase to the organic phase. This is primarily done by the reaction of suitable organic compounds with the desired metal ion that form a neutral species that is soluble in the organic phase. Most modern organic extractants can be categorised into three classes according to their mode of extraction: (1) cationic-, (2) anionic- and (3) solvating extractants.

1.4.1 Cationic extractants (acidic)

In the cationic solvent extraction process cations are exchanged between the aqueous and organic phases. The formation of the extractable neutral complex can be attributed to the removal of one acidic proton on the extractant for every positive charge on the metal ion.⁶⁵ There are two subclasses of cationic extraction processes: chelate- and acid extraction.

In chelate extraction, the metal ion is only transferred into the organic phase once an electrically neutral metal chelate is formed through the help of a chelating agent that satisfies both the valence and coordination number requirements of the metal ion.⁶⁵ There are cases where organic solvents such as diketones, oximes and oxines contain both acidic and basic functionalities that combine with a metal ion. In such cases, chelate salts are formed where both functional groups are operative.⁶⁵ Overall, the chelate extraction process can chemically be expressed as follows:



From Eq. 25, it is clear that the proton concentration increases in the aqueous phase, therefore, it is important to control this acid formation. A well-known industrial acidic chelating extractant, LIX 64 N, is successfully used in industry for the extraction of copper from dilute acidic solutions.⁶⁵

The second subclass in cationic extraction, *i.e.*, acid extraction, uses acids such as alkyl carboxylic-, phosphoric- and sulfonic acids. Unlike chelating extractions, mechanisms in cationic extractions are much more intricate because they are affected by solvent-phase properties.⁶⁵ It is known that organophosphorous and carboxylic acids form dimers (and even polymers) in the organic phase due to hydrogen bonding, which ultimately affects their extractive abilities.⁶⁵ For example, di-(2-ethylhexyl)phosphoric acid (D2EHPA) forms dimers in most non-polar organic solvents. In such cases, the extraction reaction can be written as follows:



where H_2A_2 represents the dimeric form of the extractant and m the total number of extractant molecules in the extracted species. Extraction of metal ions is improved when extractants are more basic.⁶⁵ An increase of the charge on a metal cation also increases its extractability. In cases where metal ions have the same charge, the degree of extraction will depend inversely on their ionic radii, *i.e.*, smaller cations will preferentially be extracted over larger cations.⁶⁵ The degree to which metal ions are extracted by means of carboxylic acid extractants and extractants similar to it, are pH dependent.⁶⁵ However, a close eye should always be kept on this parameter for the separation of a concoction of various metal ions.

Table 1.1: Commercial cationic extractants and their uses in industry. [Adapted from Gupta and Mukherjee⁶⁵]

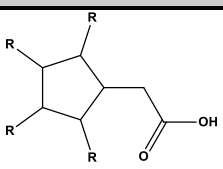
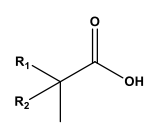
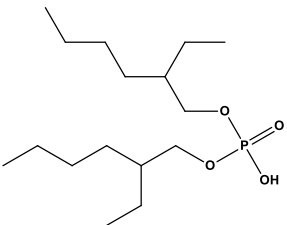
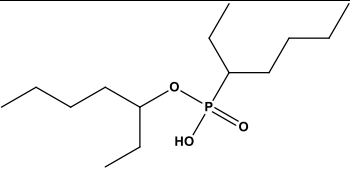
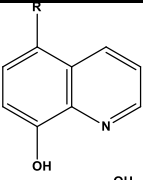
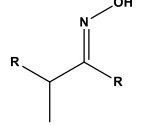
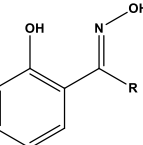
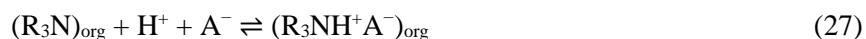
Type of extractant	Commercial name	Chemical structure	Manufacturer	Implementation
Carboxylic acid	Naphthenic acid		Shell Chemical Co.	Cu/Ni separation
	Versatic acid		Shell Chemical Co.	Cu/Ni separation
Phosphoric acid	D2EPHA		Mobile Chemicals	Co/Ni separation; U extraction from phosphoric acid
Phosphonic acid	PC-88 A		Daihachi Chemical Industries	Co/Ni separation
	Cyanex 272	Unknown (trade secret)	American Cyanamid	Co/Ni separation

Table continues...

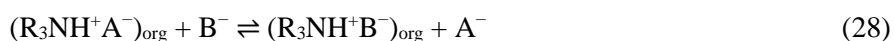
Type of extractant	Commercial name	Chemical structure	Manufacturer	Implementation
Chelating type	Kelex-100		Sherex Chemicals Co.	Cu extraction
8-hydroxy-quinoline-based	LIX 63		Cognis Inc.	Cu extraction
hydroxime	P-5000 series		Acorga Ltd.	Cu extraction

1.4.2 Anionic extractants (basic)

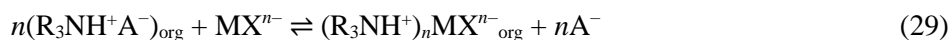
For basic extractants to be used, the metal should form an anionic complex in the aqueous solution.⁶⁸ Various anionic complexes exist, provided certain key conditions are met. Because of this, anionic extractants can selectively extract metals and afford pure solutions.⁶⁸ In industry, long-chained alkylamines are the most common forms of basic extractants (**Table 1.2**). The acid-binding property of amines with high molecular weights depend on the fact that acid salts of these bases are insoluble in water and highly soluble in organic solvents like benzene or kerosene.⁶⁸ This extraction can be thought of as an ion pair formation:



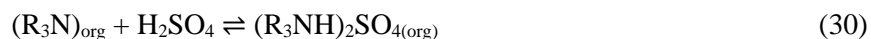
In acidic solutions the metal can be extracted due to anion exchange with an anion present in the aqueous phase. This cannot happen in basic solutions, since metal extraction will be halted:



A metal can now be extracted if it is able to form an anionic complex:



Good examples of such extractions are anionic uranium species present in sulfate solutions:⁶⁵



The uranium, however, can also be extracted through a neutral uranyl sulfate species, instead of going via anionic metal species formation:⁶⁵



The alkali amine extractants used in hydrometallurgy can be divided into three groups: primary (1° , RNH_2), secondary (2° , R_2NH) and tertiary (3° , R_3N) amines. Of course, quaternary amines (4° , R_4N^+) exist too, but these have only been able to find niche applications in industrial solvent extraction setups. Amines have specific trends and properties that make them unique:⁶⁵

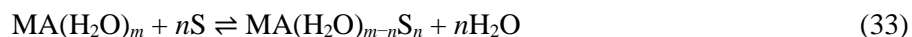
- (1) They can be arranged in the following pattern according to their solubility in water: primary > secondary > tertiary, where tertiary amines with long alkyl chains are effectively insoluble in water.
- (2) Amines are generally soluble in non-polar hydrocarbon solvents.
- (3) The extraction of anionic metal complexes by amines, where the complexing anion is chloride, is primarily governed by the rule: tertiary > secondary > primary. If extractions of sulfate complexes are performed, the order is reversed.
- (4) The extraction of singly charged anions is more effective than that of doubly- or multi-charged ones.
- (5) Chloroanions of multivalent metals are more effectively extracted compared to oxyanions.

Table 1.2: Commercial anionic extractants and their uses in industry. [Adapted from Gupta and Mukherjee⁶⁵]

Type of extractant	Commercial name	Chemical structure	Manufacturer	Typical uses
Primary amine	Primene JM-T	R-NH_2	Rohm & Haas	Fe extraction from sulfate solutions
Secondary amine	LA-1 and LA-2	$\text{R}_2\text{-NH}$ (<i>n</i> -laurylalkyl-methylamine)	Rohm & Haas	U extraction from sulfate solutions and Co extraction from chloride solutions
	Adogen 283	Di-tridecylamine	Sherex Chemicals Co.	Unknown
Tertiary amine	Alamine-336	R_3N	Cognis Inc.	U, V, Mo and W extraction from sulfate solutions
	Hostarex-A 327	R_3N , where $\text{R} = \text{C}_8\text{-C}_{10}$	Hoechst A.G.	Co and Cu extraction from chloride solutions; Separation of Zr from Hf
	Adogen 364	Tri-iso-octyl amine	Sherex Chemicals Co.	Platinum group metal (PGM) extraction from chloride solutions
Quaternary amine	Aliquat-336	$(\text{R}_3\text{N}^+\text{CH}_3)\text{Cl}^-$	Cognis Inc.	Extraction of V, Cr, W and Cu
	Adogen 464	$(\text{R}_3\text{N}^+\text{CH}_3)\text{Cl}^-$, where $\text{R} = \text{C}_8\text{-C}_{10}$	Sherex Chemicals Co.	Extraction of V, Cr, W and Cu

1.4.3 Solvating extractants (neutral)

Neutral extractants have various neutral solvating agents which facilitate extraction by coordinating with the metal, while water molecules are simultaneously displaced.⁶⁵ This leads to the formation of neutral complexes through ion association. The extraction reaction can be formulated as follows:



where MA represents the metal ion pair and S the solvent. There are innumerable organic reagents, such as alcohols, ethers, ketones, alkyl phosphates, *etc.*, with oxygen atoms as electron donors that can solvate metal ions and subsequently be used as solvating extractants.⁶⁵ Tributylphosphate (TBP) and methyl isobutyl ketone (MIBK) are two well-known examples. TBP especially, has found niche application in nuclear materials processing technology.⁶⁵ It can extract uranium from uranyl nitrate solutions in the following way:



Furthermore, TBP can extract a number of non-ferrous metals such as Zn, Cu and Co from hydrochloric acid solutions. Interestingly, TBP can extract mineral acids from effluents and acid nickel liquors produced in metallurgical industries. The key lies in its ability to solvate the proton. The order of extraction is as follows: $\text{H}_3\text{PO}_4 > \text{HNO}_3 \geq \text{HF} > \text{HCl} > \text{H}_2\text{SO}_4$.⁶⁵ Other than nitric acid media, TBP can also extract metals from hydrochloric acid solutions as $\text{MCl}_2(\text{TBP})_n$ by solvating the metal ion and as $\text{HMCl}_3(\text{TBP})_n$ by solvating the proton.⁶⁵ However, a significant drawback of TBP is its inability to extract metals from H_2SO_4 or H_3PO_4 solutions.

In general, the degree of solvation and extraction is determined by five factors:⁶⁵

- (1) The elution donor property of the solvent molecule.
- (2) The length and molecular structure of the hydrocarbon chain.
- (3) The nature of the associate anion.
- (4) The charge of the metal ion.
- (5) The ionic radius of the metal ion.

As far as phosphorous-containing compounds go, the extractability increases with the number of C–P bonds in the extractant, *i.e.*, phosphine oxides > phosphonates > phosphates.⁶⁵ The order is exactly reversed concerning the aqueous solubility of the solvent. The selectivity in extraction by solvating agents mainly depend on the change in solvation energy that takes place upon the displacement of water of hydration by the solvent.⁶⁸

Table 1.3: Commercial solvating extractants and their uses in industry. [Adapted from Gupta and Mukherjee⁶⁵]

Type of extractant	Commercial name	Chemical structure	Manufacturer	Typical uses
Phosphoric acid ester	TBP	$(\text{CH}_3\text{CH}_2\text{CH}_2\text{CH}_2\text{O})_3\text{PO}$	Union Carbide; Albright & Wilson; Daihachi Chemical Industries	Fe extraction from chloride solutions; Separation of Zr and Hf; Uranium purification for nuclear fuel processing
Phosphine oxide	TOPO	R_3PO , where $\text{R} = \text{C}_8\text{H}_{17}$	American Cyanamid; Albright & Wilson; Hokko Chemical Ind.	Extraction of U^{6+} from H_3PO_4 in combination with D2EPHA
Methyl-isobutyl ketone	MIBK	Unknown (trade secret)	Unknown	Separation of Hf from Zr; Extraction of Au from chloride solutions
Alkyl sulphides	Di- <i>n</i> -hexyl sulphides	R_2S , where $\text{R} = \text{C}_8\text{H}_{17}$	Unknown	Pd extraction from chloride solutions

1.4.4 Additives

In addition to the extractant(s), other additives such as diluents and modifiers, are often added to solvent extraction systems to optimise the extractive ability of the extraction assembly.

1.4.4.1 Diluents

At times, diluents are needed to dissolve or dilute the extractant so that its physical properties, like viscosity and density, become more favourable to enhance the mixing and separation of the two phases.² These diluents are hydrocarbons and can be aliphatic or aromatic in nature. Crucially, it is necessary to note that diluents should be inert, *i.e.*, they should not have any extractive power, whatsoever. They should, however, affect the extraction, scrubbing, stripping and phase separation in a meaningful way.

Table 1.4: Examples of commercial diluents. [Adapted from Gupta and Mukherjee⁶⁵]

	Diluent	Specific gravity (20 °C)	Boiling point (°C)
Aromatic	Benzene	0.833	80
	Toluene	0.873	110
	Xylene	0.870	138
	Solvesso 100	0.876	157
	Solvesso 150	0.931	188
Medium aromatic	Escaid 100	0.797	193
Low aromatic	Escaid 100	0.767	199
	Naptha 140 Flash	0.785	60.5
Aliphatic	Mineral Spirits	0.785	157
	Odorless 360	0.761	177
Aliphatic with naphthenes	Isoparo L	0.767	189
	Shell 140	0.790	–
	Kermac 470 B	0.810	–

1.4.4.2 Modifiers

Modifiers are only used to prevent the formation of third phases and to improve the solubility of the metal complex in the organic phase.⁶⁵ Usually, they tend to be long-chained alkyl alcohols (like isodecanol) or other neutral extractants. Like diluents, modifiers are also known to influence the extraction, scrubbing and stripping properties of the extractant. Therefore, they should be chosen with the utmost of care as to not affect the extraction system in a negative way (anti-synergism).⁶⁵

Table 1.5: Examples of commercial modifiers. [Adapted from Gupta and Mukherjee⁶⁵]

Modifier	Specific gravity (20 °C)	Flash point (°C)
2-Ethylhexanol	0.833	85
Isodecanol	0.841	104
Nonylphenol	0.950	140
Tri- <i>n</i> -butyl phosphate	0.973	193

1.5 Synergism and how its related to solvent extraction

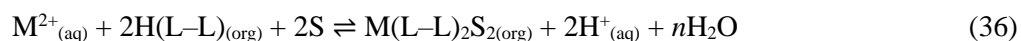
The word “synergism” is derived from two Greek words: “συν” (together) and “εργο” (to work). Therefore, “synergism” means “to work together” or “to work as a unit”.¹ Occasionally, the mixture of two extractants, from the same class or not, will enhance the extraction of a metal above and beyond the mere summed

extractions of the individual extractants.⁶⁹ The following equation describes this phenomenon in mathematical terms:

$$%E_{AB} > \%E_A + \%E_B \quad (35)$$

where $\%E_A$ represents the percentage extraction of extractant A, $\%E_B$ represents the percentage extraction of extractant B and $\%E_{AB}$ represents the combinative percentage extraction of extractants A and B in a single solvent extraction system. This phenomenon is known as “synergism” and is explored in greater detail in **Section 3.1.1**.

There are numerous examples of synergists in literature, although few of them have ever been commercialised for industrial purposes. The principal reason for this is due to the difficulty in ensuring the optimum extractant/synergist ratio in the organic phase remains constant. This optimum ratio can easily be altered through the evaporation of the extractant, poor water solubility and/or entrainment.⁶⁹ The synergistic system most common today is a mixture of a solvating and acidic extractant that acts upon a metal ion where the preferred coordination number cannot satisfactorily be met by the acidic extractant alone.⁶⁹ For example, a divalent metal ion (M^{2+}) with a preferred coordination number of 6 would form a complex with a bidentate acidic extractant, $M(L-L)_2(H_2O)_2$, where $HL-L$ is the extractant.⁶⁹ The displacement of the water molecules of the extracted complex with a solvating extractant (S) will ensure that the complex is soluble in the organic phase, *i.e.*, the complex becomes more lipophilic, $M(L-L)_2S_2$.⁶⁹ When the solvating extractant is unlikely to extract the metal ion by itself, the synergistic system can be generalised as follows:



There are a few examples of synergistic systems applicable to the separation of nickel from cobalt. Varying degrees of synergism can be achieved by adduct formation of octanol, tributyl phosphate (TBP) or trioctylphosphine oxide (TOPO) for the separation of nickel from cobalt.⁷⁰ This is not ideal, therefore, the addition of di-(2-ethylhexyl)phosphoric acid (D2EHPA) to LIX 63 greatly enhances the extraction of nickel and increases the separation factor of nickel from cobalt,⁷¹ but even greater separation factors are achieved when carboxylic acids are used instead of the phosphoric acid.⁷² Weak nickel extraction has been reported when a mixture of versatic acid and LIX 64N was used,⁷⁰ but this was greatly enhanced upon the addition of dinonylnaphthalene sulfonic acid (DNNSA) to the organic phase. Selective cobalt/nickel extraction has also been reported by varying the LIX 63/DNNSA ratios so that, depending on the metal ion sought after, either cobalt or nickel could be selectively extracted in favour of the other.⁷³

1.6 Ligand-metal compatibility

The coordination chemistry of base metal ions naturally play a major role in their separation. When metal-specific ligands are designed, it is essential to explore the properties of the metal ion of interest as well as the properties of the remaining metal ions in solution (matrix). The following criteria are important to consider in such an investigation: (1) The nature of the metal ion, (2) hydrogen ion concentration, (3) thermodynamics and kinetics of complexation and (4) coordination ability of the anion.^{74,75}

Over the past 15 years, various studies have been conducted in which the anion selectivity in the transport of metal salts were investigated.^{64,76-79} These studies focused on both the inner- and outer-sphere coordination chemistry. Furthermore, ligand pre-organisation has also been investigated as an approach for metal ion recognition.^{80,81} Likewise, this dissertation will focus on both the inner- and outer-sphere coordination chemistry as well. We will specifically investigate various factors influencing ligand-metal compatibility. An important feature to consider in the design of a ligand series lies in the selection of the most appropriate donor atoms.

1.6.1 Choosing the correct donor atoms

In hydrometallurgy, the structural design of ligands should be simple and minimalistic to curb excessive synthetic costs. Moreover, if ligands contain oxygen, nitrogen and/or sulphur donor atoms, they are generally far easier to synthesise compared to more exotic donor atoms.⁸²

In 1963, Pearson¹⁴ authored an article in which he explained the hard/soft properties of metal ions (**Table 1.6**). Today, this approach is often referred to as the hard/soft-acid/base (HSAB) theory. Later, in 1966, Pearson and Songstad⁸³ expanded this list to include certain organic moieties as well (**Table 1.7**). For this dissertation, it was of great interest to know which metal ions are preferentially extracted by which organic ligands, based on their hard/soft character. Generally speaking, though, hard organic species preferentially coordinate to hard metal ions, while soft organic species preferentially coordinate to soft metal ions.

Table 1.6: The hard- and soft metal ions as reported by Pearson.¹⁴ [Partial representation]

Hard	Soft	Borderline
H ⁺ , Li ⁺ , Na ⁺ , K ⁺ , Be ²⁺ , Mg ²⁺ , Ca ²⁺ , Sr ²⁺ , Sn ²⁺ , Al ³⁺ , Sc ³⁺ , Ga ³⁺ , In ³⁺ , La ³⁺ , Cr ³⁺ , Co ³⁺ , Fe ³⁺ , As ³⁺ , Ir ³⁺ , Si ⁴⁺ , Ti ⁴⁺ , Zr ⁴⁺ ,	Cu ⁺ , Ag ⁺ , Au ⁺ , Tl ⁺ , Hg ⁺ , Cs ⁺ , Pd ²⁺ , Cd ²⁺ , Pt ²⁺ , Hg ²⁺	Fe ²⁺ , Co ²⁺ , Ni ²⁺ , Cu ²⁺ , Zn ²⁺ , Pb ²⁺

Table 1.7: The hard- and soft organic bases as reported by Pearson and Songstad.⁸³ [Partial representation]

Hard	Soft	Borderline
H ₂ O, OH ⁻ , F ⁻ , CH ₃ CO ₂ ⁻ , PO ₄ ³⁻ , SO ₄ ²⁻ , CO ₃ ²⁻ , ClO ₄ ⁻ , NO ₃ ⁻ , ROH, RO ⁻ , R ₂ O, NH ₃ , RNH ₂ , N ₂ H ₄	R ₂ S, RSH, RS ⁻ , I ⁻ , SCN ⁻ , S ₂ O ₃ ²⁻ , Br ⁻ , R ₃ P, R ₃ As, (RO) ₃ P, CN ⁻ , RNC, CO, C ₂ H ₄ , C ₆ H ₆ , H ⁻ , R ⁻	C ₅ H ₅ NH ₂ , C ₃ H ₄ N ₂ , C ₅ H ₅ N, Cl ⁻ , NO ₂ ⁻ , SO ₃ ²⁻

As a rule of thumb, the hardness of a donor atom increases with an increase in electronegativity (for example F⁻ and H₂O), while less electronegative elements such as P and I⁻ are softer donor atoms. See **Figure 1.3** for the hard/soft distribution of non-metals.

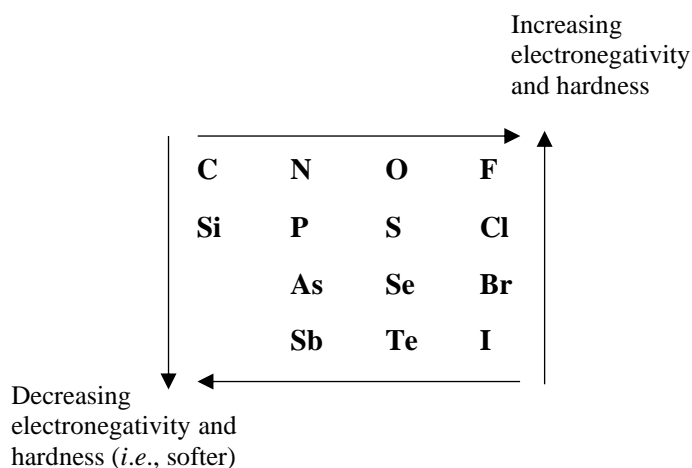


Figure 1.3: The HSAB trend for non-metals based on electronegativity. [Adapted from Martell and Hancock⁸⁴]

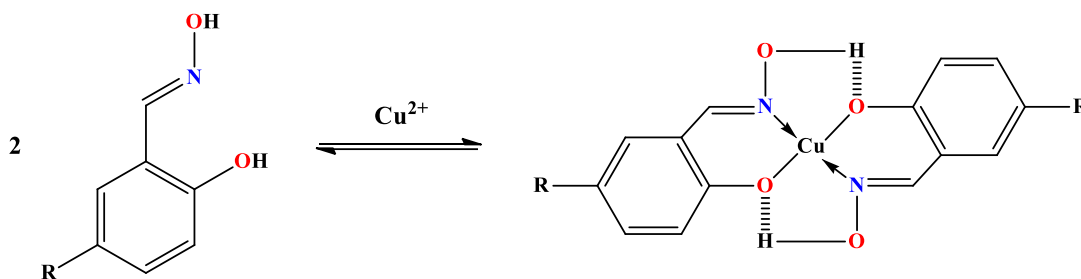
It should be noted, however, that electronegativity is not the only parameter that influences the hard/soft character of a metal ion or organic species, although it certainly plays a major role. Other notable parameters are: ionic radius, oxidation state, polarisability, HOMO energy of bases, LUMO energy of acids and bonding affinity (*e.g.*, ionic- vs. covalent bonding).^{14,83–89}

1.5.1.1 O-donor atoms

It is well known that oxygen donor ligands form more stable complexes with harder metal ions.⁸³ This can be attributed to the fact that they possess strong σ -donor properties and no π -acceptor ability. Therefore, oxygen donor ligands will theoretically coordinate to hard metal ions, and to lesser extents, later 3d transition metal ions (borderline hard/soft metal ions).

The separation of cobalt(II) from nickel(II) in the presence of other base metal ions by means of organophosphorous extractants (CYANEX-type reagents) has broadly been studied.⁹⁰ However, the reverse extraction—nickel(II) from cobalt-rich ore—has not yet been achieved in an efficient manner. Organophosphorous extractants tend to separate cobalt(II) from nickel-rich ore in mildly acidic aqueous solutions (pH 4–6). One significant drawback of organophosphorous extractants is their affinity towards harder metal ions, such as Fe^{3+} . This necessitates the precipitation of iron(III) salts prior to cobalt-nickel separation.⁹¹

Hydroxyoxime extractants (commercialised as LIX reagents) have been used extensively for the extraction of copper(II). Szymanowski⁹² reported the interaction of copper(II) and a hydroxyoxime, shown in **Scheme 1.1**. During the extraction of copper(II), two acidic phenolic protons are removed to form a 2:1 (ligand: Cu^{2+}) complex. This complex is further stabilised by the formation of 5-membered chelate rings through hydrogen bonding of the hydroxyl groups.



Scheme 1.1: The reaction of copper(II) and two hydroxyoxime reagents. [Adapted from Szymanowski⁹²]

1.5.1.2 S-donor atoms

According to Pearson and Songstad,⁸³ sulphur donor atoms are “softer” than oxygen donor atoms. Because of this, sulphur containing ligands are able to form more stable complexes with divalent 3d transition metal ions such as cobalt(II) and nickel(II). It has been reported that sulphur derivatives of di-(2-ethylhexyl)phosphoric acid (D2EHPA) are excellent extractants of cobalt(II), but predominantly at low pH values. This is somewhat of a concern, since low pH values (even negative pH values) are needed to strip cobalt from the ligand during the recycling process. A study by Chia *et al.*⁹³ showed that alkylthiomethylpyridine derivatives formed octahedral complexes with both nickel(II) and cobalt(II), but a slight preference for nickel(II) was reported. An important advantage of sulphur containing ligands is the fact that they hardly ever interact with iron(III), unlike O-donor atoms. A significant disadvantage lies in the synthesis of sulphur-containing extractants. The starting materials for the synthesis of thiol-type extractants can be harmful and are known to give off foul odours.

1.5.1.3 N-donor atoms

According to Pearson and Songstad,⁸³ nitrogen donor atoms are classified as “borderline” hard/soft donor atoms. Appreciably stable complexes are formed with later 3d transition metal ions (Co^{2+} , Ni^{2+} , Cu^{2+} and Zn^{2+}) compared with early and middle 3d transition metal ions (Ti^{2+} , V^{2+} , Cr^{3+} , Mn^{2+} and Fe^{3+}). A tremendous upsurge in the use of amine extractants has been witnessed over the past two decades. N-donor extractants are very useful in the formation of 6-coordinated nickel(II) complexes. Since nickel is known to form the most stable high-spin octahedral complex of all the base metals, the selection of N-donor extractants for the extraction of nickel(II) seems to be a fair decision. Equally, copper(II) forms stable complexes with N-donor ligands as well, and often result in 4-coordinate complex species, *i.e.*, tetrahedral or square-planar geometries.⁹¹

There has been a deliberate shift towards aromatic amine extractants because of their favourable properties when compared to their oxygen analogues.⁷⁵ Aliphatic amine extractants (R-NH_2 , where R = *n*-alkyl) tend to form complexes at relatively high pH values due to their high protonation constants which led to the hydrolysis of metal ions even under slightly acidic conditions. These aliphatic ligands—with only σ -donor character—show lack of metal ion selectivity. However, this can be improved once chelating ligands are implemented instead.⁷⁵ An example of this is the alkylated derivatives of ethylenediamine. Aromatic nitrogenous ligands, on the other hand, have excellent metal ion selectivity, possibly due to their dual σ - and π -bonding character. Moreover, these ligands can form complexes even in harsh acidic solutions due to their lower pK_a values.^{74,75}

1.7 Chelating ligands

1.7.1 The chelate effect

In the mid-twentieth century, Bjerrum⁹⁴ and Schwarzenbach⁹⁵ ushered in a bloom period of coordination chemistry with extensive studies of equilibria in solution. Of particular importance and relevance was the recognition and detailed description of the chelate effect.⁹⁶ The chelate effect, as defined by Schwarzenbach⁹⁶ is:

“the difference in stability (log equilibrium constant) of a chelate complex and the corresponding complex with simple ligands”.

In layman’s terms, the chelate effect generally implies that polydentate ligands (ligands with more than one donor atom) form thermodynamically more stable complexes than analogous complexes containing only monodentate ligands (ligands with only one donor atom). An example of this is portrayed in **Table 1.8**, where the formation constants of nickel(II) complexes with *n*-dentate polyamines are compared to analogous complexes with NH₃.

Table 1.8: The formation constants of polyamine nickel(II) complexes compared to analogous NH₃ complexes. [Data from Martell and Smith⁹⁷]

Polyamine	Denticity	log β_n (NH ₃)	log K ₁ (polyamine)
en ^a	2	5.08	7.47
dien ^b	3	6.85	10.7
trien ^c	4	8.12	14.4
tetren ^d	5	8.93	17.4
penten ^e	6	9.08	19.1

^a ethylenediamine; ^b diethylenetriamine; ^c triethylenetetramine; ^d tetraethylenepentamine; ^e pentaethylenhexamine

Schwarzenbach,⁹⁶ in explaining the chelate effect, endorsed the idea that once the first donor atom had attached itself to the metal ion, the second and subsequent donor atoms could not move freely around in solution, *i.e.*, it was restricted to a specific volume around the metal ion (**Figure 1.4**).⁸⁴ This volume was determined by the length of the chelating ligand. In effect, this meant the entropy (ΔS) of the second and subsequent donor atoms was significantly reduced as compared with an equal number of monodentate ligands.

This model, however, does have its shortcomings. It predicted that larger chelate rings (6-membered and larger) would exhibit lower complex stability compared to 5-membered chelate rings. This was theorised because of the longer bridge connecting the two donor atoms forcing the uncoordinated donor atom to move in a larger volume of sphere around the metal ion centre.⁸⁴ In general, this seems to be valid reasoning and logic, but does not agree with common observations entirely. This model predicts that the decrease in formation constants as chelate ring sizes are increased should be an entropic effect, but for 7-membered chelate rings and smaller, it seems to be predominantly an enthalpic (ΔH) effect instead.⁹⁸

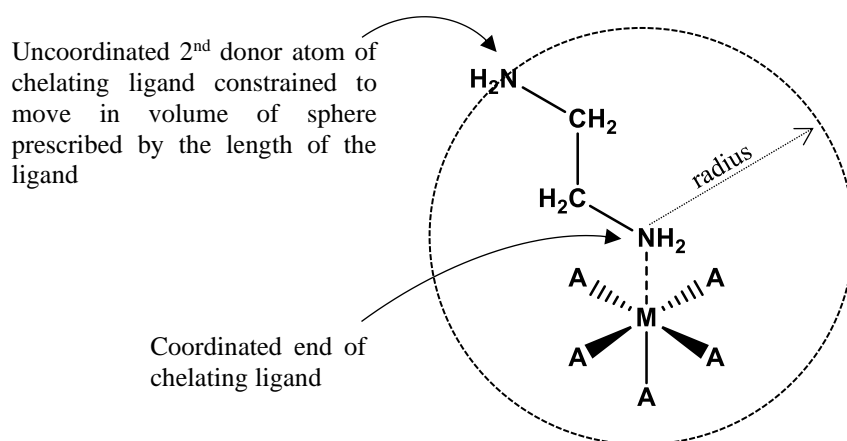


Figure 1.4: An illustration of Schwarzenbach’s model of the chelate effect. The chelating ligand, ethylenediamine, is constrained to move in a volume of sphere dictated by the length of the ethylene bridge connecting the two *N*-donor atoms. [Adapted from Martell and Hancock⁸⁴]

In contrast to the explanation of the chelate effect by Schwarzenbach,⁹⁶ was another proposed model. This model is commonly referred to as the “standard reference state model”.

1.7.2 The standard reference state and the chelate effect

In 1954, Adamson⁹⁹ noted that the units used for the concentration of the species involved in the formation constants were such that the formation constant, β_n , would have units of $l^n \text{ mol}^{-n}$, which was attributed the asymmetry of the standard reference state. This is as a result of the solvent being given an activity of unity, whereas all other species in the equilibrium are expressed as $\text{mol}\cdot\text{dm}^{-3}$.⁹⁹ This meant that monodentate and chelating ligands with equal number of donor atoms coordinated to the metal ion have different values of n , for β_n , with different units.⁹⁹ Therefore, the constants presented in **Table 1.8** are rendered erroneous. In fact, the chelate effect is actually reversed,⁹⁹ when instead of $\text{mol}\cdot\text{dm}^{-3}$, concentrations are expressed in $\text{mol}\cdot\text{cm}^{-3}$ with complexes of monodentate ligands seemingly more stable. Adamson⁹⁹ proposed that mole fractions should be used to express concentrations instead, which subsequently forces the formation constants to be dimensionless. Only now, true and valid comparisons in **Table 1.8** can be made. Adamson’s proposal resulted in the fact that, at low concentrations, the total number of moles present in the solution is effectively the molarity of pure water (55.5 M at 25 °C).⁹⁹ This was a major mathematical finding and effectually meant that each species in equilibrium can divide its molarity by 55.5 and obtain their individual mole fractions. Now, it was required that $n \cdot \log 55.5$ be added to all $\log \beta_n$ values to ensure their relatability.⁹⁹ This principally dealt with the chelate effect in a detailed mathematical way, something the Schwarzenbach model seemingly lacked.

Adamson’s proposal leads to the following equation,¹⁰⁰ for relating the formation constant of a polydentate chelating ligand to that of the analogous complex containing merely monodentate ligands:

$$\log K_1 (\text{polydentate}) = \log \beta_n (\text{monodentate}) + (n - 1) \log 55.5 \quad (37)$$

This equation predicts lower values for polyamine complexes than observed (**Table 1.9**). The main reason for this is that *N*-donor atoms of the polyamines are more basic ($pK_a = 10.6$) than the zero order nitrogen of ammonia ($pK_a = 9.2$).⁸⁴ This can be corrected by taking inductive effects into account. We can add an inductive effect factor of 1.152 ($10.6 \div 9.2$) to Eq. 37, to yield the following equation:⁸⁴

$$\log K_1 (\text{polyamine}) = 1.152 \cdot \log \beta_n (\text{NH}_3) + (n - 1) \log 55.5 \quad (38)$$

Finally, the calculated values of $\log K_1$ accord well with the observed values of $\log K_1$.

Table 1.9: A comparison of the observed formation constant, $\log K_1$, with the calculated formation constant derived from Eqs. 37 and 38. Eq. 37 only considers the asymmetry of the standard state, while Eq. 38 corrects for inductive effects as well. [Data from Martell and Smith⁹⁷]

Polyamine ^a	Denticity	$\log K_1$ calculated via Eq. 37	$\log K_1$ calculated via Eq. 38	Observed $\log K_1$
en	2	6.82	7.58	7.47
dien	3	10.33	11.37	10.96
trien	4	13.34	14.67	14.4
tetren	5	15.89	17.25	17.4
penten	6	17.78	19.16	19.1

^a Polyamine acronyms can be found below **Table 1.8**.

From the results in **Table 1.9**, we see that the formation constants of polyamine complexes are dependent on two thermodynamic contributors: (1) the entropy (ΔS) contribution from the asymmetry of the standard reference state, and (2) an enthalpy (ΔH) driven inductive effect contribution from the ethylene bridges of polyamine ligands.⁸⁴ At the core of Adamson's model is the suggestion that the chelate effect should mainly be considered as a strong entropic effect from (1), with a minor, yet vital, enthalpic contribution from (2).⁸⁴

One question still remains, however, and needs resolution: Which model, Adamson or Schwarzenbach's, describes the chelate effect more accurately? Adamson⁹⁹ and Schwarzenbach's⁹⁶ individual proposals on the origin of the chelate effect are, at their cores, very similar. The Schwarzenbach model sets the translational entropy of the second monodentate ligand close to zero by making it move in a limited spherical volume, while the Adamson model sets the translational entropy of the second monodentate ligand to exactly zero by making each reactant completely fill the space of the standard reference state once the constants are expressed as mole fractions.⁸⁴ This means that Adamson's model appears more accurate and reliable, since it doesn't make any assumptions regarding the ligand geometry or the length of the carbon bridge connecting the donor atoms.⁸⁴

1.8 Metal ion selectivity of *N*-donor ligands

It is known that smaller metal ions are more likely to form complexes with 6-membered chelate rings than 5-membered ones.⁸⁴ Conversely, 5-membered chelate rings preferentially coordinate to larger metal ions. This, by far, is one of the most powerful ligand design tools and can be used to extract specific metal ions. Metal ion sizes, in terms of the ionic radius (r^+), can be categorised as follows: $r^+ \geq 1.2 \text{ \AA}$ (very large), $1.2 > r^+ > 1.0 \text{ \AA}$ (large), $1.0 > r^+ > 0.8 \text{ \AA}$ (medium), $0.8 > r^+ > 0.7 \text{ \AA}$ (medium-small), $0.7 > r^+ > 0.5 \text{ \AA}$ (small) and $r^+ < 0.5 \text{ \AA}$ (very small).¹⁰¹

1.8.1 The chelate ring geometry and preferred metal ion sizes

It is quite easily understood why 5-membered chelate rings form more stable complexes with larger metal ions, while 6-membered chelate rings predominantly form stable complexes with smaller metal ions, when the relatively low-strain form of cyclohexane is utilised as a model backbone.^{102,103} Cyclohexane in its chair conformation exhibits the minimum strain possible (**Figure 1.5**). The torsion angles are 60° and the C–C–C bond angles are all 109.5° .

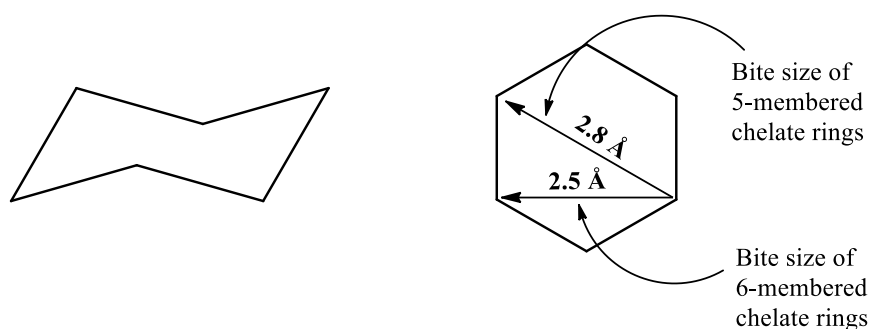


Figure 1.5: Cyclohexane in its chair conformation. Bite sizes of 5- and 6-membered chelate rings are also shown. [Adapted from Martell and Hancock⁸⁴]

The 6-membered chelate ring of 1,3-diaminopropane containing two *N*-donor atoms and a metal ion in place of three carbon atoms of cyclohexane will also exhibit very low strain energy.⁸⁴ This is obviously pre-conditional to the metal ion having roughly the same size and geometry as a sp^3 hybridised carbon atom. The ideal metal ion for coordination to 1,3-diaminopropane has a N–M–N bond angle of 109.5° , and a short M–N bond length of 1.6 \AA (**Figure 1.6a**).⁸⁴ This conformation is better suited to smaller metal ions.

The ideal metal ion size for a 5-membered chelate ring can also be derived by considering the aforementioned cyclohexane ring. One can envisage a minimally strained ethylenediamine ring by removing two adjacent carbon atoms and converting the next two *N*-donor atoms. The two lone pairs on the nitrogen atoms are extrapolated to focus them $\sim 2.5 \text{ \AA}$ away from the metal ion. This was necessary to ensure the lone pairs are in the same plane.⁸⁴ This simple pictorial diagram (**Figure 1.6b**) illustrates the M–N bond lengths at 2.5 \AA and the N–M–N bond angles at 69° , when ethylenediamine is in its least-strained conformation.⁸⁴ Because of these specific dimensions, this conformation is better suited to larger metal ions.

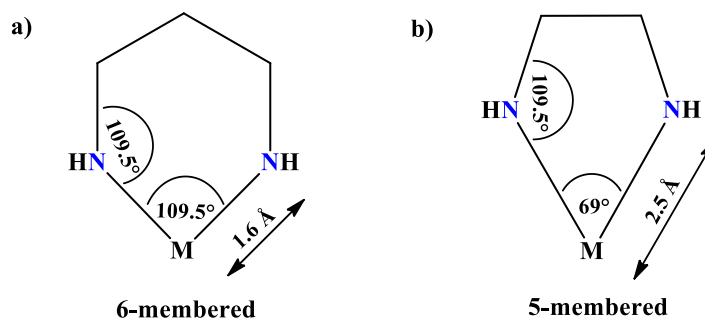


Figure 1.6: The idealised bond lengths and angles of **a)** 6-membered (1,3-diaminopropane) and **b)** 5-membered (ethylenediamine) chelate rings. [Adapted from Martell and Hancock⁸⁴]

The relation of complex stability to chelate ring sizes is readily understood in terms of the best-fit size of the metal ion for complexing with 5- and 6-membered chelate rings. In particular, smaller metal ions tend to have lower coordination numbers, and also, as the M–N bond lengths become smaller, the N–M–N bond angles become larger.⁸⁴

When the *N*-donor atoms are replaced with *O*-donor atoms, the 6-membered chelate ring's O–M–O bond angle becomes 95°, while the C–O–M bond angle becomes 126°. Moreover, the M–O bond length stretches to 1.9 Å (**Figure 1.7a**).¹⁰⁴ The 5-membered chelate ring's O–M–O bond angle becomes 58°, while the C–O–M bond angle remains 126°. The M–O bond length stretches to more than 3.2 Å (**Figure 1.7b**).¹⁰⁴

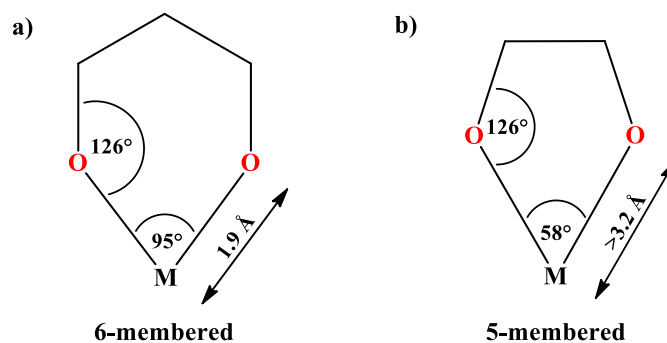


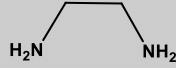
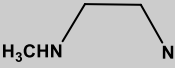
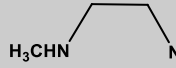
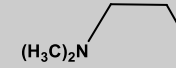
Figure 1.7: The idealised bond lengths and angles of **a)** 6-membered (1,3-propanediol) and **b)** 5-membered (1,2-ethanediol) chelate rings. [Adapted from Martell and Hancock⁸⁴]

From **Figures 1.6** and **1.7**, it is clear there are large differences in bond lengths and angles of the nitrogen and oxygen chelate rings. These differences can largely be attributed to neutral *N*-donor atoms forming tetrahedral geometries, while neutral *O*-donor atoms form trigonal planar geometries.⁸⁴

1.9 Steric- and inductive effects in *N*-donor chelating ligands


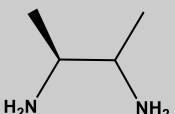
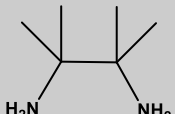
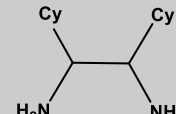
Two of the most important structural factors in chelate formation are steric- and inductive effects. The tendency of donor strength increases along the following series: $\text{NH}_3 < \text{NH}_2\text{CH}_3 < \text{NH}(\text{CH}_3)_2 < \text{N}(\text{CH}_3)_3$, but also increases the possibility of steric hindrance.⁸⁴ The inductive effects are often overshadowed by the steric hindrance of large alkyl moieties. Therefore, inductive effects are often ignored or overlooked, and when they do manifest themselves, they are misunderstood and attributed to “other effects”.⁸⁴ These inductive effects have consequently been termed as “hidden inductive effects”.¹⁰⁵ An example of inductive effects outweighing steric effects is shown in **Table 1.10**, where ethylenediamine was synthetically altered to contain various *N*-methyl substituents.

Table 1.10: Examples of steric effects outweighing inductive effects by systematically methylating the *N*-donor atoms of ethylenediamine. [Data from Martell and Smith⁹⁷]

$\log K_1 [\text{M}^{2+}]$				
$\log K_1 [\text{Cu}^{2+}]$	10.48	10.33	10.02	7.20
$\log K_1 [\text{Ni}^{2+}]$	7.35	7.17	6.89	3.57
$\log K_1 [\text{Cd}^{2+}]$	5.4	5.47	5.20	3.87

It appears from literature⁹⁷ that *N*-alkyl substitution in general leads to a decrease in complex stability, but several examples of *N*-donor ligands with adjacent carbon substitution where the inductive effect dominates, exist too (**Table 1.11**).

Table 1.11: Examples of inductive effects outweighing steric effects in *N*-alkyl ligands. [Data from Martell and Smith⁹⁷]

$\log K_1$ and $\log \beta_2$ [M^{2+}]				
$\log K_1 [\text{Cu}^{2+}]$	10.48	11.27	11.63	12.20
$\log \beta_2 [\text{Ni}^{2+}]$	13.54	14.01	14.56	14.90

Observations for monodentate amines follow this exact pattern of behaviour as well, where methyl substitution on the adjacent carbon is found to produce less serious effects than *N*-methyl substitution, *i.e.*, inductive effects can be observed with little or no impact by steric effects.¹⁰⁶ In essence, this seems to indicate that the addition of alkylating moieties may not be restricting access to the metal once it is accurately bound to adjacent carbon atoms. Generally speaking, the basicity of *N*-donor atoms increases with an increase in alkyl substitution: primary (1°) < secondary (2°) < tertiary (3°) < quaternary (4°). This is due to alkyl moieties pushing electron

density (inductive effect) onto the *N*-donor atoms. Quaternary carbons exhibit a greater inductive effect than tertiary and subsequent substituted carbons.

1.10 Factors to consider in ligand design: A concise summary

After considerable elaboration of the various factors that might influence a ligand's selectivity towards certain metal ions (Sections 1.5–1.8), we thought it useful to briefly list the factors that need to be considered when designing novel ligands for the separation of base metal ions:

- (1) The hard/soft character of both the metal ion and the relevant donor atoms. From the hard and soft acids and bases (HSAB) theory proposed by Pearson,¹² we know that soft metal ions [for example Ag(I)] prefer to form complexes with ligands containing soft donor atoms (less electronegative) such as iodide. Hard metal ions [for example In(III)] prefer to form complexes with harder (more electronegative) donor atoms such as fluoride. “Borderline” metal ions show no real preference for either hard or soft donor atoms.
- (2) The size of the metal ion (metal ion radius, r^+). A metal ion's radius that matches the bite size of an appropriate chelating ligand will have increased thermodynamic odds of forming a stable complex.
- (3) The size of the chelate ring [complimentary to (2)]. 5-Membered chelate rings preferentially form complexes with larger metal ions, while 6-membered chelate rings preferentially coordinate to smaller metal ions.
- (4) The coordination number and geometry of the metal ion of interest. Some metal ions, for example, prefer tetrahedral geometry as opposed to octahedral geometry because of the valence electrons present in specific orbitals. Metal ions and donor atoms can only form complexes when both their outer shell orbitals overlap correctly.
- (5) The denticity of the donor atoms. This is somewhat akin to (3) and (4), where the correct geometry and number of the donor atoms seriously need to be considered before a ligand is used for metal ion coordination. Both Schwarzenbach⁹⁶ and Adamson⁹⁹ showed that polydentate ligands form thermodynamically more stable complexes compared to analogous monodentate ligands.
- (6) The inductive- and steric effects. Alkyl moieties—or any electron donating moiety for that matter—bound to carbon atoms adjacent to the donor atoms can increase the electron density on the donor atoms and thereby strengthening the metal-donor atom bond. One should, however, be somewhat cautious to build too much steric bulk on the donor atoms themselves. We do know that they add positive inductive effects, but this is often overshadowed by “hidden” steric effects.
- (7) For the purposes of solvent extraction studies, one should be mindful of adding elaborate and exotic electron donating moieties to a ligand backbone, since they are often quite polar in nature and would render the overall ligand increasingly hydrophilic as well. This must be minimised at all cost to ensure the final complex species is solely soluble in the organic phase and does not bleed into the aqueous phase, thereby defeating the purpose of solvent extraction studies altogether.

1.11 Literary background on pyrazole- and imidazole-pyridinyl ligands

The solvent extraction of base metal ions by means of pyrazole- and imidazole-pyridinyl ligands are of great interest, since we know that complexes with these ligands, according to literature, are readily formed. Aromatic nitrogenous ligands show relative preference for metal ions because of their σ -donor and π -acceptor abilities. Imidazole extractants also show high formation constants with later 3d transition metal ions resulting in high extraction efficiencies.⁹¹ These extractants can also coordinate with metal ions in slightly acidic media due to their mild pK_a values (**Figure 1.8**).¹⁰⁷ Pyridine derivatives have low protonation constants and are known to interact strongly with metal ions in strongly acidic media.⁹¹ This very fact can work against it in an industrial setting due to the difficulty involved in recovering the metals. Pyrazole derivatives have lower protonation constants and should be combined, either with pyridinyl- or imidazolyl moieties for enhanced extractions.⁹¹

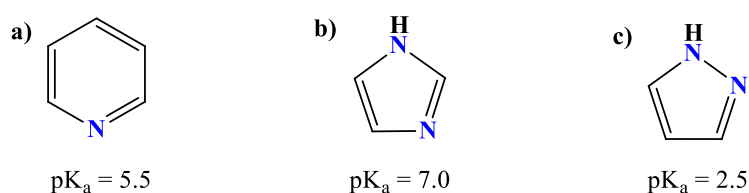


Figure 1.8: Chemical structures and pK_a values of **a)** pyridine, **b)** imidazole and **c)** pyrazole.

1.11.1 Relevant literature on various pyrazole- and imidazole-pyridinyl ligands

Gerber *et al.*¹⁰⁸ reported the use of 2-(2'-pyridyl)imidazole (pimH) in the synthesis of the rhenium(III) salt, $[\text{ReCl}_2(\text{pimH})(\text{PPh}_3)_2](\text{ReO}_4)$, and 2-(2'-pyridyl)-1-methylimidazole (pimMe) in the synthesis of the rhenium(III) complex, $[\text{ReCl}_3(\text{pimMe})(\text{PPh}_3)]$. The monooxorhenium(V) complexes $[\text{ReOCl}_3(\text{pimR})]$ (where $R = \text{H}$ or Me) were also reported. All of the complexes were characterised by X-ray crystallography, ^1H NMR and IR spectroscopy.

Okewole *et al.*¹⁰⁹ investigated 1-octyl-2-(2'-pyridyl)imidazole (OPIM), along with dinonylnaphthalene sulfonic acid (DNNSA), as a potential extractant of nickel(II). They attempted this from a mixture of base metals in a solvent extraction system which included 2-octanol and Shellsol 2325 as diluent and modifier, respectively. They were successful in the separation of nickel(II) from the various base metals at pH 0.5–3.5 (sulfate media). The interesting fact about this study was that the extraction of nickel(II) was extremely poor without the use of DNNSA. Upon addition of DNNSA, extraction of nickel(II) increased substantially.

Watson *et al.*,¹¹⁰ on the other hand, studied chiral nitrogenous heterocyclic ligands. They focused on the synthesis of 2,6-bis(pyrazol-1-ylmethyl)pyridine metal complexes and their chiral derivatives. They managed to prepare complexes with multiple divalent transition metal ions, such as iron(II), nickel(II), copper(II), ruthenium(II) and palladium(II).

Satake and Nakata¹¹¹ synthesised novel cationic η^3 -allylpalladium-pyridinylpyrazole complexes from 3-alkyl-5-(2-pyridinyl)pyrazole and a η^3 -allylpalladium chloride dimer in the presence of AgBF_4 . They converted

cationic complexes into neutral complexes under basic conditions. These complexes were characterised via ^1H , ^{13}C and ^{15}N NMR studies. Comparisons of both cationic and neutral complexes were discussed, while the reaction mechanism of cyclopropanation were investigated as well.

Pearce *et al.*¹¹² published an article with regards to bidentate pyrazole-pyridinyl ligands for the selective extraction of nickel(II) and copper(II). These ligands exhibited remarkable copper(II) selectivity, even in the absence of a synergist, but delivered somewhat underwhelming nickel(II) and copper(II) recovery results. Pearce *et al.*¹¹³ published another peer-reviewed article indicating the nickel(II) extractive ability of bidentate imidazolyl and methylpyrazolyl ligands. These ligands performed well in the presence of the synergist, sodium dodecylbenzenesulfonate (SDBS). This work pointed towards possible intermolecular interactions in the outer-coordination sphere.

1.11.2 Relevant literature on tridentate pyrazole- and imidazole-pyridinyl ligands as utilised in solvent extraction systems

The synthesis of tridentate pyrazole- and imidazole-pyridinyl ligands is by no means a novel concept. Many literature sources report the use of these ligands for various purposes, such as spin-crossover materials,¹¹⁴ macrocyclic precursors¹¹⁵ and catalysts,^{116–120} but very few ever demonstrate their usefulness as selective metal ion extractants. This opened a proverbial window of opportunity to exploit their unique properties in a solvent extraction environment. To the best of our knowledge, only two literary sources reported the implementation of a tridentate pyrazole-pyridinyl ligand in the extraction of base metal ions.

Zhou and Pesic¹²¹ illustrated that 2,6-bis(5-nonyl-1*H*-pyrazol-3-yl)pyridine was an excellent cobalt(II) and nickel(II) extractant in the presence of dinonylnaphthalene sulfonic acid (DNNSA). Roebuck *et al.*¹²² continued this train of thought and used the same nonyl-substituted tridentate ligand in a renewed attempt to extract iron(II), cobalt(II) and nickel(II) efficaciously, with Kermac 470B as diluent. Both sources reported excellent extraction ($\%E > 90\%$) and indicated that various base metal ions can selectively be extracted once the pH was finely tuned. These two sources were of tremendous help during this dissertation and was, at least in part, an inspiring force behind this dissertation.

1.12 Problem statement

There are several oxime-type reagents for the selective extraction of copper(II). For zinc(II), DE2HPA is selective and CYANEX[®] 272 has proved to be valuable in the separation of cobalt(II) over nickel(II). There are no unique extractants for the selective separation of nickel(II) from other base metal ions. This dissertation endeavours to develop such an extractant.

1.13 Aim of this dissertation

The core aim of this study was the selective extraction of six base metal ions (Co^{2+} , Ni^{2+} , Cu^{2+} , Zn^{2+} , Cd^{2+} and Pb^{2+}) by means of a series of pyrazole- and imidazole-pyridinyl ligands. These ligands were: 2,6-bis(5-methyl-1*H*-pyrazol-3-yl)pyridine (**1**), 2,6-bis(5-ethyl-1*H*-pyrazol-3-yl)pyridine (**2**), 2,6-bis(5-propyl-1*H*-pyrazol-3-yl)pyridine (**3**), 2,6-bis(5-butyl-1*H*-pyrazol-3-yl)pyridine (**4**), 2,6-bis(5-pentyl-1*H*-pyrazol-3-yl)pyridine (**5**), 2,6-bis(5-hexyl-1*H*-pyrazol-3-yl)pyridine (**6**), 2,6-bis(5-heptyl-1*H*-pyrazol-3-yl)pyridine (**7**), 2,6-bis(5-octyl-1*H*-pyrazol-3-yl)pyridine (**8**), 2,6-bis(5-(*tert*-butyl)-1*H*-pyrazol-3-yl)pyridine (**9**), 2,6-bis(5-phenyl-1*H*-pyrazol-3-yl)pyridine (**10**), 2,6-bis(1-butylimidazol-2-yl)pyridine (**11**) and 2,6-bis(1-octylimidazol-2-yl)pyridine (**12**).

1.12.1 Minor expounded objectives

Besides the abovementioned core objective, twelve other sub-objectives are listed below:

- (1) Synthesise and fully characterise pyrazolyl ligands **1–12**. These ligands are separated into two groups: pyrazolyl ligands (**1–10**) and imidazolyl ligands (**11** and **12**). Characterisation techniques such as ^1H and ^{13}C nuclear magnetic resonance (NMR), infrared (IR) spectroscopy, mass spectrometry (MS), elemental analyses (EA) and melting point (mp) analyses were utilised to verify the chemical/molecular structures of all ligands.
- (2) Perform competitive extraction studies by using ligands **1–12** as extractants. This was done as a concoction of the aforementioned six base metal ions (nitrate source) in an equimolar ratio at pH ~5.
- (3) Redo competitive extraction studies in the exact manner as objective (2), only this time in the absence of copper(II). We anticipate that copper(II) might be highly extractable and therefore exclude it in this objective to ascertain the second- and third-most extractable species in solution. Conditions remain constant.
- (4) Execute selectivity studies to probe whether our ligands are selective towards copper(II), even at a concentration ten- and hundredfold less than the remaining five base metal ions' concentration. This experiment, at its core, is another competitive extraction study, yet it delivers additional insight regarding the true selectivity of the ligands.
- (5) Study the nickel(II) and copper(II) recovery ability from ligands **1–12**. This is usually done under extreme acidic conditions ($\text{pH} \leq 1$) and is an important step in the global hydrometallurgical process.
- (6) Perform time-dependent studies of nickel(II) and copper(II) extractions to ensure that metal ion extraction equilibria is reached well within the 24-hour time frame. Only a selection of pyrazolyl ligands (**2**, **5** and **7**) and imidazolyl ligands (**11** and **12**) were used in order to minimise the use of valuable synthesised ligands. This is a critical experiment that is often overlooked in peer-reviewed studies.
- (7) Perform extensive pH isotherm studies to determine the optimum pH at which certain ligands extract nickel(II) and copper(II).

- (8) Determine the ligand-to-metal ($L:M^{2+}$) ratio by means of Job's method. It was decided to perform these experiments via UV/Vis spectroscopy instead of ICP-OES analyses.
- (9) To complement objective (8) above, cobalt(II), nickel(II) and copper(II) slope analyses were performed via ICP-OES as well. Only pyrazolyl ligands **5** and **7** were selected, since these experiments required many grams of extractant—a luxury we certainly did not have.
- (10) Study the synergistic interaction of pyrazolyl ligands **6–8** and imidazolyl ligands **11** and **12** in the presence of dodecylbenzenesulfonic acid (DBSA) as synergist. The optimum synergist concentration will first be determined, however. A proposed extraction mechanism will also briefly be discussed.
- (11) Grow crystals of various base metal ion complexes for single crystal X-ray diffraction analyses. Crystal structures yield valuable information regarding bond lengths, bond angles, coordination number and geometry. Moreover, such an investigation might provide insights with regard to inner- and outer-sphere interactions as well (both inter- and intra-molecular interactions).
- (12) Examine the nickel(II) extractive ability of aromatic oxime-type extractants (ligands **13** and **14**) and bidentate pyrazolyl extractants (ligands **15** and **16**) in the presence of sulfonic-, carboxylic- and phosphinic acid synergists. Crystals of these unique assemblies are also to be grown and analysed via single crystal X-ray diffraction.

Objective (1) is dealt with in **CHAPTER 2**, while objectives (2–10) are discussed in **CHAPTER 3**. Objectives (11) and (12) are covered in **CHAPTERS 4** and **5**, respectively. Finally, overall conclusions, future work and final remarks are reported in **CHAPTER 6**.

1.14 References

- (1) Habashi, F. *A Textbook of Hydrometallurgy*, 2nd Edition; Sainte-Foy: Métallurgie Extractive Quebec, 1999.
- (2) Gupta, C.; Mukherjee, T. *Hydrometallurgy in Extraction Processes*, Vol. 1.; CRC Press: Boca Raton, Florida, 1990.
- (3) Walton, R. Zinc cementation. In *Advances in Gold Ore Processing*; Adams, M., Wills, B., Eds.; Elsevier, 2005; Vol. 15, p 589.
- (4) Habashi, F. One hundred years of cyanidation. *CIM Bull.* **1987**, *80*, 108.
- (5) Habashi, F. A short history of hydrometallurgy. *Hydrometallurgy* **2005**, *79* (1), 15.
- (6) Habashi, F. Bayer's process for alumina production: A historical perspective. *Bull. Hist. Chem.* **1995**, *17/18*, 15.
- (7) Peligot, E. Recherches sur l'uranium. *Ann. Chim. Phys.* **1842**, *5*, 7.

- (8) Rothe, J. New procedure for the separation of iron from other elements. *Chem. News* **1892**, 66, 182.
- (9) Pomeranz, C. Sur les bergaptène. *Bull. Soc. Chim. Fr.* **1892**, 7, 171.
- (10) Langmuir, A. The determination of sulphur in bitumens. *J. Am. Chem. Soc.* **1900**, 22 (2), 99.
- (11) Berthelot, M.; Jungfleisch, E. Sur les lois qui président au partage d'un corps entre deux dissolvants. *Ann. Chim.* **1872**, 26, 396.
- (12) Nernst, W. Verteilung eines stoffes zwischen zwei lösungsmitteln und zwischen lösungsmittel und dampfraum. *Zeitschrift für Phys. Chemie* **1891**, 8 (1), 110–139.
- (13) Sangster, D. Geology. In *Encyclopedia of Life Support Systems*; De Vivo, B., Grasemann, B., Stüwe, K., Eds.; Eolss Publishers: Paris, France, 2009; p 91.
- (14) Pearson, R. Hard and soft acids and bases. *J. Am. Chem. Soc.* **1963**, 85 (22), 3533.
- (15) Critical Materials Strategy - Summary. U.S. Department of Energy 2011.
- (16) Mineral Commodities Summaries. U.S. Geological Survey 2018, p 200.
- (17) Huang, Y.; Zhang, Z.; Cao, Y.; Han, G.; Peng, W.; Zhu, X.; Zhang, T.; Dou, Z. Overview of cobalt resources and comprehensive analysis of cobalt recovery from zinc plant purification residue - A review. *Hydrometallurgy* **2020**, 193, 105327.
- (18) Banza Lubaba Nkulu, C.; Casas, L.; Haufroid, V.; De Putter, T.; Saenen, N.; Kayembe-Kitenge, T.; Musa Obadia, P.; Kyanika Wa Mukoma, D.; Lunda Ilunga, J.; Nawrot, T.; *et al.* Sustainability of artisanal mining of cobalt in DR Congo. *Nat. Sustain.* **2018**, 1 (9), 495.
- (19) Smith, C. Always the bridesmaid, never the bride: Cobalt geology and resources. *Trans. Institutions Min. Metall. Sect. B Appl. Earth Sci.* **2001**, 110 (MAY/AUG.), B75.
- (20) Liu, Q.; Sha, J.; Yan, J.; Zhou, P. Study on risk assessment and management of cobalt resource supply in China. *China Min. Mag.* **2018**, 1, 50.
- (21) Mineral Commodity Summaries. U.S. Geological Survey 2019, p 200.
- (22) Mudd, G. Global trends and environmental issues in nickel mining: Sulfides versus laterites. *Ore Geol. Rev.* **2010**, 38 (1), 9.
- (23) Kim, B. Effect of carbon on the coefficient of thermal expansion of as-cast Fe-30wt.%Ni-12.5wt.%Co-XC invar alloys. *Metals and Materials International.* 2002, p 247.
- (24) Miller, D.; Fahnestock, L.; Eatherton, M. Development and experimental validation of a nickel-titanium shape memory alloy self-centering buckling-restrained brace. *Eng. Struct.* **2012**, 40, 288.

- (25) Furrer, D.; Fecht, H. Ni-based superalloys for turbine discs. *JOM* **1999**, *51* (1), 14.
- (26) Parsons, D. The environmental impact of disposable versus re-chargeable batteries for consumer use. *Int. J. Life Cycle Assess.* **2006**, *12* (3), 197.
- (27) Akiyama, M.; Oki, Y.; Nagai, M. Steam reforming of ethanol over carburized alkali-doped nickel on zirconia and various supports for hydrogen production. *Catal. Today* **2012**, *181* (1), 4.
- (28) Burkin, A. *Extractive Metallurgy of Nickel*; Vol. 17.; Published on behalf of the Society of Chemical Industry by Wiley: Chichester; New York, 1987.
- (29) Ozberk, E.; Davenport, W.; Gibson, N. Future of nickel industry in Canada. *CIM Bull.* **1983**, *76* (857), 99.
- (30) Conry, R. Copper: Inorganic & Coordination Chemistry Based in Part on the Article Copper: Inorganic & Coordination Chemistry by Rebecca R. & Kenneth D. which appeared in the Encyclopedia of Inorganic Chemistry, 1st Edition. *Encyclopedia of Inorganic Chemistry*. September 7, 2005.
- (31) Pietrzyk, S.; Tora, B. Trends in global copper mining – A review. *IOP Conf. Ser. Mater. Sci. Eng.* **2018**, *427*, 12002.
- (32) Pietrzyk, S.; Tora, B. Processing of non-ferrous metals secondary raw materials in Poland - trends, opportunities and threats. *Inz. Miner.* **2017**, *2017* (2), 81.
- (33) Wieniewski, A.; Myczkowski, Z. Achievements and participation in development of mineral processing and waste utilization by institute of non-ferrous metals in Gliwice. *Inz. Miner.* **2017**, *2017* (2), 15.
- (34) Crundwell, F.; Moats, M.; Ramachandran, V.; Robinson, T.; Davenport, W. *Extractive Metallurgy of Nickel, Cobalt and Platinum Group Metals*, 1st Edition; Elsevier: Oxford, 2011.
- (35) Botelho Junior, A.; Dreisinger, D.; Espinosa, D. A review of nickel, copper, and cobalt recovery by chelating ion exchange resins from mining processes and mining tailings. *Mining, Metall. Explor.* **2019**, *36* (1), 199.
- (36) Jorjani, E.; Ghahreman, A. Challenges with elemental sulfur removal during the leaching of copper and zinc sulfides, and from the residues: A review. *Hydrometallurgy* **2017**, *171*, 333.
- (37) Lane, D.; Cook, N.; Grano, S.; Ehrig, K. Selective leaching of penalty elements from copper concentrates: A review. *Miner. Eng.* **2016**, *98*, 110.
- (38) Lundström, M.; Liipo, J.; Taskinen, P.; Aromaa, J. Copper precipitation during leaching of various copper sulfide concentrates with cupric chloride in acidic solutions. *Hydrometallurgy* **2016**, *166*, 136.

- (39) Lu, J.; Dreisinger, D. Copper chloride leaching from chalcopyrite and bornite concentrates containing high levels of impurities and minor elements. *Hydrometallurgy* **2013**, *138*, 40.
- (40) Lu, J.; Dreisinger, D. Copper leaching from chalcopyrite concentrate in Cu(II)/Fe(III) chloride system. *Miner. Eng.* **2013**, *45*, 185.
- (41) Fomchenko, N.; Muravyov, M. Two-step biohydrometallurgical technology for modernization of processing of sulfidic copper-zinc products. *Hydrometallurgy* **2017**, *174*, 116.
- (42) Liu, Z.; Ng, Y.; Tiong, P.; Abu Talip, R.; Jasin, N.; Jong, V.; Tay, M. Five-coordinate zinc(II) complex: Synthesis, characterization, molecular structure, and antibacterial activities of bis-[(*E*)-2-hydroxy-*N'*-{1-(4-methoxyphenyl)ethylidene}benzohydrazido]dimethylsulfoxidezinc(II) complex. *Int. J. Inorg. Chem.* **2017**, *2017*, 7520640.
- (43) Franks, M.; Gadzhieva, A.; Ghandhi, L.; Murrell, D.; Blake, A.; Davies, E.; Lewis, W.; Moro, F.; McMaster, J.; Schröder, M. Five coordinate M(II)-diphenolate [M = Zn(II), Ni(II), and Cu(II)] Schiff base complexes exhibiting metal- and ligand-based redox chemistry. *Inorg. Chem.* **2013**, *52* (2), 660.
- (44) Szlyk, E.; Wojtczak, A.; Surdykowski, A.; Goździkiewicz, M. Five-coordinate zinc(II) complexes with optically active Schiff bases derived from (1*R*,2*R*)-(-)-cyclohexanediamine: X-ray structure and CP MAS NMR characterization of [cyclohexylenebis(5-chlorosalicylideneiminato)zinc(II) pyridine] and [cyclohexylenebis(5-bromosalicylideneiminato)zinc(II)pyridine]. *Inorg. Chim. Acta* **2005**, *358* (3), 467.
- (45) Newman, J.; Bear, C.; Hambley, T.; Freeman, H. Structure of bis(glycinato)zinc(II) monohydrate, a five-coordinate zinc(II) complex. *Acta Crystallogr. Sect. C* **1990**, *46* (1), 44.
- (46) Song, X.; Gao, X.; Liu, H.; Chen, H.; Chen, C. Synthesis and characterization of a supramolecular assembly based on a pyridyl-functionalized [FeFe]-hydrogenase mimic and zinc tetraphenylporphyrin. *Inorg. Chem. Commun.* **2016**, *70*, 1.
- (47) Che, W.; Yu, T.; Jin, D.; Ren, X.; Zhu, D.; Su, Z.; Bryce, M. A simple oxazoline as fluorescent sensor for Zn²⁺ in aqueous media. *Inorg. Chem. Commun.* **2016**, *69*, 89.
- (48) Kołodziejczak-Radzimska, A.; Jesionowski, T. Zinc oxide—from synthesis to application: A review. *Materials (Basel)*. **2014**, *7* (4), 2833.
- (49) Abkhoshk, E.; Jorjani, E.; Al-Harashsheh, M.; Rashchi, F.; Naazeri, M. Review of the hydrometallurgical processing of non-sulfide zinc ores. *Hydrometallurgy* **2014**, *149*, 153.
- (50) Gordon, R.; Graedel, T.; Bertram, M.; Fuse, K.; Lifset, R.; Rechberger, H.; Spataro, S. The characterization of technological zinc cycles. *Resour. Conserv. Recycl.* **2003**, *39* (2), 107.

- (51) Gilg, H.; Boni, M.; Hochleitner, R.; Struck, U. Stable isotope geochemistry of carbonate minerals in supergene oxidation zones of Zn–Pb deposits. *Ore Geol. Rev.* **2008**, *33* (2), 117.
- (52) Balarini, J.; Polli, L.; Miranda, T.; Castro, R.; Salum, A. Importance of roasted sulphide concentrates characterization in the hydrometallurgical extraction of zinc. *Miner. Eng.* **2008**, *21* (1), 100–110.
- (53) *Base Metals Handbook*, 3rd Edition; Thompson, M., Ed.; Woodhead Publishing: Cambridge, England, 2006.
- (54) Large, D. The geology of non-sulphide zinc deposits - An overview. *Erzmetall J. Explor. Min. Metall.* **2001**, *54* (5), 264.
- (55) Boni, M.; Coppola, V.; Deiongho, L.; Fedele, L. Willemite in the Belgian non-sulfide zinc deposits: A fluid inclusion study. *Period. di Mineral.* **2005**, *74* (1), 87.
- (56) Hitzman, M.; Reynolds, N.; Sangster, D.; Allen, C.; Carman, C. Classification, genesis, and exploration guides for nonsulfide zinc deposits. *Econ. Geol.* **2003**, *98* (4), 685.
- (57) Fleischer, M.; Sarofim, A.; Fassett, D.; Hammond, P.; Shacklette, H.; Nisbet, I.; Epstein, S. Environmental impact of cadmium: A review by the panel on hazardous trace substances. *Environ. Health Perspect.* **1974**, *7*, 253.
- (58) Borsari, M. Cadmium: Coordination chemistry. *Encyclopedia of Inorganic and Bioinorganic Chemistry*. September 15, 2014, p 1.
- (59) Sadegh Safarzadeh, M.; Bafghi, M.; Moradkhani, D.; Ojaghi Ilkhchi, M. A review on hydrometallurgical extraction and recovery of cadmium from various resources. *Miner. Eng.* **2007**, *20* (3), 211.
- (60) Cotton, A.; Wilkinson, G. *Advanced Inorganic Chemistry - A Comprehensive Text*, 3rd Edition; Interscience Publishers: New York, 1972.
- (61) Abundance of elements in the earth's crust and in the sea. In *Handbook of Chemistry and Physics*; Haynes, W., Ed.; CRC Press, 2016; p 2670.
- (62) Zhang, W.; Yang, J.; Wu, X.; Hu, Y.; Yu, W.; Wang, J.; Dong, J.; Li, M.; Liang, S.; Hu, J.; *et al.* A critical review on secondary lead recycling technology and its prospect. *Renew. Sustain. Energy Rev.* **2016**, *61*, 108.
- (63) Ellis, T.; Mirza, A. The refining of secondary lead for use in advanced lead-acid batteries. *J. Power Sources* **2010**, *195* (14), 4525.
- (64) Wilson, A.; Bailey, P.; Tasker, P.; Turkington, J.; Grant, R.; Love, J. Solvent extraction: The coordination chemistry behind extractive metallurgy. *Chem. Soc. Rev.* **2014**, *43* (1), 123.

- (65) Gupta, C.; Mukherjee, T. *Hydrometallurgy in Extraction Processes*, Vol. 2.; CRC Press: Boca Raton, Florida, 1990.
- (66) Sekine, T.; Hasegawa, Y. *Solvent Extraction Chemistry: Fundamentals and Applications*; M. Dekker: New York, 1977.
- (67) Rydberg, J. *Solvent Extraction Principles and Practice*, 2nd Edition; Taylor & Francis Group, LLC: New York, 2004.
- (68) De, A.; Khopkar, S.; Chalmers, R. *Solvent Extraction of Metals*; Van Nostrand Reinhold Company: London, 1970.
- (69) Aguilar, M.; Cortina, J. *Solvent Extraction and Liquid Membranes: Fundamentals and Applications in New Materials*, 1st Edition; CRC Press: Boca Raton, Florida, 2008.
- (70) Van Hare, G. Precipitation of metal powder, especially copper, US Patent 2813020, 12 November 1957.
- (71) Schaufelberger, F. Separation of nickel and cobalt metal from acidic solution, US Patent 2694005, 9 November 1954.
- (72) Van Hare, G.; Montgomery, R. Precipitating metals in metallic form from ammoniacal ammonium salt solutions, US Patent 2733990, 7 February 1956.
- (73) Schaufelberger, F.; Roy, T. Separation of copper, nickel, and cobalt by selective reduction from aqueous solution. *Bull. - Inst. Min. Metall.* **1955**, *581*, 375.
- (74) Okewole, A.; Antunes, E.; Nyokong, T.; Tshentu, Z. The development of novel nickel selective amine extractants: 2,20'-Pyridylimidazole functionalised chelating resin. *Miner. Eng.* **2013**, *54*.
- (75) Du Preez, J. Recent advances in amines as separating agents for metal ions. *Solvent Extr. Ion Exch.* **2000**, *18* (4), 679.
- (76) Bates, G.; Davidson, J.; Forgan, R.; Gale, P.; Henderson, D.; King, M.; Light, M.; Moore, S.; Tasker, P.; Tong, C. A dual host approach to NiSO₄ extraction. *Supramol. Chem.* **2012**, *24* (2), 117.
- (77) Tasker, P.; Tong, C.; Westra, A. Co-extraction of cations and anions in base metal recovery. *Coord. Chem. Rev.* **2007**, *251* (13), 1868.
- (78) Galbraith, S.; Tasker, P. Review: The design of ligands for the transport of metal salts in extractive metallurgy. *Supramol. Chem.* **2005**, *17* (3), 191.
- (79) Forgan, R.; Davidson, J.; Galbraith, S.; Henderson, D.; Parsons, S.; Tasker, P.; White, F. Transport of metal salts by zwitterionic ligands; simple but highly efficient salicylaldoxime extractants. *Chem. Commun.* **2008**, No. 34, 4049.

- (80) Williams, N.; Gephart, R.; Hames, A.; Reibenspies, J.; Luckay, R.; de Sousa, A.; Hancock, R. Affinity of two highly preorganized ligands for the base metal ions Co(II), Ni(II) and Cu(II): A thermodynamic, crystallographic and fluorometric study. *Polyhedron* **2012**, *46* (1), 139.
- (81) Hancock, R.; Melton, D.; Harrington, J.; McDonald, F.; Gephart, R.; Boone, L.; Jones, S.; Dean, N.; Whitehead, J.; Cockrell, G. Metal ion recognition in aqueous solution by highly preorganized non-macrocyclic ligands. *Coord. Chem. Rev.* **2007**, *251* (13), 1678.
- (82) Hancock, R.; Martell, A. Ligand design for selective complexation of metal ions in aqueous solution. *Chem. Rev.* **1989**, *89* (8), 1875.
- (83) Pearson, R.; Songstad, J. Application of the principle of hard and soft acids and bases to organic chemistry. *J. Am. Chem. Soc.* **1967**, *89* (8), 1827.
- (84) Martell, A.; Hancock, R. *Metal Complexes in Aqueous Solutions*; Fackler, J., Ed.; Plenum Press: New York, 1996.
- (85) Pearson, R. Hard and soft acids and bases, HSAB, Part I: Fundamental principles. *J. Chem. Educ.* **1968**, *45* (9), 581.
- (86) Pearson, R. Hard and soft acids and bases, HSAB, Part II: Underlying theories. *J. Chem. Educ.* **1968**, *45* (10), 643.
- (87) Ayers, P. An elementary derivation of the hard/soft-acid/base principle. *J. Chem. Phys.* **2005**, *122* (14), 141102.
- (88) Miessler, G.; Tarr, D. *Inorganic Chemistry*, 4th Edition; Pearson Prentice Hall, Upper Saddle River, NJ, USA; Boston; London, 2011.
- (89) LoPachin, R.; Gavin, T.; DeCaprio, A.; Barber, D. Application of the hard and soft, acids and bases (HSAB) theory to toxicant–target interactions. *Chem. Res. Toxicol.* **2012**, *25* (2), 239.
- (90) Rickelton, W.; Flett, D.; West, D. Cobalt-nickel separation by solvent extraction with bis(2,4,4 trimethylpentyl)phosphinic acid. *Solvent Extr. Ion Exch.* **1984**, *2* (6), 815.
- (91) Du Preez, J.; Postma, J.; Ravindran, S.; van Brecht, B. Nitrogen reagents in metal ion separation. Part VI. 2-(1'-Octylthiomethyl)pyridine as extractant for later 3d transition metal ions. *Solvent Extr. Ion Exch.* **1997**, *15* (1), 79–96.
- (92) Szymanowski, J. *Hydroxyoximes and Copper Hydrometallurgy*, 1st Edition; CRC Press, 1993.
- (93) Chia, P.; Livingstone, S.; Lockyer, T. Sulphur-nitrogen chelating agents. III. Metal complexes of 2-methylthiomethylpyridine. *Aust. J. Chem.* **1967**, *20* (2), 239.

- (94) Bjerrum, J. *Metal ammine formation in aqueous solution: Theory of the reversible step reactions*; Haase and Son: Copenhagen, 1941.
- (95) Schwarzenbach, G. The general, selective and specific formation of complexes by metallic cations. In *Advances in Inorganic Chemistry and Radiochemistry*; Emeleus, H., Sharpe, A., Eds.; Academic Press, 1961; Vol. 3, p 257.
- (96) Schwarzenbach, G. The chelate effect. *Helv. Chim. Acta* **1952**, *35*, 2344.
- (97) Martell, A.; Smith, R. *Critical Stability Constants*; Plenum Press: New York, 1974, 1975, 1977, 1977, 1982 and 1986; Vols. 1–6.
- (98) Hancock, R.; Martell, A. The chelate, cryptate and macrocyclic effects. *Comments Inorg. Chem.* **1988**, *6* (5–6), 237.
- (99) Adamson, A. A proposed approach to the chelate effect. *J. Am. Chem. Soc.* **1954**, *76* (6), 1578.
- (100) Hancock, R.; Marsicano, F. The chelate effect: A simple quantitative approach. *J. Chem. Soc. Dalton Trans.* **1976**, No. 12, 1096.
- (101) Shannon, R. Revised effective ionic radii and systematic studies of interatomic distances in halides and chalcogenides. *Acta Crystallogr. Sect. A* **1976**, *32* (5), 751–767.
- (102) Hancock, R.; Bhavan, R.; Wade, P.; Boeyens, J.; Dobson, S. Ligand design for complexation in aqueous solution. 1. Neutral oxygen donor bearing groups as a means of controlling size-based selectivity for metal ions. *Inorg. Chem.* **1989**, *28* (2), 187.
- (103) Hancock, R. Molecular mechanics calculations and metal ion recognition. *Acc. Chem. Res.* **1990**, *23* (8), 253–257.
- (104) Hay, B.; Rustad, J.; Hostetler, C. Quantitative structure-stability relationship for potassium ion complexation by crown ethers. A molecular mechanics and ab initio study. *J. Am. Chem. Soc.* **1993**, *115* (24), 11158.
- (105) Hancock, R.; Nakani, B.; Marsicano, F. Relationship between Lewis acid-base behavior in the gas phase and in aqueous solution. 1. Role of inductive, polarizability, and steric effects in amine ligands. *Inorg. Chem.* **1983**, *22* (18), 2531.
- (106) Hancock, R. Polar and steric effects in the stability of silver complexes of primary amines. *J. Chem. Soc. Dalt. Trans.* **1980**, No. 3, 416.
- (107) Clayden, J.; Greeves, N.; Warren, S. *Organic Chemistry*, 2nd Edition; Oxford University Press Inc.: New York, 2012.

- (108) Gerber, T.; Hosten, E.; Mayer, P.; Tshentu, Z. Synthesis and characterization of rhenium(III) and (V) pyridylimidazole complexes. *J. Coord. Chem.* **2006**, *59* (3), 243.
- (109) Okewole, A.; Magwa, N.; Tshentu, Z. The separation of nickel(II) from base metal ions using 1-octyl-2-(2'-pyridyl)imidazole as extractant in a highly acidic sulfate medium. *Hydrometallurgy* **2012**, *121–124*, 81.
- (110) Watson, A.; House, D.; Steel, P. Chiral heterocyclic ligands. Part IV. Synthesis and metal complexes of 2,6-bis(pyrazol-1-ylmethyl)pyridine and chiral derivatives. *Inorg. Chim. Acta* **1987**, *130* (2), 167.
- (111) Satake, A.; Nakata, T. Novel η^3 -allylpalladium-pyridinylpyrazole complex: Synthesis, reactivity, and catalytic activity for cyclopropanation of ketene silyl acetal with allylic acetates. *J. Am. Chem. Soc.* **1998**, *120* (40), 10391.
- (112) Pearce, B.; Ogutu, H.; Luckay, R. Synthesis of pyrazole-based pyridine ligands and their use as extractants for nickel(II) and copper(II): Crystal structure of a copper(II)–ligand complex. *Eur. J. Inorg. Chem.* **2017**, *2017* (8), 1189–1201.
- (113) Pearce, B.; Ogutu, H.; Saban, W.; Luckay, R. Synthesis, characterization and use of imidazole and methyl-pyrazole based pyridine ligands as extractants for nickel(II) and copper(II). *Inorg. Chim. Acta* **2019**, *490*, 57–67.
- (114) Roberts, T.; Little, M.; Kershaw Cook, L.; Halcrow, M. Iron(II) complexes of 2,6-di(1*H*-pyrazol-3-yl)pyridine derivatives with hydrogen bonding and sterically bulky substituents. *Dalton Trans.* **2014**, *43* (20), 7577–7588.
- (115) Gal, M.; Tarrago, G.; Steel, P.; Marzin, C. A novel macrocyclic ligand containing 2,6-bis(pyrazol-5-yl)pyridine units. Synthesis and complexation properties. *Nouv. J. Chim.* **1985**, *9* (10), 617–620.
- (116) Yoshinari, A.; Tazawa, A.; Kuwata, S.; Ikariya, T. Synthesis, structures, and reactivities of pincer-type ruthenium complexes bearing two proton-responsive pyrazole arms. *Chem. – An Asian J.* **2012**, *7* (6), 1417–1425.
- (117) Umehara, K.; Kuwata, S.; Ikariya, T. Synthesis, structures, and reactivities of iron, cobalt, and manganese complexes bearing a pincer ligand with two protic pyrazole arms. *Inorg. Chim. Acta* **2014**, *413*, 136–142.
- (118) Li, L.; Luo, Q.; Cui, H.; Li, R.; Zhang, J.; Peng, T. Air-stable ruthenium(II)-NNN pincer complexes for the efficient coupling of aromatic diamines and alcohols to 1*H*-benzo[*d*]imidazoles with the liberation of H₂. *ChemCatChem* **2018**, *10* (7), 1607–1613.
- (119) Polezhaev, A.; Chen, C.; Kinne, A.; Cabelof, A.; Lord, R.; Caulton, K. Ligand design toward multifunctional substrate reductive transformations. *Inorg. Chem.* **2017**, *56* (16), 9505–9514.

- (120) Roberts, T.; Halcrow, M. Supramolecular assembly and transfer hydrogenation catalysis with ruthenium(II) complexes of 2,6-di(1*H*-pyrazol-3-yl)pyridine derivatives. *Polyhedron* **2016**, *103*, 79–86.
- (121) Zhou, T.; Pesic, B. A pyridine-based chelating solvent extraction system for selective extraction of nickel and cobalt. *Hydrometallurgy* **1997**, *46* (1), 37–53.
- (122) Roebuck, J.; Bailey, P.; Doidge, E.; Fischmann, A.; Healy, M.; Nichol, G.; O'Toole, N.; Pelsler, M.; Sassi, T.; Sole, K.; *et al.* Strong and selective Ni(II) extractants based on synergistic mixtures of sulfonic acids and bidentate *N*-heterocycles. *Solvent Extr. Ion Exch.* **2018**, *36* (05), 1–22.

CHAPTER 2

SYNTHESIS AND CHARACTERISATION OF TRIDENTATE PYRAZOLE- AND IMIDAZOLE-PYRIDINYL LIGANDS

2.1 Introduction

The use of amines as extractants and separating agents has been a very common practice for over seventy years.¹ These molecules were extensively researched and developed in the early years of ion exchange resins and solvent extraction reagents (1940s–1960s).¹ The main drive for the development of these molecules lied in the pursuit of obtaining ever purer metals through hydrometallurgical means. Noteworthy contributions were made by academics like Gray *et al.*² and Vidal,³ who reported on the syntheses of novel amine extractants, while Hildebrand *et al.*⁴ and Kertes^{5,6} studied the relationship between the number of carbon atoms in high molecular weight amine ligands and aqueous solubility. In addition, Bucher *et al.*⁷ and Müller *et al.*⁸ gave valuable insight regarding amine ligand compatibility in organic solvents and micelle formation in organic phases. An honourable mention should also be extended to Hall,^{9,10} Trotman-Dickenson,¹¹ Chremos *et al.*¹² and Stewart *et al.*¹³ who researched and reviewed the basicity of tertiary aliphatic amines as well as their extraction capabilities. In 1969, Marcus and Kertes¹⁴ compiled a comprehensive review textbook on amines as separating agents. To date, however, amine extractants in their neutral form have not been extensively explored as separating agents for base metal ions by means of solvent extraction systems.¹

Nitrogenous ligands can be difficult to work with in the solvent extraction arena since they are easily protonated. This inherent characteristic, coupled with the hydrolysis of metal ions at $\text{pH} > 5.5$, means that there are fine pH margins to work within. The pH must be kept high enough to prevent the protonation of the ligands, while too high a pH will force the hydrolysis of the metal ions in the aqueous phase. This gum-like metal hydroxide precipitate is incredibly difficult to filter and is a major concern and drawback for industrial purposes.¹

Early progress on amine ligands was largely made on RNH_2 -type ligands, where R typically represented alkyl or aryl moieties. These amines are only able to bond, via sigma donicity, to a hydrogen or metal ion. However, the protonation constants of these ligands are so high that there is no real preference for the metal ion over the hydrogen.¹ This can significantly be improved if chelates are used instead.¹ In the last two to three decades, significant advances were made in the use of aromatic ligands in the extraction of metal ions through their *N*-donor capabilities. Monodentate amine ligands are known to have larger protonation constants compared to their bidentate counterparts, which in turn implies that bidentate ligands can extract at lower pH values. Moreover, monodentate aromatic ligands form less stable complexes compared to bidentate aromatic ligands.¹

Over the past twenty years, imidazole- and pyrazole-pyridinyl ligands were developed and implemented as metal extractants. Examples include ligands such as *N,N,N',N'*-tetraoctylethylenediamine (TOEDA), *N,N'*-di-*n*-octyl- α -aminopicoline and various derivatives thereof.¹⁵ Du Preez *et al.*^{16,17} reported on the stability and wide pH range at which imidazole- and pyrazole-pyridinyl ligands can extract metal ions. This was a promising sign and a key reason for proceeding with these heterocyclic amine-type ligands. Furthermore, it was shown that imidazole-, pyrazole- and pyridinyl-type ligands have appreciably high affinities for later 3d transition metal ions, such as Co^{2+} , Ni^{2+} , Cu^{2+} and Zn^{2+} .

Therefore, taking all of the aforementioned into account, we set out to synthesise 2,6-bis(5-methyl-1*H*-pyrazol-3-yl)pyridine (**1**), 2,6-bis(5-ethyl-1*H*-pyrazol-3-yl)pyridine (**2**), 2,6-bis(5-propyl-1*H*-pyrazol-3-yl)pyridine (**3**), 2,6-bis(5-butyl-1*H*-pyrazol-3-yl)pyridine (**4**), 2,6-bis(5-pentyl-1*H*-pyrazol-3-yl)pyridine (**5**), 2,6-bis(5-hexyl-1*H*-pyrazol-3-yl)pyridine (**6**), 2,6-bis(5-heptyl-1*H*-pyrazol-3-yl)pyridine (**7**), 2,6-bis(5-octyl-1*H*-pyrazol-3-yl)pyridine (**8**), 2,6-bis(5-(*tert*-butyl)-1*H*-pyrazol-3-yl)pyridine (**9**), 2,6-bis(5-phenyl-1*H*-pyrazol-3-yl)pyridine (**10**), 2,6-bis(1-butylimidazol-2-yl)pyridine (**11**) and 2,6-bis(1-octylimidazol-2-yl)pyridine (**12**). See **Figure 2.1** below for a schematic summary of ligands **1–12**.

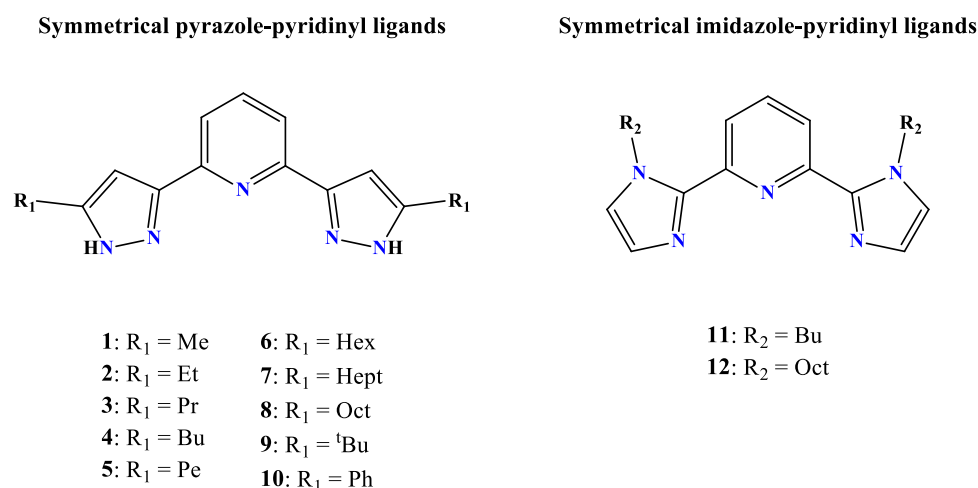


Figure 2.1: Schematic overview of ligands **1–12**.

2.2 Materials and methods

2.2.1 Chemicals and reagents

The chemicals listed in **Table 2.1** were all bought from reputable chemical suppliers and used without additional purification.

Table 2.1: List of chemicals used in alphanumeric order.

Chemical/Reagent	Purity (%)	Commercial Supplier
1-Bromobutane	99	British Drug House Chemical Company
1-Bromooctane	99	Sigma-Aldrich (Pty) Ltd.
2-Butanone	≥ 99	Sigma-Aldrich (Pty) Ltd.
2-Decanone	≥ 98	Alfa Aesar
2-Heptanone	≥ 98	Sigma-Aldrich (Pty) Ltd.
2-Hexanone	≥ 98	Sigma-Aldrich (Pty) Ltd.
2-Nonanone	≥ 99	Sigma-Aldrich (Pty) Ltd.
2-Octanone	≥ 98	Alfa Aesar
2-Pentanone	≥ 99	Sigma-Aldrich (Pty) Ltd.
3,3-Dimethyl-2-butanone	98	Sigma-Aldrich (Pty) Ltd.
Acetic acid (glacial)	≥ 98	Protea Chemicals (Pty) Ltd.
Acetone	≥ 99.5	Sigma-Aldrich (Pty) Ltd.
Acetonitrile	≥ 98	Protea Chemicals (Pty) Ltd.
Acetophenone	99	Alfa Aesar
Aminoacetaldehyde diethylacetal	98	Sigma-Aldrich (Pty) Ltd.
Benzene	≥ 99	KIMIX Chemical and Lab Supplies (CC)
Chloroform	≥ 98	KIMIX Chemical and Lab Supplies (CC)
Dichloromethane	≥ 98	KIMIX Chemical and Lab Supplies (CC)
Diethyl ether	≥ 98	KIMIX Chemical and Lab Supplies (CC)
Dimethyl pyridine-2,6-dicarboxylate	99	Sigma-Aldrich (Pty) Ltd.
Ethanol (absolute)	≥ 99	KIMIX Chemical and Lab Supplies (CC)
Ethyl acetate	≥ 98	KIMIX Chemical and Lab Supplies (CC)
Hydrazine monohydrate	98 (64–65% N ₂ H ₄)	Sigma-Aldrich (Pty) Ltd.
Hydrochloric acid solution	32 wt. % in H ₂ O	KIMIX Chemical and Lab Supplies (CC)
Methanol	≥ 97	KIMIX Chemical and Lab Supplies (CC)
<i>N,N</i> -Dimethylformamide	99	Sigma-Aldrich (Pty) Ltd.
Potassium bromide (FT-IR grade)	≥ 99	Merck (Pty) Ltd.
Potassium hydroxide (pellets)	≥ 95	KIMIX Chemical and Lab Supplies (CC)
Potassium <i>tert</i> -butoxide	≥ 97	KIMIX Chemical and Lab Supplies (CC)

Table continues to next page...

Chemical/Reagent	Purity (%)	Commercial Supplier
Pyridine-2,6-dicarbonitrile	97	Sigma-Aldrich (Pty) Ltd.
Pyridine-2,6-dicarboxylic acid	99	Merck (Pty) Ltd.
Sodium ethoxide (powder)	≥ 95	Alfa Aesar
Sodium hydride	60 wt.% in mineral oil	Sigma-Aldrich (Pty) Ltd.
Sodium hydroxide	97	Protea Chemicals (Pty) Ltd.
Sodium metal (cubes in mineral oil)	99.9	Alfa Aesar
Sodium sulfate (anhydrous)	≥ 99	Merck (Pty) Ltd.
Sulfuric acid	95–98	Protea Chemicals
Tetrabutylammonium bromide	≥ 98	Sigma-Aldrich (Pty) Ltd.
Tetrabutylammonium hydroxide	40 wt. % in H ₂ O	Sigma-Aldrich (Pty) Ltd.
Tetrahydrofuran	≥ 97	KIMIX Chemical and Lab Supplies (CC)
Toluene	99	KIMIX Chemical and Lab Supplies (CC)
Triethylamine	≥ 99.5	Sigma-Aldrich (Pty) Ltd.

2.2.2 Instrumentation

2.2.2.1 Nuclear magnetic resonance spectroscopy

Nuclear magnetic resonance (NMR) spectra were recorded at room temperature by using various NMR spectrometers. These include the *Varian UnityInova 600 Liquid State NMR Spectrometer*, *Varian UnityInova 400 Liquid State NMR Spectrometer* and the *Varian VNMRs 300 Liquid State NMR Spectrometer*. All fid/propcar files were processed using *MestReNova*, Version 6.0.2-5475. All chemical shifts (δ) are given in ppm and are relative to either deuteriochloroform [CDCl_3 , δ 7.26] or -dimethyl sulfoxide [$(\text{CD}_3)_2\text{SO}$, δ 2.50].

2.2.2.2 Infrared spectroscopy

All ligands were partially characterised via infrared (IR) spectroscopy. This was achieved by using a *Nicolet Avatar 330 FT-IR Spectrometer* for liquid or viscous samples, while the *PerkinElmer FT-IR Spectrum Two™ Spectrometer* was used for solid samples (KBr pellets). Both spectrometers were set to record the percentage transmittance (%T) in the mid-IR range (4000–500 cm^{-1}).

2.2.2.3 Mass spectrometry

Time of flight (TOF) positive electrospray ionisation (ESI+) mass spectrometry (MS) was carried out on a *Waters Synapt G2 High Resolution Mass Spectrometer*, with a cone voltage of 15 V. The ESI probe was injected into a stream of acetonitrile. All signals were recorded as a mass over charge (m/z) ratio, with the molecular ion typically observed as either an $(M + H)^+$, $(M + Na)^+$ or $(M + K)^+$ ion.

2.2.2.4 Elemental analyses

All elemental analyses were done using a *PerkinElmer 2400 Series II CHNS Elemental Analyzer* at the University of KwaZulu-Natal's (UKZN) mass spectrometry laboratory in Pietermaritzburg, South Africa.

2.2.2.5 Melting point analyses

The melting point of solid ligands and complexes were determined using a *SMP20 Stuart™ melting point apparatus*.

2.2.2.6 pH determinations

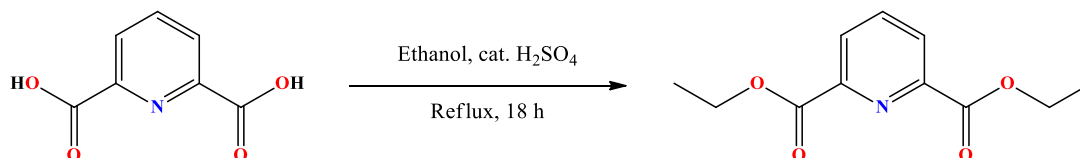
Accurate pH measurements were performed on a *Thermo Orion 420A+ pH meter*, using standards (pH 4, 7 and 10) to calibrate the system before every set of measurements.

2.2.2.7 Short path distillation

Vacuum distillation was performed using a *BÜCHI Glass oven B-585 kugelrohr* short path distillation apparatus to rid the sample of trace amounts of solvent and/or reagent.

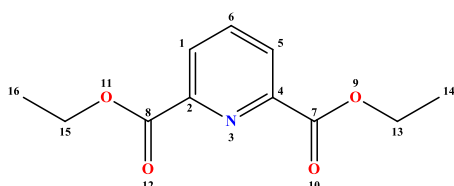
2.3 Experimental

2.3.1 Synthesis of diethyl pyridine-2,6-dicarboxylate



Scheme 2.1: Synthetic route to diethyl pyridine-2,6-dicarboxylate. [Adapted from Li *et al.*¹⁸]

A 500 mL round-bottom flask was charged with pyridine-2,6-dicarboxylic acid (20.0 g, 0.120 mol), ethanol (250 mL) and 5 drops of concentrated sulfuric acid. The resulting mixture was heated to reflux for 18 hours. After the solvent was removed via rotary evaporation, the viscous colourless residue was washed with 0.01 M NaOH solution (2 × 50 mL) and extracted with chloroform (3 × 50 mL). After the organic phase was dried overnight with anhydrous Na₂SO₄, the drying agent was filtered off and the solvent was removed via rotary evaporation to afford diethyl pyridine-2,6-dicarboxylate as colourless needle-like crystals (24.2 g, 90.3%).

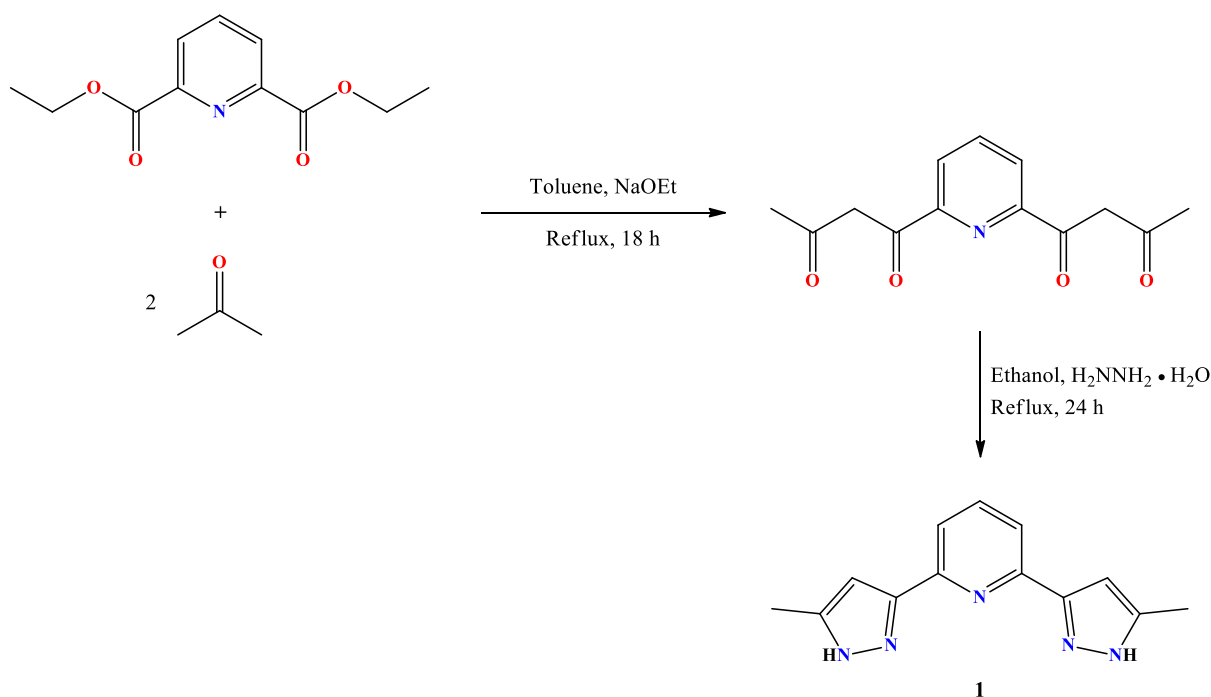


FT-IR (ATR, cm⁻¹) 3075 (aromatic C–H str), 2981 (aliphatic C–H str), 1742/1715 (C=O str), 1582 (pyridine C=N str), 1466 (–CH₂– bend), 1449 (–CH₃ bend), 1369 (–CH₃ bend). **¹H NMR (400 MHz, CDCl₃)** δ 8.26 (d, *J* = 7.8 Hz, *H*₁/*H*₅, 2H), 7.99 (t, *J* = 7.8 Hz, *H*₆,

1H), 4.47 (q, *J* = 7.2 Hz, *H*₁₃/*H*₁₅, 4H), 1.44 (dd, *J* = 8.1, 6.2 Hz, *H*₁₄/*H*₁₆, 6H). **¹³C NMR (100 MHz, CDCl₃)** δ 164.7 (*C*₇/*C*₈), 148.7 (*C*₂/*C*₄), 138.4 (*C*₆), 127.9 (*C*₁/*C*₅), 62.5 (*C*₁₃/*C*₁₅), 14.3 (*C*₁₄/*C*₁₆).

Calculated exact mass (μ) 223.08. **ESI-MS (*m/z*)** 224.09 (M + H)⁺, 246.07 (M + Na)⁺. **EA calculated (%)** C, 59.19; H, 5.87; N, 6.27. **EA found (%)** C, 59.30; H, 5.96; N, 6.02. **m.p.** 42–43 °C. See full range of spectra on pages 2–5 of *Appendix A — SPECTRA*.

2.3.2 Synthesis of 2,6-bis(5-methyl-1H-pyrazol-3-yl)pyridine (1)



Scheme 2.2: Synthetic route to 2,6-bis(5-methyl-1H-pyrazol-3-yl)pyridine (1). [Based on *Method 4*]

Method 1 [Adapted from Fenton *et al.*¹⁹ and Zhou & Chen²⁰]

A 250 mL two-necked round-bottom flask, under constant flow of N₂, was charged with sodium metal (1.05 g, 45.7 mmol) and dry ethanol (50.0 mL). Following the consumption of the sodium metal, the ethanol was removed by rotary evaporation, yielding a fresh batch of off-white sodium ethoxide powder (2.82 g, 90.7%).

Analytical reagent grade acetone (2.50 mL, 34.0 mmol) in benzene (50.0 mL) was added to the round-bottom flask containing the freshly prepared sodium ethoxide, followed swiftly by diethyl pyridine-2,6-dicarboxylate (3.00 g, 13.4 mmol). The mixture was stirred for 12 hours at room temperature, followed by an additional 2 hours at 50 °C. The mixture was allowed to cool to room temperature and gravity filtered to remove minor suspended black impurities. Distilled water (30.0 mL) and a few drops of glacial acetic acid was added to the mixture until pH 7–8. The yellow organic layer was separated from the milky aqueous layer and dried over anhydrous Na₂SO₄ overnight. The drying agent was filtered off and the solvent was removed under reduced pressure to yield a crude viscous yellow-brown oil. The oil was redissolved in chloroform (50.0 mL), washed with brine (3 × 30 mL) and distilled water (2 × 50 mL). The organic layer was subsequently dried over anhydrous Na₂SO₄ overnight. The drying agent was filtered off and the solvent was removed via rotary evaporation, yielding the crude tetraketone species (1.02 g, 29.6%) as a yellow-brown solid.

A mixture of the crude tetraketone (1.02 g, 4.13 mmol), hydrazine monohydrate (0.420 mL, 8.66 mmol) in methanol (50.0 mL) was immediately refluxed for 24 hours. The solvent was removed by rotary evaporation and the residue was redissolved in chloroform (50.0 mL) and washed with distilled water (3 × 50 mL). The pale-yellow organic layer was dried over anhydrous Na₂SO₄ overnight and subsequently filtered. The solvent was removed via rotary evaporation and dried *in vacuo* at 100 °C to yield ligand **1** (0.619 g, 19.3%) as an off-white solid.

Method 2 [Adapted from Satake and Nakata²¹]

In a 250 mL round-bottom flask, analytical reagent grade acetone (3.80 mL, 51.8 mmol) was added to a suspension of NaH (60 wt.% in mineral oil, 2.30 g, 57.5 mmol) in THF (50.0 mL). After the mixture was stirred for 20 minutes at room temperature, it was heated to 50 °C. This was followed by the immediate dropwise addition of diethyl pyridine-2,6-dicarboxylate (4.46 g, 20.0 mmol) in THF (40.0 mL). Upon complete addition of the diester species, the mixture was stirred for an additional 30 minutes at 50 °C, whereafter, 32% HCl was added at 0 °C until pH 7–8. The mixture was extracted with diethyl ether (4 × 30 mL) and the combined organic layers were washed with brine (2 × 30 mL), dried over anhydrous Na₂SO₄ and concentrated *in vacuo* to give the crude intermediary tetraketone species (1.33 g, ~26.9%) as a yellow-brown solid.

To a refluxing solution of the crude tetraketone species (1.33 g, ~5.38 mmol) in ethanol (50.0 mL) was added 2 drops of concentrated H₂SO₄ and hydrazine monohydrate (0.600 mL, 12.4 mmol) in ethanol (20.0 mL) over a period of 15 minutes. After a refluxing period of 2 hours, the solvent was removed via rotary evaporation. Purification was done via gravitational column chromatography on silica gel, with toluene as initial eluent (R_f = 0.198) to rid the sample of unwanted impurities and side products. The eluent was subsequently changed to an EtOAc/CHCl₃ (v/v, 8:2) system (R_f = 0.877) in order to flush the desired product from the column. The solvent was removed on a high vacuum system to yield ligand **1** (0.789 g, 16.5%) as an off-white solid.

Method 3 [Adapted from Gal *et al.*²²]

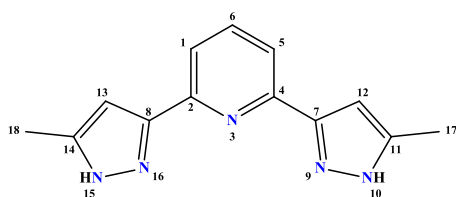
A 250 mL round-bottom flask was charged with commercial high-grade sodium ethoxide (3.4 g, 50.0 mmol) and dry diethyl ether (120 mL). To this stirring dispersion was added diethyl pyridine-2,6-dicarboxylate (4.46 g, 20.0 mmol) in dry diethyl ether (30.0 mL) dropwise at room temperature. After addition of analytical reagent grade acetone (3.10 mL, 42.2 mmol) in dry diethyl ether (30.0 mL) the reaction mixture was refluxed for 3 hours. After cooling the mixture, it was acidified with glacial acetic acid (3.00 mL) and the precipitate was dissolved in distilled water (100 mL). The organic and aqueous layers were separated and additional extractions of the aqueous layer with diethyl ether (3 × 50 mL) were done. The combined organic phases were washed with distilled water (2 × 50 mL), dried over anhydrous Na₂SO₄ and concentrated *in vacuo* to yield the crude tetraketone species (1.58 g, ~31.9%) as a viscous yellow-brown oil.

To a solution of the crude tetraketone (1.58 g, ~6.39 mmol) in ethanol (50.0 mL) and 1 drop of HCl, hydrazine monohydrate (0.700 mL, 14.4 mmol) in ethanol (15.0 mL) was added dropwise. The mixture was refluxed for 18 hours. After evaporation of the solvent the residue was dissolved in dichloromethane (50.0 mL), washed with distilled water (2 × 50 mL), dried over anhydrous Na₂SO₄ and concentrated *in vacuo* to yield ligand **1** (1.20 g, 25.1%) as an off-white solid.

Method 4 [Combination of **Methods 1, 2** and **3**]

A 250 mL round-bottom flask was charged with commercial high-grade sodium ethoxide powder (2.18 g, 32.0 mmol) and toluene (50.0 mL). To this mixture was added analytical reagent grade acetone (2.20 mL, 30.0 mmol) followed immediately by diethyl pyridine-2,6-dicarboxylate (2.80 g, 12.5 mmol). The pale-yellow mixture was refluxed for 18 hours, eventually turning mustard-yellow. After the mixture was cooled to room temperature, distilled water (50.0 mL) was added, which immediately discharged the colour from the organic phase. Concentrated H₂SO₄ was added dropwise to the biphasic mixture until the colour permanently returned to the organic phase (pH 6–7). The organic layer was separated from the aqueous layer and washed several times with brine (3 × 30 mL) and distilled water (3 × 50 mL). The organic layer was dried over anhydrous Na₂SO₄ and concentrated *in vacuo* to yield the crude intermediary tetraketone species, 1,1'-(pyridine-2,6-diyl)bis(butane-1,3-dione), as a viscous yellow-brown oil (1.18 g, ~38.0%).

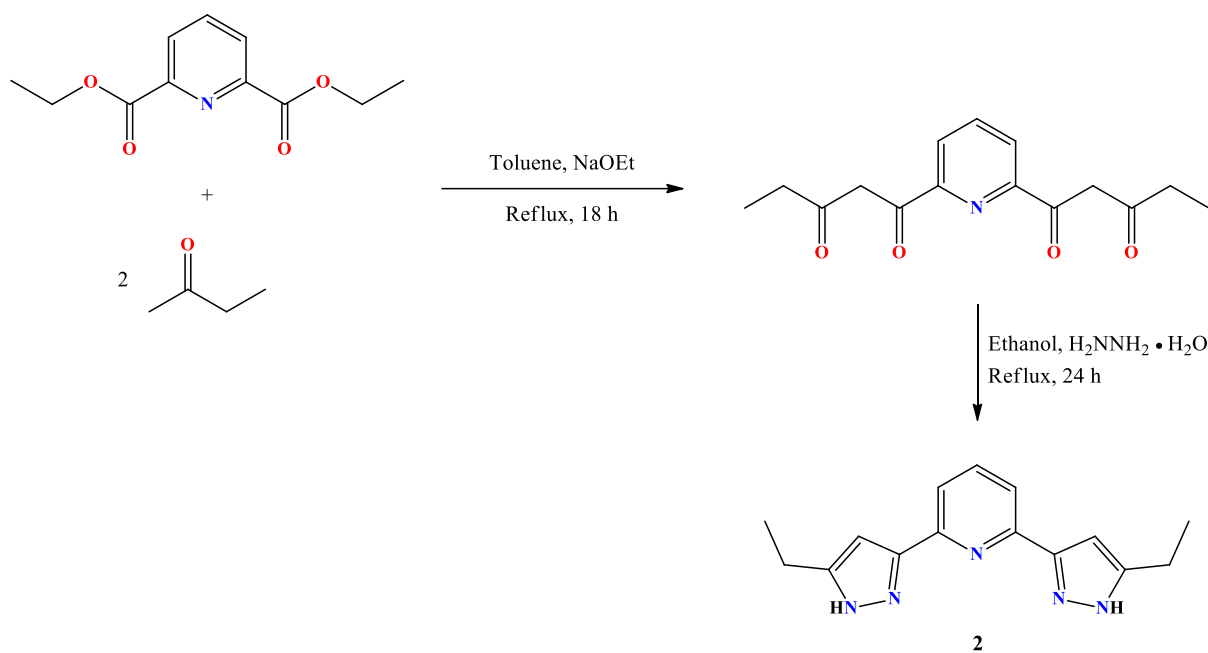
To a refluxing solution of the crude tetraketone species (1.18 g, ~4.77 mmol) in ethanol (50.0 mL) was added hydrazine monohydrate (0.600 mL, 12.4 mmol) in ethanol (20.0 mL) and 2 drops of concentrated H₂SO₄. After a refluxing period of 24 hours, the solvent was removed via rotary evaporation. The crude product was redissolved in chloroform (50.0 mL) and washed with distilled water several times (5 × 50 mL) until the aqueous phase became clear. The organic phase was separated, dried over anhydrous Na₂SO₄, and concentrated to ~10 mL. The concentrated product was transferred to a kugelrohr bulb and purified by means of vacuum distillation using a kugelrohr short path distillation apparatus, yielding ligand **1** (1.01 g, 33.7%) as an off-white solid.



FT-IR (KBr pellet, cm⁻¹) 3191 (pyrazole C–H str), 3129/3099 (aromatic C–H str), 2983/2926/2861 (aliphatic C–H str), 1599 (pyridine C=N str), 1578 (pyrazole C=N str), 1564, 1461 (–CH₃ bend). **¹H NMR (600 MHz, CDCl₃)** δ 7.57 (t, *J* = 7.8 Hz, *H*₆, 1H), 7.30 (d, *J* = 7.8 Hz, *H*_{1/5}, 2H), 6.34 (s, *H*_{12/13}, 2H), 2.24 (s, *H*_{17/18}, 6H). **¹³C{¹H} NMR (100 MHz, CDCl₃)** δ 148.6 (*C*_{2/4}), 147.7 (*C*_{7/8}), 144.7 (*C*_{11/14}), 137.4 (*C*₆), 118.3 (*C*_{1/5}), 102.7 (*C*_{12/13}), 12.9 (*C*_{17/18}). **Calculated exact mass (μ)** 239.12. **ESI-MS (*m/z*)** 240.13 (*M* + *H*)⁺, 262.11 (*M* + *Na*)⁺. **EA calculated (%)** C, 65.25; H, 5.48; N, 29.27. **EA found (%)** C, 65.80; H, 5.33; N, 28.97. **m.p.** 165–166 °C.

See full range of spectra on pages 6–9 of **Appendix A — SPECTRA**.

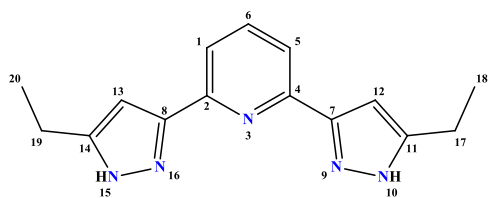
2.3.3 Synthesis of 2,6-bis(5-ethyl-1H-pyrazol-3-yl)pyridine (2)



Scheme 2.3: Synthetic route to 2,6-bis(5-ethyl-1H-pyrazol-3-yl)pyridine (2). [Adapted from Fenton *et al.*,¹⁹ Zhou *et al.*,²⁰ Satake *et al.*,²¹ and Gal *et al.*²²]

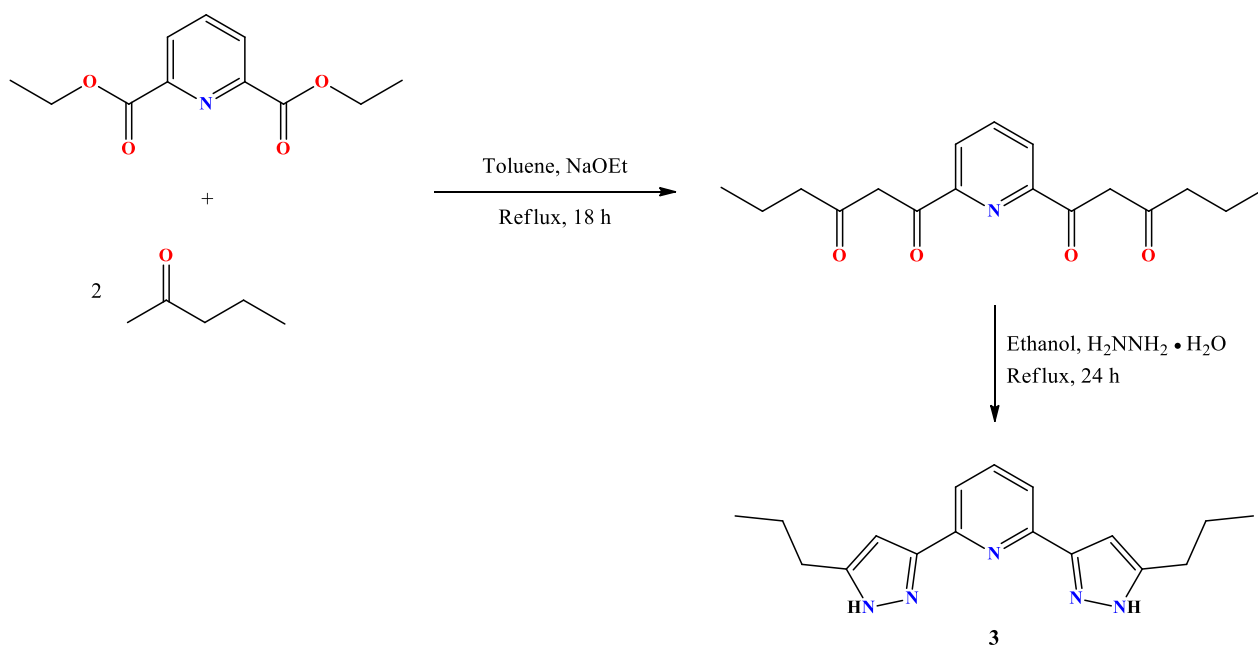
A 250 mL round-bottom flask was charged with commercial high-grade sodium ethoxide powder (2.50 g, 36.7 mmol) and toluene (50.0 mL). To this mixture was added 2-butanone (3.00 mL, 33.5 mmol) followed immediately by diethyl pyridine-2,6-dicarboxylate (3.00 g, 13.4 mmol). The pale-yellow mixture was refluxed for 18 hours, eventually turning a dark yellow-brown hue. After the mixture cooled to room temperature, distilled water (50.0 mL) was added, which immediately drained the colour from the organic phase. Concentrated H₂SO₄ was added dropwise to the biphasic mixture until the colour permanently returned to the organic phase (pH 6–7). The organic layer was separated from the aqueous layer and washed several times with brine (2 × 30 mL) and distilled water (3 × 50 mL). The organic layer was dried over anhydrous Na₂SO₄ and concentrated *in vacuo* to yield the crude intermediary tetraketone species, 1,1'-(pyridine-2,6-diyl)bis(pentane-1,3-dione), as a viscous yellow-brown oil (1.74 g, ~47.0%).

To a refluxing solution of the crude tetraketone species (1.74 g, ~6.32 mmol) in ethanol (50.0 mL) was added hydrazine monohydrate (0.650 mL, 13.4 mmol) in ethanol (20.0 mL) and 2 drops of concentrated H₂SO₄. After a refluxing period of 24 hours, the solvent was removed via rotary evaporation. The crude product was redissolved in chloroform (50.0 mL) and washed with distilled water several times (3 × 50 mL) until the aqueous phase became clear. The organic phase was separated, dried over anhydrous Na₂SO₄, and concentrated to ~10 mL. The concentrated product was transferred to a kugelrohr bulb and purified by means of vacuum distillation using a kugelrohr short path distillation apparatus, yielding ligand **2** (1.49 g, 41.5%) as an ochre-yellow solid.



FT-IR (KBr pellet, cm^{-1}) 3201 (pyrazole C–H str), 3106 (aromatic C–H str), 2969 (aliphatic C–H str), 1599 (pyridine C=N str), 1570 (pyrazole C=N str), 1479 (pyridine C=C str), 804 (aromatic C–H bend). **^1H NMR (300 MHz, CDCl_3)** δ 10.76 (br, NH10/15, 2H), 7.51 (t, $J = 7.8$ Hz, H6, 1H), 7.24 (d, $J = 7.8$ Hz, H1/5, 2H), 6.32 (s, H12/13, 2H), 2.58 (q, $J = 7.6$ Hz, H17/19, 4H), 1.17 (t, $J = 7.6$ Hz, H18/20, 6H). **$^{13}\text{C}\{^1\text{H}\}$ NMR (75 MHz, CDCl_3)** δ 154.6 (C7/8), 148.3 (C2/4), 144.1 (C11/14), 137.2 (C6), 117.9 (C1/5), 101.1 (C12/13), 21.0 (C17/19), 13.7 (C18/20). **Calculated exact mass (μ)** 267.15. **ESI-MS (m/z)** 268.16 ($\text{M} + \text{H}$)⁺. **EA calculated (%)** C, 67.14; H, 6.76; N, 26.10. **EA found (%)** C, 66.72; H, 6.28; N, 26.44. **m.p.** 199–200 °C. See full range of spectra on pages 10–14 of **Appendix A — SPECTRA**.

2.3.4 Synthesis of 2,6-bis(5-propyl-1H-pyrazol-3-yl)pyridine (3)

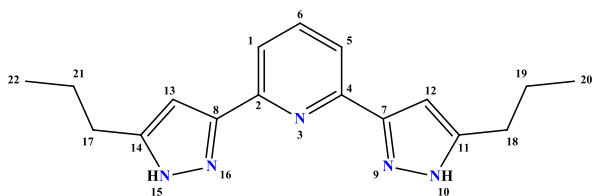


Scheme 2.4: Synthetic route to 2,6-bis(5-propyl-1H-pyrazol-3-yl)pyridine (**3**). [Adapted from Fenton *et al.*,¹⁹ Zhou *et al.*,²⁰ Satake *et al.*,²¹ and Gal *et al.*²²]

To a 250 mL round-bottom flask was added high-grade sodium ethoxide powder (1.95 g, 28.7 mmol) and toluene (50.0 mL). This was followed by 2-pentanone (3.00 mL, 28.2 mmol) and diethyl pyridine-2,6-dicarboxylate (3.00 g, 13.4 mmol). The light orange mixture was refluxed for 18 hours, eventually becoming dark brown. After the mixture was allowed to cool to room temperature, distilled water (50.0 mL) was added, resulting in the colour bleeding from the organic- to the aqueous phase. Concentrated HCl was added dropwise to the biphasic mixture until the colour returned to the organic phase (pH 6–7). The organic layer was separated from the aqueous layer and washed several times with brine (2 × 30 mL) and distilled water (3 × 50 mL). The organic layer was dried over anhydrous Na_2SO_4 and concentrated *in vacuo* to yield the

crude intermediary tetraketone species, 1,1'-(pyridine-2,6-diyl)bis(hexane-1,3-dione), as a yellow-orange solid (2.01 g, ~49.3%).

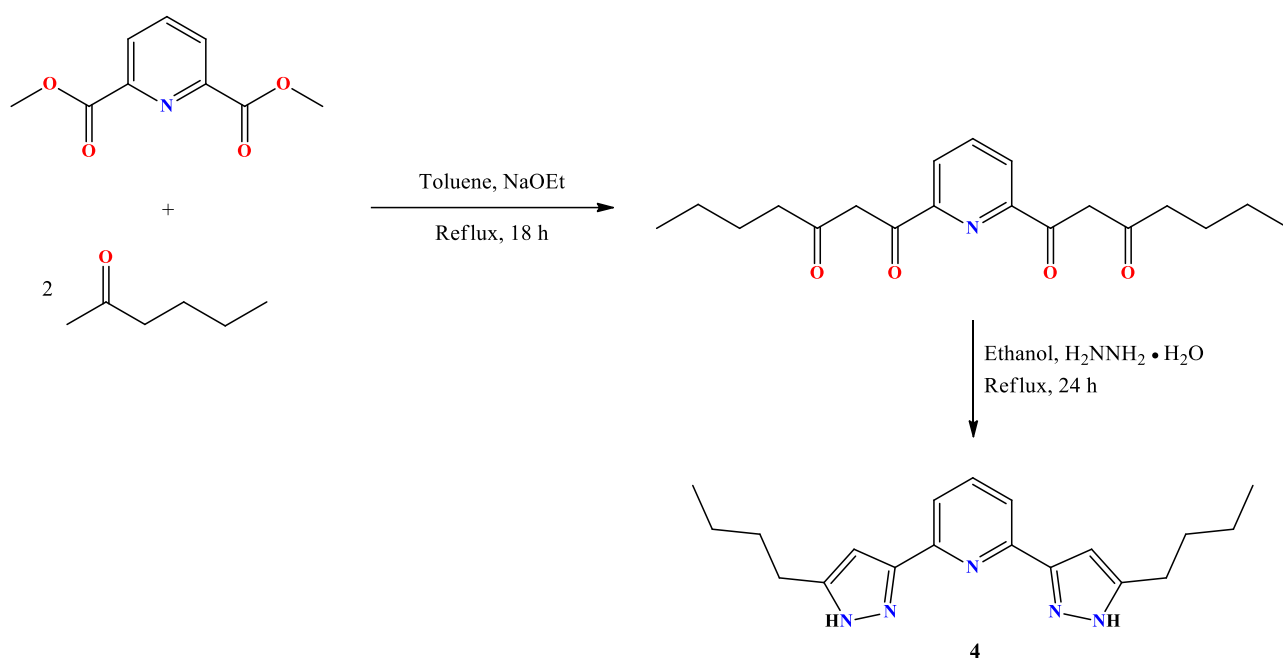
To a refluxing solution of the crude tetraketone species (1.93 g, ~6.36 mmol) in ethanol (50.0 mL) was added 2 drops of concentrated H₂SO₄ and hydrazine monohydrate (0.650 mL, 13.4 mmol) in ethanol (20.0 mL). After a refluxing period of 24 hours, the solvent was removed via rotary evaporation. The crude product was redissolved in chloroform (50.0 mL) and washed with distilled water (3 × 50 mL) until the aqueous phase became transparent. The organic phase was separated, dried over anhydrous Na₂SO₄, and concentrated to ~10 mL. The concentrated product was purified by means of vacuum distillation using a kugelrohr short path distillation apparatus, yielding ligand **3** (1.69 g, 42.6%) as a pastel orange-brown solid.



FT-IR (KBr pellet, cm⁻¹) 3191 (pyrazole C–H str), 3102 (aromatic C–H str), 2959/2931/2871 (aliphatic C–H str), 1598 (pyridine C=N str), 1575 (pyrazole C=N str), 1465 (–CH₂– bend), 1378 (–CH₃ bend), 811 (aromatic C–H bend). **¹H NMR (400 MHz, DMSO-d₆)**

δ 7.78 (m, *H*_{1/5/6}, 3H), 6.76 (s, *H*_{12/13}, 2H), 2.61 (t, *J* = 7.4 Hz, *H*_{17/18}, 4H), 1.67 (sex, *J* = 7.4 Hz, *H*_{19/21}, 4H), 0.94 (t, *J* = 7.4 Hz, *H*_{20/22}, 6H). **¹³C{¹H} NMR (100 MHz, DMSO-d₆)** δ 151.5 (*C*_{7/8}), 144.6 (*C*_{2/4}), 137.4 (*C*_{11/14}), 137.2 (*C*₆), 117.5 (*C*_{1/5}), 101.9 (*C*_{12/13}), 27.5 (*C*_{17/18}), 22.3 (*C*_{19/21}), 13.7 (*C*_{20/22}). **Calculated exact mass (μ)** 295.18. **ESI-MS (*m/z*)** 148.60 (M + 2H)²⁺, 296.19 (M + H)⁺. **EA calculated (%)** C, 69.12; H, 7.17; N, 23.71. **EA found (%)** C, 69.09; H, 7.00; N, 23.46. **m.p.** 176–177 °C. See full range of spectra on pages 15–18 of **Appendix A — SPECTRA**.

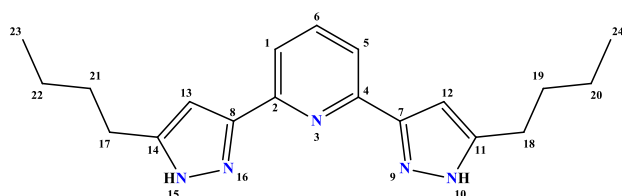
2.3.5 Synthesis of 2,6-bis(5-butyl-1H-pyrazol-3-yl)pyridine (4)



Scheme 2.5: Synthetic route to 2,6-bis(5-butyl-1H-pyrazol-3-yl)pyridine (4). [Adapted from Fenton *et al.*,¹⁹ Zhou *et al.*,²⁰ Satake *et al.*,²¹ and Gal *et al.*²²]

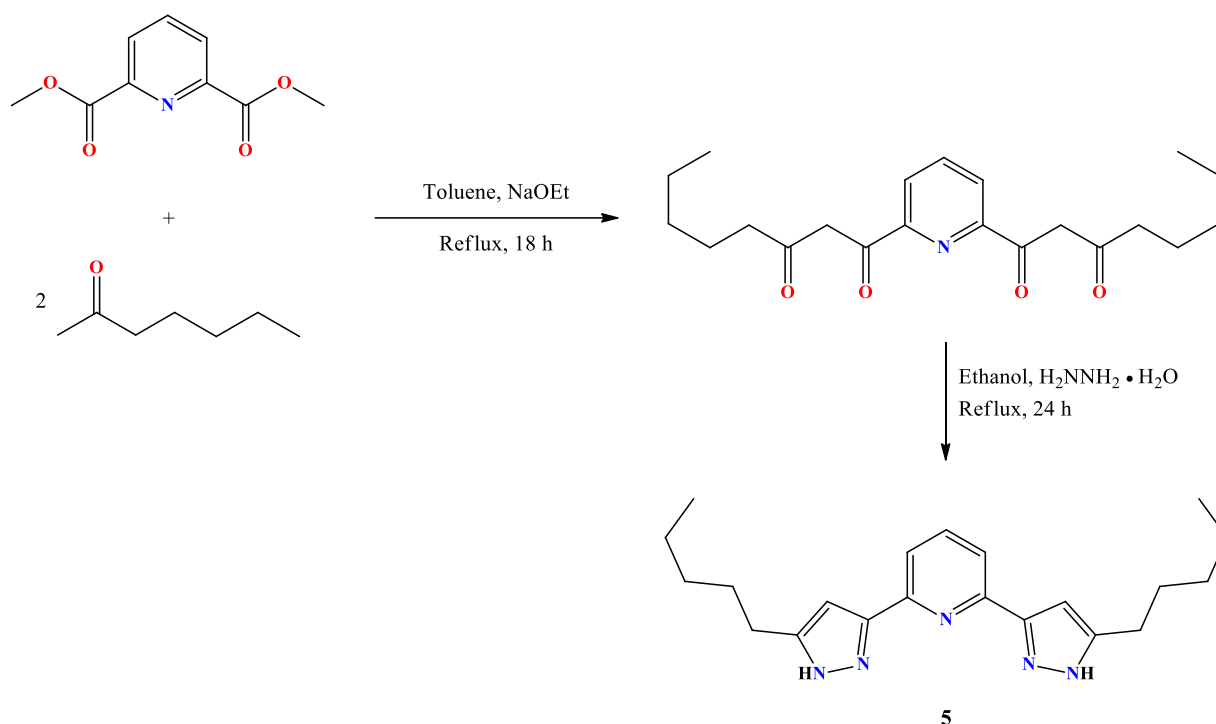
A 250 mL round-bottom flask was charged with high-grade sodium ethoxide powder (3.20 g, 47.0 mmol) and toluene (50.0 mL). To this mixture was added 2-hexanone (5.50 mL, 44.6 mmol) followed immediately by dimethyl pyridine-2,6-dicarboxylate (4.00 g, 20.5 mmol). The yellow-orange mixture was refluxed for 18 hours, eventually becoming dark brown. After the mixture cooled to room temperature, distilled water (50.0 mL) was added, which immediately drained the colour from the organic phase. Concentrated H₂SO₄ was added dropwise to the immiscible layers until the colour permanently returned to the organic phase (pH 6–7). The organic layer was separated from the aqueous layer and washed several times with brine (2 × 30 mL) and distilled water (3 × 50 mL). The organic layer was dried over anhydrous Na₂SO₄ and concentrated *in vacuo* to yield the crude intermediary tetraketone species, 1,1'-(pyridine-2,6-diyl)bis(heptane-1,3-dione), as a dark orange solid (5.35 g, ~78.7%).

To a refluxing solution of the crude tetraketone species (5.35 g, ~16.1 mmol) in ethanol (50.0 mL) was added 2 drops of concentrated H₂SO₄ and hydrazine monohydrate (1.60 mL, 33.0 mmol) in ethanol (20.0 mL). After a refluxing period of 24 hours, the solvent was removed via rotary evaporation. The crude product was redissolved in chloroform (50.0 mL) and washed with distilled water several times (3 × 50 mL) until the aqueous phase became clear. The organic phase was separated, dried over anhydrous Na₂SO₄, and concentrated to ~10 mL. The concentrated product was purified by means of vacuum distillation using a kugelrohr short path distillation apparatus, yielding ligand 4 (4.89 g, 73.7%) as a white fluffy solid.



FT-IR (KBr pellet, cm^{-1}) 3186 (pyrazole C–H str), 3102 (aromatic C–H str), 2954/2927/2859 (aliphatic C–H str), 1600 (pyridine C=N str), 1576 (pyrazole C=N str), 1465 (–CH₂– bend), 812 (aromatic C–H bend). **¹H NMR (400 MHz, CDCl₃)** δ 7.58 (t, $J = 7.8$ Hz, *H*₆, 1H), 7.36 (d, $J = 7.6$ Hz, *H*_{1/5}, 2H), 6.40 (s, *H*_{12/13}, 2H), 2.61 (t, $J = 7.7$ Hz, *H*_{17/18}, 4H), 1.61 (p, $J = 7.7$ Hz, *H*_{19/21}, 4H), 1.34 (sex, $J = 7.7$ Hz, *H*_{20/22}, 4H), 0.87 (t, $J = 7.3$ Hz, *H*_{23/24}, 6H). **¹³C{¹H} NMR (100 MHz, CDCl₃)** δ 152.1 (*C*_{7/8}), 148.9 (*C*_{2/4}), 145.1 (*C*_{11/14}), 137.3 (*C*₆), 118.2 (*C*_{1/5}), 101.6 (*C*_{12/13}), 31.8 (*C*_{17/18}), 27.3 (*C*_{19/21}), 22.6 (*C*_{20/22}), 14.0 (*C*_{23/24}). **Calculated exact mass (μ)** 323.21. **ESI-MS (m/z)** 324.22 (*M* + *H*)⁺, 346.20 (*M* + *Na*)⁺, 362.17 (*M* + *K*)⁺. **EA calculated (%)** C, 70.56; H, 7.79; N, 21.65. **EA found (%)** C, 70.31; H, 7.66; N, 21.20. **m.p.** 189–190 °C. See full range of spectra on pages 19–22 of Appendix A — SPECTRA.

2.3.6 Synthesis of 2,6-bis(5-pentyl-1*H*-pyrazol-3-yl)pyridine (5)

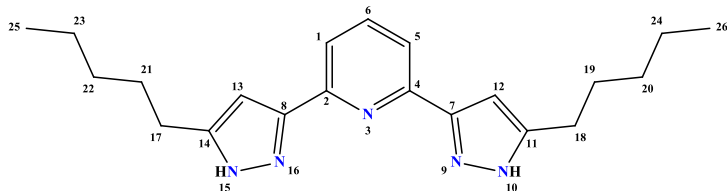


Scheme 2.6: Synthetic route to 2,6-bis(5-pentyl-1*H*-pyrazol-3-yl)pyridine (5). [Adapted from Fenton *et al.*,¹⁹ Zhou *et al.*,²⁰ Satake *et al.*,²¹ and Gal *et al.*,²²]

High-grade sodium ethoxide powder (2.50 g, 36.7 mmol) and toluene (50.0 mL) was added to a 250 mL round-bottom flask, followed momentarily by the addition of 2-heptanone (4.40 mL, 31.6 mmol) and dimethyl pyridine-2,6-dicarboxylate (3.00 g, 15.4 mmol). The resulting orange mixture was stirred under refluxing conditions for 18 hours, eventually turning ruby red. After the mixture was allowed to cool to room temperature, distilled water (50.0 mL) was added, which immediately sapped the colour from the organic phase. Concentrated H₂SO₄ was added dropwise to the immiscible layers until the colour was restored to the

organic phase (pH 6–7). The organic layer was separated from the aqueous layer and washed several times with brine (2 × 30 mL) and distilled water (3 × 50 mL). The organic layer was dried over anhydrous Na₂SO₄ and concentrated *in vacuo* to yield the crude intermediary tetraketone species, 1,1'-(pyridine-2,6-diyl)bis(octane-1,3-dione), as a dark orange solid (3.99 g, ~72.1%).

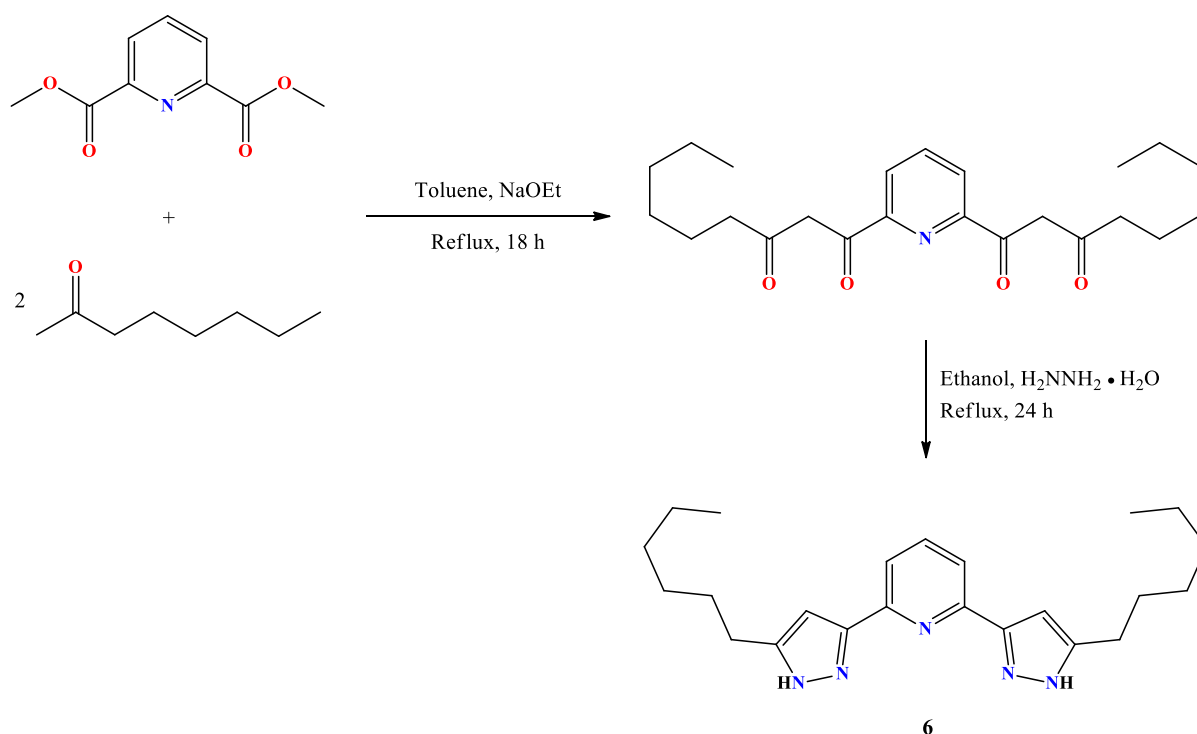
To a refluxing solution of the crude tetraketone species (3.99 g, ~11.1 mmol) in ethanol (50.0 mL) was added hydrazine monohydrate (1.30 mL, 26.8 mmol) in ethanol (20.0 mL) and 2 drops of concentrated H₂SO₄. After a refluxing period of 24 hours, the solvent was removed via rotary evaporation. The crude product was redissolved in chloroform (50.0 mL) and washed with distilled water several times (3 × 50 mL) until the aqueous phase became clear. The organic phase was separated, dried over anhydrous Na₂SO₄, and concentrated to ~10 mL. The concentrated product was purified by means of vacuum distillation using a kugelrohr short path distillation apparatus, yielding ligand **5** (3.72 g, 68.7%) as bright orange crystals.



FT-IR (ATR, cm⁻¹) 3193 (pyrazole C–H str), 3131 (aromatic C–H str), 2953/2925/2856 (aliphatic C–H str), 1596 (pyridine C=N str), 1564 (pyrazole C=N str), 1503 (N–H bend), 1465 (–CH₂– bend), 1376

(–CH₃ bend), 798 (aromatic C–H bend), **¹H NMR (400 MHz, CDCl₃)** δ 9.18 (br, NH_{10/15}, 2H), 7.63 (t, *J* = 7.8 Hz, *H*₆, 1H), 7.42 (d, *J* = 7.7 Hz, *H*_{1/5}, 2H), 6.46 (s, *H*_{12/13}, 2H), 2.65 (t, *J* = 7.7 Hz, *H*_{17/18}, 4H), 1.64 (p, *J* = 7.2 Hz, *H*_{19/21}, 4H), 1.31 (m, *H*_{20/22–24}, 8H), 0.86 (t, *J* = 6.9 Hz, *H*_{25/26}, 6H). **¹³C{¹H} NMR (100 MHz, CDCl₃)** δ 151.6 (*C*_{7/8}), 149.1 (*C*_{2/4}), 145.5 (*C*_{11/14}), 137.4 (*C*₆), 118.4 (*C*_{1/5}), 101.7 (*C*_{12/13}), 31.7 (*C*_{17/18}), 29.4 (*C*_{19/21}), 27.5 (*C*_{20/22}), 22.6 (*C*_{23/24}), 14.1 (*C*_{25/26}). **Calculated exact mass (μ)** 351.24. **ESI-MS (*m/z*)** 296.19 (*M* – C₄H₇)⁺, 352.25 (*M* + H)⁺. **EA calculated (%)** C, 71.76; H, 8.32; N, 19.92. **EA found (%)** C, 71.68; H, 8.02; N, 20.12. **m.p.** 102–103 °C. See full range of spectra on pages 23–26 of Appendix A — SPECTRA.

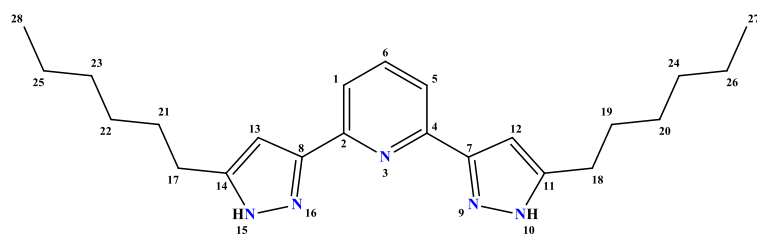
2.3.7 Synthesis of 2,6-bis(5-hexyl-1H-pyrazol-3-yl)pyridine (6)



Scheme 2.7: Synthetic route to 2,6-bis(5-hexyl-1H-pyrazol-3-yl)pyridine (6). [Adapted from Fenton *et al.*,¹⁹ Zhou *et al.*,²⁰ Satake *et al.*,²¹ and Gal *et al.*²²]

A 250 mL round-bottom flask was charged with high-grade sodium ethoxide powder (2.50 g, 36.7 mmol) and toluene (50.0 mL). To this mixture was added 2-octanone (5.00 mL, 31.9 mmol) followed immediately by dimethyl pyridine-2,6-dicarboxylate (3.00 g, 15.4 mmol). The pale-yellow mixture was refluxed for 18 hours, eventually becoming orange-brown. After the mixture cooled to room temperature, distilled water (50.0 mL) was added, which immediately drained the colour from the organic phase. Concentrated H₂SO₄ was added dropwise to the immiscible layers until the colour permanently returned to the organic phase (pH 6–7). The organic layer was separated from the aqueous layer and washed several times with brine (2 × 30 mL) and distilled water (3 × 50 mL). The organic layer was dried over anhydrous Na₂SO₄ and concentrated *in vacuo* to yield the crude intermediary tetraketone species, 1,1'-(pyridine-2,6-diyl)bis(nonane-1,3-dione), as a dark orange solid (4.78 g, ~80.1%).

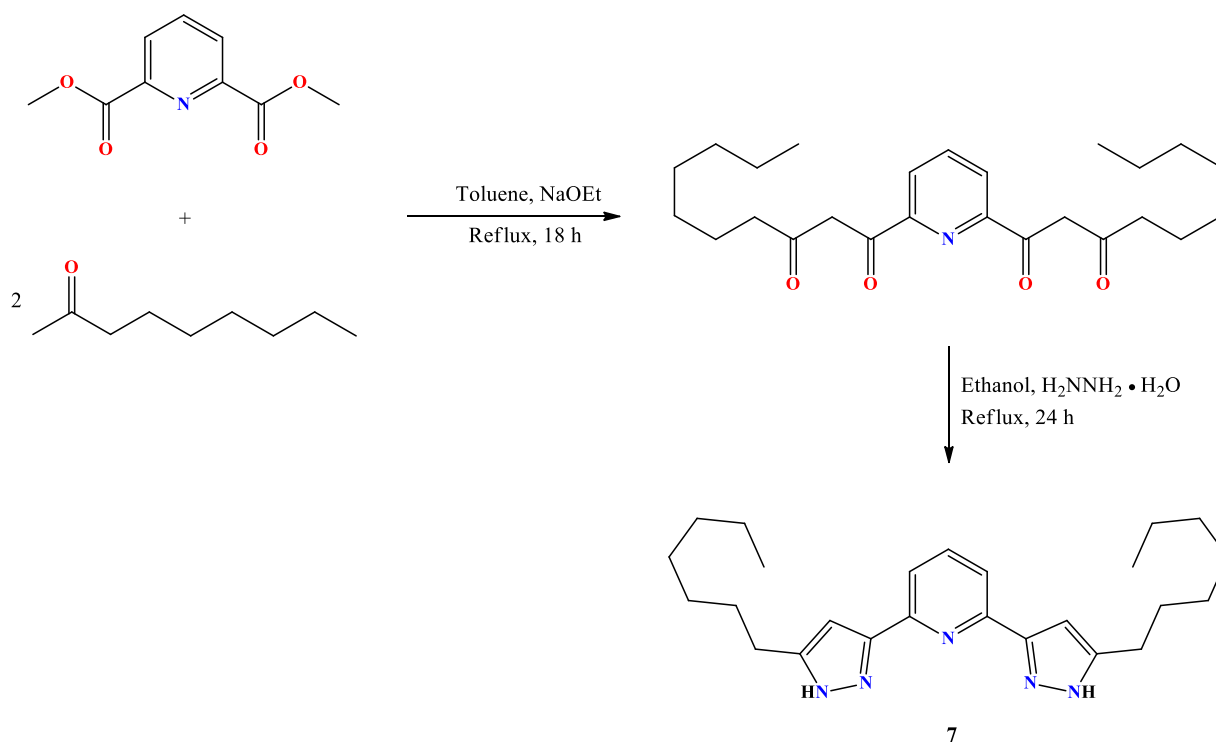
To a refluxing solution of the crude tetraketone species (4.78 g, ~12.3 mmol) in ethanol (50.0 mL) was added hydrazine monohydrate (1.30 mL, 26.8 mmol) in ethanol (20.0 mL) and 2 drops of concentrated H₂SO₄. After a refluxing period of 24 hours, the solvent was removed via rotary evaporation. Purification was done via gravitational column chromatography on silica gel, using ethanol as eluent ($R_f = 0.811$) to separate the desired product from impurities. The solvent was removed on a high vacuum system to yield ligand **6** (4.23 g, 72.4%) as a light brown solid.



FT-IR (KBr pellet, cm^{-1}) 3194 (pyrazole C–H str), 3106 (aromatic C–H str), 2958/2928/2856 (aliphatic C–H str), 1600 (pyridine C=N str), 1577 (pyrazole C=N str), 1476 (pyridine C=C str), 812

(aromatic C–H bend). **^1H NMR (400 MHz, CDCl_3)** δ 7.57 (t, $J = 7.8$ Hz, H_6 , 1H), 7.36 (m, $H_{1/5}$, 2H), 6.39 (s, $H_{12/13}$, 2H), 2.59 (t, $J = 7.7$ Hz, $H_{17/18}$, 4H), 1.62 (p, $J = 7.7$ Hz, $H_{19/21}$, 4H), 1.26 (m, $H_{20/22-26}$, 12H), 0.84 (t, $J = 6.8$ Hz, $H_{27/28}$, 6H). **$^{13}\text{C}\{^1\text{H}\}$ NMR (100 MHz, CDCl_3)** δ 152.6 ($C_{7/8}$), 148.8 ($C_{2/4}$), 145.0 ($C_{11/14}$), 137.3 (C_6), 118.2 ($C_{1/5}$), 101.6 ($C_{12/13}$), 31.8 (C_{17-18}), 29.6 (C_{19-24}), 29.2 (C_{19-24}), 27.7 (C_{19-24}), 22.7 ($C_{25/26}$), 14.2 ($C_{27/28}$). **Calculated exact mass (μ)** 379.27. **ESI-MS (m/z)** 380.28 ($M + H$)⁺. **EA calculated (%)** C, 72.78; H, 8.76; N, 18.45. **EA found (%)** C, 73.01; H, 8.88; N, 18.42. **m.p.** 77–78 °C. See full range of spectra on pages 27–30 of *Appendix A — SPECTRA*.

2.3.8 Synthesis of 2,6-bis(5-heptyl-1H-pyrazol-3-yl)pyridine (7)

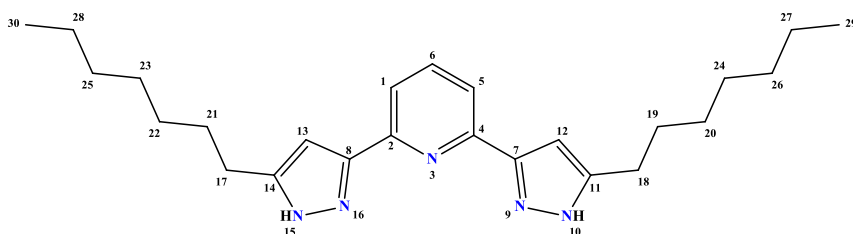


Scheme 2.8: Synthetic route to 2,6-bis(5-heptyl-1H-pyrazol-3-yl)pyridine (7). [Adapted from Fenton *et al.*,¹⁹ Zhou *et al.*,²⁰ Satake *et al.*,²¹ and Gal *et al.*²²]

A 250 mL round-bottom flask was charged with high-grade sodium ethoxide powder (2.75 g, 40.4 mmol) and toluene (50.0 mL). To this mixture was added 2-nonanone (6.50 mL, 37.5 mmol) followed immediately by dimethyl pyridine-2,6-dicarboxylate (3.50 g, 17.9 mmol). The yellow-orange mixture was refluxed for 18 hours, eventually turning a dark brown. After the mixture was allowed to cool to room temperature, distilled water (50.0 mL) was added, which immediately drained the colour from the organic phase.

Concentrated H₂SO₄ was added dropwise to the immiscible layers until the colour permanently returned to the organic phase (pH 6–7). The organic layer was separated from the aqueous layer and washed several times with brine (2 × 30 mL) and distilled water (3 × 50 mL). The organic layer was dried over anhydrous Na₂SO₄ and concentrated *in vacuo* to yield the crude intermediary tetraketone species, 1,1'-(pyridine-2,6-diyl)bis(decane-1,3-dione), as a dark orange solid (5.71 g, ~76.8%).

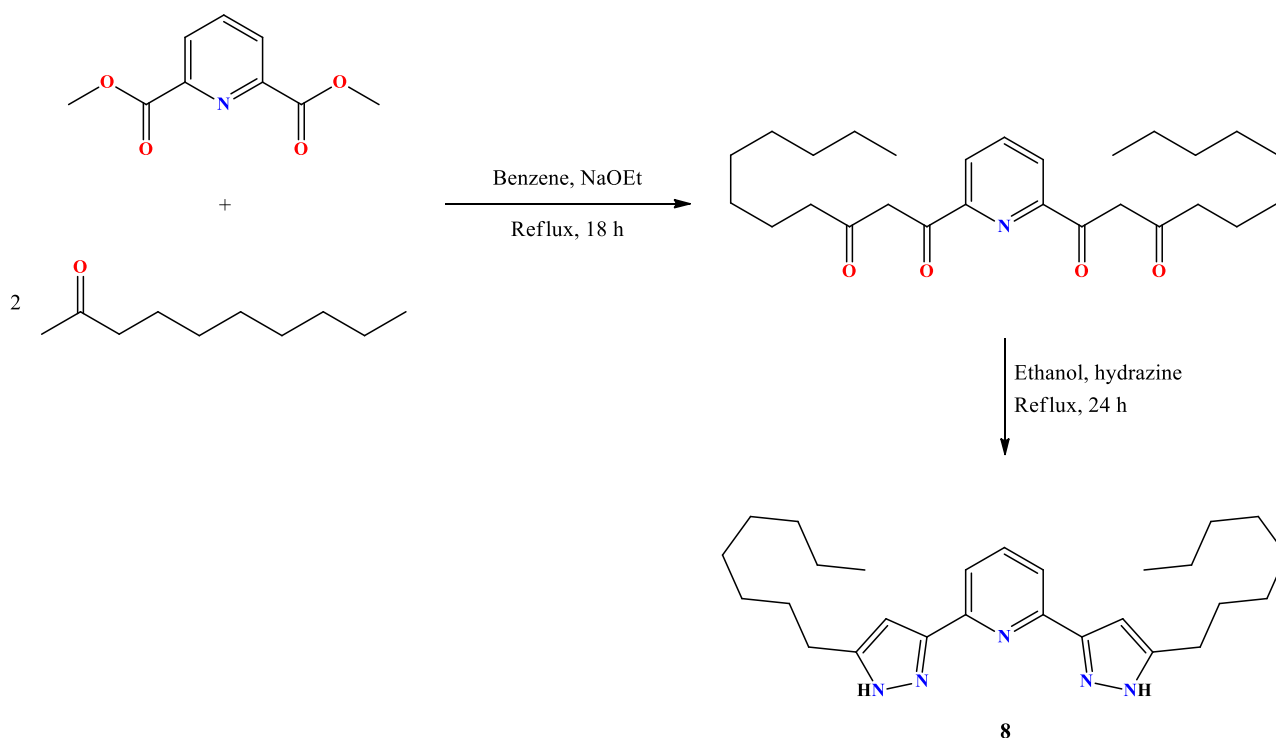
To a refluxing solution of the crude tetraketone species (5.71 g, ~13.7 mmol) in ethanol (50.0 mL) was added hydrazine monohydrate (1.40 mL, 28.9 mmol) in ethanol (20.0 mL) and 2 drops of concentrated H₂SO₄. After a refluxing period of 24 hours, the solvent was removed via rotary evaporation. The crude product was redissolved in chloroform (50.0 mL) and washed with distilled water several times (3 × 50 mL) until the aqueous phase became clear. The organic phase was separated, dried over anhydrous Na₂SO₄, and concentrated to ~10 mL. The concentrated product was purified by means of vacuum distillation using a kugelrohr short path distillation apparatus, yielding ligand **7** (5.03 g, 68.9%) as a brown toffee-like substance.



FT-IR (ATR, cm⁻¹) 3186 (pyrazole C–H str), 3102 (aromatic C–H str), 2953/2922/2852 (aliphatic C–H str), 1673, 1597 (pyridine C=N

str), 1567 (pyrazole C=N str), 1465 (–CH₂– bend), 1377 (–CH₃ bend), 796 (aromatic C–H bend), 723 (–CH₂– bend, long chain band). **¹H NMR (600 MHz, CDCl₃)** δ 7.66 (t, *J* = 7.5 Hz, *H*₆, 1H), 7.48 (d, *J* = 7.5 Hz, *H*_{1/5}, 2H), 6.50 (s, *H*_{12/13}, 2H), 2.66 (t, *J* = 7.2 Hz, *H*_{17/18}, 4H), 1.66 (p, *J* = 7.2 Hz, *H*_{19/21}, 4H), 1.29 (m, *H*_{20/22–28}, 16H), 0.86 (t, *J* = 6.9 Hz, *H*_{29/30}, 6H). **¹³C{¹H} NMR (100 MHz, CDCl₃)** δ 151.8 (*C*_{7/8}), 149.4 (*C*_{2/4}), 145.6 (*C*_{11/14}), 137.5 (*C*₆), 118.5 (*C*_{1/5}), 101.8 (*C*_{12/13}), 31.9 (*C*_{17/18}), 29.7 (*C*_{19–26}), 29.5 (*C*_{19–26}), 29.3 (*C*_{19–26}), 27.6 (*C*_{19–26}), 22.8 (*C*_{27/28}), 14.2 (*C*_{29/30}). **Calculated exact mass (μ)** 407.30. **ESI-MS (*m/z*)** 204.66 (*M* + 2*H*)²⁺, 244.18 (*M* – C₁₀H₁₅N₂)⁺, 258.20 (*M* – C₉H₁₃N₂)⁺, 324.22 (*M* – C₆H₁₁)⁺, 408.31 (*M* + *H*)⁺. **EA calculated (%)** C, 73.67; H, 9.15; N, 17.18. **EA found (%)** C, 73.60; H, 8.85; N, 16.89. See full range of spectra on pages 31–34 of **Appendix A — SPECTRA**.

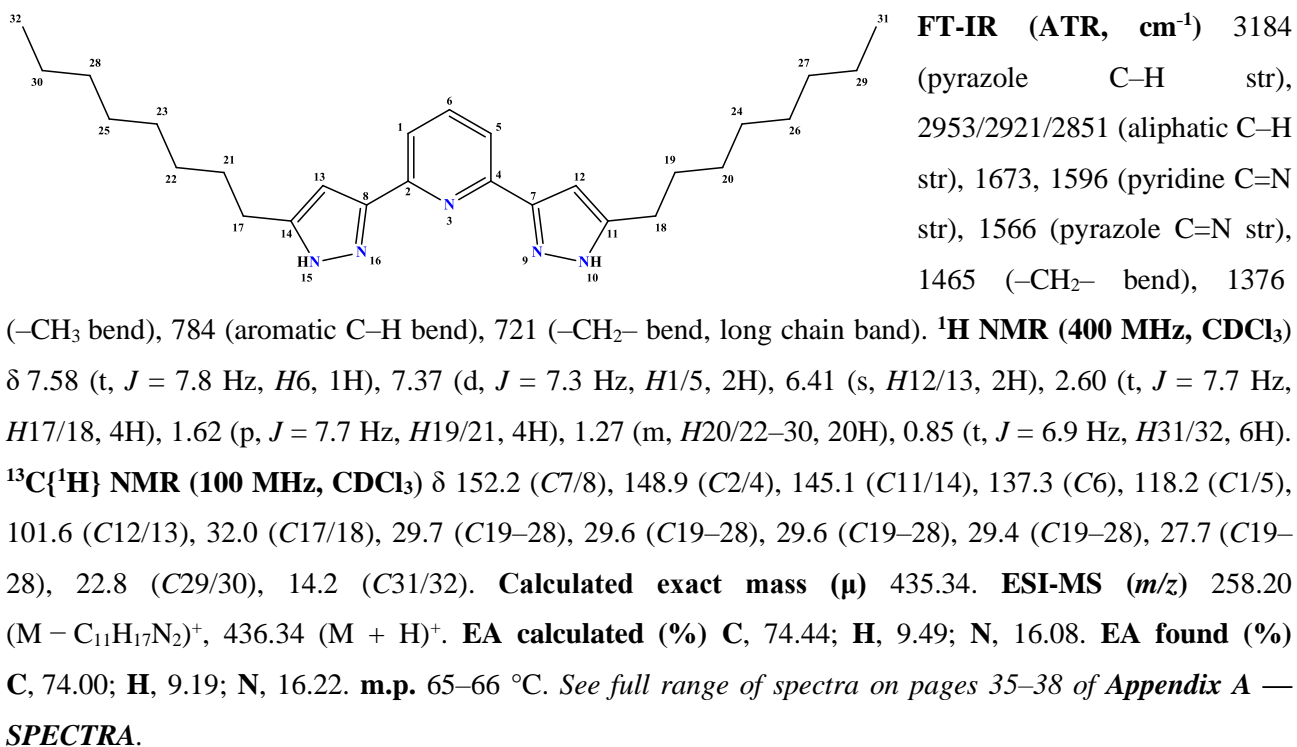
2.3.9 Synthesis of 2,6-bis(5-octyl-1H-pyrazol-3-yl)pyridine (**8**)



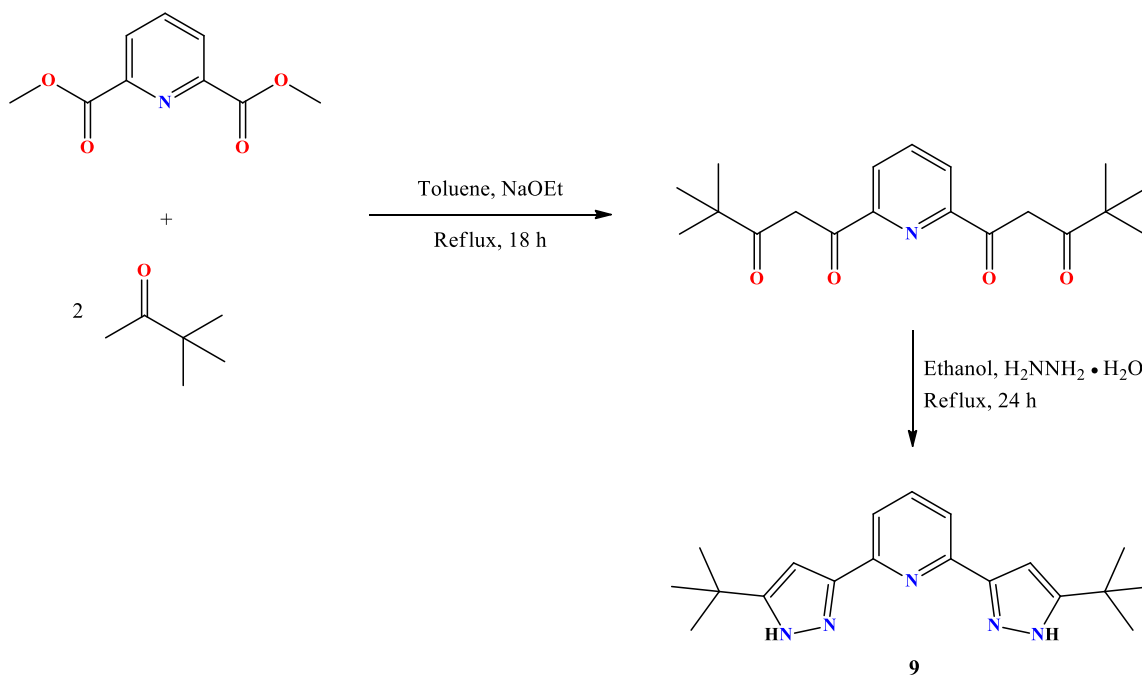
Scheme 2.9: Synthetic route to 2,6-bis(5-octyl-1H-pyrazol-3-yl)pyridine (**8**). [Adapted from Fenton *et al.*,¹⁹ Zhou *et al.*,²⁰ Satake *et al.*,²¹ and Gal *et al.*²²]

A 250 mL round-bottom flask was charged with high-grade sodium ethoxide powder (2.50 g, 36.7 mmol) and benzene (50.0 mL). To this mixture was added 2-decanone (6.00 mL, 31.7 mmol) followed immediately by dimethyl pyridine-2,6-dicarboxylate (3.00 g, 15.4 mmol). The yellow mixture was refluxed for 18 hours, eventually turning yellow-brown. After the mixture cooled to room temperature, distilled water (50.0 mL) was added, which immediately drained the colour from the organic phase. Concentrated H₂SO₄ was added dropwise to the immiscible layers until the colour permanently returned to the organic phase (pH 6–7). The organic layer was separated from the aqueous layer and washed several times with brine (2 × 30 mL) and distilled water (3 × 50 mL). The organic layer was dried over anhydrous Na₂SO₄ and concentrated *in vacuo* to yield the crude intermediary tetraketone species, 1,1'-(pyridine-2,6-diyl)bis(undecane-1,3-dione), as an orange-brown solid (5.73 g, ~83.9%).

To a refluxing solution of the crude tetraketone species (5.73 g, ~12.9 mmol) in ethanol (50.0 mL) was added hydrazine monohydrate (1.30 mL, 26.8 mmol) in ethanol (20.0 mL) and 2 drops of concentrated H₂SO₄. After a refluxing period of 24 hours, the solvent was removed via rotary evaporation. Purification was done via gravitational column chromatography on silica gel, using ethanol as eluent ($R_f = 0.846$) to separate the desired product from impurities. The solvent was removed on a high vacuum system to yield ligand **8** (5.40 g, 80.5%) as a yellow opaque solid.



2.3.10 Synthesis of 2,6-bis(5-(*tert*-butyl)-1*H*-pyrazol-3-yl)pyridine (**9**)

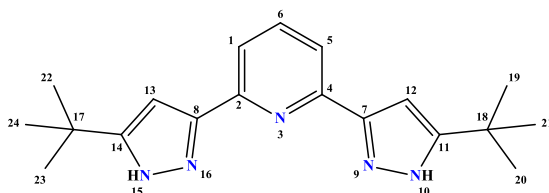


Scheme 2.10: Synthetic route to 2,6-bis(5-(*tert*-butyl)-1*H*-pyrazol-3-yl)pyridine (**9**). [Adapted from Fenton *et al.*,¹⁹ Zhou *et al.*,²⁰ Satake *et al.*,²¹ and Gal *et al.*,²²]

A 250 mL round-bottom flask was charged with high-grade sodium ethoxide powder (2.50 g, 36.7 mmol) and toluene (50.0 mL). To this mixture was added 3,3-dimethyl-2-butanone (4.00 mL, 32.0 mmol) followed immediately by dimethyl pyridine-2,6-dicarboxylate (3.00 g, 15.4 mmol). The pale yellow-orange mixture

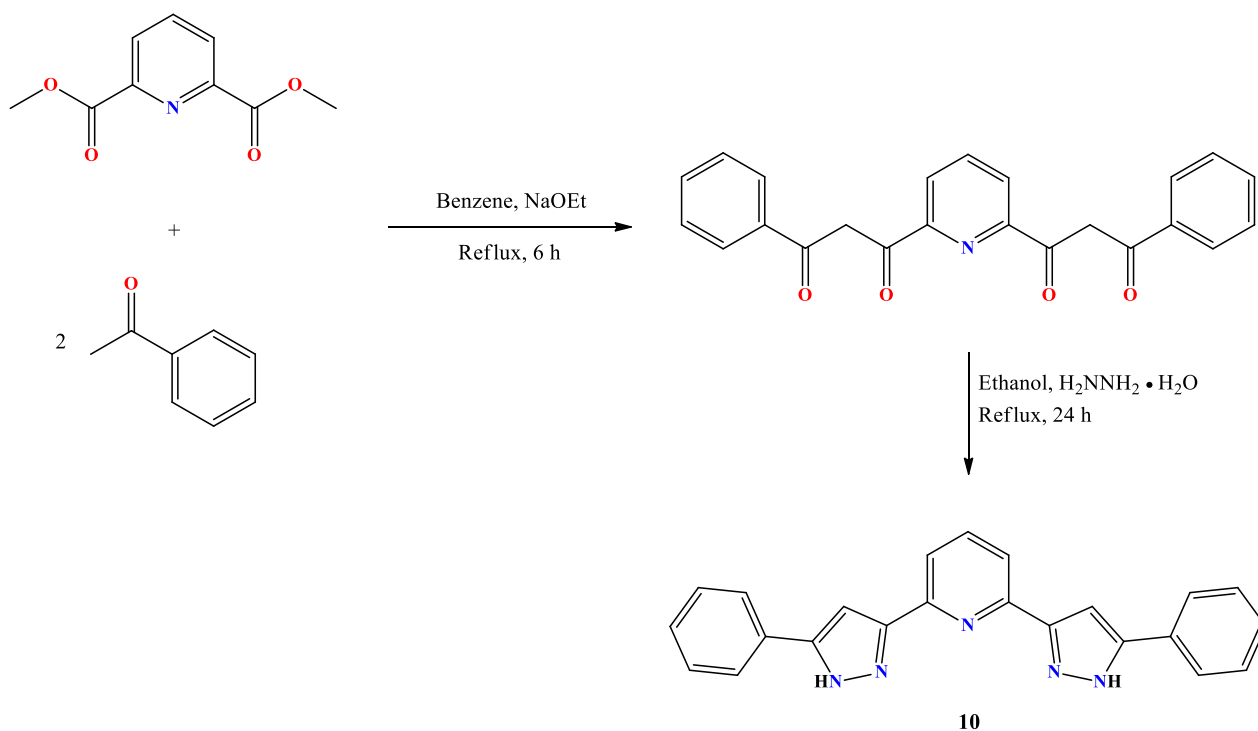
was refluxed for 18 hours, eventually turning a dark yellow-orange hue. After the mixture was allowed to cool to room temperature, distilled water (50.0 mL) was added, which immediately drained the colour from the organic phase. Concentrated H₂SO₄ was added dropwise to the immiscible layers until the colour permanently returned to the organic phase (pH 6–7). The organic layer was separated from the aqueous layer and washed several times with brine (2 × 30 mL) and distilled water (3 × 50 mL). The organic layer was dried over anhydrous Na₂SO₄ and concentrated *in vacuo* to yield the crude intermediary tetraketone species, 1,1'-(pyridine-2,6-diyl)bis(4,4-dimethylpentane-1,3-dione), as a pale-yellow solid (2.95 g, ~57.8%).

To a refluxing solution of the crude tetraketone species (2.95 g, ~8.90 mmol) in ethanol (50.0 mL) was added hydrazine monohydrate (1.00 mL, 20.6 mmol) in ethanol (20.0 mL) and 2 drops of concentrated H₂SO₄. After a refluxing period of 24 hours, the solvent was removed via rotary evaporation. The crude product was redissolved in chloroform (50.0 mL) and washed with distilled water several times (3 × 50 mL) until the aqueous phase became clear. The organic phase was separated, dried over anhydrous Na₂SO₄, and concentrated to ~10 mL. The concentrated product was purified by means of vacuum distillation using a kugelrohr short path distillation apparatus, yielding ligand **9** (2.49 g, 50.0%) as an off-white solid.



FT-IR (KBr pellet, cm⁻¹) 3210 (pyrazole C–H str), 3102 (aromatic C–H str), 2961 (aliphatic C–H str), 1598 (pyridine C=N str), 1575 (pyrazole C=N str), 1364 (–CH₃ bend), 804 (aromatic C–H bend). **¹H NMR (300 MHz, CDCl₃)** δ 8.90 (br, NH10/15, 2H), 7.64 (m, H6, 1H), 7.55 (m, H1/5, 2H), 6.60 (s, H12/13, 2H), 1.34 (s, H19–

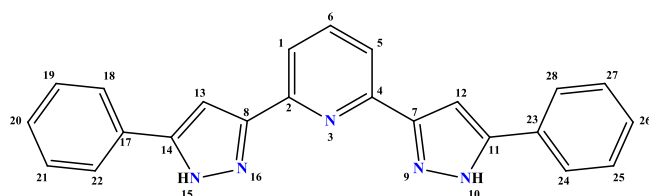
24, 18H). **¹³C{¹H} NMR (75 MHz, CDCl₃)** δ 159.6 (C7/8), 149.6 (C2/4), 146.2 (C11/14), 137.5 (C6), 118.7 (C1/5), 99.9 (C12/13), 31.8 (C17/18), 30.5 (C19–24). **Calculated exact mass (μ)** 323.21. **ESI-MS (m/z)** 162.61 (M + 2H)²⁺, 324.22 (M + H)⁺. **EA calculated (%)** C, 70.56; H, 7.79; N, 21.65. **EA found (%)** C, 70.50; H, 7.82; N, 21.31. **m.p.** 158–159 °C. See full range of spectra on pages 39–42 of *Appendix A — SPECTRA*.

2.3.11 Synthesis of 2,6-bis(5-phenyl-1H-pyrazol-3-yl)pyridine (**10**)

Scheme 2.11: Synthetic route to 2,6-bis(5-phenyl-1H-pyrazol-3-yl)pyridine (**10**). [Adapted from Zhou *et al.*²⁰ and Pons *et al.*²³]

A 250 mL round-bottom flask was charged with high-grade sodium ethoxide powder (2.50 g, 36.7 mmol) and benzene (50.0 mL). To this mixture was added acetophenone (3.80 mL, 32.6 mmol) followed immediately by dimethyl pyridine-2,6-dicarboxylate (3.00 g, 15.4 mmol). The light orange mixture was refluxed for 6 hours, eventually becoming an orange-brown hue. To this organic mixture was added 50.0 mL distilled water, followed slowly by the dropwise addition of 32% HCl until the benzene layer was yellow in colour (pH 6–7). The organic layer was separated and concentrated *in vacuo* to yield the crude intermediary tetraketone species, 3,3'-(pyridine-2,6-diyl)bis(1-phenylpropane-1,3-dione), as a yellow oil (4.41 g, ~77.1%).

To a refluxing solution of the crude tetraketone species (4.41 g, ~11.9 mmol) in ethanol (50.0 mL) was added hydrazine monohydrate (2.00 mL, 41.2 mmol) in ethanol (20.0 mL) and 2 drops of concentrated H₂SO₄. After refluxing for 24 hours, the mixture was allowed to reach the ambient temperature and remained undisturbed in the fumehood overnight. This led to the formation of white needle-like crystals and was collected by filtration. The product was dried in an oven at 100 °C overnight, yielding ligand **10** (3.92 g, 70.0%).



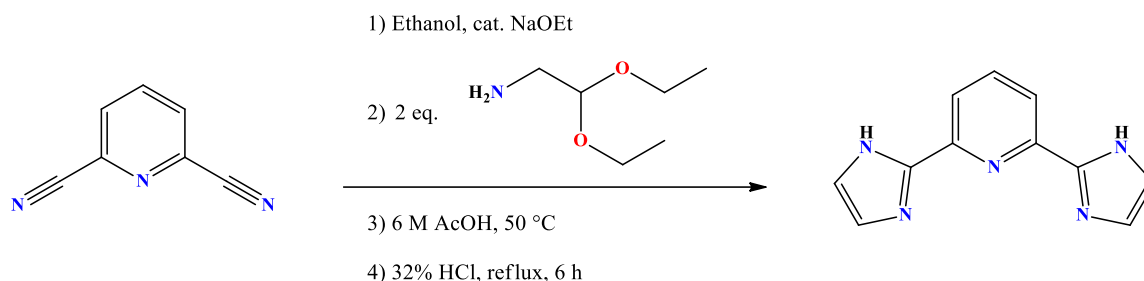
FT-IR (KBr pellet, cm^{-1}) 3461 (N–H str), 3196 (pyrazole C–H str), 1602 (pyridine C=N str), 1562 (pyrazole C=N str), 1468 (aromatic C=C str), 1452, 801 (aromatic C–H bend), 762 (=C–H out-of-plane bend), 692 (=C–H out-of-plane bend).

^1H NMR (600 MHz, $\text{DMSO-}d_6$) δ 7.90 (m, 7.5H), 7.44 (m, 7.5H).

$^{13}\text{C}\{^1\text{H}\}$ NMR (150 MHz, $\text{DMSO-}d_6$) δ 152.1 (C7/8), 147.5 (C2/4), 143.1 (C11/14), 139.3 (C6), 133.9 (C17/23), 129.1 (C19/21/25/27), 128.0 (C20/26), 125.6 (C18/22/24/28), 118.9 (C1/5), 101.2 (C12/13).

Calculated exact mass (μ) 363.15. **ESI-MS (m/z)** 364.16 ($\text{M} + \text{H}^+$), 386.14 ($\text{M} + \text{Na}^+$). **EA calculated (%)** C, 76.01; H, 4.71; N, 19.27. **EA found (%)** C, 75.95; H, 4.80; N, 19.10. **m.p.** 157–158 °C. See full range of spectra on pages 43–46 of *Appendix A — SPECTRA*.

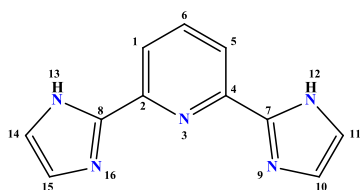
2.3.12 Synthesis of 2,6-bis(1H-imidazol-2-yl)pyridine



Scheme 2.12: Synthetic route to 2,6-bis(1H-imidazol-2-yl)pyridine. [Adapted from Stupka *et al.*,²⁴ Voss *et al.*,²⁵ Rigsby *et al.*,²⁶ and Hashiguchi *et al.*,²⁷]

Pyridine-2,6-dicarbonitrile (1.00 g, 7.74 mmol) was quantitatively transferred to a 100 mL round-bottom flask and dissolved using absolute ethanol (10 mL). To this dissolved mixture, was added high-grade sodium ethoxide (0.100 g, 1.47 mmol), followed by gentle stirring at room temperature for 2 hours. Aminoacetaldehyde diethylacetal (2.25 mL, 15.5 mmol) and 6 M acetic acid (0.500 mL) was added to the reaction mixture and stirred for 1 hour at 50 °C, followed by the addition of 32% HCl (2.00 mL). This pale-yellow mixture was vigorously stirred under refluxing conditions for 6 hours.

The solvent was removed from the ambiently cooled reaction mixture via rotary evaporation and the remaining light-yellow oil was redissolved in deionised water (20 mL). The aqueous phase was extracted with diethyl ether (3×20 mL) and the organic layers were discarded. The pH of the aqueous layer was modified with 2 M NaOH to pH 6–7, resulting in the precipitation of a white solid. The solid was collected by filtration, dried overnight in an oven at 80 °C and recovered as a fluffy white solid (1.31 g, 80.1%).

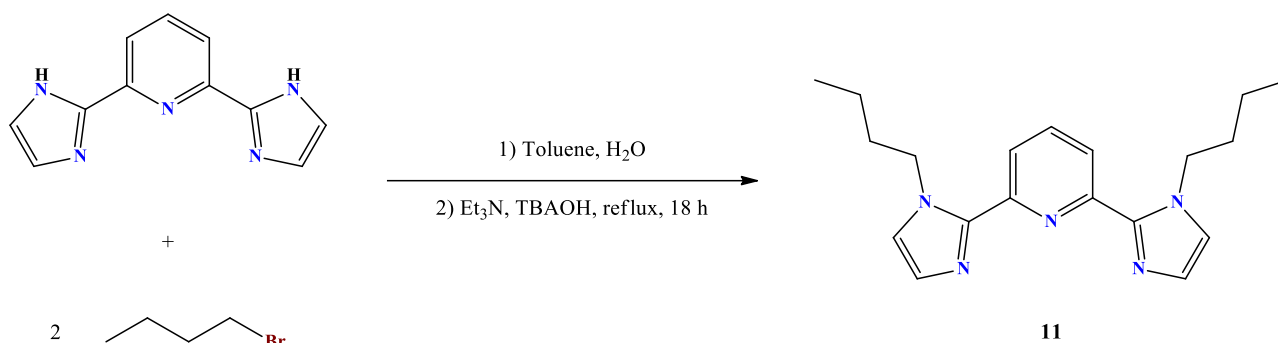


FT-IR (KBr pellet, cm^{-1}) 3479 (N–H str), 3041 (aromatic C–H str), 1614 (pyridine C=N str), 1583 (imidazole C=N str). **^1H NMR (400 MHz, $\text{DMSO-}d_6$)** δ 7.94 (m, *H*6, 1H), 7.87 (m, *H*1/5, 2H), 7.46 (s, *H*11/14, 2H), 7.12 (s, *H*10/15, 2H). **$^{13}\text{C}\{^1\text{H}\}$ NMR (100 MHz, $\text{DMSO-}d_6$)** δ 147.7 (*C*7/8),

145.7 (*C*2/4), 138.5 (*C*6), 129.8 (*C*10/15), 118.5 (*C*11/14), 117.3 (*C*1/5). **Calculated exact mass (μ)** 211.09.

ESI-MS (*m/z*) 212.09 ($\text{M} + \text{H}^+$), 234.08 ($\text{M} + \text{Na}^+$), 250.05 ($\text{M} + \text{K}^+$). **EA calculated (%)** C, 62.55; H, 4.29; N, 33.16. **EA found (%)** C, 62.84; H, 4.40; N, 32.77. **m.p.** >250 °C. See full range of spectra on pages 47–50 of *Appendix A — SPECTRA*.

2.3.13 Synthesis of 2,6-bis(1-butylimidazol-2-yl)pyridine (**11**)



Scheme 2.13: Synthetic route to 2,6-bis(1-butylimidazol-2-yl)pyridine (**11**). [Based on *Method 3*]

Method 1 [Adapted from Rigsby *et al.*²⁶ and Zhang *et al.*²⁸]

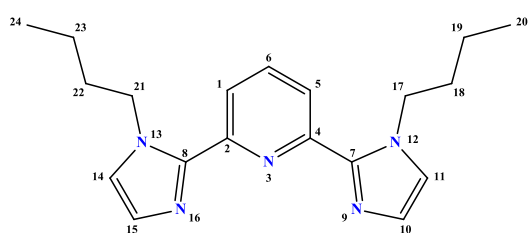
To a stirring suspension of 2,6-bis(1*H*-imidazol-2-yl)pyridine (0.500 g, 2.37 mmol) in acetone (20 mL) was added KOH (0.300 g, 5.34 mmol). The mixture was stirred at room temperature for 10 minutes, followed by the addition of 1-bromobutane (0.600 mL, 5.56 mmol) and subsequent stirring at room temperature for 8 hours. Thereafter, 2 M NaOH (20 mL) was added and the mixture was extracted multiple times with DCM (5 × 20 mL). The combined organic layers were collected, dried over anhydrous Na_2SO_4 and filtered. The solvent and unreacted starting material were removed under reduced pressure and the product was dried using a high vacuum pump, whereafter ligand **11** (0.0810 g, 10.6 %) was obtained as a yellow-brown oil.

Method 2 [Adapted from Wang *et al.*²⁹]

A mixture of 2,6-bis(1*H*-imidazol-2-yl)pyridine (0.500 g, 2.37 mmol) and 40% aqueous NaOH (5 mL) in DMF (20 mL) was stirred for 1 hour at room temperature. 1-Bromobutane (0.600 mL, 5.56 mmol) was slowly added to this mixture and stirred for 18 hours at room temperature. The resulting solution was poured into deionised water (20 mL) and extracted multiple times with chloroform (4 × 20 mL). The combined organic layers were washed with H_2O (3 × 20 mL) and dried over anhydrous Na_2SO_4 . The solvent and unreacted starting material were removed under reduced pressure and the product was dried using a high vacuum pump, whereafter ligand **11** (0.122 g, 15.9 %) was obtained as a yellow-brown oil.

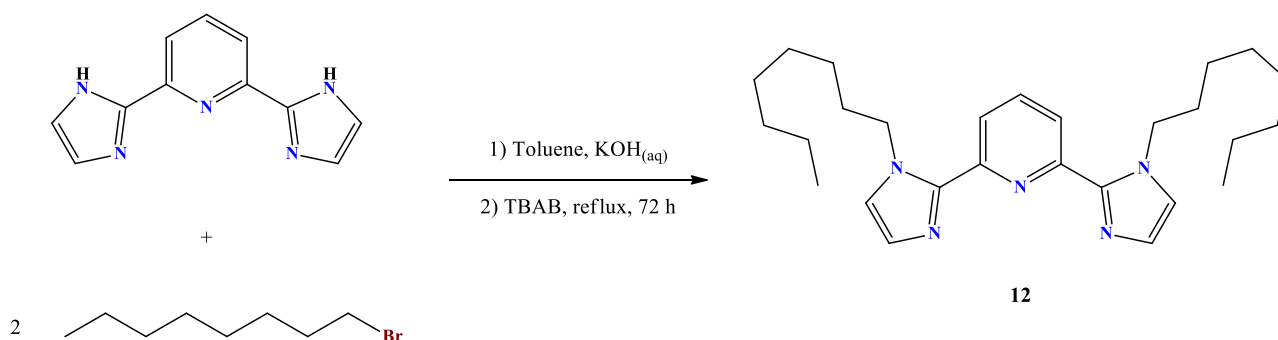
Method 3 [Unique method]

A 100 mL round-bottom flask was charged with toluene (20 mL), deionised water (20 mL) and 2,6-bis(1*H*-imidazol-2-yl)pyridine (0.500 g, 2.37 mmol). While stirring at room temperature, Et₃N (1.60 mL, 11.5 mmol) and tetrabutylammonium hydroxide (3 drops) were added, followed by the incremental addition of 1-bromobutane (0.600 mL, 5.56 mmol). The reaction mixture was heated to reflux and stirred for 18 hours. After the reaction cooled to room temperature, the yellow organic layer was separated from the aqueous phase and washed with brine (2 × 20 mL) and distilled H₂O (3 × 20 mL). The organic phase was dried over anhydrous Na₂SO₄, filtered and the product was concentrated using a rotary evaporator. No additional purification steps were necessary, ultimately yielding ligand **11** (0.493 g, 64.4 %) as a yellow-brown oil.



FT-IR (ATR, cm⁻¹) 2956 (aliphatic C–H str), 1572 (imidazole C=N str), 1466 (–CH₂– bend). **¹H NMR (400 MHz, CDCl₃)** δ 8.00 (d, *J* = 7.6 Hz, *H*_{1/5}, 2H), 7.84 (m, *H*₆, 1H), 7.13 (d, *J* = 1.1 Hz, *H*_{10/15}, 2H), 7.03 (d, *J* = 1.1 Hz, *H*_{11/14}, 2H), 4.49 (t, *J* = 7.3 Hz, *H*_{17/21}, 4H), 1.66 (p, *J* = 7.3 Hz, *H*_{18/22},

4H), 1.18 (sex, *J* = 7.3 Hz, *H*_{19/23}, 4H), 0.77 (t, *J* = 7.3 Hz, *H*_{20/24}, 6H). **¹³C{¹H} NMR (100 MHz, CDCl₃)** δ 149.8 (*C*_{7/8}), 145.1 (*C*_{2/4}), 137.7 (*C*₆), 128.6 (*C*_{10/15}), 123.0 (*C*_{11/14}), 122.5 (*C*_{1/5}), 47.4 (*C*_{17/21}), 33.4 (*C*_{18/22}), 19.8 (*C*_{19/23}), 13.6 (*C*_{20/24}). **Calculated exact mass (μ)** 323.21. **ESI-MS (*m/z*)** 324.22 (*M* + *H*)⁺, 346.20 (*M* + *Na*)⁺, 362.17 (*M* + *K*)⁺. **EA calculated (%)** C, 70.56; H, 7.79; N, 21.65. **EA found (%)** C, 70.50; H, 7.68; N, 21.31. See full range of spectra on pages 51–54 of **Appendix A — SPECTRA**.

2.3.14 Synthesis of 2,6-bis(1-octylimidazol-2-yl)pyridine (12)

Scheme 2.14: Synthetic route to 2,6-bis(1-octylimidazol-2-yl)pyridine (**12**).

Method 1 [Adapted from Rigsby *et al.*²⁶ and Li *et al.*³⁰]

To a 100 mL round-bottom flask was added 2,6-bis(1*H*-imidazol-2-yl)pyridine (1.00 g, 4.73 mmol), potassium *tert*-butoxide (0.540 g, 4.81 mmol) and reagent grade acetone (50 mL). After this yellow mixture was stirred for 3 hours at room temperature, 1-bromooctane (1.65 mL, 9.55 mmol) was added dropwise and

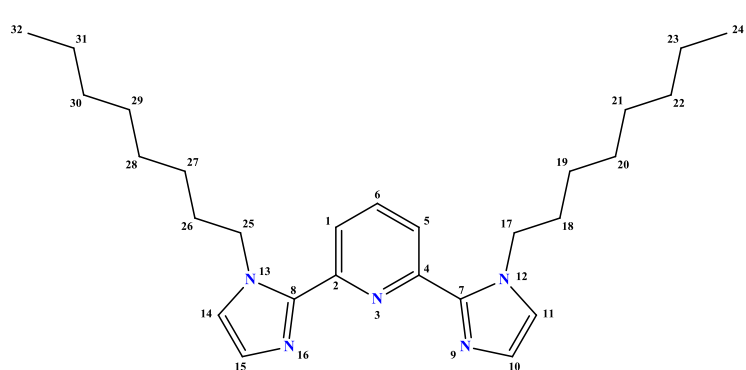
the mixture was refluxed for 18 hours using a narrow-bore condenser to avoid excessive loss of acetone from the system. Upon cooling to room temperature, the solvent was removed *in vacuo* and the resulting residual brown oil was extracted using DCM (2×30 mL). The combined organic solution was washed with brine and the solvent was removed under reduced pressure to yield a crude product that was further purified via gravitational column chromatography using silica gel, with a DCM/EtOAc (v/v, 7:3) eluent system ($R_f = 0.388$). Ligand **12** (0.220 g, 10.7%) was obtained as a viscous yellow-brown oil.

Method 2

A 50 mL round-bottom flask was charged with 2,6-bis(1*H*-imidazol-2-yl)pyridine (1.00 g, 4.73 mmol), NaOH (0.397 g, 9.93 mmol) and distilled water (10 mL), followed by vigorous stirring at ambient conditions until the suspended solution became homogeneous. This was followed by the gradual addition of 1-bromooctane (1.65 mL, 9.55 mmol) in acetonitrile (20 mL) and 5 drops of tetrabutylammonium hydroxide, whereafter the mixture was refluxed for 24 hours. The yellow solution was concentrated under reduced pressure and redissolved in DCM. The organic solution was washed with brine (2×25 mL) and distilled water (2×25 mL), followed by the removal of the solvent *in vacuo*. The crude product was purified by means of gravitational column chromatography using silica gel with DCM/EtOAc (v/v, 1:1) as the eluent system ($R_f = 0.450$). After the removal of the solvent system *in vacuo*, ligand **12** (0.271 g, 13.1%) was obtained as a yellow-brown oil.

Method 3 [Unique method]

2,6-Bis(1*H*-imidazol-2-yl)pyridine (2.00 g, 9.47 mmol), potassium hydroxide (1.33 g, 23.7 mmol) and 20 mL distilled water was added to a 100 mL round-bottom flask and allowed to stir at room temperature for 2 hours. To this cloudy aqueous solution was added 1-bromooctane (3.30 mL, 19.1 mmol) in toluene (20 mL) and tetrabutylammonium bromide (50,0 mg, 0.155 mmol). The resulting biphasic mixture was refluxed for 72 hours, whereafter a yellow organic layer was observed. The organic layer was separated, washed with brine (3×30 mL) and distilled water (2×30 mL), followed by the addition of anhydrous Na₂SO₄ as drying agent. After filtering off the Na₂SO₄, the solution was concentrated *in vacuo* at 100 °C. Additional purification via column chromatography (silica gel) was required as residual alkyl halide was still present. Initially, CHCl₃ was used as eluent ($R_f = 0.0890$) to rid the column of residual alkyl halide, followed by EtOAc as eluent ($R_f = 0.664$) to flush out the pure product. After the removal of the solvent under reduced pressure, ligand **12** (2.49 g, 60.4%) was obtained in moderate yield as a yellow-brown oil.



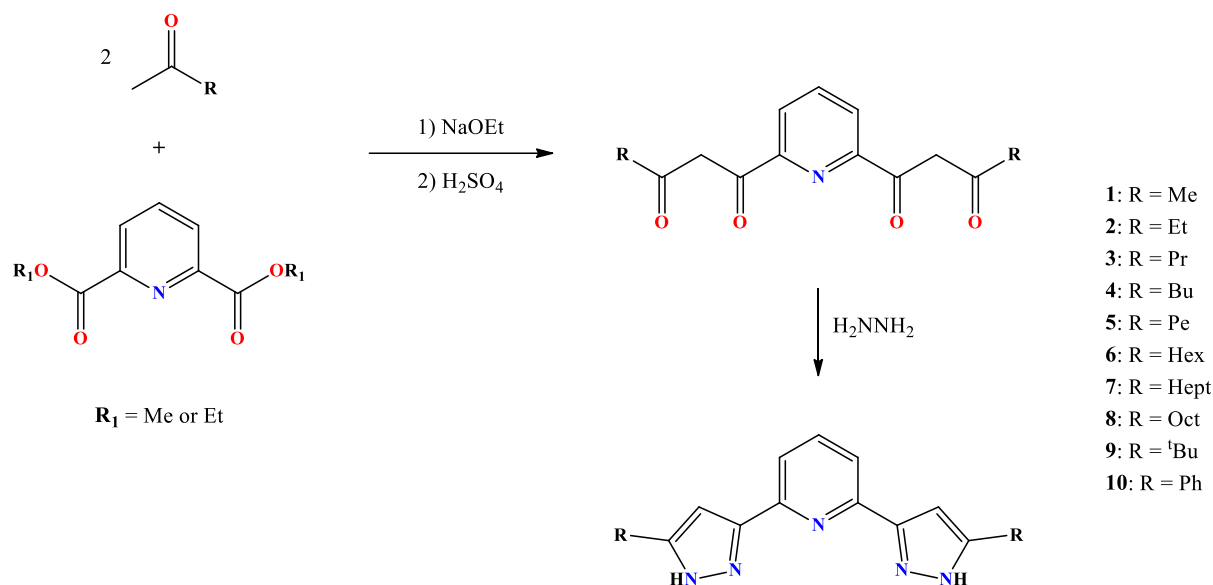
FT-IR (ATR, cm^{-1}) 3104 (aromatic C–H str), 2922/2853 (aliphatic C–H str), 1573 (imidazole C=N str), 1466 ($-\text{CH}_2-$ bend). **^1H NMR (300 MHz, CDCl_3)** δ 8.00 (m, $H_{1/5}$, 2H), 7.84 (m, H_6 , 1H), 7.12 (d, $J = 1.1$ Hz, $H_{10/15}$, 2H), 7.02 (d, $J = 1.1$ Hz, $H_{11/14}$, 2H), 4.47 (t, $J = 7.2$ Hz, $H_{17/25}$, 4H), 1.66 (p, $J = 7.0$ Hz, $H_{18/26}$,

4H), 1.19 (m, $H_{19-23/27-31}$, 20H), 0.81 (t, $J = 7.0$ Hz, $H_{24/32}$, 6H). **$^{13}\text{C}\{^1\text{H}\}$ NMR (75 MHz, CDCl_3)** δ 149.8 ($C_{7/8}$), 145.0 ($C_{2/4}$), 137.7 (C_6), 128.6 ($C_{10/15}$), 123.0 ($C_{11/14}$), 122.5 ($C_{1/5}$), 47.6 ($C_{17/25}$), 31.7 ($C_{18/26}$), 31.4 ($C_{19/27}$), 29.2 ($C_{20/28}$), 29.1 ($C_{21/29}$), 26.6 ($C_{22/30}$), 22.6 ($C_{23/31}$), 14.1 ($C_{24/32}$). **Calculated exact mass (μ)** 435.34. **ESI-MS (m/z)** 324.22 ($\text{M} - \text{C}_8\text{H}_{15}$)⁺, 436.34 ($\text{M} + \text{H}$)⁺, 458.33 ($\text{M} + \text{Na}$)⁺. **EA calculated (%)** C, 74.44; H, 9.49; N, 16.08. **EA found (%)** C, 74.02; H, 9.63; N, 16.30. See full range of spectra on pages 55–58 of **Appendix A — SPECTRA**.

2.4 Results and discussion

2.4.1 Pyrazole-pyridinyl ligands

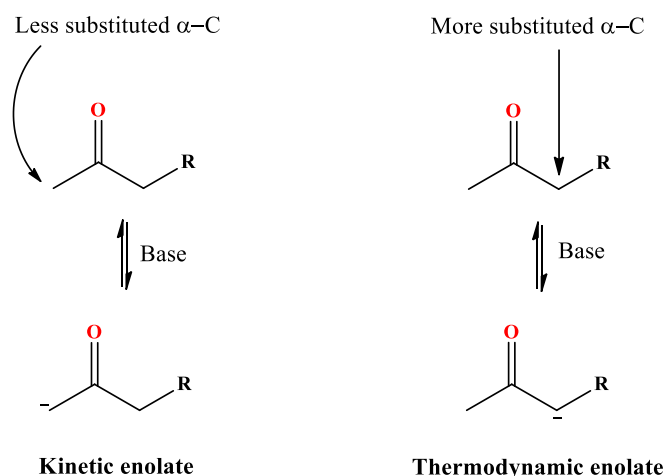
The immense synthetic part of this study was initiated with the “trial and error” approach to the synthesis of the first ligand in a series of ten pyrazole-pyridinyl ligands. In general, ligands **1–10** were obtained via the Claisen-Schmidt condensation of either dimethyl- or diethyl pyridine-2,6-dicarboxylate with the appropriate alkyl ketone, yielding a crude symmetrical bis(1,3-dicarbonyl) intermediary species. This crude product was used immediately without any additional purification. Subsequently, the classic Knorr pyrazole synthesis³¹ with hydrazine was performed to afford the desired pyrazole-pyridinyl ligands **1–10** (**Scheme 2.15**).



Scheme 2.15: A general framework for the syntheses of ligands **1–10**.

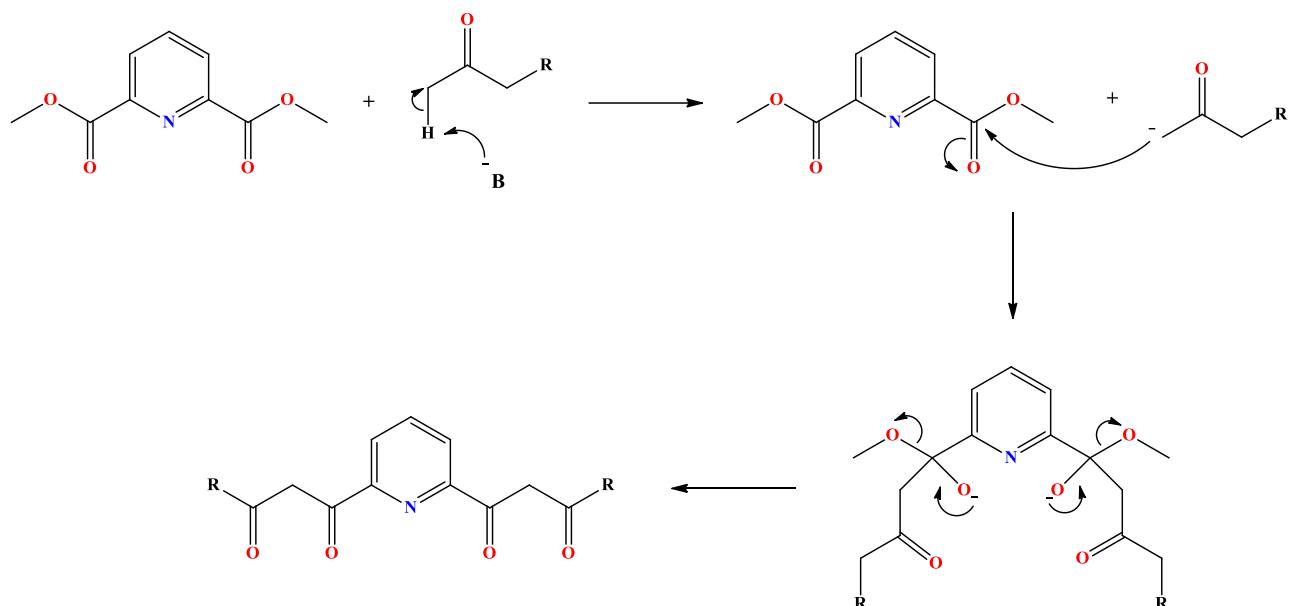
After numerous purification procedures of the crude intermediary tetraketone species, it was decided to forego any additional purification processes (recrystallisation/column chromatography/kugelrohr distillation) due to incremental losses of valuable product. Instead, the final pyrazole-pyridinyl product was purified in order to maximise yields. The final product seemed somewhat easier to purify compared to the intermediary tetraketone species.

These Claisen-Schmidt condensation reactions are classic enolate-type chemistry and care should be taken to ensure that the correct reagents and conditions are selected prior to performing these reactions. Firstly, the major tetraketone product is formed via the deprotonation of the least substituted α -carbon - in this case the terminal α -carbon. This gives rise to what is commonly referred to as the “kinetic” enolate (**Scheme 2.16**). Two independent enolates subsequently attack the carbonyls on either side of the pyridine and form an additional single bond, followed by the evacuation of two methoxides in order to maintain 8 valence electrons in carbon’s outermost electron shell ($2s^2, 2p^6$). See **Scheme 2.17** for the general Claisen-Schmidt condensation reaction mechanism for the formation of the major regioselective product.

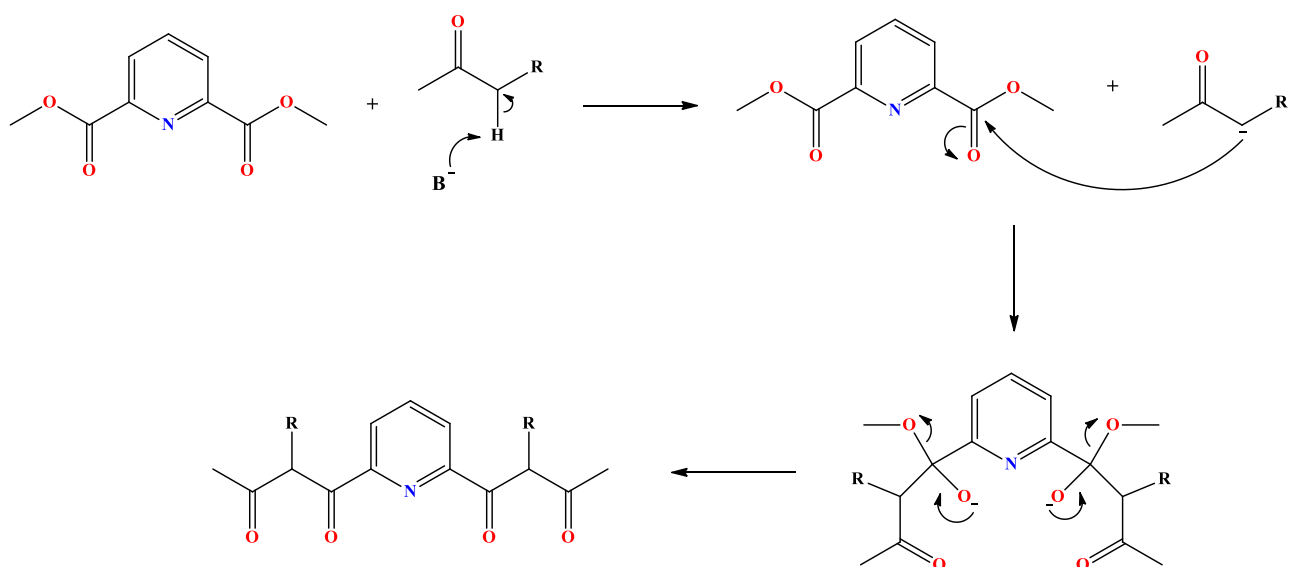


Scheme 2.16: Kinetic- and thermodynamic enolate formation.

On the other hand, once a suitable base deprotonates the internal and more substituted α -carbon, one might end up with unwanted minor products by means of “thermodynamic” enolate attack (**Scheme 2.18**). “Kinetic” enolates are called such because their early predominant formation depends on relative rate constants for enolate formation, *i.e.*, they form much faster but are less stable as well. “Thermodynamic” enolates get their designation due to their ultimate predominance depending on overall equilibrium constants, *i.e.*, they are slower to form but are by and large more stable once they do form. Products from “kinetic” enolates are said to arise from “kinetic control”, while products that arise from “thermodynamic” enolates are said to arise from “thermodynamic control”.^{32,33}



Scheme 2.17: General Claisen-Schmidt condensation reaction mechanism using dimethyl 2,6-pyridinedicarboxylate and the appropriate alkyl ketone to form the tetraketone species as the major intermediary product.



Scheme 2.18: Claisen-Schmidt condensation reaction mechanism for the attack of the “thermodynamic” enolate on dimethyl 2,6-pyridinedicarboxylate, yielding the unwanted minor tetraketone species.

In this synthetic study, it was imperative that the appropriate alkyl ketone along with the corresponding diester was immediately available in solution to counter the formation of the thermodynamic products. Various bases were evaluated, but sodium ethoxide seemed to work well. To limit the formation of the thermodynamic intermediates, one might employ bulkier organic bases such as lithium diisopropylamide (LDA), potassium *tert*-butoxide (^tBuOK) or *tert*-butyllithium (^tBuLi). The use of strong

and less bulky bases such as sodium hydride and sodium hydroxide, are strongly discouraged, as this will promote the formation of unwanted thermodynamic products. It was interesting to note that ligands **9** and **10** had no hydrogens available on their internal α -carbons, which eliminated the possibility of “thermodynamic” side-products being formed. In theory, this should mean an increased overall yield for these ligands, yet maximum yields of merely 50 and 70% were recorded for ligands **9** and **10**, respectively. This indicates deprotonation by means of NaOEt is slow and that temperature is an important variable to consider.

An increase in temperature favours the formation of the thermodynamic enolate, while lower temperatures favour kinetic enolate formation.³⁴ In this study, higher refluxing temperatures were often introduced for two significant reasons: 1) dimethyl 2,6-pyridinedicarboxylate was poorly soluble in most organic solvents at lower temperatures and 2) LDA was a reasonably expensive organic base to use on large scale. In the syntheses of ligands **1–3** (**Schemes 2.2–2.4**), diethyl 2,6-pyridinedicarboxylate was first prepared via an esterification reaction of pyridine-2,6-dicarboxylic acid with absolute ethanol and a few drops of concentrated H₂SO₄ (**Scheme 2.1**). This was primarily done to circumvent the use of the less soluble dimethyl 2,6-pyridinedicarboxylate, but it was quickly realised that the reaction system did not have enough thermal energy to promote product formation, *i.e.*, the reaction was static. It was concluded that sodium ethoxide was most probably a weaker base ($pK_a \approx 15.5$; $pK_b \approx -1.50$) that needed the extra thermal energy to deprotonate the terminal α -carbon to form the carbanion/enolate in solution.

Once the synthesis of 2,6-bis(5-methyl-1*H*-pyrazol-3-yl)pyridine (**1**) commenced, it was realised that the ¹H NMR of the tetraketone intermediate species, 1,1'-(pyridine-2,6-diyl)bis(butane-1,3-dione), was slightly off. Additional purification via column chromatography [eluent: EtOAc:DCM (9:1)] was performed to rid the sample of most impurities and to determine whether the tetraketone intermediate product was in fact obtained. The sample was rerun, and it was noticed that the two –CH₂– proton environments at 6.86 ppm did not integrate for 4, but rather integrated for approximately 2 (**Figure 2.1**). At first, this seemed perplexing, especially since the rest of the spectrum appeared correct. It was subsequently concluded that a classic case of “keto-enol tautomerism” was present, whereby the keto tautomer was largely converted to the enol tautomer, even though the –OH proton was not observed in the ¹H NMR spectrum.^{33,34}

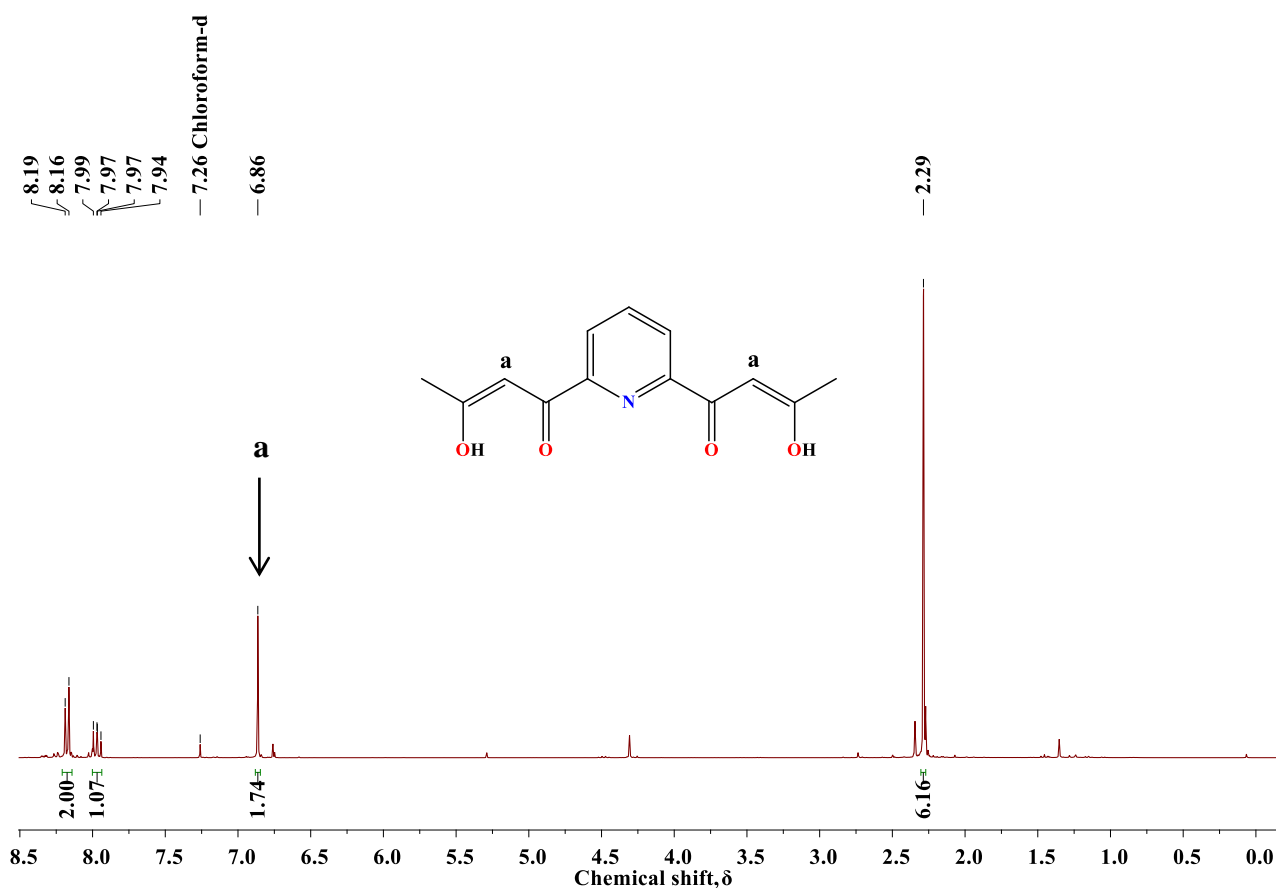
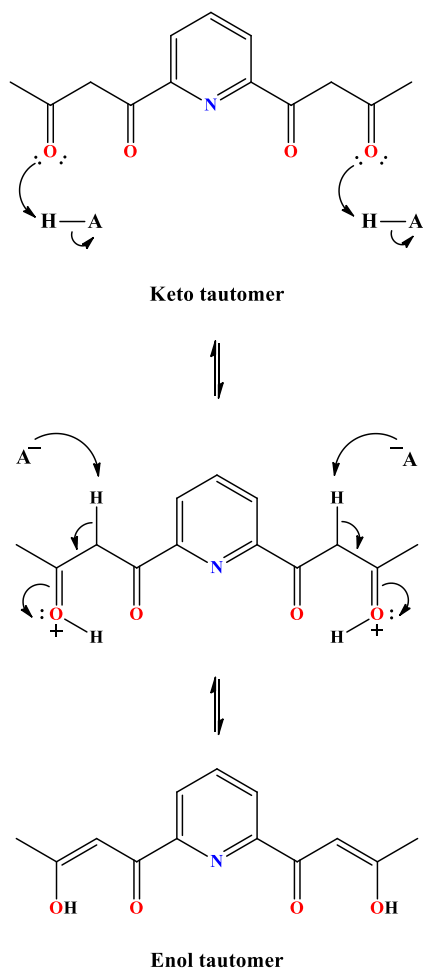


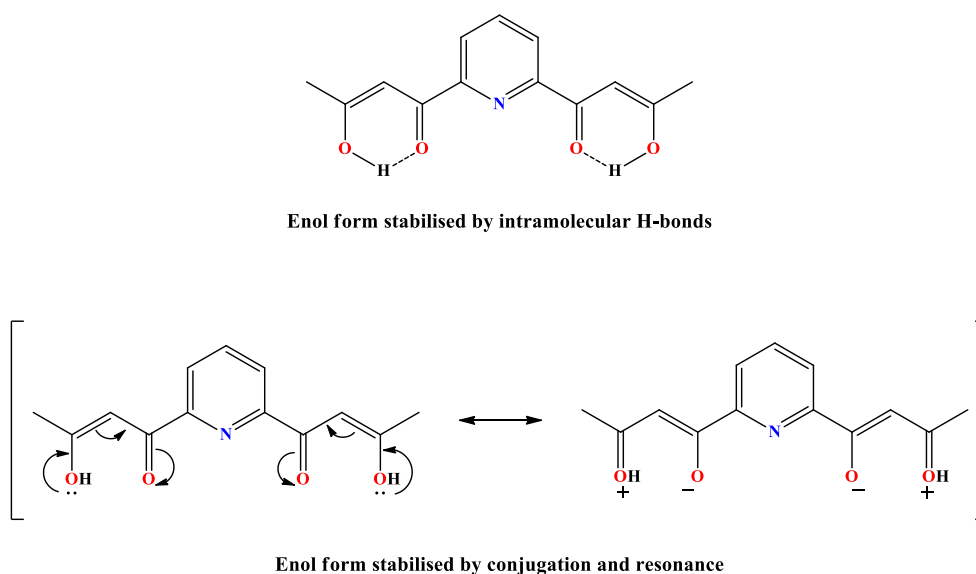
Figure 2.1: ^1H NMR spectrum of 1,1'-(pyridine-2,6-diyl)bis(3-hydroxybut-2-en-1-one), the precursor intermediate to 2,6-bis(5-methyl-1*H*-pyrazol-3-yl)pyridine (**1**).

Keto-enol tautomerism of carbonyl compounds is catalysed by both acids and bases, but since the syntheses of all the ligands involved acidic workups (pH 6–7), one can confidently assume that acid catalysed tautomerism was solely encountered. Acid catalysis occurs via protonation of the carbonyl oxygen atom to give an intermediate cation that loses a H^+ from its α -carbon by reaction with a base (A^-) to yield a neutral enol tautomer and the regeneration of the acid (HA) catalyst (**Scheme 2.19**).

In general, a carbonyl compound with a hydrogen atom on its α -carbon rapidly equilibrates or tautomerises to its corresponding enol. Most carbonyl compounds exist almost exclusively in the keto form at equilibrium, and it is typically quite difficult to isolate the pure enol.³⁴ In this study, the opposite was found to be true. This required further investigation regarding these pyridinyl-enol intermediates. It was recognised that the tetraketone species was a unique symmetrical bis(1,3-dicarbonyl) species and that additional stabilising factors were present: 1) favourable hydrogen bonding in a 6-membered ring and 2) stabilisation via conjugation (**Scheme 2.20**).³³ This, along with the aforementioned keto-enol chemistry via acid catalysis, appears to corroborate the integration oddity ($J \approx 2$) at 6.86 ppm in **Figure 2.1**.



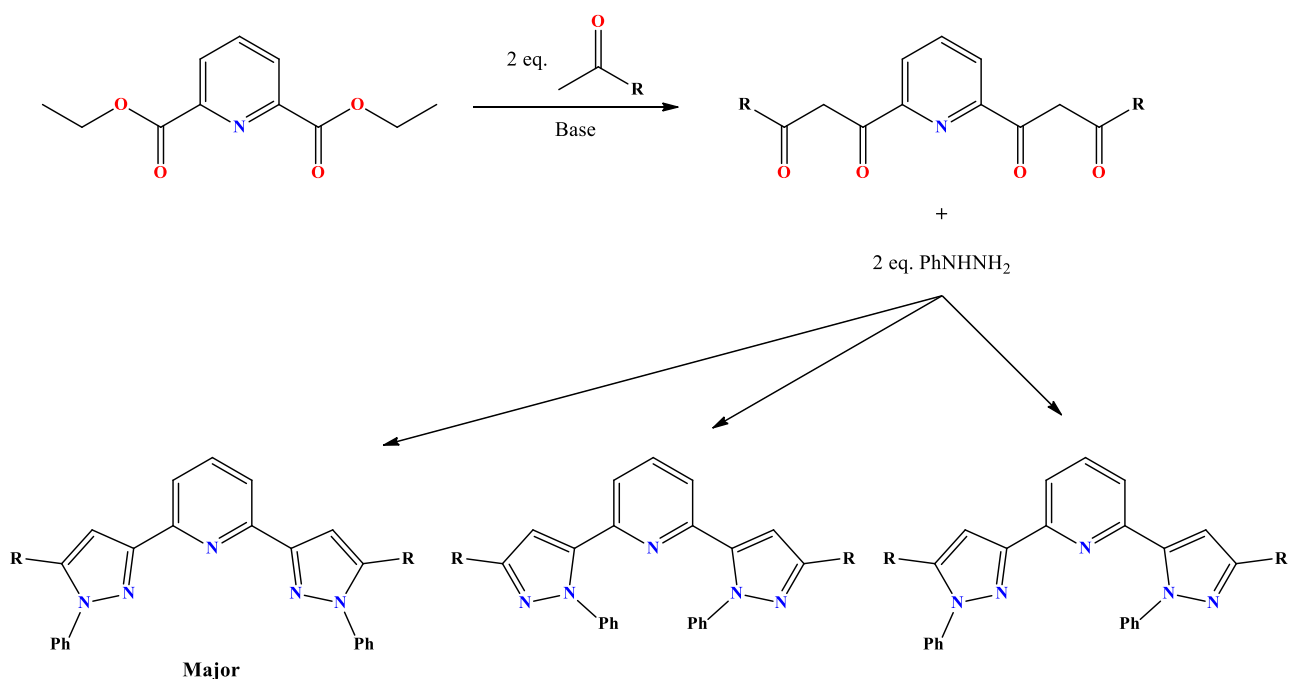
Scheme 2.19: Keto- and enol tautomers of 1,1'-(pyridine-2,6-diyl)bis(3-hydroxybut-2-en-1-one), the precursor intermediate to 2,6-bis(5-methyl-1*H*-pyrazol-3-yl)pyridine (**1**).



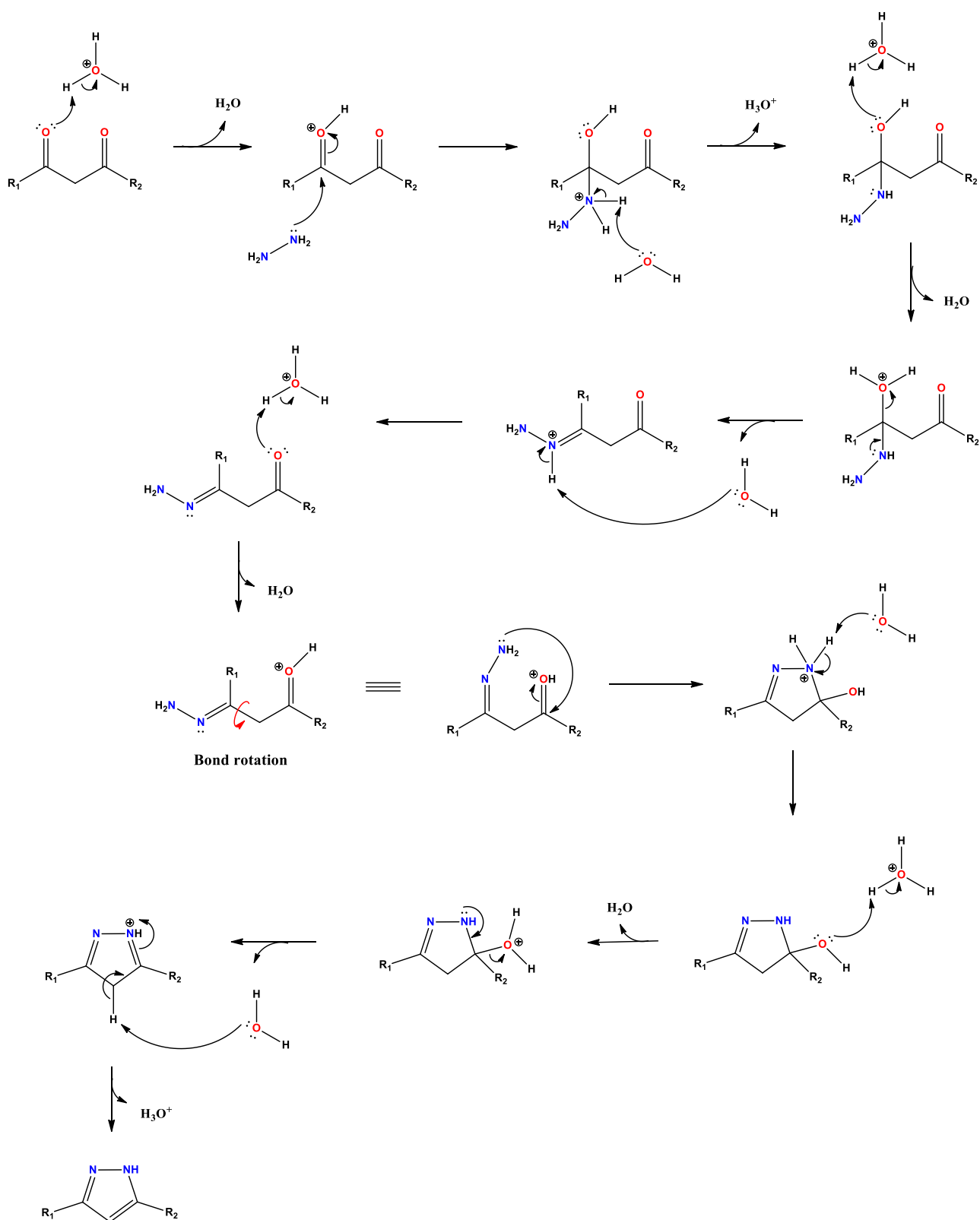
Scheme 2.20: Enol forms of 1,1'-(pyridine-2,6-diyl)bis(3-hydroxybut-2-en-1-one), the precursor to 2,6-bis(5-methyl-1*H*-pyrazol-3-yl)pyridine (**1**), stabilised via conjugation and intramolecular H-bonding.

The Claisen-Schmidt condensation reaction was followed by the cyclisation reaction of the bis(1,3-dicarbonyl) species with hydrazine in the presence of a catalytic amount of H₂SO₄ to generate the final bispyrazolyl ligand. This, as previously mentioned, was preferably done without any additional purification of the crude bis(1,3-dicarbonyl) intermediate species. The heterocyclisation reaction was experimentally straightforward and afforded excellent yields in excess of 90%. The mechanism of the heterocyclisation reaction was, however, difficult to piece together. This was eventually achieved by using information garnered from multiple sources to assemble a 12-step jigsaw reaction mechanism (**Scheme 2.22**).^{33–36} The cyclisation reaction is dependent on having a 1,3-carbonyl species in solution, which is not a problem since we know that the keto and enol forms (enol form favoured) of the intermediate species are in slow equilibrium with each other. It does however mean that the reaction is slow, and that ample time should be allowed for this reaction to go to completion. In this study, extended reaction times of up to 24 hours were allowed while refluxing in ethanol (**Schemes 2.2–2.11**).

Since simple “symmetrical” hydrazine was used for these syntheses, relatively uncomplicated final ligands were obtained. It should be noted, however, that a plethora of creative substituted pyrazolyl ligands are possible if one uses a hydrazine derivative to begin with.^{37,38} One drawback of this approach is the formation of pyrazolyl isomers with the substituents bound to either one of the two pyrazolyl nitrogens (**Scheme 2.21**). This approach was not deemed useful in this study, since the NH proton was a necessary component for hydrogen bonding during complexation in future solvent extraction experiments.



Scheme 2.21: Syntheses of possible phenyl substituted bispyrazolyl ligands using “unsymmetrical” phenylhydrazine. [Adapted from Ali³⁷ and Polezhaev *et al.*³⁸]



Scheme 2.22: A 12-step mechanism for the pyrazole cyclisation reaction with a 1,3-dicarbonyl species and hydrazine as reagents in the presence of a catalytic amount of acid. [Compiled from Clayden *et al.*,³³ McMurry,³⁴ Katritzky *et al.*³⁵ and Singh *et al.*³⁶]

The synthesis of ligand **1** was performed several times using four different methods, each time attempting to increase its meagre yield. At first, reaction conditions as outlined by Fenton *et al.*¹⁹ were closely replicated in their attempt to synthesise 1,1'-(pyridine-2,6-diyl)bis(butane-1,3-dione), the tetraketone precursor to ligand **1** (**Method 1, Section 2.3.2**). A poor overall yield of 19.3% was obtained, while an even poorer result of 16.5% was obtained by means of **Method 2**. Satake & Nakata²¹ reported a good yield of 71%, but care should be taken to compare results directly, seeing that they synthesised the monosubstituted pyrazolyl ligand and not the doubly substituted ligand as in this study. **Method 2** was repeated several times, yet yields above 16.5% were never attained. Therefore, another synthetic approach (**Method 3**) as reported by Gal *et al.*²² was used and incrementally improved yields to a maximum of 25.1%. This led to the combination of critical aspects of **Methods 1–3** into a new synthetic approach (**Method 4**). After numerous attempts, the yield of ligand **1** was marginally increased to 33.7% by using commercial high-grade sodium ethoxide powder as base, instead of synthesising it in-house. This, in addition to refluxing the mixture overnight, only seemed to increase its yield ever so slightly. The low yield proved to be a significant obstacle, seeing that large quantities (gram scale) of ligands were required for future solvent extraction purposes.

We proceeded to synthesise ligands **2–10** and noticed an interesting trend regarding the overall yields of the pyrazolyl ligands. In general, it appeared as though the yields of ligands **1–10** increased with an increase in the alkyl chain length. In the experimental section of this study (**Section 2.3**), the overall yields were reported and are summarised in **Table 2.2**, in addition to the boiling points of the appropriate ketone reagents.

Table 2.2: Percentage yields of ligands **1–10** compared to their corresponding ketone reagent's boiling point.

Ligand	R-substituent	Ketone reagent	Boiling point (° C) ^{†‡}	Yield (%)
1	Methyl	Acetone	56	33.7
2	Ethyl	2-Butanone	80	41.5
3	Propyl	2-Pentanone	101	42.6
4	Butyl	2-Hexanone	127	73.7
5	Pentyl	2-Heptanone	151	68.7
6	Hexyl	2-Octanone	173	72.4
7	Heptyl	2-Nonanone	192	68.9
8	Octyl	2-Decanone	211	80.5
9	<i>tert</i> -Butyl	3,3-Dimethyl-2-butanone	106	50.0
10	Phenyl	Acetophenone	202	70.0

[†] Boiling points of the ketone reagents retrieved from www.sigmaaldrich.com [‡] Measured at 760 mmHg

It became clear that there was a direct relationship between the boiling point of the ketone reagent and the overall yields of ligands **1–10**. In essence, this meant that the ketones with shorter alkyl chain lengths had a higher rate of evaporation that led to the loss of ketone starting material, even though excess amounts of

ketones were started with. For future purposes, one should look at employing more efficient cooling systems and perhaps use a Liebig condenser with a narrower bore or a Dimroth/Allihn condenser to increase the surface area for more efficient cooling to “lock in” as much of the volatile starting material in the reaction system as possible.

The ^1H and ^{13}C NMR spectra of ligands **1–10** were akin, with differing resonance signals in their upfield alkyl region (^1H : 0–3 ppm; ^{13}C : 0–35 ppm) depending on the length of the alkyl chain substituent. Therefore, 2,6-bis(5-butyl-1*H*-pyrazol-3-yl)pyridine (**4**) was selected as a representative ligand with its ^1H and ^{13}C NMR spectra illustrated by **Figures 2.2** and **2.3** respectively. The ^1H NMR spectrum appeared relatively clean after thorough purification, with all the proton signals accounted for and further substantiated with their accompanying integration values and splitting patterns. Ligand **4** had four characteristic resonances between 0.86 and 2.63 ppm that was assigned to the butyl moiety (*H17–H24*). Another telling feature, that indicated whether ligand **4** had successfully been synthesised, was the presence of a singlet at 6.40 ppm that integrated for 2. This resonance was attributed to the protons on the pyrazole rings and integrated for 2 due to symmetry (*H12/13*). An interesting observation, however, was the slight broadening of these pyrazolyl protons. This was likely due to rapid tautomerism in solution (**Scheme 2.23**). The last two signals in the aromatic region (7.35–7.60 ppm) were assigned to the three protons present on the pyridine ring, appearing as a doublet (*H1/5*) and a sharp triplet (*H6*) in two distinct chemical environments.

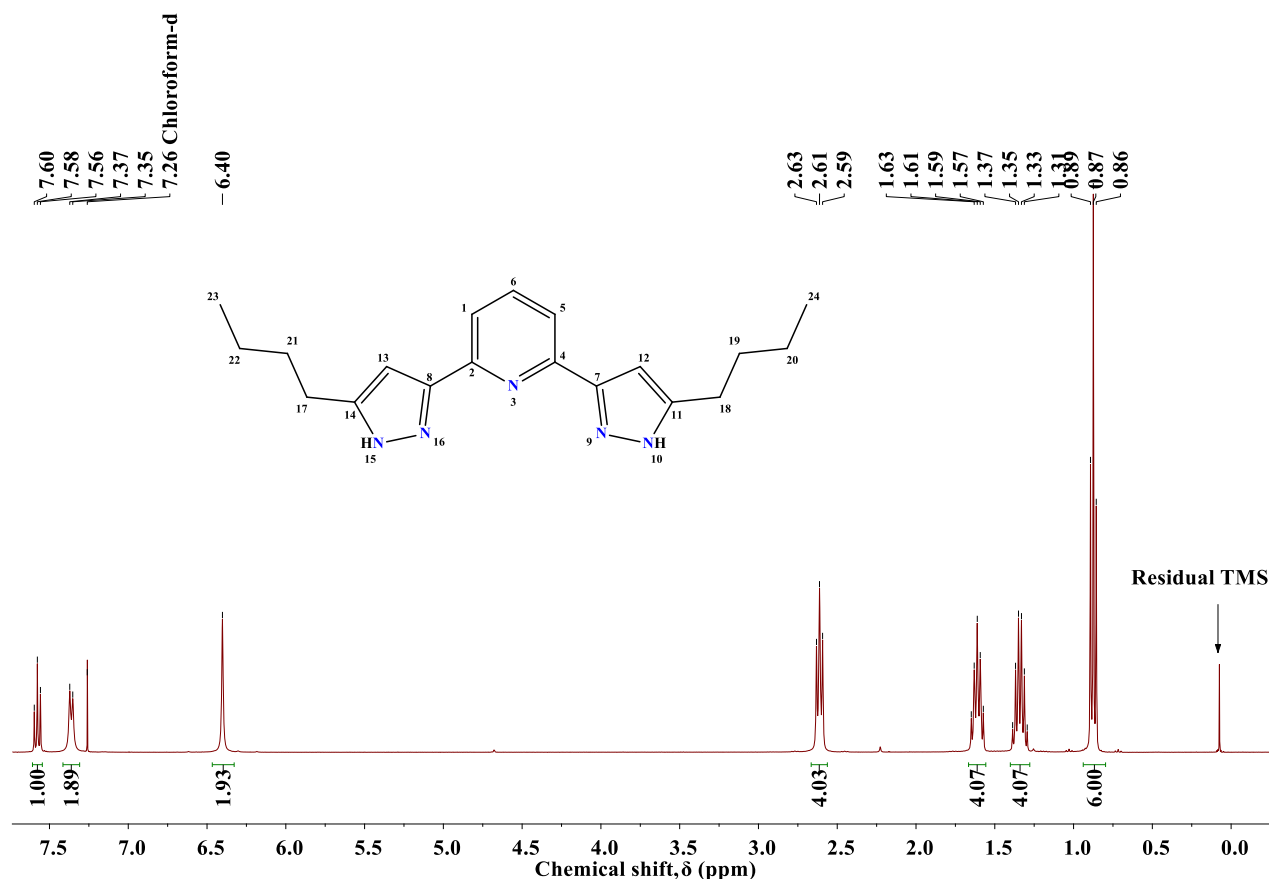
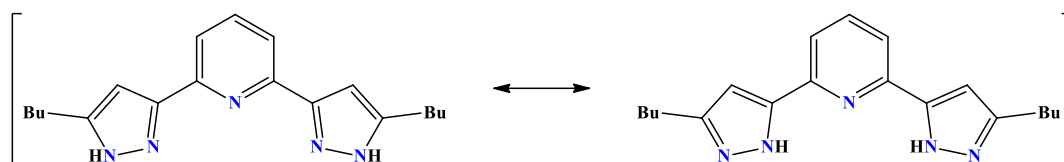


Figure 2.2: ^1H NMR spectrum of 2,6-bis(5-butyl-1*H*-pyrazol-3-yl)pyridine (**4**) [400 MHz, CDCl_3 , 25 °C].



Scheme 2.23: Tautomeric forms of 2,6-bis(5-butyl-1*H*-pyrazol-3-yl)pyridine (**4**) in solution.

The ^{13}C NMR spectrum of ligand **4** was also relatively easy to assign, with the four upfield resonances, between 14.0 and 31.8 ppm, attributable to the butyl moiety ($\text{C}17\text{--}24$). The aromatic pyridinyl ^{13}C signals at 118.2, 137.3 and 148.9 ppm were assigned to $\text{C}1/5$, $\text{C}6$ and $\text{C}2/4$, respectively, while the pyrazolyl ring had three distinct chemical environments with resonances at 101.6 ppm ($\text{C}12/13$), 145.1 ppm ($\text{C}11/14$) and 152.1 ppm ($\text{C}7/8$). The aforementioned tautomerism (**Scheme 2.23**) was now clearly evident in the ^{13}C NMR spectrum with broadened resonance signals at 152.1 and 145.1 ppm. The rapid shifting of the NH proton between $\text{N}9/10$ and $\text{N}15/16$ results in two chemically inequivalent environments, giving rise to broad ^{13}C signals. Similar monosubstituted pyrazolyl ligands have previously been reported by Pearce *et al.*,³⁹ and signal broadening was clearly evident as well. This was corroborated by Satake & Nakata²¹ and Henkelis *et al.*⁴⁰ who likewise saw the same tautomeric effects as reported in this study. The infrared (IR), mass spectrometry (MS) and elemental analyses (EA) results were consistent with expected results and point toward the successful synthesis of ligand **4**, although these are not shown here.

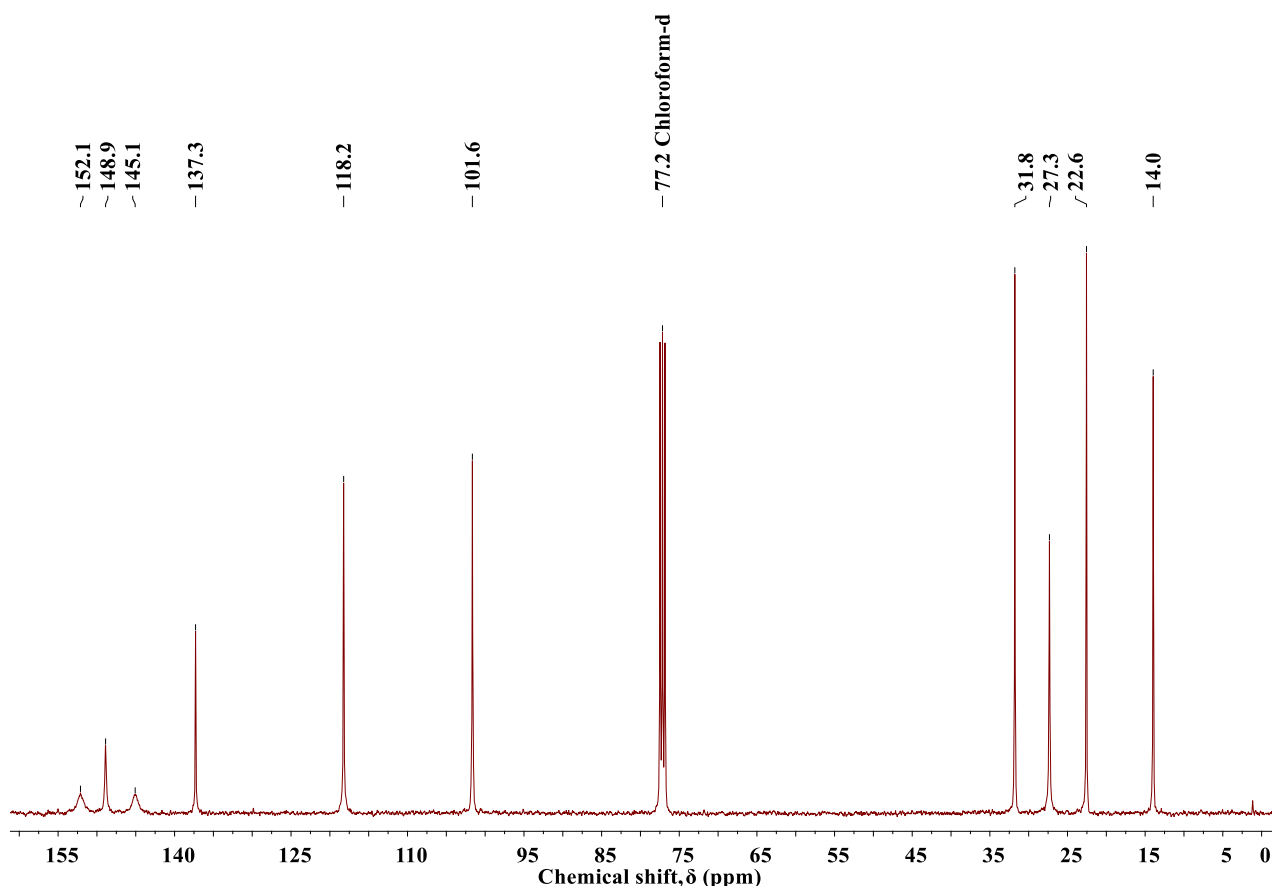
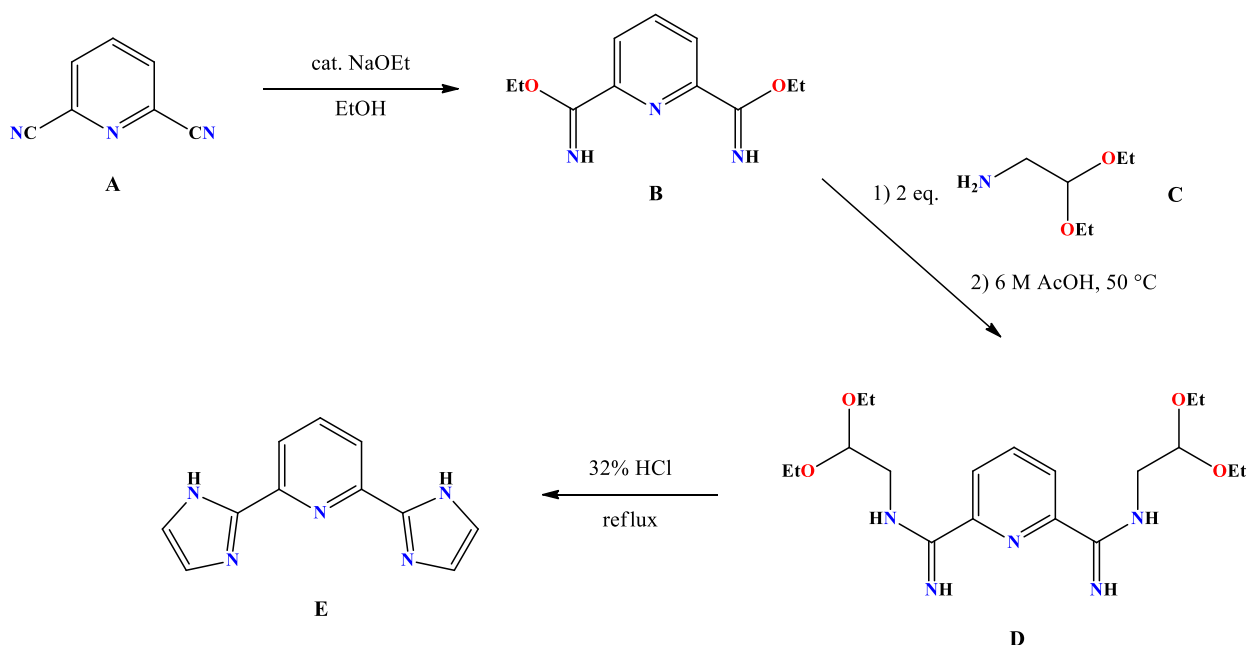


Figure 2.3: $^{13}\text{C}\{^1\text{H}\}$ NMR spectrum of 2,6-bis(5-butyl-1*H*-pyrazol-3-yl)pyridine (**4**) [100 MHz, CDCl_3 , 25 °C].

2.4.2 Imidazole-pyridinyl ligands

There are various ways in which one could synthesise aryl-2-imidazoles. The most common being the classic Debus-Radziszewski approach for imidazoles.^{41,42} This synthetic pathway always includes three typical starting materials: a dicarbonyl species (usually glyoxal), an aldehyde and two equivalents of ammonia. The second approach includes fairly recent examples of transition metal catalysed 2-arylation of imidazoles under Negishi or Stille conditions, but the downside of this approach is the necessity of protecting and deprotecting the NH-group of imidazole.^{24,43,44} Additionally, the use of *n*-butyllithium and strict water- and oxygen-free conditions make this reaction unsuitable for large-scale syntheses. The third approach involves the conversion of the corresponding nitrile into the imidazoline followed by oxidation to the desired imidazole by using an array of metal salts.^{45–49} This synthetic approach became unappealing due to high initial reaction temperatures (> 200 °C), the need for the subsequent separation of inorganic side-products and low to moderate overall yields.

The last set of ligands in this chapter, 2,6-bis(1-butylimidazol-2-yl)pyridine (**11**) and 2,6-bis(1-octylimidazol-2-yl)pyridine (**12**), were ultimately synthesised via a multiple-step synthetic procedure. But first, the precursor ligand, 2,6-bis(1*H*-imidazol-2-yl)pyridine (**E**), needed to be prepared via the nucleophilic substitution of an imidate (**B**) with the diethylacetal-protected aminoacetaldehyde (**C**) followed by deprotection-cyclisation under acidic conditions (**Scheme 2.24**).^{25,50–52} The imidate was initially formed from the alkaline catalysis of pyridine-2,6-dicarbonitrile, followed by the *in situ* reaction with aminoacetaldehyde diethylacetal and the subsequent deprotection-cyclisation under acidic (32% HCl) refluxing conditions.

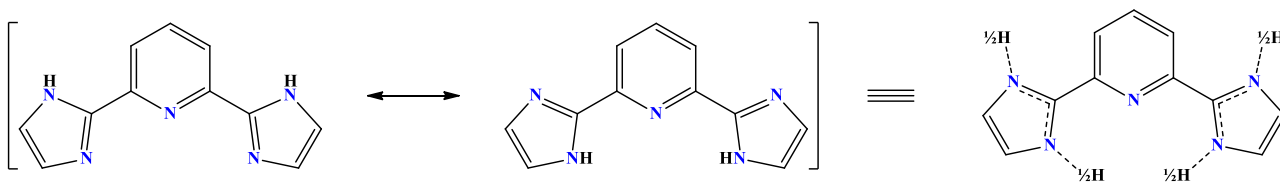


Scheme 2.24: Stepwise synthesis of 2,6-bis(1*H*-imidazol-2-yl)pyridine (**E**) from pyridine-2,6-dicarbonitrile (**A**) and aminoacetaldehyde diethylacetal (**C**) via an imidate- (**B**) and acetal-protected imidamide intermediate (**D**). [Adapted from Voss *et al.*,²⁵ Lawson⁵⁰ and Clews *et al.*⁵²]

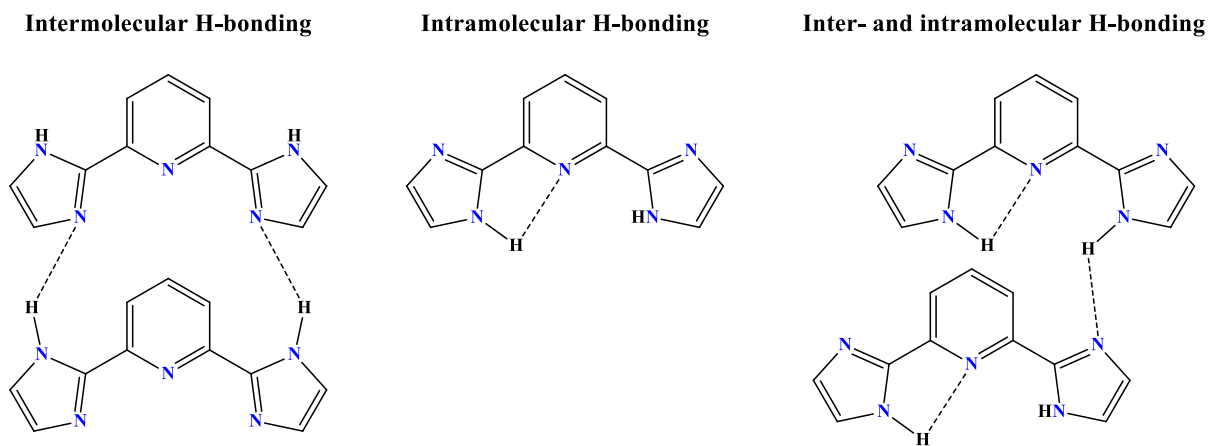
The most important step in the one-pot synthesis of the imidazole precursor ligand, was the formation of the initial imidate intermediate (**A**→**B**). This crucial step requires at least one hour of gentle stirring at room temperature, but it was found that the overall yield of the final product significantly improved upon increasing the imidate formation to two hours. Voss *et al.*²⁵ suggested the use of sodium methoxide as catalytic base in methanol, but a solvent with a slightly higher boiling point was sought to maximise the overall yield, hence the use of high-grade sodium ethoxide in ethanol. This does mean, however, that the imidate formation might be slower and therefore the increase in the reaction time was justified. After the acidic reflux, workup and purification, a maximum yield of 80.1% was recorded of fluffy cotton-like white solid—slightly less than Voss and co-workers²⁵ yield of 85%. This indicated the refluxing temperature not to be the major contributing factor in the attempted increase of yield, but that the imidazole formation was principally driven by the initial imidate formation instead.

The IR, MS and EA of 2,6-bis(1*H*-imidazol-2-yl)pyridine indicated the successful synthesis of the precursor imidazolyl ligand. However, the ¹H and ¹³C NMR spectra were puzzling, especially since the same tautomerism as encountered with pyrazolyl ligands **1–10** (Section 2.4.1) was expected. If tautomerism was present, one should simply expect three ¹H NMR signals and five ¹³C NMR signals due to tautomeric-induced quasi-symmetry of the precursor ligand (Scheme 2.25). This was not the case, since four ¹H NMR signals and six ¹³C NMR signals were observed (Figures 2.4 and 2.5). The only way one could make sense of this was on the assumption that the imidazolyl protons and carbons were in non-equivalent chemical environments, *i.e.*, symmetry was somehow disrupted. We, therefore, propose that the *NH* protons are either hydrogen bonded in an inter- or intramolecular fashion (or a combination thereof), subsequently fixing the *NH* protons in a specific conformation and thereby rendering the imidazolyl hydrogens and carbons as appearing in non-equivalent chemical environments (Scheme 2.26). It should also be noted that intermolecular hydrogen bonding between the imidazolyl ligand and the solvent (DMSO-*d*₆) is another possible mode of “locking in” the *NH* functional group, although it is not depicted in Scheme 2.26. Unfortunately, this precursor ligand was insoluble in most laboratory solvents, let alone deuterated solvents. This halted attempts to run NMR experiments in non-coordinating deuterated solvents, such as CDCl₃.

Therefore, due to the “locked” *NH* protons, we observe two slightly broad ¹H signals at 7.12 and 7.46 ppm respectively, both integrating for two (Figure 2.4), while two distinct resonances appear for the *CH* imidazolyl carbons (Figure 2.5) at 117.3 and 118.5 ppm, respectively.



Scheme 2.25: Expected tautomerism in 2,6-bis(1*H*-imidazol-2-yl)pyridine with averaged proton distribution. [Similar monosubstituted imidazolyl tautomerism in CDCl₃ previously reported by Pearce, *et al.*⁵³]



Scheme 2.26: Possible modes of hydrogen bonding of 2,6-bis(1*H*-imidazol-2-yl)pyridine in DMSO- d_6 .

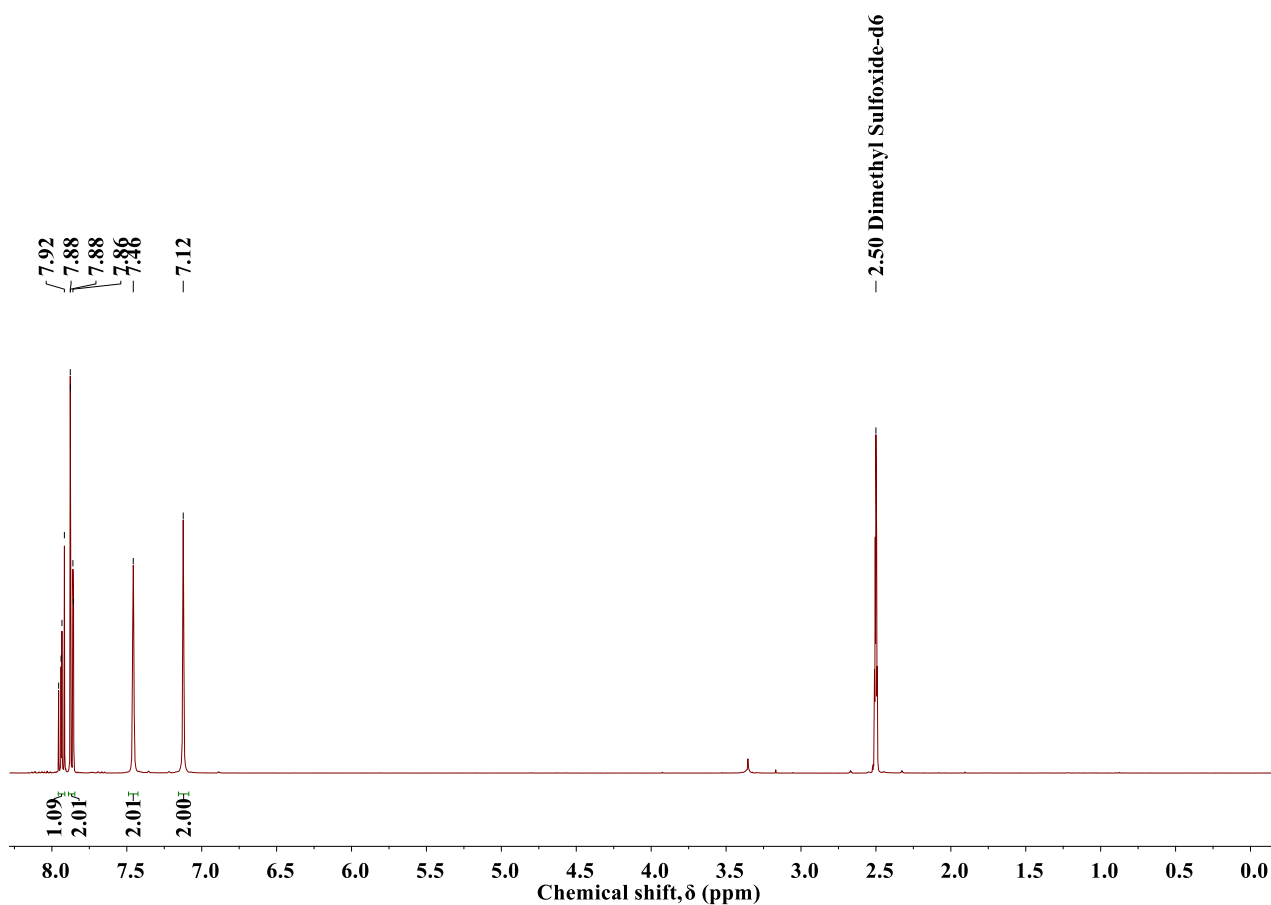


Figure 2.4: ^1H NMR spectrum of 2,6-bis(1*H*-imidazol-2-yl)pyridine [400 MHz, DMSO- d_6 , 25 °C].

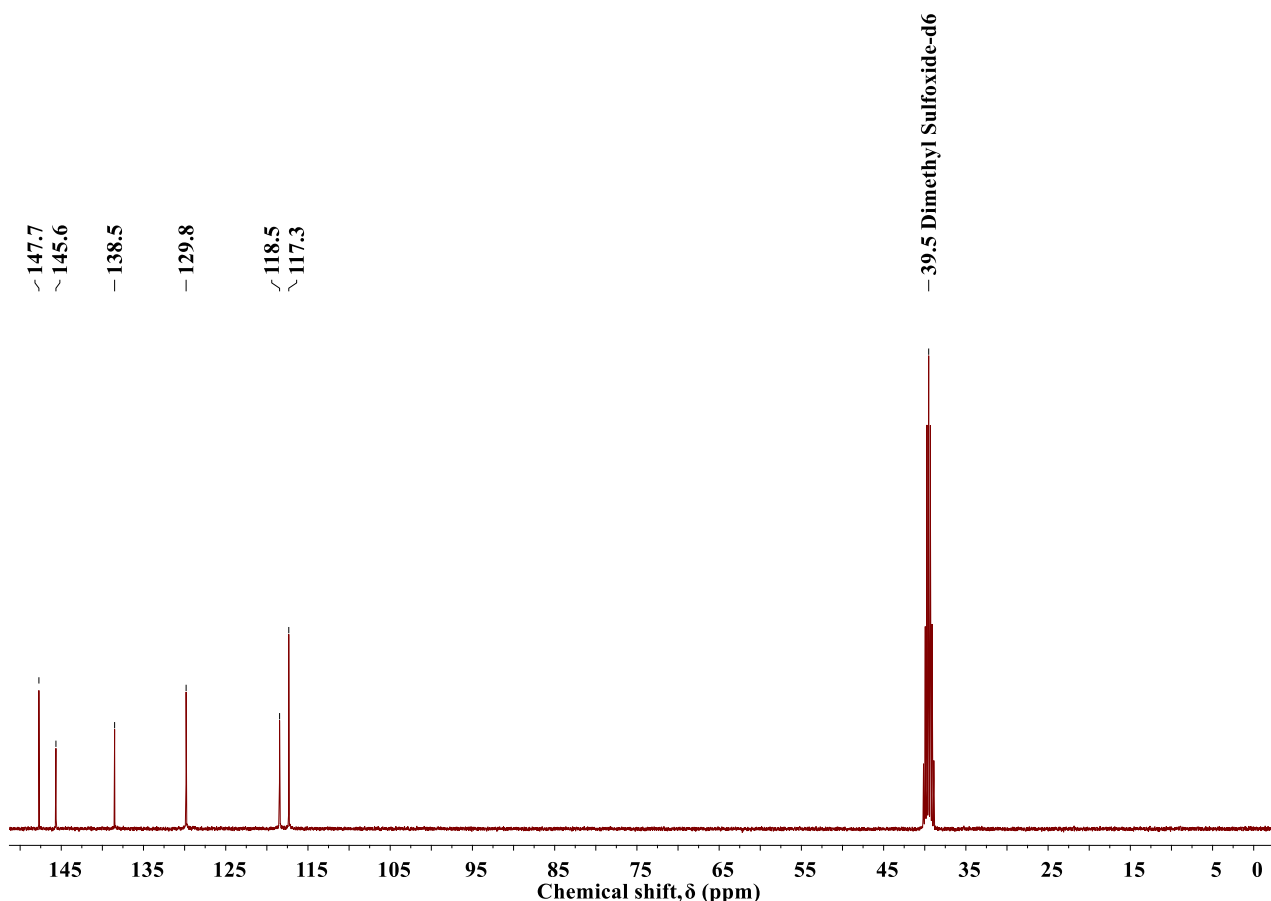


Figure 2.5: $^{13}\text{C}\{^1\text{H}\}$ NMR spectrum of 2,6-bis(1*H*-imidazol-2-yl)pyridine [100 MHz, DMSO- d_6 , 25 °C].

The next step in synthesising 2,6-bis(1-butylimidazol-2-yl)pyridine (**11**) and 2,6-bis(1-octylimidazol-2-yl)pyridine (**12**), was by far the most challenging synthetic alkylation encountered during this study. Not because it had a complex multiple-step synthetic pathway, but rather due to its practical difficulties. The precursor imidazolyl ligand, as previously mentioned, was nigh impossible to dissolve in common organic solvents we had at our disposal at the time. See list of solvents used below:

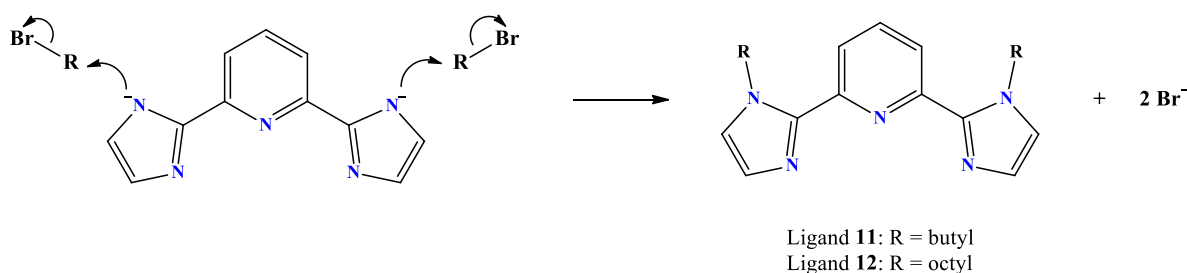
1-Butanol, 1-octanol, 1,2-dichloroethylene, benzene, carbon tetrachloride, chloroform, cyclohexane, dichloromethane, diethyl ether, dimethylformamide (slightly soluble), ethanol, ethyl acetate, heptane, hexane methanol, *p*-xylene, *tert*-butyl methyl ether and toluene.

The precursor ligand was solely soluble in DMSO, which led to the formation of various side-products during the alkylation procedure. DMSO was also difficult to remove once the reaction went to completion and purification became cumbersome and tedious. Therefore, the use of DMSO as solvent was abandoned altogether. Both Rigsby *et al.*²⁶ and Li *et al.*³⁰ reported the alkylation of 2,6-bis(1*H*-imidazol-2-yl)pyridine by using iodomethane (73% yield) and 1-bromohexane (80% yield) as alkylating agent, respectively. The former suggested stirring potassium hydroxide and the imidazolyl precursor ligand as a suspension in acetone at room temperature, while the latter implemented alkylation in acetone under refluxing conditions with potassium *tert*-butoxide as base. These procedures were followed as accurately as possible, but never managed to simulate the yields of the aforementioned authors—obtaining a maximum yield of 10.6% for

ligand **11** (Section 2.3.14, Method 1) and 10.7% for ligand **12** (Section 2.3.15, Method 1). For ligand **11**, experimental conditions and parameters were often altered while mixing the precursor ligand with DMF and aqueous sodium hydroxide at room temperature for 18 hours. Refluxing was not an option in this case, since it leads to the formation of unwanted side-products (Section 2.3.14, Method 2). This method only marginally increased the yield to 15.9%, forcing a change of experimental parameters once more. Lastly, a biphasic reaction setup was implemented whereby the precursor ligand was dissolved in a H₂O/Et₃N homogeneous solution and added to 1-bromobutane in toluene, followed by an 18-hour refluxing period (Section 2.3.14, Method 3). At last, this set of reaction parameters seemed to work well, ultimately affording ligand **11** as a yellow-brown oil in good yield (64.4%).

For ligand **12**, the alkylation process was even more challenging, since contact between the precursor ligand and 1-bromooctane was extremely poor. To improve contact, the precursor ligand was dissolved in aqueous sodium hydroxide until the solution became clear, followed by the gradual addition of 1-bromooctane in acetonitrile and five drops of tetrabutylammonium hydroxide (TBAOH) as a phase-transfer catalyst (Section 2.3.15, Method 2). It was hoped that the miscibility of acetonitrile in water would increase contact between the reagents, but after a 24-hour refluxing period a meagre yield of 13.1% was reported. This result led to the reintroduction of a biphasic reaction setup in an attempted synthetic protocol to obtain ligand **12**. The precursor ligand was dissolved in aqueous potassium hydroxide and allowed to stir for two hours at room temperature to ensure the deprotonation step was complete. Thereafter, 1-bromooctane and tetrabutylammonium bromide (TBAB) in toluene was added to the aqueous mixture and allowed to reflux for 72 hours. After a tedious workup procedure and purification via column chromatography, a yield of 60.4% was obtained. It is theorised that alkylation only occurred at the water/toluene interface, given that 1-bromooctane was insoluble in water and that the precursor ligand was poorly soluble in toluene, hence the need for a 72-hour refluxing period. The phase-transfer catalyst, TBAB, is a necessary inclusion in this reaction as it assists the alkylation reaction.

Mechanistically, the deprotonated nitrogens acted as nucleophiles that attacked the electrophilic carbons of the alkylbromides in these theoretically simple nucleophilic substitution (S_N2) reactions (Scheme 2.27).



Scheme 2.27: Nucleophilic substitution (S_N2) mechanism by which ligands **11** and **12** were formed.

The ^1H and ^{13}C NMR spectra of ligands **11** and **12** were relatively similar, therefore, only the octyl substituted imidazolyl ligand (**12**) spectra will be discussed in this section. A clear-cut way in which one might discern whether the precursor imidazolyl ligand was successfully alkylated, lies in two key observations: 1) the presence of the *n*-octyl resonances in both ^1H and ^{13}C NMR spectra and 2) the correct integration values for the pendant arm protons. This might seem trivial, but the presence of unreacted 1-bromooctane will appear at similar chemical shifts with the same splitting patterns. **Figure 2.6** evidently shows resonance signals for 34 protons in the mid- to upfield region (0.79–4.49 ppm), corresponding exactly to the number of protons on the alkyl pendant arms of ligand **12**. The pyridinyl (7.83–8.01 ppm) and imidazolyl (7.02–7.13 ppm) proton signals are also accounted for in the downfield region. Fine splitting of the imidazolyl protons were also noticed due to *J*-coupling ($J = 1.1$ Hz) to their immediate proton neighbour, which was not visible in the ^1H NMR spectrum of the precursor ligand, 2,6-bis(1*H*-imidazol-2-yl)pyridine.

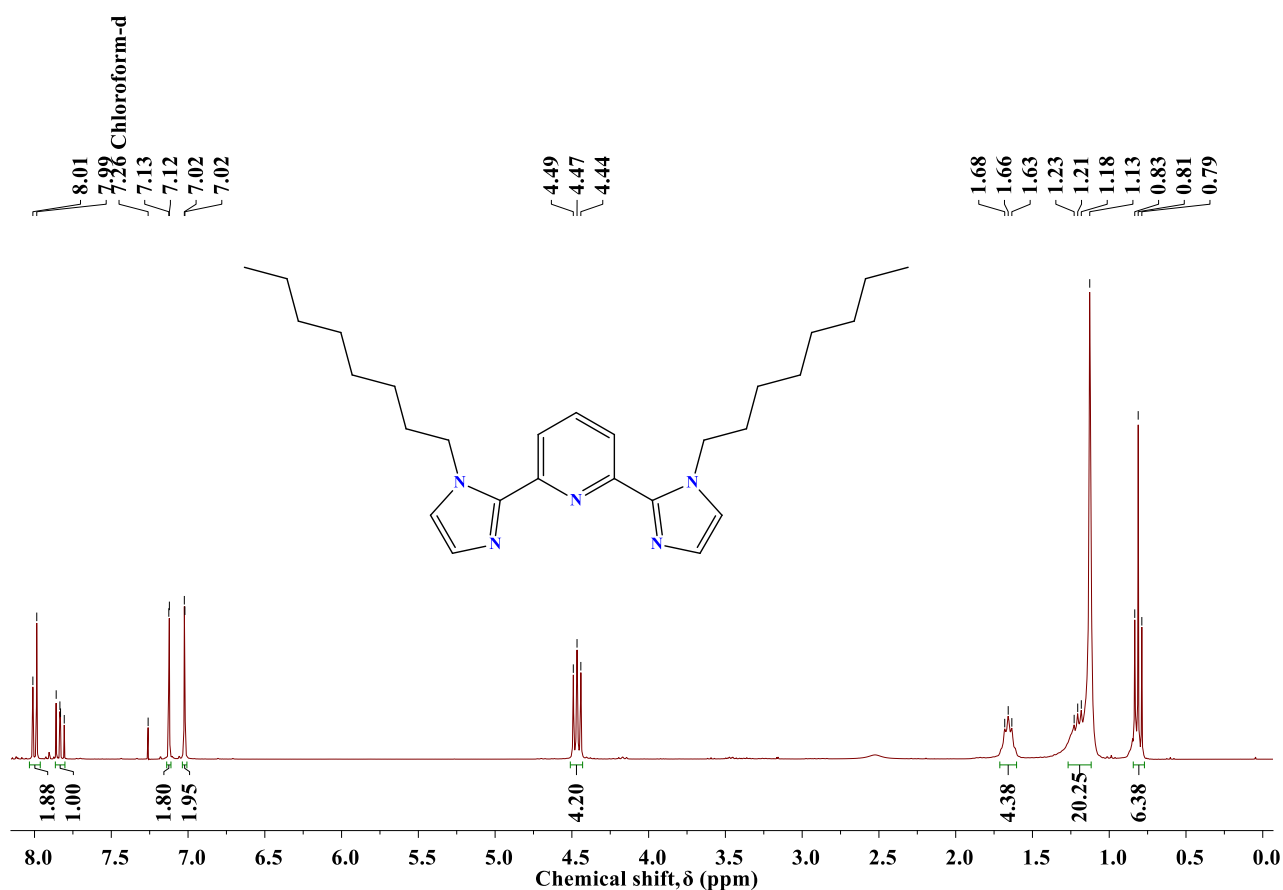


Figure 2.6: ^1H NMR spectrum of 2,6-bis(1-octylimidazol-2-yl)pyridine (**12**) [300 MHz, CDCl_3 , 25 °C].

The ^{13}C NMR spectrum appeared to represent the characteristics of ligand **12** well, with eight ^{13}C resonances in the upfield region (14.1–47.6 ppm)—indicating the presence of two *n*-octyl pendant tethers (**Figure 2.7**). Six aromatic and heterocyclic ^{13}C resonances were attributed to the pyridinyl (128.6–145.0 ppm) and imidazolyl carbons (122.5–123.0 and 149.8 ppm), with the lack of nuclear Overhauser enhancement (NOE) of carbons without bound hydrogens making it easy to identify the protonless pyridinyl (145.0 ppm) and

imidazolyl carbons (149.8 ppm).⁵⁴ Additionally, the IR, MS and EA analyses results corroborated the successful synthesis of ligand **12**.

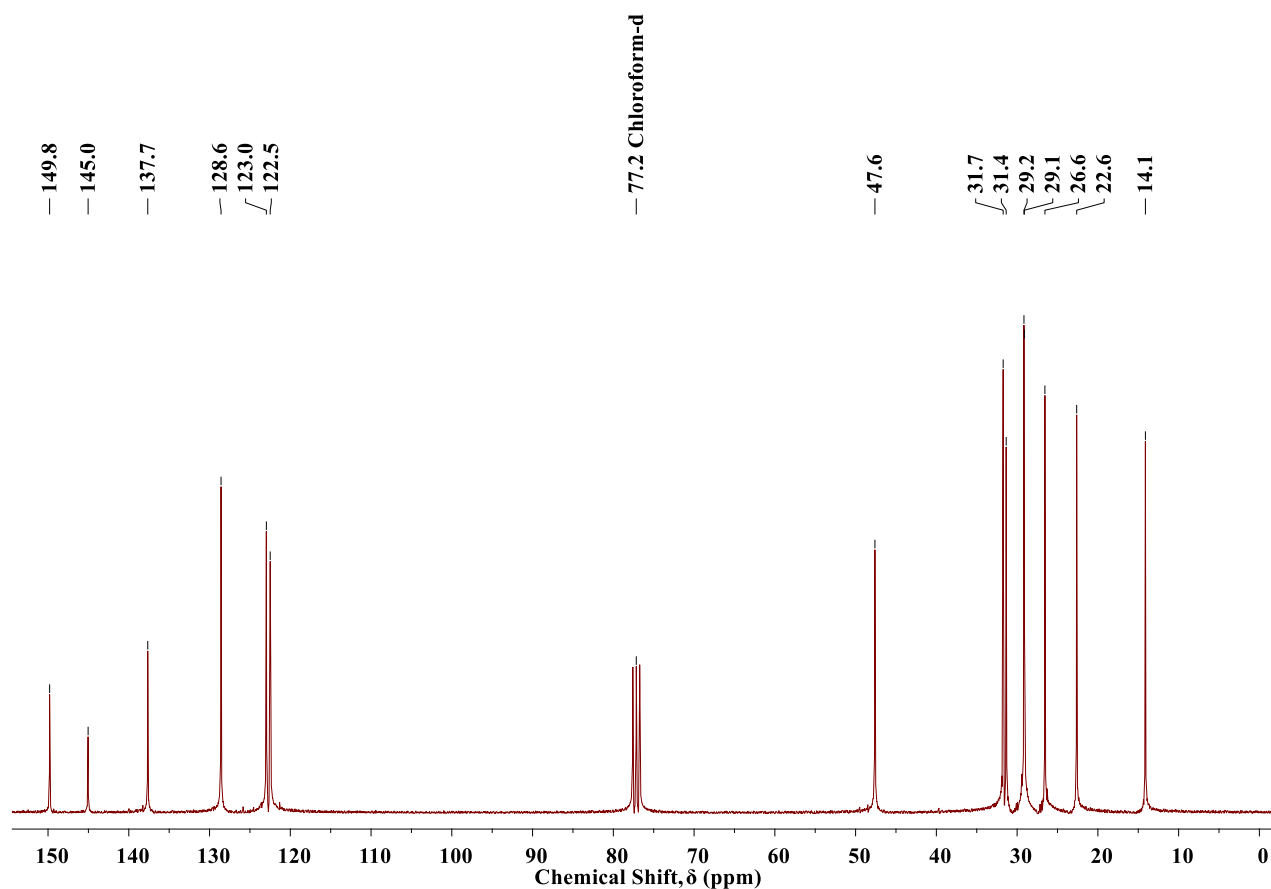


Figure 2.7: ¹³C{¹H} NMR spectrum of 2,6-bis(1-octylimidazol-2-yl)pyridine (**12**) [75 MHz, CDCl₃, 25 °C].

2.5 Conclusions

One of the most challenging aspects in the syntheses of pyrazolyl ligands **1–10** were the exceptionally low yields initially obtained. This was subsequently overcome with optimised reaction conditions and parameters. Specifically, a general increase in yields from ligand **1** (33.7%) to **8** (80.5%) were noticed, as *n*-alkyl ketone lengths of the reagents increased from acetone to 2-decanone. This was primarily attributed to the boiling points of the ketone reagents. Impure products were often encountered at the tail end of a synthetic process, mainly due to excess starting materials. Because of this, these products required purification via recrystallisation, vacuum distillation and/or column chromatography. These techniques were extremely time-consuming and cumbersome, and in certain cases took up to three weeks to complete. Another negative in implementing these techniques, was the loss of a small percentage of product during these extensive purification processes. Either the product was not amenable to conventional recrystallisation protocols or could not be subjected to column chromatography. At times, product decomposition was observed during vacuum distillation (kugelrohr short path apparatus) as well. Therefore, the overarching difficulty during the syntheses of ligands **1–10** was the challenge of synthesising sufficient amounts of pure

product for future solvent extraction experiments. This was especially true for ligands **1–3** and **9**, with overall yields of less than 50%.

The imidazolyl syntheses of ligands **11** and **12** were by no means theoretically challenging, but rather practically challenging due to poor contact between the alkylating agent and the precursor imidazolyl ligand. This forced the implementation of a biphasic reaction system to maximise yields. This reaction was easily tracked by visually taking note of the organic layer's hue. Once the organic layer had a yellow-brown tinge, the reaction was proceeding forward, albeit quite slowly. As with pyrazolyl ligands **1–10**, the same purification challenges were encountered with imidazolyl ligands **11** and **12**.

In this investigation, a series of pyrazole- (**1–10**) and imidazole-pyridinyl ligands (**11** and **12**) were successfully synthesised and characterised. On the whole, it was a tussle to match the good yields reported by the various authors cited in this study. This might be due to our uniquely adapted synthetic methods coupled with cumbersome workup procedures and purification processes, especially column chromatography. All ligands were characterised by means of ^1H and ^{13}C NMR, IR, MS and EA.

Finally, for the first time the syntheses of 2,6-bis(5-pentyl-1*H*-pyrazol-3-yl)pyridine (**5**), 2,6-bis(5-heptyl-1*H*-pyrazol-3-yl)pyridine (**7**) and 2,6-bis(1-octylimidazol-2-yl)pyridine (**12**) is reported, which to the best of our knowledge are novel. There are a couple of instances where ligands have been mentioned in patents, but reaction conditions and parameters were not expounded on in any way. Reagents and various chemicals were distinctly absent as well. Therefore, the following ligands—as alluded to by Geist *et al.*⁵⁵ and Zheng *et al.*⁵⁶—are classified as “new in their application of base metal solvent extraction systems”: 2,6-bis(5-hexyl-1*H*-pyrazol-3-yl)pyridine (**6**), 2,6-bis(5-octyl-1*H*-pyrazol-3-yl)pyridine (**8**) and 2,6-bis(1-butylimidazol-2-yl)pyridine (**11**).

2.6 References

- (1) Du Preez, J. Recent advances in amines as separating agents for metal ions. *Solvent Extr. Ion Exch.* **2000**, *18* (4), 679–701.
- (2) Gray, A.; O'Dell, T. Reaction of ethylene bromide with trimethylamine and the neuromuscular blocking activity of ethylenebis-(trimethylammonium). *Nature* **1958**, *181* (4609), 634–635.
- (3) Vidal, F. Reaction of ethylene dibromide with triethylamine and the restoring action of some alkanebis(triethylammonium) ions upon sodium-deficient nerve fibers. *J. Org. Chem.* **1959**, *24* (5), 680–683.
- (4) Hildebrand, J.; Scott, R. *Regular Solutions*; Prentice-Hall: Englewood Cliffs, N.J., 1962.
- (5) Kertes, A. Solubility parameters of long-chain alkylamines and their activities in organic solvents. *J. Inorg. Nucl. Chem.* **1964**, *26* (10), 1764–1766.

- (6) Kertes, A. Solubility and activity of high-molecular amine hydrochlorides in organic solvents. *J. Inorg. Nucl. Chem.* **1965**, 27 (1), 209–217.
- (7) Bucher, J.; Diamond, R. The extraction of perchloric acid by trilaurylamine. Part I. Aromatic diluents. *J. Phys. Chem.* **1965**, 69 (5), 1565–1574.
- (8) Müller, W.; Diamond, R. The extraction of hydrohalic acids by trilaurylamine. *J. Phys. Chem.* **1966**, 70 (11), 3469–3479.
- (9) Hall, H. Potentiometric determination of the base strength of amines in non-protolytic solvents. *J. Phys. Chem.* **1956**, 60 (1), 63–70.
- (10) Hall, H. Correlation of the base strengths of amines. *J. Am. Chem. Soc.* **1957**, 79 (20), 5441–5444.
- (11) Trotman-Dickenson, A. The basic strength of amines. *J. Chem. Soc.* **1949**, No. 0, 1293–1297.
- (12) Chremos, G.; Zimmerman, H. Polar and steric contributions of saturated substituents to the acid-base equilibria of aqueous amines. *Chimia (Aarau)*. **1964**, 18 (8), 265.
- (13) Stewart, R.; O'Donnell, J. Strongly basic systems. Part IV. Substituent effects on the acidity of aromatic amines. *Can. J. Chem.* **1964**, 42 (7), 1694.
- (14) Marcus, Y.; Kertes, A. *Ion Exchange and Solvent Extraction of Metal Complexes*; Wiley-Interscience: London & New York, 1969.
- (15) Du Preez, J.; Schanknecht, S.; Shillington, D. Polynitrogen reagents in metal separation. Part III. The extraction of Co^{2+} , Ni^{2+} , Cu^{2+} and Zn^{2+} using novel ditertiary-amine extractants. *Solvent Extr. Ion Exch.* **1987**, 5 (5), 789–809.
- (16) Du Preez, J.; Sumter, N.; Mattheüs, C.; Ravindran, S.; Van Brecht, B. Nitrogen reagents in metal ion separation. Part VII. The development of a novel copper(II) extractant. *Solvent Extr. Ion Exch.* **1997**, 15 (6), 1007–1021.
- (17) Du Preez, J.; Mattheüs, C.; Sumter, N.; Ravindran, S.; Potgieter, C.; Van Brecht, B. Nitrogen reagents in metal ion separation. Part VIII. Substituted imidazoles as extractants for Cu^{2+} . *Solvent Extr. Ion Exch.* **1998**, 16 (2), 565–586.
- (18) Li, X.; Zhan, C.; Wang, Y.; Yao, J. Pyridine-imide oligomers. *Chem. Commun. (Camb)*. **2008**, No. 21, 2444–2446.
- (19) Fenton, D.; Tate, J.; Casellato, U.; Tamburini, S.; Vigato, P.; Vidali, M. Metal complexes of some tetraketones and their schiff bases. *Inorg. Chim. Acta* **1984**, 83 (1), 23–31.
- (20) Zhou, Y.; Chen, W. Novel neutral octanuclear copper(I) complexes stabilized by pyridine linked bis(pyrazolate) ligands. *Dalton Trans.* **2007**, 1 (44), 5123.

- (21) Satake, A.; Nakata, T. Novel η^3 -allylpalladium-pyridinylpyrazole complex: Synthesis, reactivity, and catalytic activity for cyclopropanation of ketene silyl acetal with allylic acetates. *J. Am. Chem. Soc.* **1998**, *120* (40).
- (22) Gal, M.; Tarrago, G.; Steel, P.; Marzin, C. A novel macrocyclic ligand containing 2,6-bis(pyrazol-5-yl)pyridine units. Synthesis and complexation properties. *Nouv. J. Chim.* **1985**, *9* (10), 617–620.
- (23) Pons, J.; Chadghan, A.; García-Antón, J.; Ros, J. Phenyl and pyridyl bis-pyrazoles: Synthesis from the bis(β -diketone) precursors and characterization by analytical and spectroscopic methods. *Lett. Org. Chem.* **2010**, *7* (2), 178–181.
- (24) Stupka, G.; Gremaud, L.; Bernardinelli, G.; Williams, A. Redox state switching of transition metals by deprotonation of the tridentate ligand 2,6-bis(imidazol-2-yl)pyridine. *Dalton Trans.* **2004**, No. 3, 407–412.
- (25) Voss, M.; Beer, C.; Mitchell, S.; Blomgren, P.; Zhichkin, P. A simple and convenient one-pot method for the preparation of heteroaryl-2-imidazoles from nitriles. *Tetrahedron* **2008**, *64* (4), 645–651.
- (26) Rigsby, M.; Mandal, S.; Nam, W.; Spencer, L.; Llobet, A.; Stahl, S. Cobalt analogs of Ru-based water oxidation catalysts: Overcoming thermodynamic instability and kinetic lability to achieve electrocatalytic O₂ evolution. *Chem. Sci.* **2012**, *3* (10).
- (27) Hashiguchi, B.; Young, K.; Yousufuddin, M.; Goddard, W.; Periana, R. Acceleration of nucleophilic CH activation by strongly basic solvents. *J. Am. Chem. Soc.* **2010**, *132* (36), 12542–12545.
- (28) Zhang, W.; Sun, W.; Zhang, S.; Hou, J.; Wedeking, K.; Schultz, S.; Fröhlich, R.; Song, H. Synthesis, characterization, and ethylene oligomerization and polymerization of [2,6-bis(2-benzimidazolyl)pyridyl]chromium chlorides. *Organometallics* **2006**, *25* (8), 1961–1969.
- (29) Wang, R.; Xiao, J.; Twamley, B.; Shreeve, J. Efficient Heck reactions catalyzed by a highly recyclable palladium(II) complex of a pyridyl-functionalized imidazolium-based ionic liquid. *Org. Biomol. Chem.* **2007**, *5* (4), 671–678.
- (30) Li, L.; Luo, Q.; Cui, H.; Li, R.; Zhang, J.; Peng, T. Air-stable Ru(II)-NNN pincer complexes for efficient coupling of aromatic diamines and alcohols to 1*H*-benzo[*d*]imidazoles with the liberation of H₂. *ChemCatChem* **2018**, *10* (7), 1607–1613.
- (31) Knorr, L.; Blank, A. Einwirkung substituierter acetessigester auf phenylhydrazin. *Berichte der Dtsch. Chem. Gesellschaft* **1884**, *17* (2).
- (32) Neuman, R. Reaction of enolate ions and enols. *Organic Chemistry*; University of California, Riverside, 2013; pp 3–13.

- (33) Clayden, J.; Greeves, N.; Warren, S. *Organic Chemistry*, 2nd Edition; Oxford University Press Inc.: New York, 2012.
- (34) McMurry, J. *Organic Chemistry*, 7th Edition.; Graphic World Inc., Eds.; Thomson Learning, Inc.: Belmont, USA, 2008.
- (35) Katritzky, A.; Ostercamp, D.; Yousaf, T. The mechanisms of heterocyclic ring closures. *Tetrahedron* **1987**, *43* (22), 5171–5186.
- (36) Singh, S.; Kumar, D.; Batra, H.; Naithani, R.; Rozas, I.; Elguero, J. The reaction between hydrazines and β -dicarbonyl compounds: proposal for a mechanism. *Can. J. Chem.* **2000**, *78* (8), 1109–1120.
- (37) Ali, K. A new convenient synthesis of some novel 2,6-disubstituted-pyridine derivatives. *Arkivoc* **2010**, *2010* (11), 55–63.
- (38) Polezhaev, A.; Chen, C.; Kinne, A.; Cabelof, A.; Lord, R.; Caulton, K. Ligand design toward multifunctional substrate reductive transformations. *Inorg. Chem.* **2017**, *56* (16), 9505–9514.
- (39) Pearce, B.; Ogutu, H.; Luckay, R. Synthesis of pyrazole-based pyridine ligands and their use as extractants for nickel(II) and copper(II): Crystal structure of a copper(II)–ligand complex. *Eur. J. Inorg. Chem.* **2017**, *2017* (8), 1189–1201.
- (40) Henkelis, J.; Kilner, C.; Halcrow, M. New insights into the aggregation of silver pyrazolides using sterically hindered bidentate pyrazole ligands. *Chem. Commun.* **2011**, *47* (18), 5187–5189.
- (41) Debus, H. Ueber die einwirkung des ammoniaks auf glyoxal. *Justus Liebigs Ann. Chem.* **1858**, *107* (2).
- (42) Radziszewski, B. Ueber glyoxalin und seine homologe. *Berichte der Dtsch. Chem. Gesellschaft* **1882**, *15* (2).
- (43) Bell, A.; Roberts, D.; Ruddock, K. A synthesis of 2- and 4(5)-(2-pyridinyl)imidazoles by palladium-catalysed cross-coupling reactions. *Tetrahedron Lett.* **1988**, *29* (39), 5013–5016.
- (44) Li, G.; Peterson, J.; Albaugh, P.; Currie, K.; Cai, G.; Gustavson, L.; Lee, K.; Hutchison, A.; Singh, V.; Maynard, G.; *et al.* Aryl or heteroaryl fused imidazoles as selective GABAA receptor ligands, 27 June 2002.
- (45) Oxley, P.; Short, W. Amidines. Part VI. Preparation of 2-substituted 4,5-dihydroglyoxalines and ring homologues from cyanides and alkylenediamines. *J. Chem. Soc.* **1947**, 497–505.
- (46) Hughey, J.; Knapp, S.; Schugar, H. Dehydrogenation of 2-imidazolines to imidazoles with barium manganate. *Synth.* **1980**, *1980* (6), 489–490.

- (47) Rousselet, G.; Capdevielle, P.; Maumy, M. Copper(I)-induced addition of amines to unactivated nitriles: The first general one-step synthesis of alkyl amidines. *Tetrahedron Lett.* **1993**, *34* (40), 6395–6398.
- (48) Satake, A.; Koshino, H.; Nakata, T. Interconvertible cationic and neutral pyridinylimidazole η^3 -allylpalladium complexes. Structural assignment by ^1H , ^{13}C , and ^{15}N NMR and X-Ray diffraction. *Organometallics* **1999**, *18* (24), 5108–5111.
- (49) Ishihara, M.; Togo, H. An efficient preparation of 2-imidazolines and imidazoles from aldehydes with molecular iodine and (diacetoxyiodo)benzene. *Synlett* **2006**, No. 2, 227–230.
- (50) Lawson, A. The reaction of imidates with α -amino-acetals and α -amino-aldehydes. *J. Chem. Soc.* **1957**, 4225–4228.
- (51) Jensen, N.; Schmitt, S.; Windholz, T.; Shen, T.; Mandel, L.; Lopez-Ramos, B.; Porter, C. Inhibition of adrenal phenethanolamine-*N*-methyltransferase by substituted imidazoles. *J. Med. Chem.* **1972**, *15* (4), 341–344.
- (52) Clews, J.; Morgan, N.; Ramsden, C. Preparation of the I_3 imidazoline receptor antagonist KU14R and related 2,3-dihydrobenzo[*b*]furan derivatives. *Synthesis (Stuttg.)* **2001**, No. 10, 1546–1550.
- (53) Pearce, B.; Ogutu, H.; Saban, W.; Luckay, R. Synthesis, characterization and use of imidazole and methyl-pyrazole based pyridine ligands as extractants for nickel(II) and copper(II). *Inorg. Chim. Acta* **2019**, 57–67.
- (54) Lampman, G.; Pavia, D.; Kriz, G.; Vyvyan, J. *Spectroscopy*, 4th Intern. Edition; Brooks/Cole, Cengage Learning: Belmont, USA, 2010.
- (55) Geist, A.; Muellich, U.; Zevaco, T.; Karpov, A.; Mueller, T. Preparation of alkylated bis(pyrazolyl)pyridines for the selective extraction of actinides, DE102009003783, 21 October 2010.
- (56) Zheng, C.; Yin, Y.; Wei, W.; Liu, M.; Zhang, Y.; Deng, P. Composite corrosion inhibitor and its preparation method, CN105603436, 25 May 2016.

CHAPTER 3

SOLVENT EXTRACTION OF SIX DIVALENT BASE METAL IONS BY MEANS OF TRIDENTATE PYRAZOLE- AND IMIDAZOLE-PYRIDINYL LIGANDS

3.1 Introduction

The use of amine extractants for nickel and cobalt solvent extraction purposes is generally well-known, especially from chloride solutions. Typically, these systems include generic extractants such as Alamine 336, Alamine 308 and Alamine 300, all of which are long *n*-alkyl-chained tertiary amines.¹ Aromatic amine extractants, on the other hand, have been studied to a much lesser extent due to their general inability to be exclusively soluble in the organic phase. This hindrance has been a major drawback in hydrometallurgical research and can only be surmounted by the incorporation of lipophilic or hydrophobic moieties, such as *n*-alkyl chains.

During the latter part of the 1990s, Du Preez *et al.*²⁻⁵ published a series of articles in which they reported the use of pyridinyl-, pyrazolyl- and imidazolyl-type ligands as selective extractants for later 3d transition metal ions. The imidazolyl ligands were of particular interest, since they showed promising selectivity towards copper(II), and once these ligands were modified, showed increased selectivity towards nickel(II) and cobalt(II) as well. It was noticed that these South African workers merely used pyridinyl, pyrazolyl and imidazolyl ligands as monodentate extractants, never attempting to combine these moieties into a single extractant. Therefore, this window of opportunity to use tridentate *N*-type ligands in base metal solvent extraction systems was the opportune time to exploit their combinative extractive abilities.

It is known that the late 3d transition metal ions (Cu^{2+} , Co^{2+} , Ni^{2+} and Zn^{2+}) form relatively stable complexes with *N*-donor ligands in aqueous solutions as compared to early 3d transition metal ions (Ti^{2+} , VO^{2+} , Cr^{3+} , Mn^{2+} , Fe^{2+} and Fe^{3+}).³ This provides metallurgists ample opportunities to not only separate these two groups of metals, but creates room for the separation of individual metal ions from the former group as well.

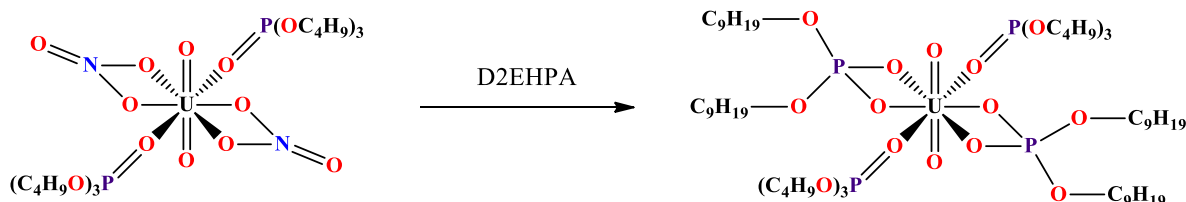
Although numerous tridentate aromatic amine ligands have been reported, very few were ever implemented for base metal solvent extraction purposes. They are often used as ligands in complexes which behave as spin-crossover materials,⁶ macrocyclic precursors,⁷ catalytic precursors,⁸⁻¹² biomolecular reagents¹³ or single-molecule magnets¹⁴—which allows us to probe their usefulness as solvent extractants. To the best of our knowledge, only a handful of literature reports mentioned the use of tridentate aromatic amine ligands as selective metal extractants, most of which studied lanthanoid(III)/actinoid(III) extractions via non-solvent extraction techniques.¹⁵⁻²¹ Only Zhou *et al.*¹⁵ and Roebuck *et al.*¹⁶ reported the use of 2,6-bis(5-nonyl-1*H*-pyrazol-3-yl)pyridine as an efficient cobalt(II) and nickel(II) extractant from sulfate sources. Because of the

apparent lack of research in base metal solvent extraction systems by means of tridentate aromatic amine ligands, it was decided to investigate a series of pyrazole- and imidazole-pyridinyl ligands with regard to their extractive ability of six base metal ions (Cu^{2+} , Co^{2+} , Cd^{2+} , Ni^{2+} , Zn^{2+} and Pb^{2+}) from nitrate sources.

3.1.1 Synergism and synergistic additives

Over the past sixty years, the hydrometallurgical field witnessed an exponential output of peer-reviewed articles relating to synergistic solvent extraction systems. The term “synergism” was first coined by Blake *et al.*²² in 1958 with the introduction of di-(2-ethylhexyl)phosphoric acid (D2EHPA) as an additive to neutral organophosphorous reagents, such as dibutyl butylphosphonate (DBBP) and tributyl phosphate (TBP). By implementing these combinations, they noticed a marked increase in the extraction of uranium(VI) compared to the neutral organophosphorous reagents alone. This intermolecular phenomenon between two or more reagents, causing the enhanced extraction of metal ions, is called “synergism” and can mathematically be expressed according to Eq. 35 in **Section 1.5 of CHAPTER 1**.

To gain additional insight, the synergistic extraction of uranium(VI) as $[\text{UO}_2]^{2+}$ from nitric acid media was further investigated. Initially, the uranium species was present in the acid medium as $[\text{UO}_2(\text{NO}_3)_2(\text{OH}_2)_2]$, which was strongly hydrogen bonded to proximate water molecules. The addition of TBP displaced two coordinated water molecules and gave the stable neutral bisolvated species, $[\text{UO}_2(\text{NO}_3)_2(\text{TBP})_2]$, which was poorly extractable into the organic phase. To take advantage of D2EHPA’s synergistic influence, it was added to the aqueous layer to yield the neutral species, $[\text{UO}_2(\text{D2EHPA})_2(\text{TBP})_2]$. This species was 1000 times more extractable than either of the complexes containing only one of the phosphorous ligands, due to the addition of extended alkyl chains that rendered it highly hydrophobic (**Scheme 3.1**).^{22,23}



Scheme 3.1: The addition of D2EHPA to $[\text{UO}_2(\text{NO}_3)_2(\text{TBP})_2]$ to form the neutral species, $[\text{UO}_2(\text{D2EHPA})_2(\text{TBP})_2]$. [Adapted from Laing²³]

3.1.1.1 Sulfonic acid synergists

Various literature sources^{1,24–27} report the use of synergists for base metal ion extraction—all with their own unique end-purposes in mind. It was noticed, however, that very few hydrometallurgists reported the use of sulfonic acid synergists, although this trend is rapidly expiring, ostensibly as more and more benefits of sulfonic acid synergists emerge.

Flett²⁸ reported the use of a carboxylic acid and 5,8-diethyl-7-hydroxy-6-dodecanone oxime (commercially known as LIX63) extractant system for the selective extraction of nickel(II) over cobalt(II). Although

reasonable separation was observed, it was recognised that separation was “poor” in industrial terms. Work done by Finnish workers Nyman *et al.*²⁹ and Hummelstedt *et al.*³⁰ was duly acknowledged for showing that the addition of dinonylnaphthalene sulfonic acid (DNNSA) significantly enhanced the rate of nickel(II) extraction in such systems. Flett,²⁸ therefore, set out to determine the extractive ability of DNNSA by performing a series of tests under experimental conditions as defined by the aforementioned Finnish collaborators. He subsequently proved that DNNSA did in fact extract nickel(II). As he incrementally increased the equilibrium pH, the concentration of nickel(II) in the aqueous phase lessened while the nickel(II) concentration in the organic phase increased (**Table 3.1**). This was clear evidence that DNNSA was transporting nickel(II) from the aqueous to the organic phase.

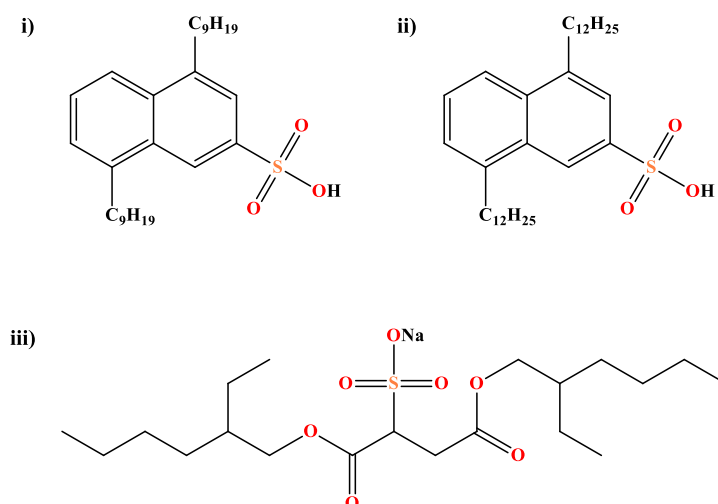
Table 3.1: Extraction of Ni²⁺ by means of DNNSA[†] by increasing the equilibrium pH. [Adapted from Flett²⁸]

Equilibrium pH	Equilibrium Ni ²⁺ concentration [‡]		log <i>D</i>
	Organic phase (g.L ⁻¹)	Aqueous phase (g.L ⁻¹)	
2.03	0.22	0.37	-0.22
2.46	0.50	0.09	+0.74
3.03	0.58	0.01	+1.76

[†] [DNNSA] = 2×10⁻³ M in hexane

[‡] [Ni²⁺] = 1×10⁻³ M in 1 M KNO₃

Osseo-Asare and Keeney³¹ did a comparative study of the nickel(II) extraction efficacy with LIX63 using three related sulfonic acid/sulfonate extractants. These extractants were dinonylnaphthalene sulfonic acid (DNNSA), didodecyl naphthalene sulfonic acid (DDNSA) and di-(2-ethylhexyl) sodium sulfosuccinate (DEHSS) (**Scheme 3.2**).



Scheme 3.2: Schematic representation of sulfonic acid/sulfonate extractants i) DNNSA, ii) DDNSA and iii) DEHSS.

In their opinion, the acidic extractants acted in a synergistic manner with LIX63. They subsequently continued to probe the interfacial (aqueous and organic phase contact point) tension of their extraction systems and adequately demonstrated the formation of reverse micelles (hydrophobic alkyl chains flaring outward with

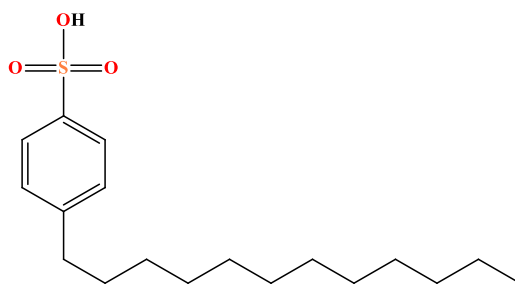
inward facing hydrophilic sulfonate heads) in non-polar solvents. They theorised that the reverse micelles catalysed the extraction process by specific solubilisation of both the ligand and nickel(II), resulting in an increased interfacial concentration of the reacting species. When Osseo-Asare and Keeney³¹ made their concluding remarks regarding the use of sulfonic acids as synergists, they encouragingly said the following:

“It appears therefore that the sulfonic acids have tremendous potential as catalysts for the liquid-liquid extraction of metals if used in conjunction with the appropriate secondary extractant.”

More recently, in 2012, Okewole *et al.*³² performed synergistic studies using 1-octyl-2-(2'-pyridyl)imidazole (OPIM) and DNNSA as synergist. They attempted to extract nickel(II) from a mixture of borderline and hard metal ions (Co²⁺, Cu²⁺, Zn²⁺, Fe²⁺, Fe³⁺, Mn²⁺, Mg²⁺ and Ca²⁺) by incorporating a diluent (2-octanol) and modifier (Shellsol 2325) in an 8:2 ratio respectively at a pH range of 0.5–3.5 in sulfate and sulfate/chloride media. Intriguingly, in the absence of DNNSA, nickel(II) extraction was exceptionally poor. However, upon the addition of DNNSA (concentration 15 times that of [Ni²⁺]), they observed nearly 100% nickel(II) extraction at pH ≥ 2. Some co-extraction of copper(II) and cobalt(II) was also noticed, but this was minimised once extraction was performed at the following optimised conditions: [M²⁺] = 0.01 M, [OPIM] = 0.025 M, [DNNSA] = 0.02 M and pH ~1.7, where M²⁺ = Ni²⁺, Cu²⁺ or Co²⁺.

In 2018, Roebuck *et al.*¹⁶ published an in-depth article outlining the strong and selective extraction of nickel(II) based on synergistic mixtures of sulfonic acid synergists and a plethora of bidentate and tridentate *N*-heterocycles. They, interestingly, used DNNSA as synergist along with 2,6-bis(5-octyl-1*H*-pyrazol-3-yl)pyridine as ligand and reported nickel(II) and cobalt(II) extraction of just shy of 100% in extremely acidic sulfate media (pH ~0)—at times going to negative pH values using 10 N H₂SO₄. Moreover, they made a sound case for the mode of extraction by means of tridentate and sulfonic acid synergists, suggesting that the incorporation of DNNSA allows for hydrogen bonding to occur on the periphery (outer coordination sphere and not directly coordinating to the metal centre) of the Ni-ligand-synergist assembly. They claim that the H-bonded assembly drives the efficient extraction of nickel(II) by providing additional stability and hydrophobic moieties. This was shown by means of crystal structure data—something this dissertation studied as well with similar results obtained (**CHAPTER 4**).

Taking all of the aforementioned information into account, a sulfonic acid synergist with similar properties to that of DNNSA was opted for. Therefore, *p*-dodecylbenzenesulfonic acid (DBSA) was selected as an appropriate synergist for synergistic solvent extraction studies (**Scheme 3.3**). DBSA, like DNNSA, also has a characteristic hydrophobic alkyl tail, an aromatic torso and a hydrophilic sulfonic acid head. DBSA is akin to a previously reported analogous synergist by Pearce *et al.*,³³ with the only difference being the presence of a sulfonic acid (–SO₃H) head instead of a sodium sulfonate (SO₃[–]Na⁺) head. This was done to eliminate any interferences that sodium cations might have during solvent extraction studies, although it was merely anticipated to act as a spectator ion in solution. It must be mentioned that DBSA is only applicable to experimental work done in **CHAPTER 3** of this study. The use of different acid synergists in **CHAPTER 5** is mentioned accordingly.

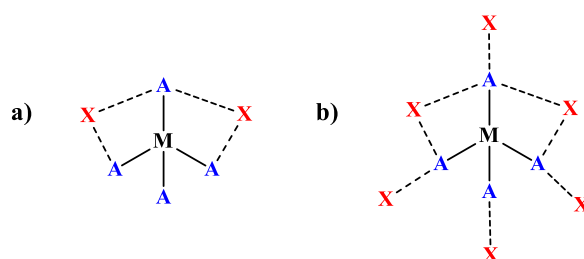


Scheme 3.3: Schematic representation of the sulfonic acid synergist (DBSA) used in this study.

3.1.1.2 Defining the roles of ligands and synergists in this study

To date, there have been no consensus on defining the roles that *ligands* and *synergists* play in modern extractive metallurgy. Synergistic studies are still, relatively speaking, in its infancy with no regulatory chemistry organisations, such as IUPAC, publishing systematic naming protocols regarding this issue. In this study, numerous examples of synergistic systems with an inner-sphere (coordinated) compound and an outer-sphere (uncoordinated) compound providing stabilisation via intermolecular forces have been encountered. Assigning which of these compounds carry the title of “ligand/extractant” or “synergist” has therefore been a matter that required resolution to avoid confusion and misinterpretation. There are a couple of ways to interpret and define ligand/synergist relationships:

- (1) The compound in mole excess should bear the title of “ligand”, while the remaining compound(s) should be assigned as “synergist(s)”, irrespective of their coordination status (**Scheme 3.4**).
- (2) The coordinated compound should always be assigned as the “ligand” (inner coordination sphere) and the non-coordinated compound as the “synergist” (outer coordination sphere), irrespective of their relative stoichiometric ratios (**Scheme 3.4**).



Scheme 3.4: A schematic diagram representing unofficial ligand/synergist conventions **1** and **2**. Convention **1** considers compound A as the “ligand” in **a**) and the “synergist” in **b**), while the opposite is true for compound X. Convention **2** regards compound A as the “ligand” in both **a**) and **b**), while compound X is considered the “synergist” as a result of its exclusive outer coordination sphere involvement.

We are of the mindset, however, that the latter method of assignment (**2**) seems chemically more accurate and avoids the pitfall of regularly having to change the status of a ligand/synergist based on their stoichiometric

ratios. Therefore, throughout this study the primary coordinated species are continually referred to as the “ligand” or “extractant” while the outer-sphere uncoordinated species hold the title of “synergist”. In cases where both compounds A and B are directly coordinated to a metal, the compound with a higher mole value is considered the “ligand” and the compound with lower mole value the “synergist”. It must be emphasised, however, that this unofficial nomenclature convention is only applicable to synergistic solvent extraction systems in this study and is by no means attempting to suggest the blanket adoption thereof.

3.2 Materials and methods

3.2.1 Chemicals and reagents

All chemicals listed in **Table 3.2** were bought from reputable commercial suppliers and used without additional purification.

Table 3.2: List of chemicals used in alphanumeric order.

Chemical/Reagent	Purity (%)	Commercial Supplier
2-(<i>N</i> -Morpholino)ethanesulfonic acid	≥ 99	Sigma-Aldrich (Pty) Ltd.
Acetic acid (glacial)	≥ 99.7	KIMIX Chemical and Lab Supplies (CC)
Cadmium(II) nitrate tetrahydrate	98	Honeywell Fluka™
Chloroform	98	Alfa Aesar
Cobalt(II) nitrate hexahydrate	≥ 98	Merck (Pty) Ltd.
Copper(II) nitrate trihydrate	≥ 99	Sigma-Aldrich (Pty) Ltd.
Lead(II) nitrate	≥ 99	Sigma-Aldrich (Pty) Ltd.
Methanol	≥ 97	Sigma-Aldrich (Pty) Ltd.
Nickel(II) nitrate hexahydrate	≥ 96	Merck (Pty) Ltd.
Nitric acid	1 & 10 N	KIMIX Chemical and Lab Supplies (CC)
<i>p</i> -Dodecylbenzenesulfonic acid	≥ 95	Sigma-Aldrich (Pty) Ltd.
<i>p</i> -Toluenesulfonic acid monohydrate	≥ 98.5	Sigma-Aldrich (Pty) Ltd.
Sodium acetate	≥ 99	KIMIX Chemical and Lab Supplies (CC)
Sodium hydroxide	≥ 97	Alfa Aesar
Sodium nitrate	≥ 99	Sigma-Aldrich (Pty) Ltd.
Zinc(II) nitrate hexahydrate	≥ 98	Sigma-Aldrich (Pty) Ltd.

The following ligands were used as synthetically described in **Section 2.3** of **CHAPTER 2**: 2,6-bis(5-methyl-1*H*-pyrazol-3-yl)pyridine (**1**), 2,6-bis(5-ethyl-1*H*-pyrazol-3-yl)pyridine (**2**), 2,6-bis(5-propyl-1*H*-pyrazol-3-yl)pyridine (**3**), 2,6-bis(5-butyl-1*H*-pyrazol-3-yl)pyridine (**4**), 2,6-bis(5-pentyl-1*H*-pyrazol-3-yl)pyridine (**5**), 2,6-bis(5-hexyl-1*H*-pyrazol-3-yl)pyridine (**6**), 2,6-bis(5-heptyl-1*H*-pyrazol-3-yl)pyridine (**7**), 2,6-bis(5-octyl-1*H*-pyrazol-3-yl)pyridine (**8**), 2,6-bis(5-*tert*-butyl-1*H*-pyrazol-3-yl)pyridine (**9**), 2,6-bis(5-phenyl-1*H*-pyrazol-3-yl)pyridine (**10**), 2,6-bis(1-butylimidazol-2-yl)pyridine (**11**) and 2,6-bis(1-octylimidazol-2-yl)pyridine (**12**).

3.2.2 Instrumentation

3.2.2.1 pH determinations

All pH measurements were performed using a *Thermo Orion 420A+* pH meter, using standards (pH 4, 7 and 10) to calibrate the instrument before every set of measurements.

3.2.2.2 Ultraviolet/visible spectrometry

UV/Vis data were collected using a *Specord® 210 plus* and a *PerkinElmer Lambda 2* spectrophotometer.

3.2.2.3 Laboratory shakers

The organic and aqueous phases were thoroughly mixed during extraction studies using either a *SPO 15-MP Labcon* orbital platform shaker or a *Heidolph Reax 2* overhead shaker/rotator.

3.2.2.5 Inductively Coupled Plasma – Optical Emission Spectrometry

Metal concentrations in the mg/L (ppm) to µg/L (ppb) range were measured using a *Spectro Arcos FHS12 ICP-OES* instrument or a *Perkin-Elmer Optima 2000™ DV*. The former instrument relayed all data via *AMATEK's SPECTRO ICP-OES Smart Analyzer Vision Software, Version 4.02.0834*. Metal concentrations were determined from intensities measured at wavelengths of 214.438 (Cd), 230.786 (Co), 224.700 (Cu), 221.648 (Ni), 172.680 (Pb) and 206.200 (Zn) nm.

3.2.2.6 Data processing software

Data generated via ICP-OES analyses were stored in a *Microsoft Office Excel (Version 2004, Build 12730.20150)* spreadsheet where all calculations were done and extraction plots/curves were produced.

3.2.3 Preparation of buffered solutions

3.2.3.1 NaOAc/AcOH buffer

To prepare a pH 5.0 buffered solution, acetic acid (74.0 mL, 0.200 M) and sodium acetate solution (176 mL, 0.200 M) were quantitatively transferred to a 500 mL volumetric flask and filled to the mark with deionised water.^{34,35} Alternatively, sodium acetate solution (34.7 mL, 2.00 M) and acetic acid (15.3 mL, 2.00 M) were quantitatively transferred to a 500 mL volumetric flask and topped up to the etched mark with deionised water.^{35,36}

Nota bene: Depending on the experimental requirements, these buffered solutions contained various base metal nitrates as well (as listed in **Table 3.2**). The exact pH was measured pre- and post-extraction to ensure that pH changes were kept to a minimum (± 0.2) and the buffered solution was maintaining a constant pH.

3.2.3.2 MES/NaOH buffer with NaNO₃ as ionic strength agent

To a 100 mL volumetric flask was added NaNO₃ (0.425 g, 0.0500 M) and MES (0.976 g, 0.0500 M) with the appropriate base metal. After the flask was three-quarters filled with deionised water, 1.0 M NaOH was added in a dropwise manner until a pH of 5.5 was obtained.

3.2.4 General solvent extraction procedure and conditions

All solvent extraction experiments were carried out in a temperature-monitored laboratory at $20 (\pm 2) ^\circ\text{C}$. Equal volumes (3 mL) of the buffered metal nitrate solution (aqueous phase) and chloroform (organic phase)—containing the appropriate ligand and synergist—were transferred into a 24 mL glass vial (no. 6 polytop) using either a *Gilson* or an *Eppendorf* pipette. Once the glass vials contained the appropriate aqueous and organic contents, they were sealed with tight-fitting plastic tops and parafilm to ensure no leakages occurred. Subsequently, these vials were clamped onto a large laboratory orbital shaker for 24 hours (automatic timer) at an optimised speed of 200 rpm (**Figure 3.1**).

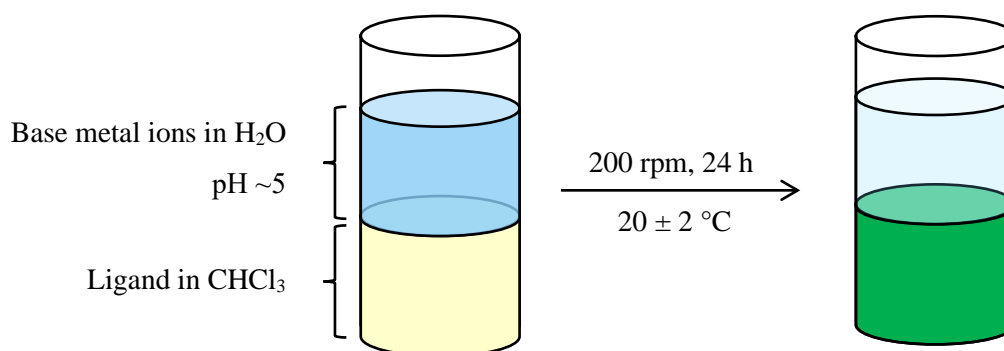


Figure 3.1: General experimental setup and execution of the solvent extraction process.

After the 24-hour extraction period, 1 mL of the aqueous phase was transferred to a 15 mL graded ICP tube and diluted to 5 mL with 0.1 M high-quality nitric acid. These ICP samples were immediately analysed via ICP-OES to avoid evaporation that may lead to higher base metal ion concentrations. Percentage extraction ($\%E$) of the various base metal ions were calculated as follows:

$$\%E = \left(\frac{C_i - C_s}{C_i} \right) \times 100 \quad (39)$$

where C_i represents the initial stock concentration ($\text{mg}\cdot\text{L}^{-1}$) of the metal-rich aqueous solution and C_s represents the concentration ($\text{mg}\cdot\text{L}^{-1}$) of the aqueous solution after extraction as determined via ICP-OES analyses.

Generally, the pH of the aqueous solutions was maintained at ~ 5 , except in the cases of metal ion stripping studies (**Section 3.3.3**) and pH isotherm studies (**Section 3.3.5**). Solvent extraction experiments were performed either in duplicate ($\times 2$) or triplicate ($\times 3$) to guarantee accurate and trustworthy results.

3.3 Results and discussion

There are many factors to consider when planning and preparing solvent extraction experiments. The most challenging aspect throughout this study by far, has been the large quantities of synthesised ligands required to successfully run a wide range of experiments, especially since these experiments had to be performed either in duplicate or triplicate. Therefore, special care was taken with each measurement and experimental setup in order to negate the unnecessary loss of valuable ligand. It was determined that the maximum ligand concentration to be used throughout this study should be limited to 2×10^{-2} M. This was purely done to limit the use of excess ligands and saved many months in the laboratory performing ligand syntheses. Additionally, it had the added benefit of minimising the cost of solvents, reagents and common laboratory consumables as well.

3.3.1 Competitive extraction studies

3.3.1.1 Competitive extraction studies (Cu²⁺ included)

It was decided that the solvent extraction section of this study would commence with competitive extraction studies in the absence of synergist. Competitive (or simultaneous) extraction of six equimolar base metal ions (Cd²⁺, Co²⁺, Cu²⁺, Ni²⁺, Pb²⁺ and Zn²⁺, 1:1:1:1:1:1 ratio) by means of ligands **1–12** was performed to determine their selectivity for any of the aforementioned metal ions. Many hydrometallurgists would argue that competitive extraction studies are better representations of real-world conditions and mimics what one would encounter in industry today, albeit on a much smaller scale.

Two extremely cumbersome and tedious competitive extraction studies were performed. The first being an experiment where the ligand and metal ion concentrations were fixed in a 1:1 (L:M²⁺) ratio (**Figure 3.4**). The data showed an obvious trend for the selective extraction of copper(II) by means of pyrazolyl-pyridine ligands, **1–8**, where the general percentage extraction (%*E*) of copper(II) was arranged as follows:

$$\text{ligand } \mathbf{1} < \text{ligand } \mathbf{2} < \text{ligand } \mathbf{3} < \text{ligand } \mathbf{4} < \text{ligand } \mathbf{5} < \text{ligand } \mathbf{6} \approx \text{Ligand } \mathbf{7} \approx \text{ligand } \mathbf{8}$$

Ligand **1** exhibited the weakest extraction of copper(II) with 12.4 (± 1.7)%, while ligands **6**, **7** and **8** exhibited good and comparable extractions of 78.4 (± 0.2)%, 77.9 (± 0.3)% and 76.9 (± 1.2)%, respectively. This trend can primarily be attributed to the increase in alkyl chain length from ligand **1** (methyl) to ligand **8** (octyl). The tethered alkyl arms served two main functions: the first being related to induction effects and the second being solubility-related. Martell and Smith³⁷ have shown the inclusion of alkyl moieties on ligands increase their ability to form more stable copper(II) and nickel(II) complexes due to a higher electron density being pushed onto the *N*-donor atoms (see **Section 1.9** of **CHAPTER 1**). In this study, however, electron effects were incorporated into the pyrazolyl heterocycle first, which in turn affected electron density on the donor atom. One must also be mindful of the location of alkyl moieties onto the ligands, since alkyl moieties directly tethered to donor atoms negatively affect copper(II) and nickel(II) complex stabilities and subsequent extraction results. The second function of the pendant alkyl moieties is related to the solubility of the ligands in the chloroform organic phase. An increase in the *n*-alkyl pendant lengths (**1–8**) or an increase in branched

moieties (ligand **9**) largely leads to improved solubility of the extracted complex species in the organic phase. In their purest uncoordinated forms, ligands **1–12** were all hydrophobic in nature and merely floated as solid suspensions or as oils on water. It was only once complexation occurred during extraction that the ligand-complex assembly became water soluble, especially in the cases of ligands **1** (methyl) and **2** (ethyl)—and to a lesser extent, ligand **3** (propyl). This too, was clearly a contributing factor to the copper(II) extraction trend seen in **Figure 3.4**. This fact was made even more obvious with a blue-green hue visibly observed in the top aqueous layers of extractants **1–3** (**Figure 3.2**). From **Figure 3.2**, it was also clear that complexation by means of ligands **4–8** were successful due to the presence of a bottle green band at the bottom of the polytop, but more importantly, the complexes remained solubilised in the organic phase, *i.e.*, transport of copper(II) from the aqueous phase was indeed effective.

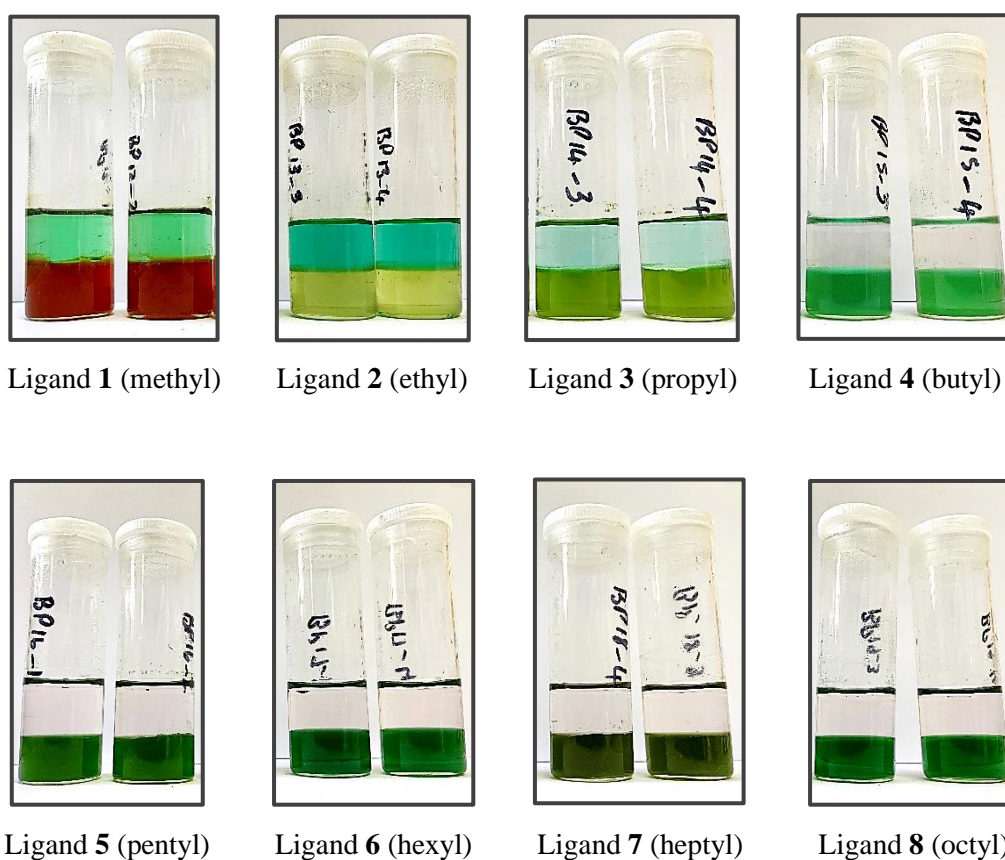


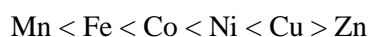
Figure 3.2: Photos of duplicate samples immediately after competitive solvent extraction studies of extractants **1–8**. [Complimentary to **Figure 3.4**]

From **Figure 3.4**, it was apparent that copper(II) extraction plateauing occurred from ligand **6** (hexyl) to **8** (octyl), with these ligands nearing their peak extractive abilities when 1:1 (L:M²⁺) ratios were implemented. An important piece of evidence regarding the ligand:Cu²⁺ (L:Cu²⁺) ratio was also obtained from this data. Since ligands **4–8** and **10** extracted copper(II) in excess of 50%, it can confidently be assumed that L:Cu²⁺ ratios equalled 1:1. If this was not the case, extractions must have been limited to ≤ 50%. Complexes with a 2:1 (L:M²⁺) ratio have a maximum extractive ability of 50%, while 3:1 (L:M²⁺) complexes theoretically hit an extraction ceiling at 33.3% [applicable to 1:1 (L:Cu²⁺) complexes only, **Figure 3.4**]. With that being said, it is

suspected that all copper(II) pyrazolyl complexes probably exist in 1:1 (L:M²⁺) ratios in solution, but due to the less organic soluble complexes (Cu²⁺ complexes with ligands **1–3** and **9**) bleeding into the aqueous phase, this ratio is difficult to prove via solvent extraction experiments. The alternative might be that ligands **1–3** and **9** do in fact coordinate in a 2:1 (L:M²⁺) fashion, but was not observed for ligands **4–8** and **10** due to steric hindrances caused by their extended pendant arms, preventing a second ligand from coordinating to the copper(II) centre. This ligand-to-metal ratio conundrum was further investigated in **Sections 3.3.6** and **3.3.7**.

From **Figure 3.4**, it was clear that the majority of pyrazolyl ligands had selective affinities for copper(II), although ligand **10** (phenyl) showed some extractive affinity for cobalt(II) at 15.2 (± 4.1)% as well. Ligand **10** was the only ligand to be used as a solid due to its insolubility in most common water-immiscible organic solvents. It was therefore decided to use it as a suspended solid extractant. This was probably the reason for large discrepancies observed between measurements and their subsequent inherent errors (see error bars in **Figure 3.4**), since ligand **10** had to be weighed off manually for each polytop. This does, however, bring into question the comparability of ligand **10** to ligands **1–9** and whether it can sensibly be compared to extractants in solution. One must thoroughly consider the necessary caveats when comparisons are made. It is of vital importance that the “solvation factor” not be underestimated, even though all other conditions were kept constant throughout the competitive experiments. Ligand **10** is a promising starting point for additional studies regarding solid phase extractions. It can be tethered to a resin- or polymeric backbone, just like Okewole *et al.*³⁸ synthesised a chelating resin by functionalising the chloromethylated Merrifield resin with 2-(2'-pyridyl)imidazole in their attempt to extract nickel(II). A similar study was also conducted by Ndayambaje *et al.*³⁹ where they managed to adsorb nickel(II) onto polyacrylonitrile (PAN) nanofibers modified with 2-(2'-pyridyl)imidazole.

Figure 3.5 displays a similar type of experiment as **Figure 3.4**, only in this case a 2:1 (L:M²⁺) ratio was implemented. Again, the same copper(II) extraction trend was witnessed as previously discussed, with ligand **1** being the weakest extractant at 15.0 (± 1.7)% and ligand **8** the best extractant at 99.0 (± 0.03)%. Typically, one would expect to observe a significant increase in the extraction of the remaining base metal ions, since “free” extractant was now available to coordinate after nearly 100% copper(II) extraction was achieved. Although some nickel(II) was extracted, it was not as effective as one might anticipate it to be, but it appeared to be the predominant secondary extracted base metal ion. This accords well with the trend proposed by Irving and Williams⁴⁰, that divalent transition metal ions form stable complexes with *N*-donor ligands in the following order:



We noticed that ligand **2** extracted more than triple the original amount of copper(II) at 46.1 (± 0.7)% and ligand **9** extracting just over double the original amount at 88.5 (± 1.2)%. At first, these results were counted as significant evidence for a complex assembly existing in a 2:1 (L:M²⁺) ratio, but this was later countered by extensive Job plot analyses that suggested this cannot be the case (**Section 3.3.6**). It was interesting to note that these dramatic multi-factor increases were not observed for ligand **1**, although healthy increases were

observed for the rest of the pyrazolyl ligands. This can mainly be attributed to the poor solubility of the complex assembly (ligand **1**) in the organic phase. Ligand **10** was the only pyrazolyl ligand that showed some extractive ability for cobalt(II) and nickel(II) with 27.0 (\pm 4.6) and 28.8 (\pm 2.0)%, respectively. This makes ligand **10** a good extractant for a broad range of base metal ions, yet its downfall remains its poor selectivity toward copper(II) when compared to ligands **4–9**.

From **Figure 3.4**, the use of imidazolyl ligands **11** (butyl) and **12** (octyl) as extractants initially seemed somewhat uneventful, with ligand **11** showing no preference for any base metal ion and ligand **12** exhibiting tentative preference for copper(II) at a meagre 25.0 (\pm 0.5)%. This was indicative of poor extractants, but due to ligand **12**'s extended pendant arms, extraction marginally increased owing to its improved organic phase solubility. It was visibly noticeable that both ligands **11** and **12** formed complexes that were preferentially soluble in the top-layered aqueous phase with vibrant blue-green hues (**Figure 3.3**). This was particularly unexpected for ligand **12**, since the analogous pyrazolyl complexes were poorly water-soluble. This result can only be attributed to the lack of *NH* protons, which eliminates the key stabilisation of the complex assemblies via hydrogen bonding.

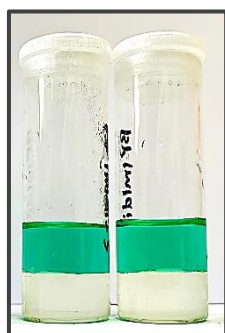
Ligand **11** (butyl)Ligand **12** (octyl)

Figure 3.3: Photos of duplicate samples immediately after competitive extraction studies by means of ligands **11** and **12**. [Complimentary to **Figure 3.4**]

Once the ligand concentration was doubled, ligand **12** doubled its copper(II) extraction as well to 51.5 (\pm 0.4)%. This was expected, but the 34.0 (\pm 1.4)% extraction of nickel(II) by means of ligand **11** was surprising to say the least (**Figure 3.5**). To verify this result, this experiment was rerun under the same conditions and did not yield any noticeable differences. It can only be surmised that both ligands **11** and **12** coordinated to nickel(II) in a 2:1 fashion, but in the case of ligand **12**, the long alkyl arms of the first coordinated ligand interfered with the coordination of the second incoming ligand. Since ligand **11** had shorter arms, this seemed less of an issue, hence the selective extraction of nickel(II), albeit $< 40\%$. Its poor extraction of copper(II), compared to that of ligand **12**, was poignant evidence that the 1:1 (L:M²⁺) copper(II) complex remained in the aqueous phase, while the 2:1 (L:M²⁺) nickel(II) complex was extracted into the organic phase due to an improved solubility overall.

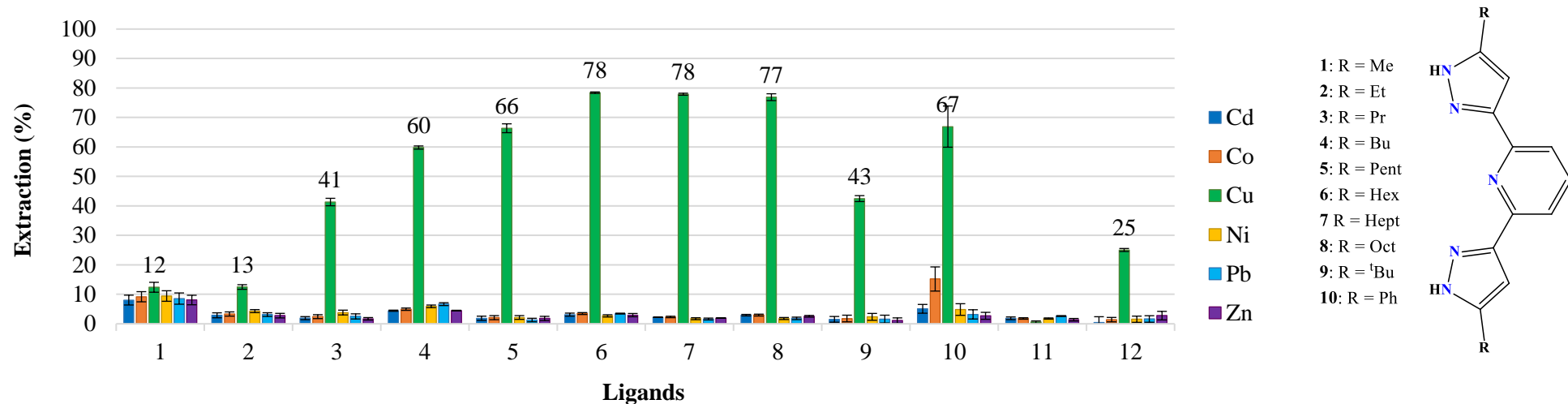


Figure 3.4: Competitive 1:1 (L:M²⁺) extraction of six base metal ions using ligands 1–12. [Ligands] $\approx 1 \times 10^{-2}$ M; [M²⁺] $\approx 1 \times 10^{-2}$ M; NaOAc/AcOH buffer; pH 5.03–5.10. [Data labels are rounded to two significant figures. See corresponding data in **Table 1** of **Appendix B — DATA TABLES**]

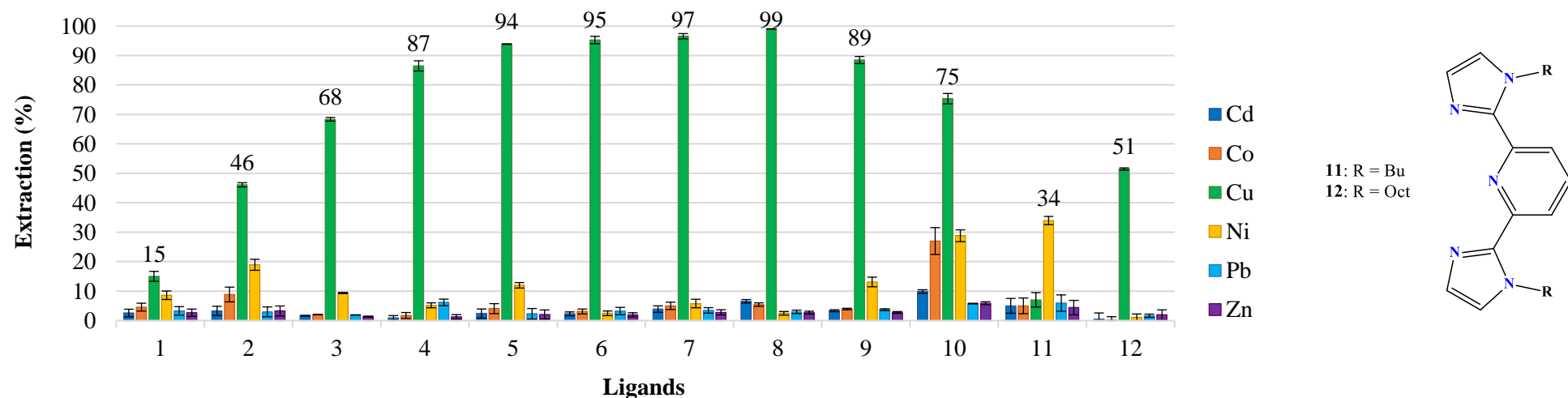


Figure 3.5: Competitive 2:1 (L:M²⁺) extraction of six base metal ions using ligands 1–12. [Ligands] $\approx 2 \times 10^{-2}$ M; [M²⁺] $\approx 1 \times 10^{-2}$ M; NaOAc/AcOH buffer; pH 5.03–5.07. [Data labels are rounded to two significant figures. See corresponding data in **Table 2** of **Appendix B — DATA TABLES**]

3.3.1.2 Competitive extraction studies (Cu²⁺ excluded)

After both pyrazolyl- and imidazolyl ligands (**1–12**) showed excellent copper(II) extractive abilities, it was decided to determine which base metal ion was the second-most extracted species. This can be probed by simply increasing the L:M²⁺ ratio incrementally until all copper(II) is extracted, followed by the extraction of the second metal ion species in solution. However, this approach was not deemed economical and therefore the use of copper(II) in the next set of competitive extraction experiments was omitted altogether. This yielded valuable insight regarding the predominant second-most extractable base metal ion species.

All experimental conditions were kept close to that of previous competitive extraction setups. A 2:1 (L:M²⁺) ratio in sodium acetate/acetic acid buffered solutions (pH ~5) were maintained, since this approach led to efficient copper(II) extractions. From **Figure 3.6**, it became clear that nickel(II) was in fact the second-most affinitive metal ion species, albeit not particularly selective. Ligand **5** (pentyl) was most effective in this regard with a generous nickel(II) extraction of 69.2 (± 2.5)%. The octyl-functionalised imidazolyl ligand (**12**) emerged as the weakest nickel(II) extractant with 5.01 (± 2.5)% and extracted 14.5 (± 0.3)% of cobalt(II)—its most selective metal ion during this experiment.

In general though, ligands **2–5** and **9** (*tert*-butyl) performed about the same, with nickel(II) extraction typically observed in the low-to-high 60% range. If experimental errors were taken into account, it would be hard to separate these ligands' nickel(II) extractive abilities. Here, however, selectivity was not nearly as clear-cut as previously seen in **Figure 3.5**. Cobalt(II) was co-extracted in many cases and would make future cobalt(II)/nickel(II) separations extremely difficult and cumbersome. Experimental conditions, such as pH, may be required to change in order to achieve this. This third stepwise metal ion separation was not attempted, since other members of the Extractive Metallurgy Research Group (EMRG) at Stellenbosch University (SU) are currently researching this exact problem.

A fascinating phenomenon was observed when ligands **6–8** and **12** were implemented as nickel(II) extractants. These ligands did not follow the preceding trend of extraction whatsoever, with sharp declines in nickel(II) extractions and notable surges in cadmium(II) extractions in the cases of ligands **6–8**. It is postulated to once again be a consequence of steric hindrance, where the coordination of two ligands to nickel(II) is made difficult due to their long alkyl pendant arms limiting their *N*-donor atoms access to nickel(II). Ligands **6–8** extracted both cobalt(II) and cadmium(II) over nickel(II), which in part can be explained by looking at these ions' divalent ionic radii. In 1976, Shannon⁴¹ showed Ni²⁺, Co²⁺ and Cd²⁺ radii to be 83, 89 and 109 pm, respectively (coordination number of 6). This could mean that cobalt and cadmium's larger divalent ionic radii created more room for two bulky tridentate pyrazolyl ligands to effectively coordinate with lessened steric interference, hence their improved extraction results by means of ligands **6–8**. This theory was further substantiated with ligand **8** extracting mostly cadmium(II) at 41.4 (± 1.0)%, probably due to its octyl moiety limiting its coordinative ability to both nickel(II) and cobalt(II).

Ligand **11** showed relative selectivity towards nickel(II) at 45.8 (± 2.1)% with the remaining metal ions weakly extracted at < 7%. This result makes it an excellent candidate for synergistic studies in the presence of

p-dodecylbenzenesulfonic acid (DBSA) to promote an increase of nickel(II) uptake in a selective manner. This is discussed in greater detail in **Section 3.3.8**.

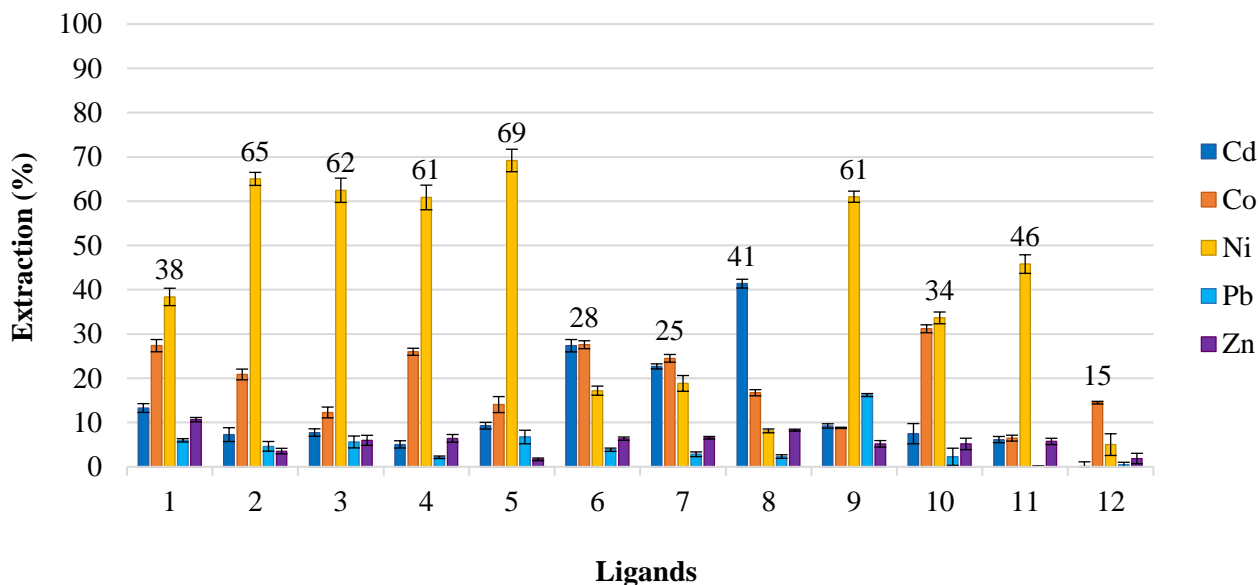


Figure 3.6: Competitive 2:1 (L:M²⁺) extraction of five base metal ions using ligands 1–12 (Cu²⁺ excluded). [Ligands] $\approx 2 \times 10^{-2}$ M; [M²⁺] $\approx 1 \times 10^{-2}$ M; NaOAc/AcOH buffer; pH 4.95–5.04. [Data labels are rounded to two significant figures. See corresponding data in **Table 3 of Appendix B — DATA TABLES**]

3.3.2 Selectivity studies

After the pyrazolyl ligands showed successful competitive extraction results for copper(II), it was decided to perform selectivity studies using ligands 3–10. Pyrazolyl ligands 1 and 2 in addition to imidazolyl ligands 11 and 12 were excluded from this study, since they did not display particularly effective competitive copper(II) extractive abilities (**Figures 3.4** and **3.5**).

Selectivity studies are akin to competitive extraction studies, with the key difference being the intentional decrease of the metal ion of interest's concentration by a pre-determined factor. This provides useful insight regarding a ligand's selectivity for a specific base metal ion, whilst being confronted with other base metal ions present at much higher concentrations. It is common practice to decrease a particular metal ion's concentration tenfold ($\times \frac{1}{10}$) or hundredfold ($\times \frac{1}{100}$), but in this case it was agreed to perform two selectivity experiments by decreasing the copper(II) concentration tenfold ($\times \frac{1}{10}$) and sixtyfold ($\times \frac{1}{60}$). Initially, a hundredfold experiment was conducted, but it was soon realised during ICP-OES analyses that the samples were skirting the instrument's detection limit for copper(II). We did not trust the analyses fully and felt uncomfortable to continue with the experiment after preliminary data yielded speculative results. This experiment was duly repeated and modified by altering the copper(II) concentration to a factor of 60 to allow the instrument to operate well above its detection limit.

In these studies, the same selection of base metal ions were present (Cd^{2+} , Co^{2+} , Cu^{2+} , Ni^{2+} , Pb^{2+} and Zn^{2+}) in a 1:1:0.1:1:1:1 ratio ($[\text{M}^{2+}] = 1 \times 10^{-2} \text{ M}$, $[\text{Cu}^{2+}] = 1 \times 10^{-3} \text{ M}$). With a decrease in the copper(II) concentration it was expected to observe increased %*E* for the other base metal ions in solution, especially nickel(II). This, upon closer inspection of **Figure 3.7**, was confirmed when noteworthy increases for nickel(II) were noticed for ligands **3–5** and **9**. Unsurprisingly by now, cobalt(II) and cadmium(II) made significant extraction gains as well in the cases of ligands **6–8**. Still phenomenal copper(II) extractions were witnessed for ligands **4–8** with results ranging from 90.0 (± 0.8)% for ligand **4** to 93.5 (± 1.1)% for ligand **8**. Ligands **3** and **9** yielded decent above-average results with 75.8 (± 0.7) and 84.1 (± 0.4)%, respectively, while ligand **10** performed quite poorly with 50.4 (± 1.1)%. These results reinforce the fact that these tridentate pyrazole-pyridinyl ligands are truly selective copper(II) extractants, with ligand **8** narrowly the best performer.

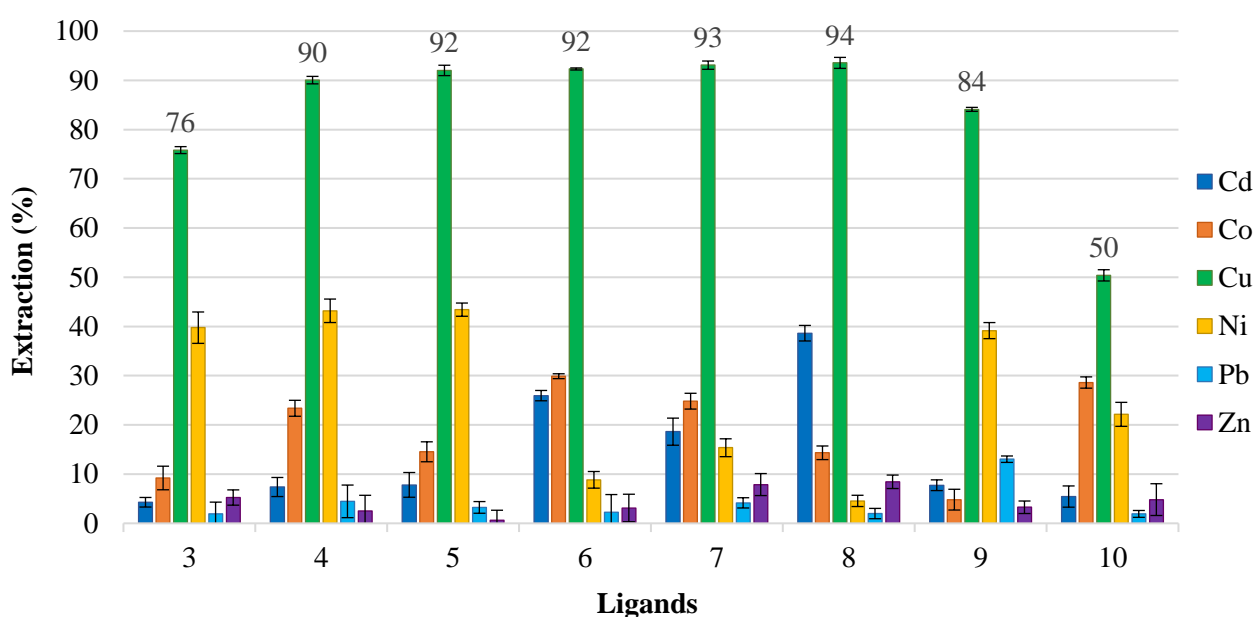


Figure 3.7: Copper(II) selectivity study using pyrazolyl ligands **3–10**. Copper(II) concentration decreased tenfold. $[\text{Ligands}] \approx 2 \times 10^{-2} \text{ M}$; $[\text{M}^{2+}] \approx 1 \times 10^{-2} \text{ M}$; $[\text{Cu}^{2+}] = 1.09 \times 10^{-3} \text{ M}$; NaOAc/AcOH buffer; pH 4.90. [Data labels are rounded to two significant figures. See corresponding data in **Table 4** of **Appendix B — DATA TABLES**]

The next selectivity study (**Figure 3.8**) was similar to the aforementioned study, only this time the copper(II) concentration was decreased sixtyfold to $1.67 \times 10^{-4} \text{ M}$. Now, the metal ion ratios can be summarised as follows: 1:1:0.0167:1:1:1 for Cd^{2+} , Co^{2+} , Cu^{2+} , Ni^{2+} , Pb^{2+} and Zn^{2+} , respectively. Once again, remarkable copper(II) extractions were observed with %*E* ranging from the mid- to high-80 percentiles. Ligand **10**'s %*E* was average at best with 49 (± 1.4)%, while ligands **3** and **9** delivered good extraction values of 75.6 (± 0.7) and 78.9 (± 0.9)%, respectively.

Nickel(II) extractions increased considerably to levels previously seen during Cu²⁺-excluded competitive studies (**Figure 3.6**). This was heartening evidence indicating the results were uniform across multiple experiments. Here too, ligands **3–5** and **9** exhibited good nickel(II) extractive abilities with results comparable to that seen in **Figure 3.6**. Similar cadmium(II) extractions were noticed when compared to **Figure 3.6** as well. For ligands **6–8**, cadmium(II) was the predominant second-most extracted base metal ion with extraction values of 25.8 (± 1.8), 23.4 (± 1.2) and 41.6 (± 2.2)%, respectively. Throughout this study, it was clear that the ligands showed very little affinity towards either lead(II) or zinc(II).

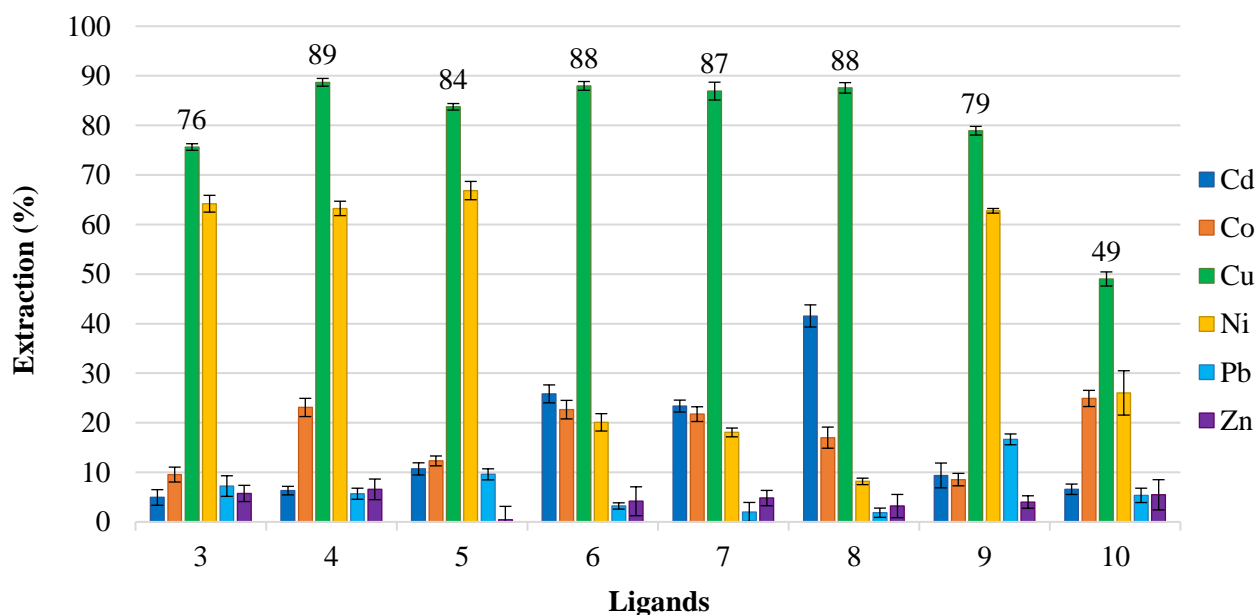


Figure 3.8: Copper(II) selectivity study using pyrazolyl ligands **3–10**. Copper(II) concentration decreased sixtyfold. [Ligands] $\approx 2 \times 10^{-2}$ M; $[M^{2+}] \approx 1 \times 10^{-2}$ M; $[Cu^{2+}] = 1.67 \times 10^{-4}$ M; NaOAc/AcOH buffer; pH 4.89. [Data labels are rounded to two significant figures. See corresponding data in **Table 5** of **Appendix B — DATA TABLES**]

3.3.3 Extraction and metal ion recovery of copper(II) and nickel(II)

The art of designing ligands for the sole purpose of metal ion extraction, is proverbial suicide for modern-day industries. It does not make sense, either economically or monetarily, for such companies to exist unless they find tangible ways to recover their extracted materials. In solvent extraction applications, this is usually done by substantially lowering the aqueous pH to < 2 in order to increase proton competition on the extractants' active donor sites. This liberates extracted metal ions back into the aqueous phase and regenerates uncoordinated ligands, which in turn, can theoretically be recycled indefinitely. Typically, this process can be followed visually with the organic phase gradually losing its vibrant colour, while the aqueous phase gains a slight blue or green tint as a result of an increased metal ion concentration (**Figure 3.9**). However, reality proves that extractants are often hydrolysed or rendered ineffective after multiple uses due to constant contact with aqueous phases at varying pH values (extraction pH: ~ 5 ; recovery pH: < 2).

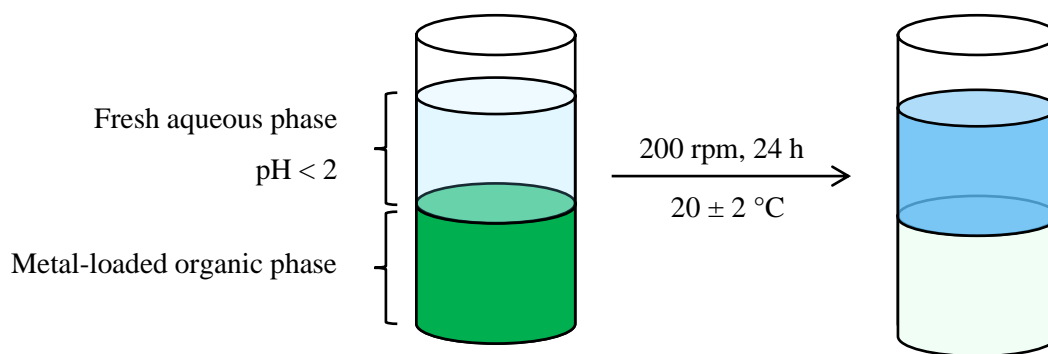


Figure 3.9: Typical experimental setup and execution of the metal ion recovery process.

3.3.3.1 Copper(II) extraction and recovery

Before the metal ion releasing abilities of ligands **1–12** could be investigated, it was first necessary to determine each ligand's copper(II) extractive ability in the absence of any other metal ion. **Figure 3.10** depicts exactly this, with generally similar trends observed as previously discussed for competitive copper(II) extractions. Ligands **4–8** are by now known to be excellent copper(II) extractants with extraction results in the low to high ninety percent range. The shorter alkyl-tethered pyrazolyl ligands, **1–3**, were expectantly the weakest performers with 27.6 (± 0.9), 52.3 (± 0.3) and 63.1 (± 0.5)%, respectively. Imidazolyl ligand **11** was by far the worst extractant at 16.8 (± 0.8)%, while ligand **12** exhibited a mediocre copper(II) extraction of 55.1 (± 0.6)%.

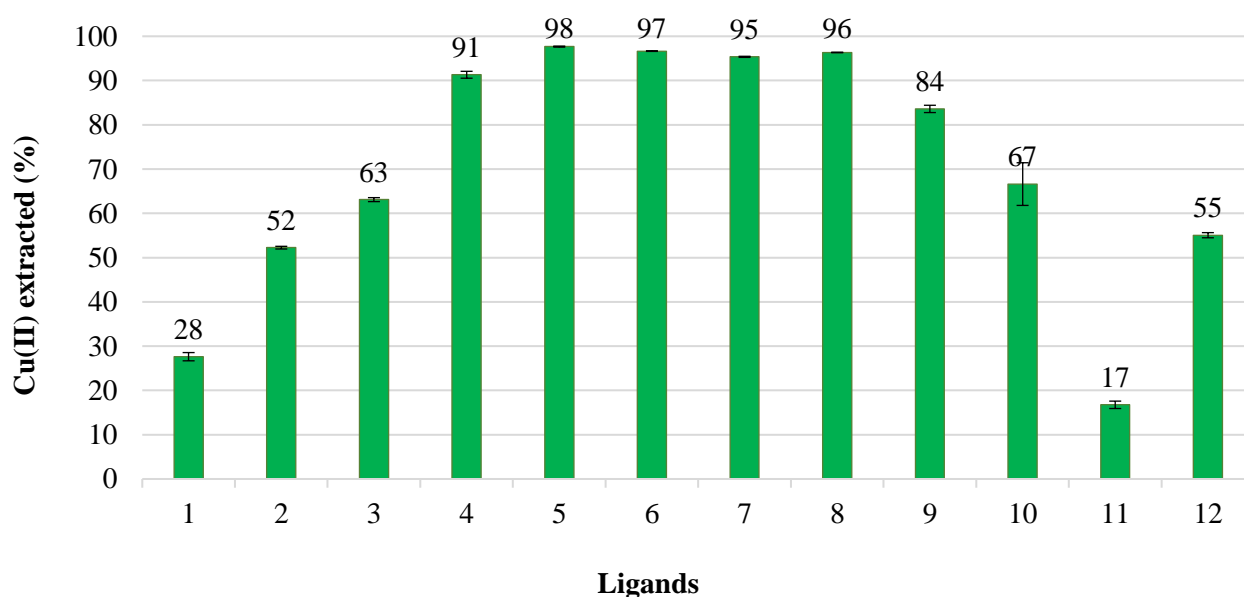


Figure 3.10: Copper(II) extraction (loading) by means of ligands, **1–12**, in a 2:1 (L:Cu²⁺) ratio. [Ligands] $\approx 2 \times 10^{-2}$ M; [Cu²⁺] = 1.05×10^{-2} M; NaOAc/AcOH buffer; pH 4.93. [Data labels are rounded to two significant figures. See corresponding data in **Table 6** of **Appendix B — DATA TABLES**]

Now, the recovery of copper(II) could commence by subjecting the loaded organic phases (containing the coordinated metal ion species) to a fresh and heavily acidic aqueous phase. It was decided to kick off the metal ion recovery process with an aqueous pH of 1 by using analytically pure 0.1 M HNO₃. After the loaded organic

phases were brought into contact with the acidic aqueous phase and allowed to mix for 24 hours, merely negligible amounts of recovered copper(II) were noticed. At pH 1, a maximum release of 1.81 (± 0.4)% was observed for ligand **3**. This highlighted the extraordinary affinity these ligands showed towards copper(II). It was quickly realised that lower pH was required to effect some sort of copper(II) release. The experiment was subsequently rerun—this time using 1 M HNO₃ to obtain an aqueous pH of 0. After many days in the laboratory and innumerable ICP analyses, it was somewhat surprising and disheartening to learn that this experiment too was unsuccessful. A maximum copper(II) release of 5.52 (± 0.4)% for ligand **3** was observed, with the majority of ligands releasing less than 2%. After much deliberation, it was therefore decided to use 10 M HNO₃ to introduce an aqueous pH of -1 . Due to these extreme acidic experimental conditions, the utmost of care was taken to ensure all precautionary personal protective equipment (PPE) was worn and that at least one other laboratory assistant/technician was present at all times.

We realised these severe conditions may in fact hydrolyse the ligands, therefore it was paramount to determine whether they would “survive” such conditions. Control experiments were performed, whereby each ligand (in chloroform) was subjected to an aqueous phase (pH -1) for 24 hours. No metal whatsoever was introduced—these were merely tests to determine the ligands’ acidic susceptibilities. After 24 hours, the aqueous phases were decanted off, followed by the *in vacuo* concentration of the organic phases and resubmission of these samples for ¹H NMR analyses. Remarkably, these ligands appeared quite resilient, with only tiny decomposition blips observed throughout the various spectra. With that being said, these ligands were not anticipated to perform effectively in more than two or three metal ion extraction-recovery cycles, with acidic decomposition being the obvious culprit.

Since the relative acidic stability of ligands **1–12** were confirmed via ¹H NMR, copper(II) recovery at pH -1 could begin. The recovery percentage (%*R*) was calculated according to Eq. 40 and was based on the amount of copper(II) initially extracted (**Figure 3.10** and **Table 6** in **Appendix B — DATA TABLES**):

$$\%R = \frac{C_R}{C_E} \times 100 \quad (40)$$

where %*R* is the percentage metal ion recovered, *C_R* is the concentration (mg.L⁻¹) of the metal ion in the aqueous phase after recovery and *C_E* is the original concentration (mg.L⁻¹) of metal ion extracted into the organic phase.

From **Figure 3.11**, it was apparent that copper(II) recovery from pyrazolyl extractants, **1–8**, shadowed the following numerical trend: **1** > **2** > **3** > **4** > **5** > **6** > **7** > **8**. The highest percentage of copper(II) was recovered from ligand **1** (methyl) at 95.4 (± 2.9)%, while only 9.07 (± 0.7)% was recovered from ligand **8** (octyl). This trend only made sense once both solubility and electronic (inductive) effects were taken into account. The longer alkyl-tethered ligands are more shielded from the acidic aqueous phase due to their inherent hydrophobic nature and is therefore not readily protonated at their donor sites (less time spent at the interface). Therefore, these ligands released copper(II) with a greater degree of difficulty. Moreover, electron density is forced into the pyrazolyl heterocycle and strengthens the N–Cu coordination bond, hence ligand **8**’s

exceptional ability to hold fast to its copper ion. The exact opposite was true for ligand **1**, with reduced hydrophobicity and lessened electron density in the pyrazole heterocycle resulting in near maximum copper(II) recovery. Although ligand **1** showed excellent releasing abilities, this result must be evaluated with its extractive power in mind (**Figure 3.10**) in order to assess its overall extractive-releasing ability. When this dual nature is thoroughly considered, it is easy to recognise ligand **1**'s poor overall performance. Ligand **8**, on the other hand, is an excellent copper(II) extractant, but incredibly poor in its copper(II) releasing ability. This is a proverbial catch-22 situation, whereby the pros and cons weigh heavily on opposite sides of this extraction conundrum. Perhaps the answer lies with ligand **4** (butyl)—the golden middle. It extracted copper(II) rather efficiently (not as good as ligand **8**, but better than ligand **1**) at 91.3 (\pm 0.8)% and showed a comparatively effective releasing ability too (better than ligand **8**, but worse than ligand **1**) at 54.9 (\pm 1.4)%.

It was interesting to note the similar extractive and releasing performances of ligands **4** (butyl) and **9** (*tert*-butyl). Both ligands released more than 52% of their > 83% extracted copper(II). This can most likely be attributed to their comparable alkyl pendant arms (both consisting of four carbons). Imidazolyl ligand **11** was poor at transporting copper(II) from the aqueous phase, while ligand **12** was average at best. However, they were both excellent in their releasing abilities with 95.2 (\pm 3.1) and 87.7 (\pm 1.9)%, respectively recovered. Again, these results can be attributed to their inability to form strong coordination bonds to copper(II), hence the high recovery percentages for ligands **11** and **12**. All in all, one probably would not implement either ligands **11** or **12** as effective copper(II) extractants in industry today—at least not without an effective synergist to boost their extractive abilities (see **Section 3.3.8**).

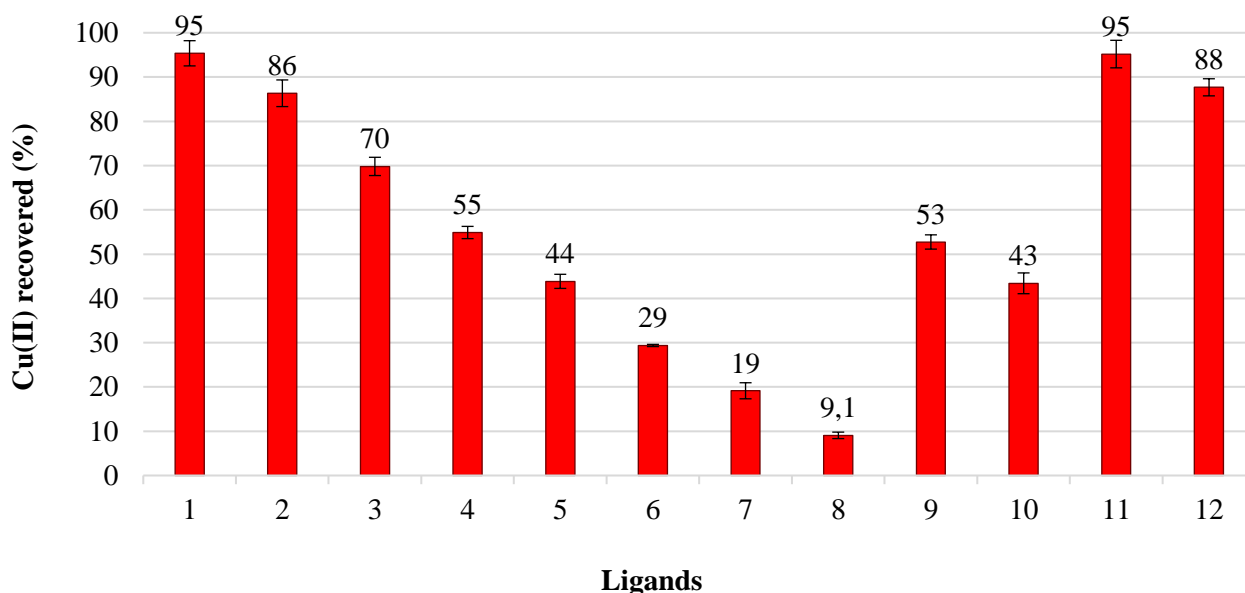


Figure 3.11: Copper(II) recovery from loaded organic phases containing ligands **1–12**. 10 M HNO₃ aqueous phase (pH -1). [Data labels are rounded to two significant figures. See corresponding data in **Table 7** of **Appendix B — DATA TABLES**]

3.3.3.2 Nickel(II) extraction and recovery

To determine whether ligands **1–12** were efficient in their nickel(II) releasing abilities, it was necessary to first conduct nickel(II) extraction studies in the absence of any other base metal ions. This allowed accurate deductions to be made without added interferences or the unknown influence of additional base metal ions in solution. As seen with previously discussed selectivity studies (**Figure 3.8**), a clear nickel(II) extraction trend seemed to repeat itself once more when **Figure 3.12** was studied. The short- to mid-ranged alkyl-tethered pyrazolyl ligands (**2–5** and **9**) appeared to have reached a nickel(II) extraction ceiling with low 70 percentile extractions. Ligands **1** (methyl) and **10** (phenyl), on the other hand, only managed to extract 48.9 (± 0.8) and 50.0 (± 4.1)%, while the longer alkyl-tethered pyrazolyl ligands, **6–8**, were the weakest performers at 30.1 (± 0.9), 28.9 (± 1.4) and 20.5 (± 0.8)%, respectively. The noticeable drop in ligands **6–8**'s extractive performance was not a new occurrence and has previously been observed in **Figures 3.6–3.8** and were explained in theoretical terms in **Sections 3.3.1.2** and **3.3.2**.

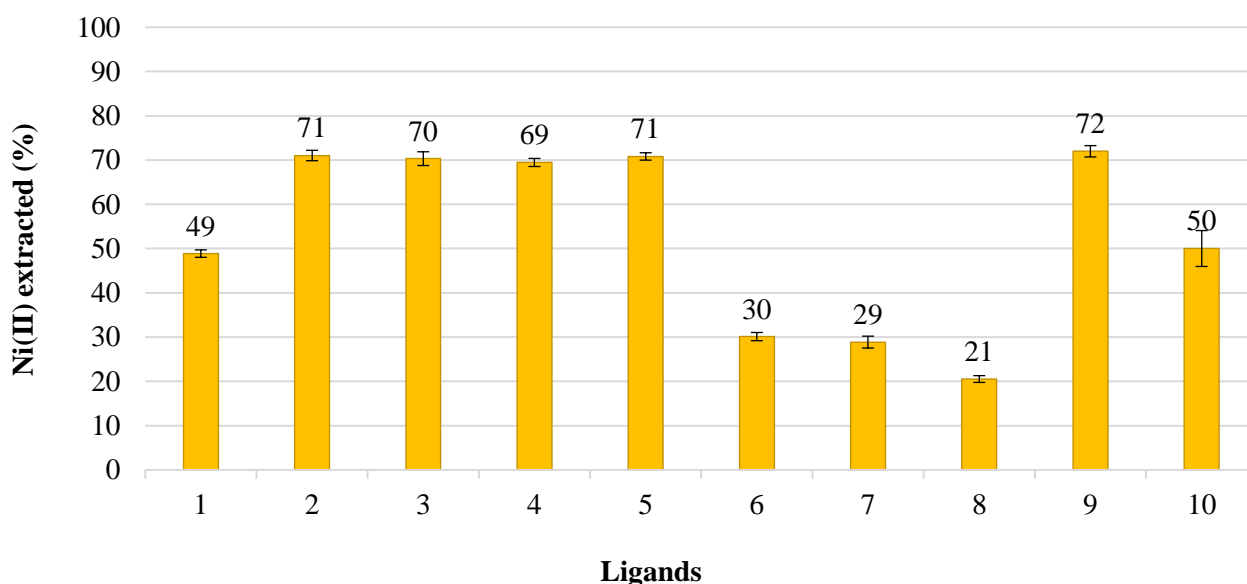


Figure 3.12: Nickel(II) extraction (loading) by means of pyrazolyl ligands, **1–10**, in a 2:1 (L:Ni²⁺) ratio. [Ligands] $\approx 1 \times 10^{-2}$ M; [Ni²⁺] = 5.61×10^{-3} M; NaOAc/AcOH buffer; pH 5.00. [Data labels are rounded to two significant figures. See corresponding data in **Table 8** of **Appendix B — DATA TABLES**]

Next, the nickel(II) extractive abilities of imidazolyl ligands were put to the test in the absence of other base metal ions. The pyrazolyl and imidazolyl ligands were separated in order to ascertain the effect that 1:1 and 2:1 (L:Ni²⁺) ratios might have on the imidazolyl ligands' metal loading results. This came after **Figure 3.6** in **Section 3.3.1.2** was studied, where promising nickel(II) loading results in the presence of cadmium(II), cobalt(II), lead(II) and zinc(II) were witnessed. It was postulated that a doubling of the loading percentage, from a 1:1 to a 2:1 (L:Ni²⁺) ratio, might be indicative of the nature of the coordination mechanism, *i.e.*, whether one or two ligands actively coordinate to nickel(II). From **Figure 3.13**, relatively poor 1:1 (L:Ni²⁺) loading results were observed with imidazolyl ligands **11** and **12** extracting 18.9 (± 0.6) and 4.36 (± 1.4)%, yet a doubling of the loading percentages did occur when the ligand concentration was doubled. Ligand **11** and **12**

increased their nickel(II) loading to 44.4 (\pm 0.7) and 9.88 (\pm 1.1)%, possibly pointing towards a 2:1 (L:Ni²⁺) complex. Of course, this data on its own did not meet all the evidential requirements to prove that this was indeed the case—it was merely a hint pointing to what was happening at the molecular level. Additional studies were performed to determine this as best we could and can be seen in **Sections 3.3.6** and **3.3.7**.

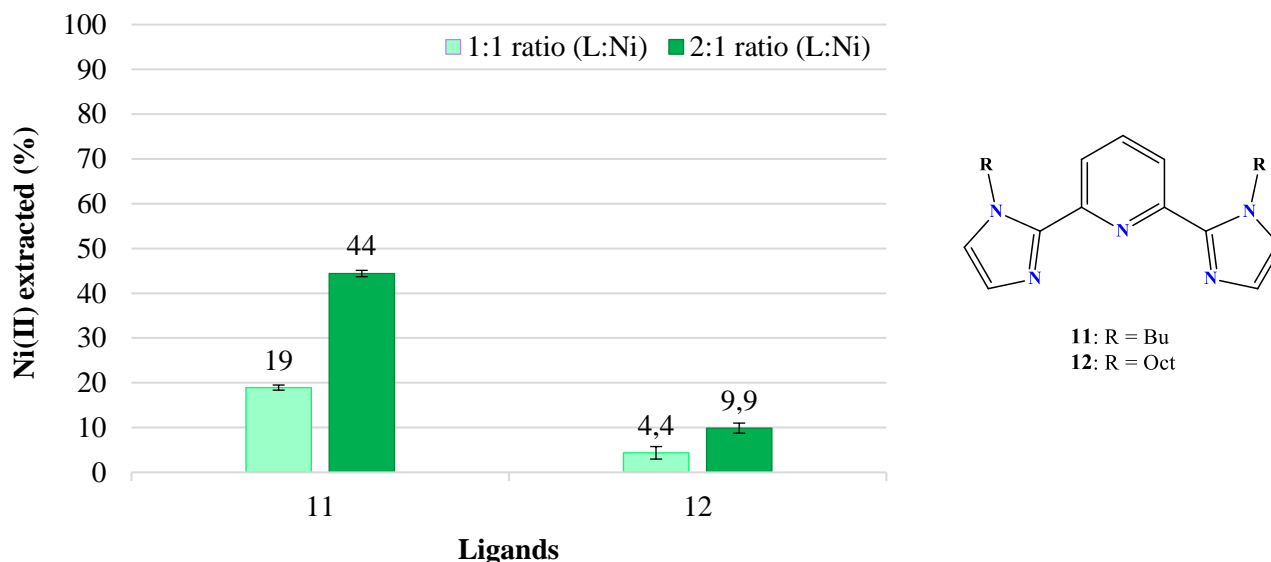


Figure 3.13: Nickel(II) extraction via imidazolyl ligands **11** and **12** with varying L:Ni²⁺ ratios. [Ligands] \approx 5×10^{-3} M (1:1 ratio); [Ligands] \approx 1×10^{-2} M (2:1 ratio); [Ni²⁺] = 5.61×10^{-3} M; NaOAc/AcOH buffer; pH 5.00. [Data labels are rounded to two significant figures. See corresponding data in **Table 9** of **Appendix B — DATA TABLES**]

Finally, the recovery of nickel(II) from ligands **1–12** can now be introduced (**Figure 3.14**). It is crucial, however, to analyse this graph in conjunction with the pyrazolyl and imidazolyl nickel(II) loading graphs (**Figures 3.12** and **3.13**) to make accurate sense of it. First, it was decided to execute this experiment at pH 0 instead of the ultra-harsh pH -1 condition implemented during the recovery of copper(II) in **Section 3.3.3.1**. This was done after Roebuck *et al.*¹⁶ demonstrated that 2,6-bis(5-nonyl-1*H*-pyrazol-3-yl)pyridine along with DNNSA as synergist, extracted nickel(II) efficiently at pH $>$ 0. In this study, no stabilising synergists were included in the extraction systems, therefore, pH 0 was presumed to be an optimum condition during this recovery study as well.

The short- to mid-ranged alkyl-tethered pyrazolyl ligands showed clear nickel(II) recovery diminution from ligand **1** [97.2 (\pm 1.2)%] to **5** [59.4 (\pm 2.2)%]. This was a similar trend to that observed for copper(II) recovery, only this time the nickel(II) recovery decline ceased at ligand **5** and did not continue to ligand **6**, **7** or **8**. At first, this appeared counterintuitive, but the poor nickel(II) extractive performance of ligands **6–8** were indicative of their weak affinity towards nickel(II) and would therefore discard their bound nickel(II) ion with more ease once the conditions became slightly unfavourable. Nickel(II) affinity decreased from ligands **6–8** (**Figure 3.12**), while the subsequent release of nickel(II) at pH 0 incrementally increased from

ligand **6** [87.5 (\pm 0.8)%] to **8** [91.3 (\pm 0.8)%]. Ligand **9** (*tert*-butyl) [65.9 (\pm 1.9)%] yielded similar results to that of ligand **4** (butyl) [68.4 (\pm 1.9)%], with ligand **10** releasing 83.5 (\pm 2.3)% of its originally extracted nickel(II).

Imidazolyl ligands **11** and **12** displayed good releasing abilities too, with 85.7 (\pm 1.5) and 89.7 (\pm 0.6)%, respectively. Again, exceptional nickel(II) releasing abilities were observed in the case of ligand **12** due to its comparably weak affinity for nickel(II).

If a single ligand had to be selected for an overall effective and efficient nickel(II) extraction and recovery cycle, pyrazolyl ligand **2** (ethyl) would most likely be the most effective—primarily due to an extraction of 71.0 (\pm 1.2)% and nickel(II) release of 88.4 (\pm 1.3)%. It must be noted, however, that these results are heavily dependent on pH, temperature, ligand concentration and ionic strength. Therefore, the best suited ligand for one specific set of circumstances might not be the best suited ligand for another. It is imperative that the cyclical extraction-recovery setup is fully optimised for the envisaged end use of the implementer.

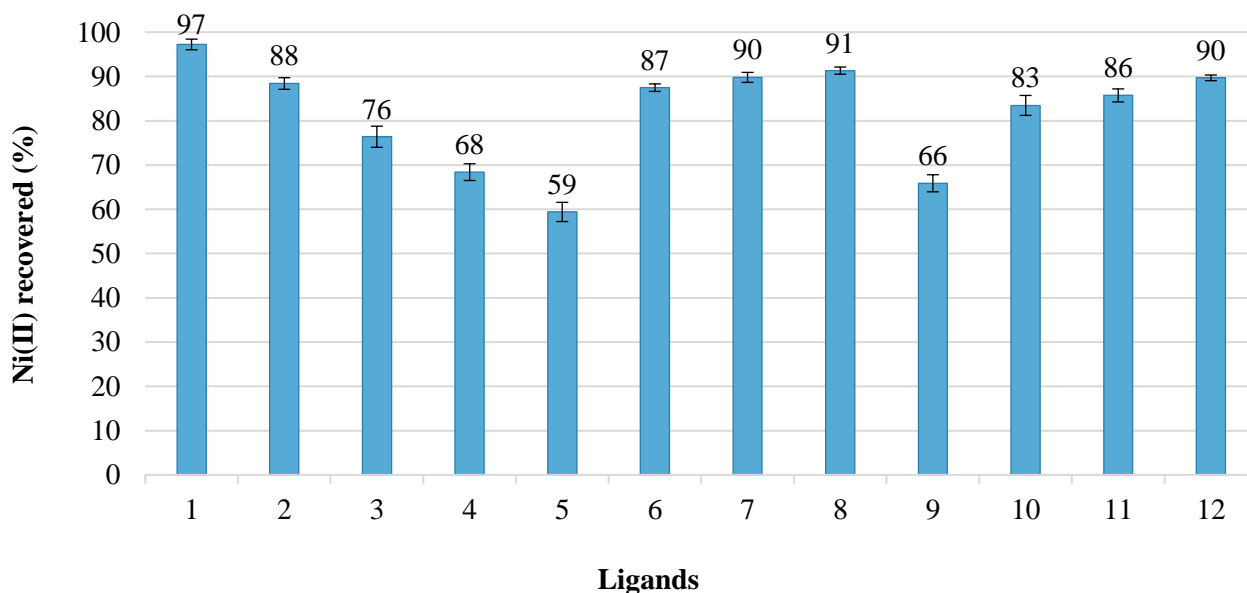


Figure 3.14: Nickel(II) recovery from loaded organic phases containing ligands **1–12**. 1 M HNO₃ aqueous phase (pH 0). [Data labels are rounded to two significant figures. See corresponding data in **Table 10** of **Appendix B — DATA TABLES**]

3.3.4 Time-dependent extraction study of copper(II) and nickel(II)

To ensure that the aforementioned copper(II) and nickel(II) extraction and stripping studies (**Sections 3.3.3**) were accurate and reliable, multiple 24-hour time-dependent studies were performed to ascertain whether or not the extractions reached equilibrium before the 24-hour mark. These experiments are exhaustively tedious and cumbersome to execute, but equally important and necessary too. Without knowing whether the solvent extraction systems reached equilibrium, it was nigh impossible to assess the results with a fair degree of

confidence. Industrially speaking, these time-dependent studies allow companies the added benefit of adjusting their extraction timeframes to < 24 hours, resulting in improved productivity and maximised profit margins.

Figure 3.15A illustrates the extraction of copper(II) over a 24-hour period by using a selection of short, intermediate and long alkyl-armed pyrazolyl ligands (**2**, **5** and **7**) as extractants. It was well noted that all three ligands reached equilibrium well before the 24-hour mark, with ligands **2** and **5** achieving this after approximately 30 minutes. Ligand **7**, however, had a much shallower 8-hour approach to its state of extractive equilibrium. The longer *n*-heptyl chains inherently attributed more hydrophobic character to the ligand, making it less prone to coordinate to the water-solubilised copper(II) in the short term (< 8 hours). Outliers do exist, but can readily be attributed to human timing errors, since these experiments were extraordinarily difficult to execute manually. Without a shadow of a doubt, these experiments would gain tremendous accuracy and precision if automatic samplers were to be introduced. Moreover, these experiments were only performed in duplicate to limit the use of synthesised ligands, thereby generating the odd outlier.

From **Figure 3.15B** it was noticed that both imidazolyl ligands **11** and **12** took approximately 16 hours to reach their respective extraction equilibria. This was far longer than initially anticipated, but in hindsight can most probably be attributed to their lack of NH moieties, with no H-bonds assisting the stabilisation of the extracted complex assembly. This prolonged equilibrium approach highlighted the fact that ligands **11** and **12** were not particularly affinitive towards copper(II).

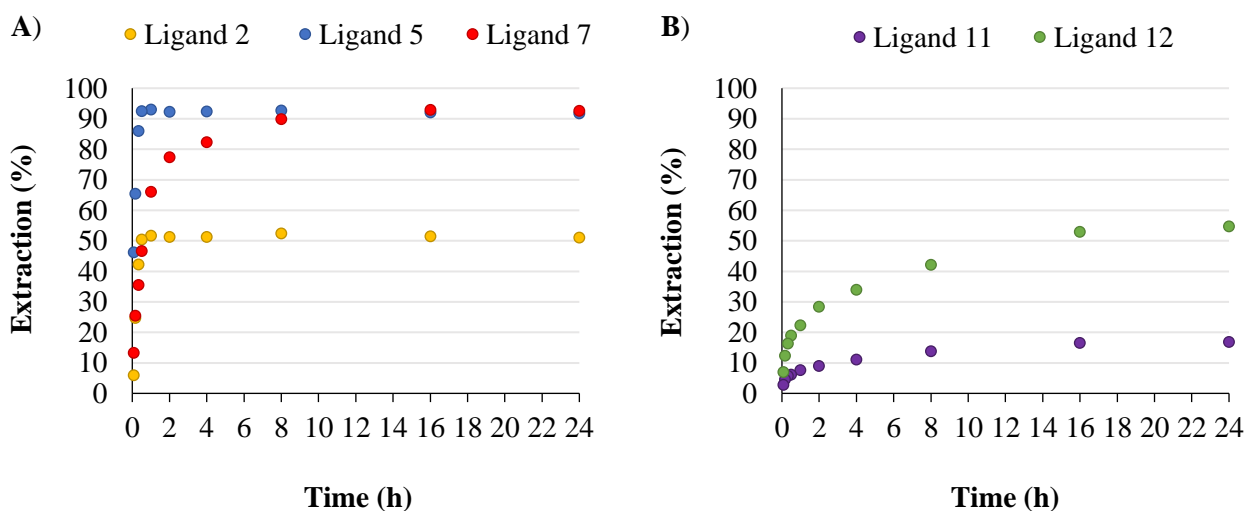


Figure 3.15: Extraction of copper(II) over a 24-hour period using **A)** pyrazolyl ligands **2**, **5** and **7** as well as **B)** imidazolyl ligands **11** and **12**. [Ligands] $\approx 2 \times 10^{-2}$ M; [Cu²⁺] = 1.01×10^{-2} M; NaOAc/AcOH buffer; pH 4.89. [No error bars added for the sake of clarity. See corresponding data in **Table 11** of **Appendix B — DATA TABLES**]

Similar experiments, as shown in **Figure 3.15**, were conducted to ascertain whether both pyrazolyl and imidazolyl ligands reached equilibrium during nickel(II) extraction experiments (**Figure 3.16**). Again, pyrazolyl ligands **2**, **5** and **7** were observed to achieve equilibrium in a timely manner with ligand **7** doing this at the 2-hour mark, whereas ligands **2** and **5** appeared to equilibrate after ~8 hours (**Figure 3.16C**). From **Figure 3.16D**, imidazolyl ligands **11** and **12** seemingly equilibrated during nickel(II) extractions only at the 16-hour mark, indicating that these ligands are much slower in their coordinative and transport ability. Compared to copper(II), it seemed clear that pyrazolyl ligands exhibited slower nickel(II) extraction rates—probably due to their slow rate of water substitution in the inner coordination sphere.^{15,42} It might also be indicative of 2:1 (L:Ni²⁺) complex ratios, which was explored in greater detail in **Sections 3.3.6** and **3.3.7**.

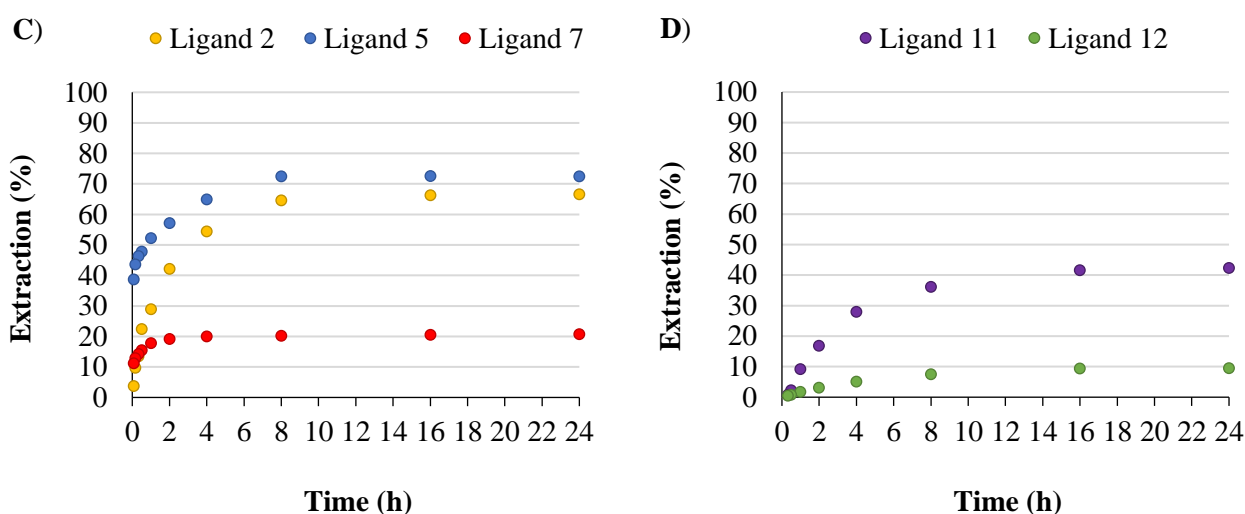


Figure 3.16: Extraction of nickel(II) over a 24-hour period using **C)** pyrazolyl ligands **2**, **5** and **7** as well as **D)** imidazolyl ligands **11** and **12**. [Ligands] $\approx 2 \times 10^{-2}$ M; [Ni²⁺] = 9.93×10^{-3} M; NaOAc/AcOH buffer; pH 5.02. [No error bars added for the sake of clarity. See corresponding data in **Table 12** of **Appendix B — DATA TABLES**]

3.3.5 pH isotherm studies

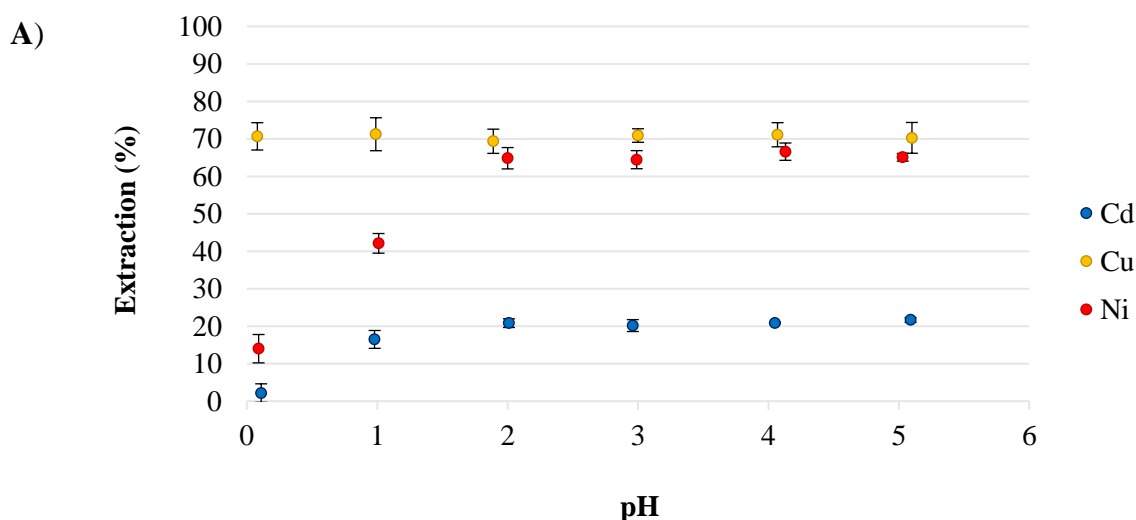
In these studies, the conditions for the extraction of nickel(II), copper(II) and cadmium(II) were altered by varying the pH of the metal-rich aqueous phase. The pH was varied by charging 25 mL volumetric flasks with predetermined amounts of metal nitrate salts, followed by premade HNO₃ aqueous solutions. All-in-all, each metal was present in an aqueous solution at pH values ranging from 0–5. The metal (1×10^{-2} M) to ligand ($\sim 5 \times 10^{-3}$ M) was maintained at 2:1 throughout this study and was kept synergist-free, since the aforementioned metals were extracted by pyrazolyl ligands **3** (propyl), **5** (pentyl) and **8** (octyl) at relatively high efficiencies.

Figure 3.17A–C represents the percentage extractions of nickel(II), copper(II) and cadmium(II) over a pH range of 0–5, using ligands **3** (**A**), **5** (**B**) and **8** (**C**). None of these ligands were able to produce a *S*-type copper(II) extraction plot, indicating the phenomenal extractive power these tridentate ligands maintained,

even at low pH values. Ligand **3** sustained %*E* values of ~70%, while ligands **5** and **8** consistently held %*E* values in the mid-90%.

Both ligands **3** and **5** appeared to extract nickel(II) at ~65% at pH ≥ 2 , while a steady decline in their extractive power was observed at pH < 2 . Remarkably, ligand **5** still extracted 38.6 (± 1.7)% nickel(II) at pH 0.09, once again revealing the robustness of these ligands under extreme acidic environments. Ligand **8**, on the other hand, produced a broad nickel(II) *S*-curve plot with maximum extractions of ~25%, which generally is not ideal for metal ion separation. A steep curve is often desired to effect metal ion separation based on a narrow window of varying pH values. Okewole *et al.*³² reported steep nickel(II) pH isotherm curves whereby the difference between the minimum and maximum %*E* values merely stretched from pH 1–2. This implies that metal ion recovery can be implemented at pH < 1 and extraction at pH > 2 .

Due to above-average %*E* values for cadmium(II) by means of ligand **8** (Figures 3.6–3.8, Sections 3.3.1.2 and 3.3.2), it was decided to investigate this phenomenon in more detail. The first striking result was observed when ligand **8** extracted cadmium(II) more efficiently than nickel(II) over the entire pH range (Figure 3.17C). This seemed counter-intuitive and does not follow the Irving-Williams series⁴⁰ as previously alluded to in Section 3.3.1.1. Interestingly, a clear cadmium(II) %*E* trend (pH ≥ 2) was observed with values of ~58, ~40 and ~20% relating to ligands **8** (octyl), **5** (pentyl) and **3** (propyl), respectively. The increase in *n*-alkyl tethers distinctly enables the higher uptake of cadmium(II) into the organic phase. This was an exciting finding and one that has not been seen in the literature. From Figure 3.17C, excellent Cd²⁺/Ni²⁺ separation at pH 1 of ~40% was observed, while ~30% separation was observed at pH 4–5.



Caption and remaining graphs continue to next page...

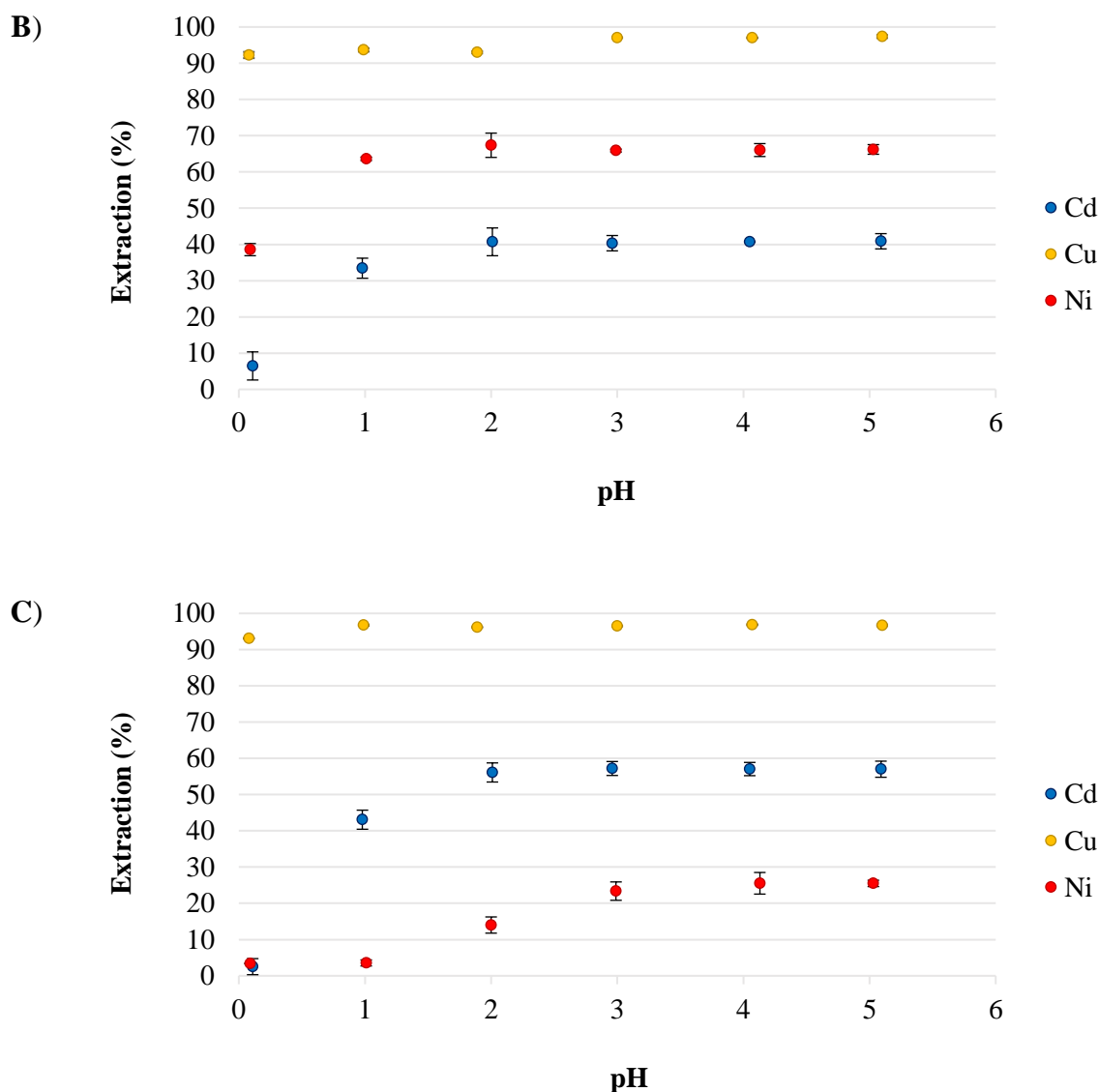


Figure 3.17: Extraction of cadmium(II), copper(II) and nickel(II) at varying pH values by means of pyrazolyl ligands **A) 3**, **B) 5** and **C) 8**. [Ligands] $\approx 1 \times 10^{-2}$ M; $[\text{Cd}^{2+}] = 5.71 \times 10^{-3}$ M; $[\text{Cu}^{2+}] = 5.03 \times 10^{-3}$ M; $[\text{Ni}^{2+}] = 5.05 \times 10^{-3}$ M; 1 M HNO_3 used to adjust pH 0–5. [See corresponding data in **Tables 13–15** of **Appendix B — DATA TABLES**]

3.3.6 Determining ligand-to-metal ($\text{L}:\text{M}^{2+}$) ratio by means of Job's method

3.3.6.1 Concise background information on Job's method

Numerous techniques have been developed to ascertain the stoichiometry of chemical equilibrium reactions, including the method of continuous variance,^{43–47} the mole ratio method⁴⁸ and the slope ratio method,⁴⁹ to name but a few. Due to its relatively uncomplicated nature, the method of continuous variance (commonly referred to as Job's method)—as originally expressed by Ostromisslensky,⁴³ Denison⁴⁴ and Job⁴⁵—is broadly considered to be the most popular of these methods.^{50,51} The most prevalent use of Job's method is the determination of the ratio of the reaction coefficients x and y in an association equilibrium of the following form:



where A and B represent the free species at equilibrium (*i.e.*, a ligand and a metal substrate), A_xB_y represent a molecular complex of A and B, while x and y represent mole coefficients (integers > 0).^{45,50,52–56} According to this method, the measured concentration of the complex A_xB_y —or a parameter that is directly proportional to its concentrations, such as its UV/Vis or IR absorbance⁵⁷ or the integrated NMR resonance intensity⁵⁸—is plotted against the mole fraction of one reactant while the sum of the reactant concentrations, c_{SUM} , is kept constant. This plot is subsequently referred to as a “Job plot”.⁵⁹ From Eq. 41, Eqs. 42 and 43 can now be derived:

$$c_A^t = c_A + x c_{A_xB_y} \quad (42)$$

$$c_B^t = c_B + y c_{A_xB_y} \quad (43)$$

where c_A^t and c_B^t represents the total concentrations of reactants A and B, while c_A , c_B and $c_{A_xB_y}$ represent the species in solution. The former are related to c_{SUM} at any given mole fraction, f , of species A and B as follows:

$$c_A^t = f \times c_{\text{SUM}} \quad (44)$$

$$c_B^t = (1 - f) \times c_{\text{SUM}} \quad (45)$$

Following association equilibria of this kind, the highest concentration of complex A_xB_y and the maximum in the Job plot is expressed as follows:

$$f_A = \frac{x}{x + y} \quad (46)$$

where f_A signifies the mole fraction of A at the maximum point on the curve.⁵¹ This simple relationship makes Job’s method a tremendously powerful tool to determine the stoichiometries of equilibrium reactions and is the overarching reason for its continuous popularity in all fields of science.⁵⁹ It is important to note that while conventional interpretations of Job plots allow for the immediate determination of the empirical ratio of the reactants in a chemical equilibrium by finding the exact position of the maximum on the plot, differentiating between 1:1, 2:2, 3:3... (and other $n:n$ ratios) stoichiometries on the basis of Job plots is a far more difficult prospect, since the maxima of such ratios will occur at the same mole fraction ($f = 0.5$).⁵⁹ In 2005, Sayago *et al.*⁵² managed to differentiate between $n:n$ stoichiometries of the types 1:1 and 2:2 by means of spectrophotometry in an adaptation of Job’s method. Throughout this study, however, the tridentate pyrazolyl or -imidazolyl ligands were not foreseen to coordinate in such a manner.

Job⁴⁵ demonstrated that by plotting UV absorption versus mole fraction, f , one can clearly observe a 1:1 molecular association ($f = 0.5$) of $\text{Tl}(\text{NO}_3)$ in mixtures of $\text{Tl}(\text{NO}_3)/\text{NH}_3$, which can be read from a plot akin to the idealised plot of **Figure 3.18**.



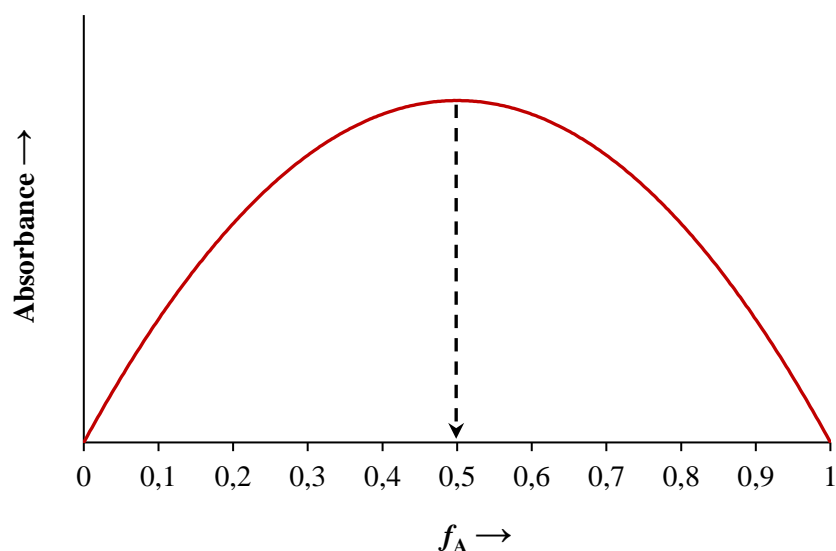


Figure 3.18: An idealised Job plot of the simplest form, where a 0.5 mole fraction of A (f_A) indicates a 1:1 (ligand: M^{2+}) complexation ratio. [Adapted from Renny *et al.*⁶⁰]

3.3.6.2 General experimental setup and procedure

At the outset of this part of the study, it was anticipated to perform mini extractions in 2 mL plastic vials (1 mL organic phase and 1 mL aqueous phase) under typical solvent extraction conditions as previously outlined in **Section 3.2.4**. This experiment was attempted on numerous occasions, using varying mole fractions of pyrazolyl ligands **2** (ethyl), **8** (octyl) and **9** (*tert*-butyl) in addition to $Cu(NO_3)_2 \cdot 3H_2O$, but could never seem to obtain reproducible results via UV/Vis analyses. This could possibly be due to micro-droplets of water suspended in the organic phase (and *vice versa*) immediately after the 24-hour overhead shaking period, thereby altering the absorbance properties of the organic phase. One could argue that the samples should ideally be “rested” and the micro-droplets allowed to find their way back to the top-layered aqueous phase. This was attempted on multiple occasions for different periods of time (30 min up to 24 hours), but any period less than 6 hours still yielded irreproducible UV/Vis results, while periods of more than 6 hours allowed for the evaporation of the vial contents (even in tightly sealed cases). Besides the formation of micro-droplets, leaching appeared to be another cause for concern, especially in the case of the shorter alkyl-tethered pyrazolyl ligand, **2**. Therefore, it was decided to forego a biphasic extraction setup and to implement a monophasic setup in high-purity methanol instead. This solvent was primarily chosen due to the dissolution of metal nitrate salts and the synthesised pyrazolyl and imidazolyl ligands. Of course, solvents such as ethanol or other polar non-coordinating organic solvents that readily dissolve both metal nitrates and synthetic ligands should work perfectly well too.

Equimolar (1×10^{-2} M) stock solutions of $M(NO_3)_2 \cdot xH_2O$, pyrazolyl ligands **1–9** and imidazolyl ligands **11** and **12** were prepared in methanol. Varying amounts of these solutions were mixed to obtain pre-determined mole fractions (0–1), making sure the total concentration of the ligands and metal nitrate salts (previously defined as c_{SUM} in **Section 3.3.6.1**) remained constant throughout this study. These combinative solutions were placed on a *Heidolph Reax 2* overhead shaker (**Figure 3.19**) for 24 hours at 25 ± 1 °C, followed immediately by

UV/Vis analyses in order to limit evaporation and its concentrative effect (performed at TU Dresden, Germany).

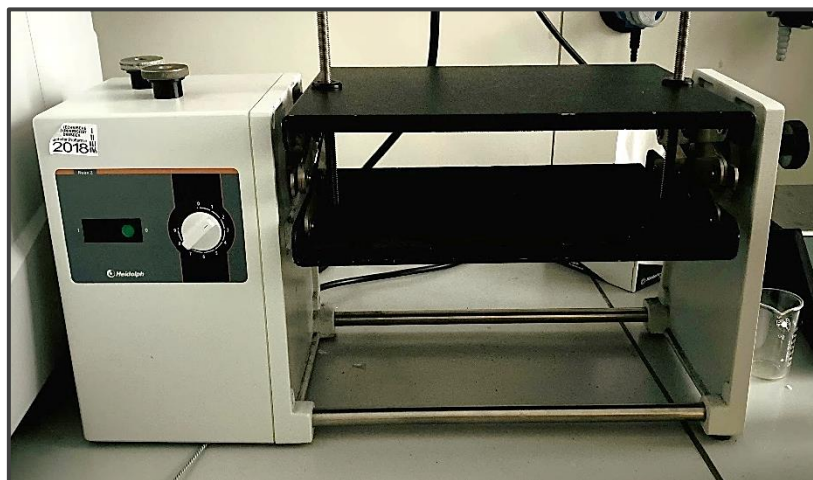


Figure 3.19: A Heidolph Reax 2 overhead shaker/rotator, equipped with a universal adapter, on which all Job plot samples were placed for 24 hours.

3.3.6.3 Job plot analyses of pyrazolyl and imidazolyl ligands' coordination to copper(II)

To kick off the experimental Job plot analyses, it was first necessary to run a series UV/Vis experiments in which mole fractions were altered according to Eq. 46 or by means of the following descriptive equation:

$$f_{\text{ligand}} = \frac{[\text{ligand}]}{[\text{ligand}] + [\text{M}^{2+}]} \quad (48)$$

where f_{ligand} represents the mole fraction of the ligand, while the square bracketed entities represent their respective concentrations. To elaborate on the manner in which Job's method was applied, focus will first be on 2,6-bis(5-hexyl-1H-pyrazol-3-yl)pyridine (**6**) and its coordination to copper(II) as a representative example of all analyses. The UV/Vis spectrum, as depicted in **Figure 3.20**, was obtained after various mole fractions were mixed for 24 hours on the aforementioned overhead shaker (**Figure 3.19**) and run on either a *Specord*[®] 210 plus or a *PerkinElmer 2* UV/Vis spectrophotometer. All UV/Vis spectra not shown in the main body of work can be found on pages 72–78 of **Appendix A — SPECTRA**.

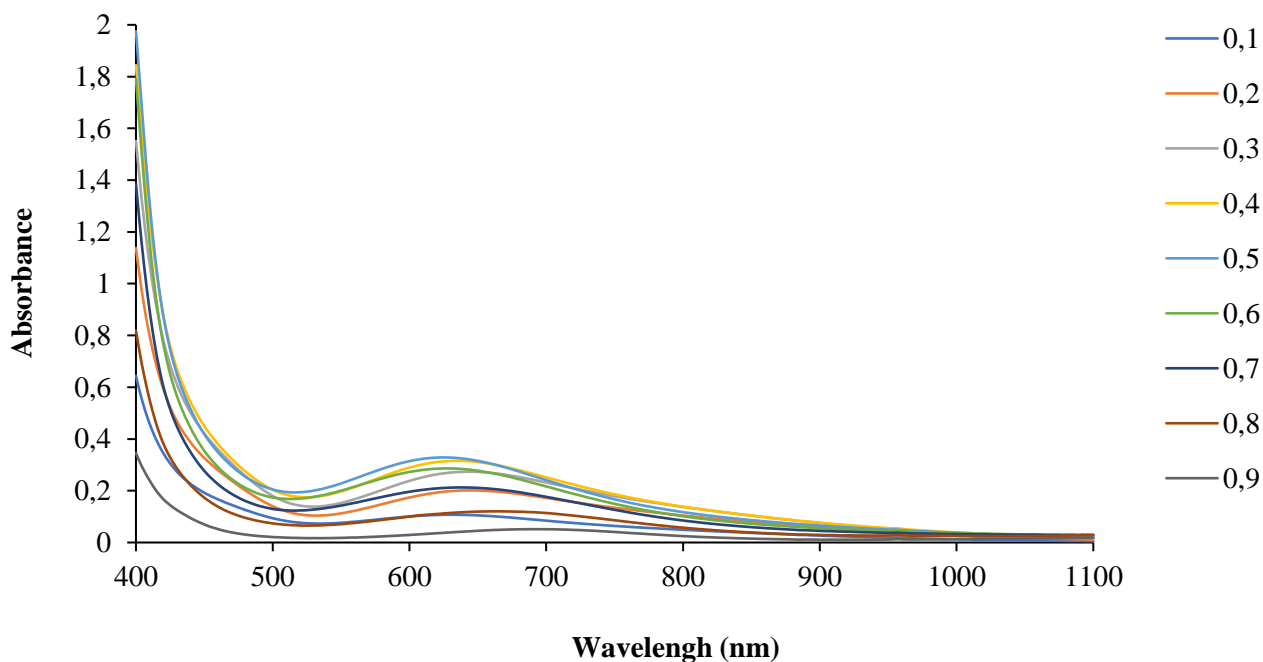


Figure 3.20: Stacked UV/Vis spectrum depicting increasing mole fractions of ligand **6** and $\text{Cu}(\text{NO}_3)_2 \cdot 3\text{H}_2\text{O}$ complex. Stock methanolic solutions: $[\text{Cu}^{2+}] = [\mathbf{6}] = 1 \times 10^{-2} \text{ M}$. Wavelength: $\lambda = 630 \text{ nm}$.

The absorbances at $\lambda = 630 \text{ nm}$ of the various mole fractions were plotted to generate **Figure 3.21**, a graphically uncorrected Job plot. It is common to find peer-reviewed papers with uncorrected Job plots, since it does not alter the intersection of the positively- and negatively sloped lines of fit in any significant way. In this study, however, it was decided to correct all Job plots to obtain aesthetic roof-shaped curves with symmetrical “rooflines”. The blue and green corrective lines on **Figure 3.21** represent the literal y-values (absorbances) that were subtracted from each experimental data point at their respective x-values (mole fractions, f). In the case of **Figure 3.21**, this shifts the overall graph downward to yield **Figure 3.22**, a graphically corrected Job plot without a slanted “roofline”.

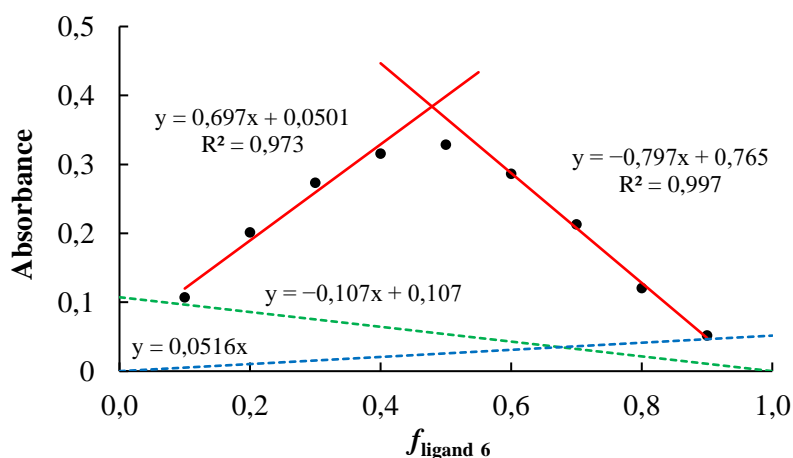


Figure 3.21: Uncorrected Job plot for the ligand **6**- Cu^{2+} complex. Absorbance measured at $\lambda = 630 \text{ nm}$.

The x-value of the exact intersection of both positively- and negatively sloped lines of fit (red lines) signify the mole fraction, f , at which the maximum complex absorbance occurs. **Figure 3.22** shows an intersectional f -value ($f_{\text{INTERSECTION}}$) of 0.490, implying a 1:1 (ligand **6**:Cu²⁺) complex ratio. To put it differently, when equimolar amounts of ligand **6** and copper(II) make contact, the absorbance of the resultant complex yields its maximum crest, signifying a 1:1 (ligand **6**:Cu²⁺) complex ratio. In mathematical terms, this phenomenon is most accurately described by means of Eq. 48.

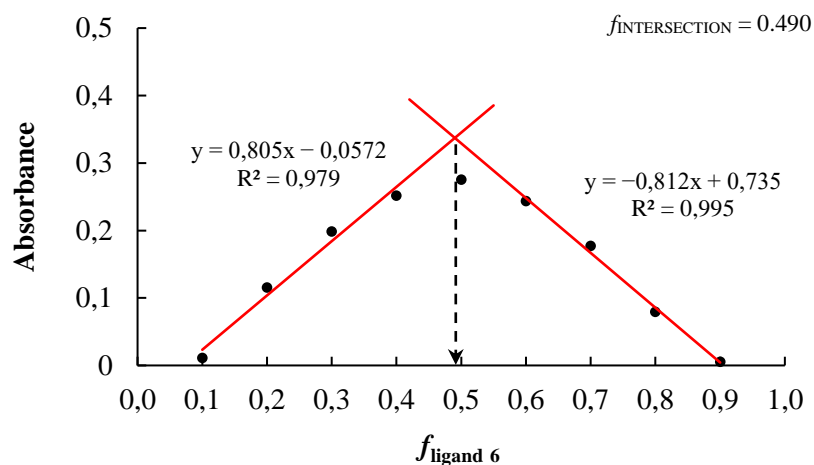
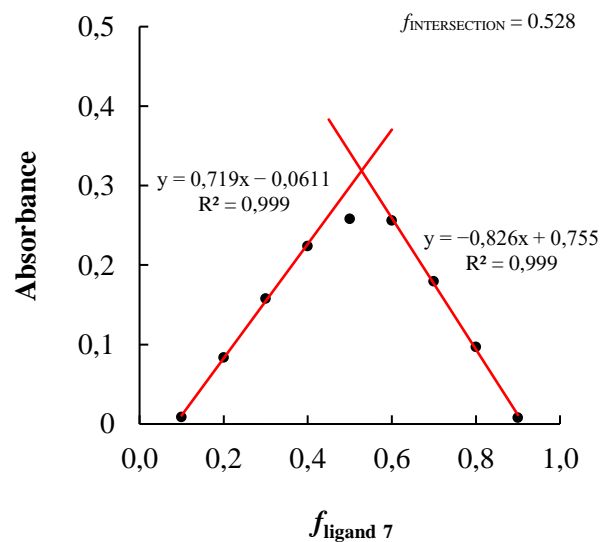
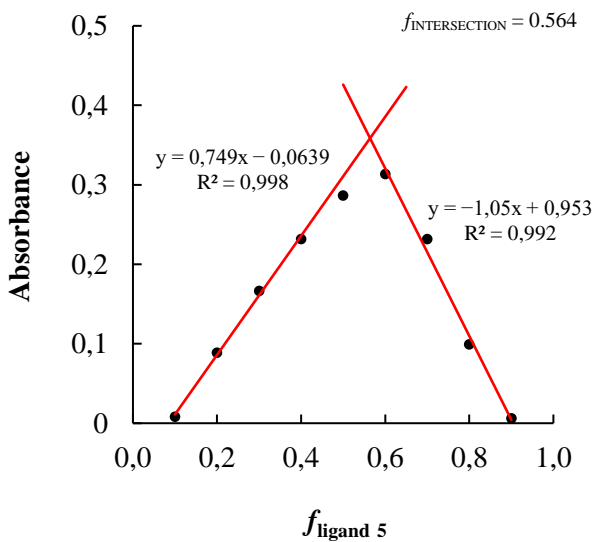
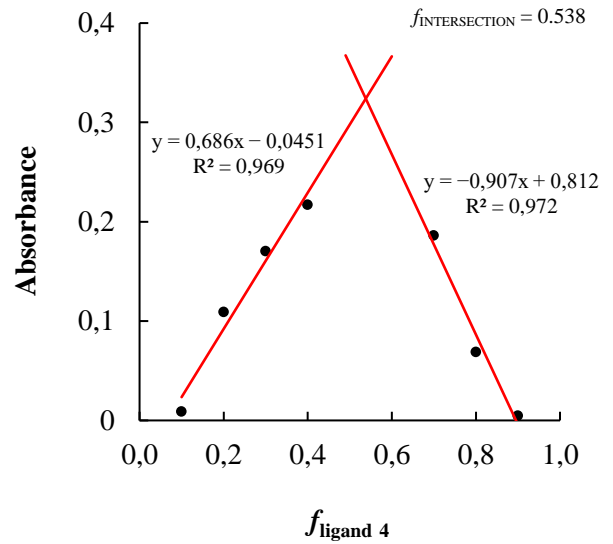
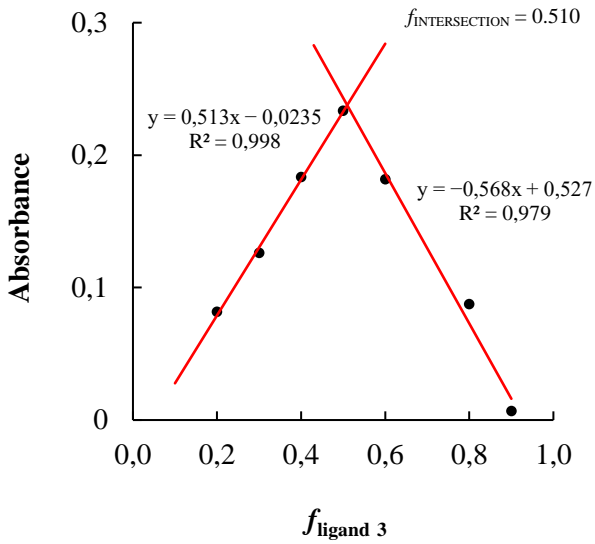
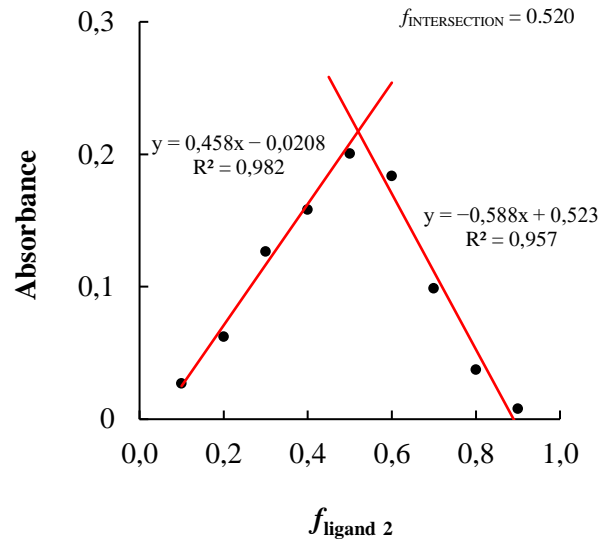
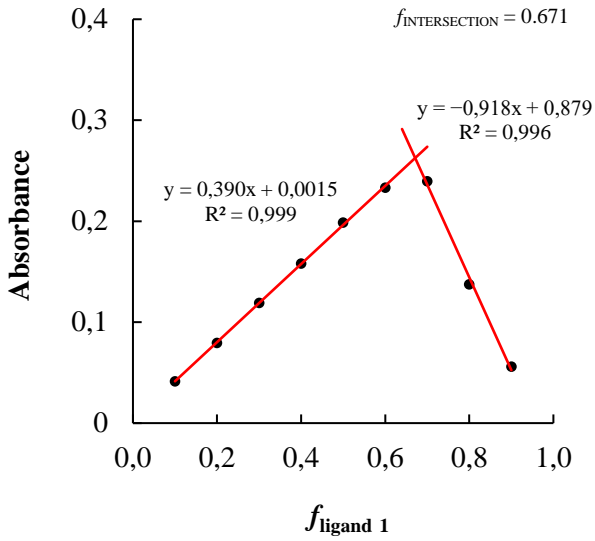


Figure 3.22: Graphically corrected Job plot for the ligand **6**-Cu²⁺ complex. Lines of fit intersect at $f_{\text{ligand 6}} = 0.490$, indicating a 1:1 (ligand **6**:Cu²⁺) ratio in solution. Absorbance measured at $\lambda = 630$ nm.

Job plot analyses were performed for all pyrazolyl and imidazolyl ligands, with the exception of 2,6-bis(5-phenyl-1*H*-pyrazol-3-yl)pyridine (**10**) due to its previously mentioned (**Section 3.3.1.1**) poor solubility in a wide range of common laboratory solvents (**Figure 3.23**). It was revealed that pyrazolyl ligands **2–9** coordinated to copper(II) in a 1:1 (ligand:Cu²⁺) fashion with $f_{\text{INTERSECTION}}$ -values of ~ 0.5 , which fittingly aligns with copper(II) extraction results as portrayed in **Figure 3.4**. Theoretically speaking, if ligands **4–8** had coordinated to copper(II) in a 2:1 (ligand:Cu²⁺) manner, extraction of $> 50\%$ would have been impossible. Ligands **2**, **3** and **9** are also expected to coordinate to copper(II) in a 1:1 manner, but due to their short carbon tethers merely extracted copper(II) at $< 50\%$. However, an inexplicable oddity, concerning ligand **1**'s Job plot result was encountered. It shows an $f_{\text{INTERSECTION}}$ -value of 0.671, which in turn indicates a 2:1 (ligand **1**:Cu²⁺) complex ratio. An idealised and theoretical 2:1 Job plot reveals a mole fraction of $0.\bar{6}$, which is not too dissimilar from the reported value. This experiment has been repeated twice with similar results obtained. Currently, the only line of defence rests on the fact that copper(II) has a relatively small ionic radius of 87 pm,^{41,61} that due to ligand **1**'s short methyl pendant arms, are now able to allow two ligands to coordinate to copper(II) without steric interference.

Imidazolyl ligands **11** and **12** yielded somewhat biased $f_{\text{INTERSECTION}}$ -values of 0.562 and 0.572, respectively. This indicates that these ligands—for the majority—coordinated in a 1:1 (ligand:Cu²⁺) manner, yet also had a small percentage of 2:1 copper(II) complexes in solution.



Caption and remaining Job plots continue to next page...

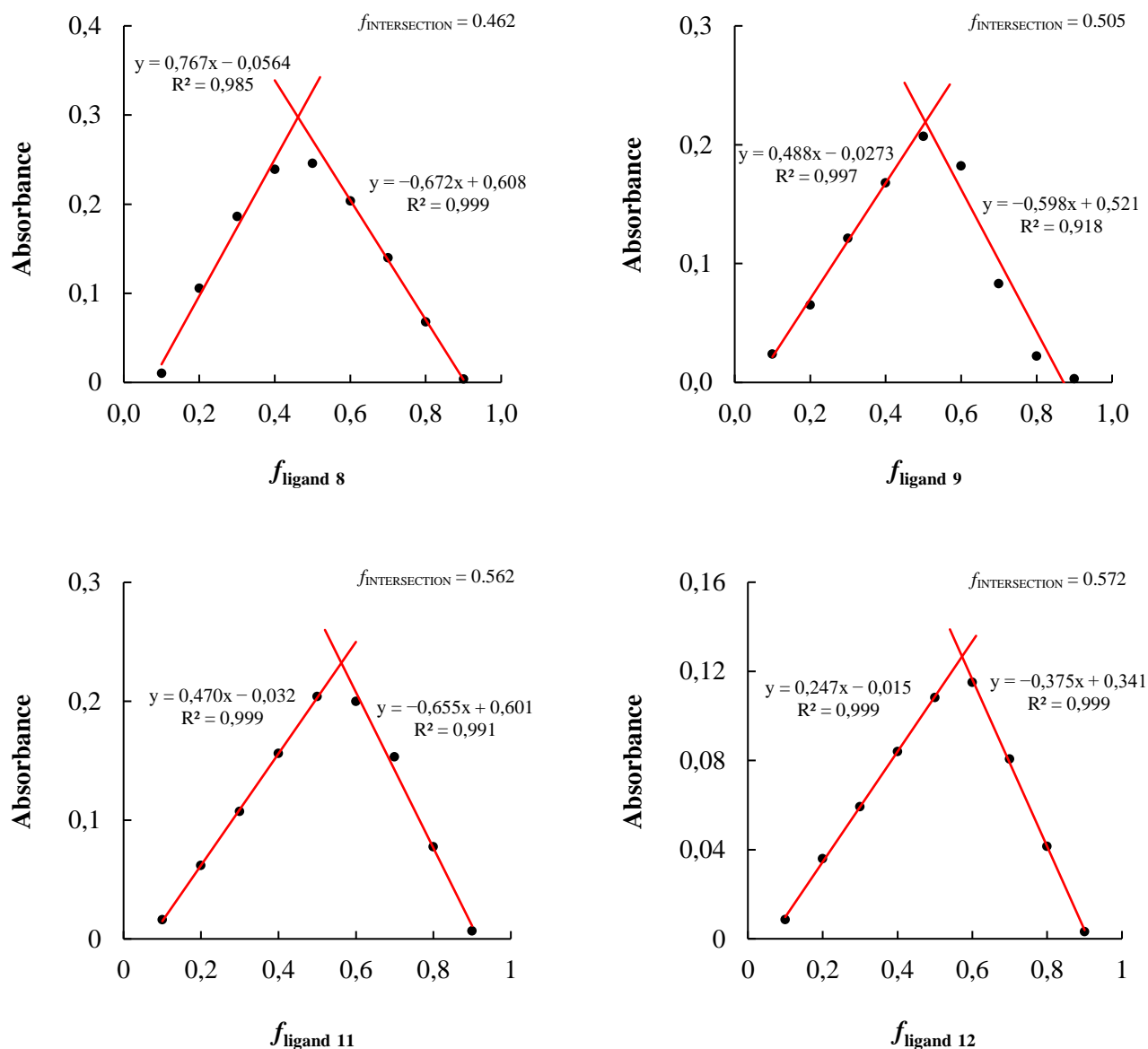


Figure 3.23: Copper(II) coordination Job plots of pyrazolyl ligands 1–5 & 7–9 in addition to imidazolyl ligands 11 and 12.

Table 3.3: Summary of $f_{\text{INTERSECTION}}$ -values and suggested L:Cu²⁺ ratios of ligands 1–12 (excluding 10).

Ligand	$f_{\text{INTERSECTION}}$ -value	Implied L:Cu ²⁺ ratio
1	0.671	2:1
2	0.520	1:1
3	0.510	1:1
4	0.538	1:1
5	0.564	~1:1
6	0.490	1:1
7	0.528	1:1
8	0.462	1:1
9	0.505	1:1
11	0.562	~1:1
12	0.572	~1:1

3.3.6.4 Job plot analyses of ligand **2** and **12**'s coordination to Co(II), Ni(II), Zn(II), Pb(II) and Cd(II)

The method of continuous variance (MCV) experiments were expanded to the remaining divalent base metal ions: cobalt(II), nickel(II), zinc(II), lead(II) and cadmium(II). These experiments were incredibly cumbersome and time intensive; therefore, it was agreed to select one pyrazolyl [**2** (ethyl)] and one imidazolyl ligand [**12** (octyl)] to represent their respective structural classes. **Figure 3.24**, depicting five Job plots, evidently showed ligand **2** preferably forming 2:1 (ligand **2**:M²⁺) complexes with the exception of lead(II). This showed that ligand **2** (and in general pyrazolyl ligands) truly had poor affinity for lead(II)—even when a 1:1 (ligand **2**:Pb²⁺) complex ratio seemed to be stoichiometrically preferred. Although odd, this was in line with previously discussed lead(II) extraction results. Co²⁺ ($f_{\text{INTERSECTION}} = 0.707$), Ni²⁺ ($f_{\text{INTERSECTION}} = 0.714$), Zn²⁺ ($f_{\text{INTERSECTION}} = 0.698$) and Cd²⁺ ($f_{\text{INTERSECTION}} = 0.685$) complexes appeared to be coordinated by two ligands in an octahedral meridional (*mer*) geometry with a coordination number of 6. These $f_{\text{INTERSECTION}}$ -values closely resembled the idealised mole fraction of 0.6. Data points in all five cases accurately formed roof-shaped (or tepee-shaped) curves, in spite of high degrees of possible human and experimental errors that may have crept into the practical execution of these experiments. Relatively high R²-values were observed, with merely one outlying datapoint omitted in the instances of Co ($f_{\text{ligand 2}} = 0.1$) and Cd ($f_{\text{ligand 2}} = 0.7$).

Imidazolyl ligand **12** yielded fairly similar results to that of pyrazolyl ligand **2**, with Co²⁺ ($f_{\text{INTERSECTION}} = 0.657$), Ni²⁺ ($f_{\text{INTERSECTION}} = 0.669$) and Zn²⁺ ($f_{\text{INTERSECTION}} = 0.639$) suggesting ligand **12**:M²⁺ complex ratios of 2:1 (**Figure 3.24**). Cd²⁺ revealed a $f_{\text{INTERSECTION}}$ -value of 0.576, once again pointing towards a possible combination of both 1:1 and 2:1 (ligand **12**:M²⁺) complexes in solution. In the case of ligand **12**, lead(II) coordination was especially poor, making it impossible to record usable UV/Vis spectra, hence its omission from **Table 3.4** and **Figure 3.24**.

Table 3.4: Summary of $f_{\text{INTERSECTION}}$ -values and suggested L:M²⁺ ratios of pyrazolyl ligand **2** and imidazolyl ligand **12**.

Ligand	Divalent metal ion	$f_{\text{INTERSECTION}}$ -value	Implied L:M ²⁺ ratio*
2,6-bis(5-ethyl-1H-pyrazol-3-yl)pyridine (2)	Co	0.707	2:1
	Ni	0.714	2:1
	Zn	0.698	2:1
	Cd	0.685	2:1
	Pb	0.534	1:1
2,6-bis(1-octylimidazol-2-yl)pyridine (12).	Co	0.657	2:1
	Ni	0.669	2:1
	Zn	0.639	2:1
	Cd	0.576	~1:1

* M = Co, Ni, Zn, Cd and Pb

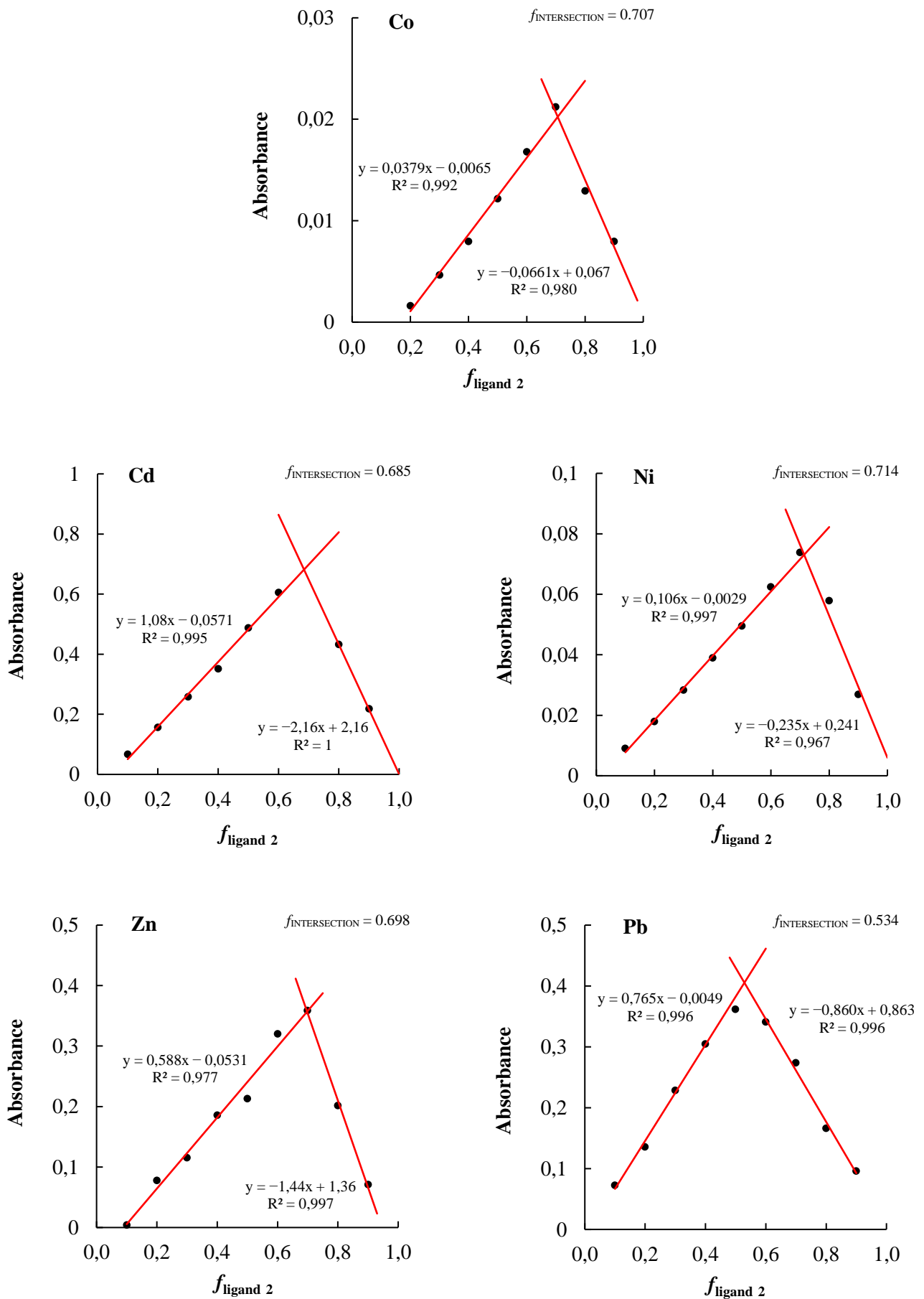


Figure 3.24: Job plots of pyrazolyl ligand 2 coordinating to Co(II), Ni(II), Zn(II), Pb(II) and Cd(II).

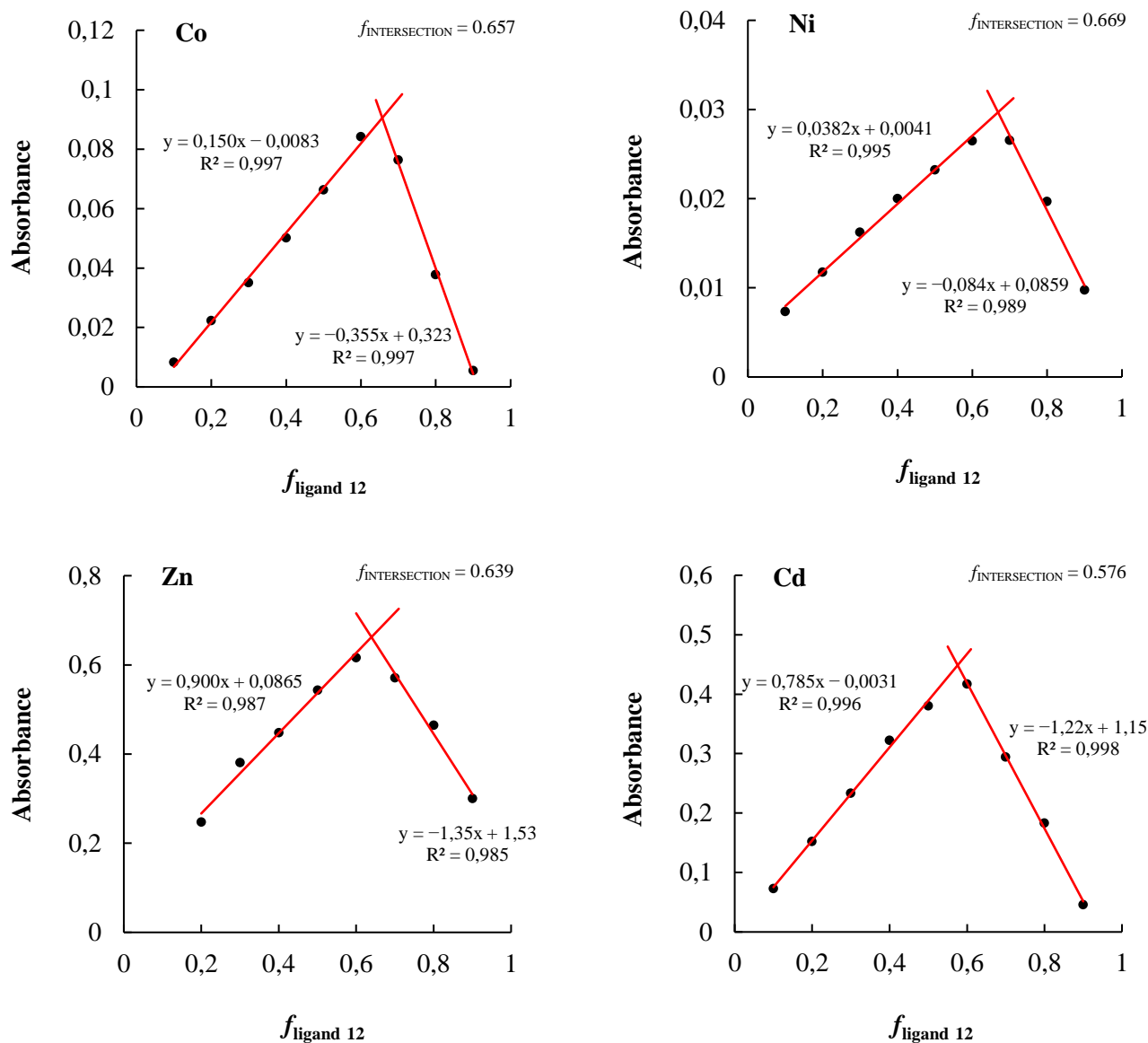


Figure 3.25: Job plots of imidazolyl ligand **12** coordinating to Co(II), Ni(II), Zn(II) and Cd(II).

3.3.7 Slope analyses via ICP-OES

Slope analyses are insightful ways in which one can determine ligand: M^{2+} ratios by means of solvent extraction processes, contrary to the method of continuous variance (Job's method) as utilised in **Section 3.3.6**. Slope analyses were performed in addition to Job's method to verify the results are in accordance with each other.

This is an opportune time to reintroduce the distribution ratio, D , which can be defined as the ratio of concentration of metal in the organic phase to the concentration of metal in the aqueous phase. For a given divalent base metal ion, M^{2+} , partitioned between an organic and aqueous phase, the extraction can mathematically be described as follows:

$$D = \frac{\text{Total concentration of metal in the organic phase}}{\text{Total concentration of metal in the aqueous phase}} = \frac{[M^{2+}]_{\text{org}}}{[M^{2+}]_{\text{aq}}} \quad (49)$$

It is interesting to note that percentage extraction (%*E*) is related to the distribution ratio as follows:

$$D = \frac{\left(\frac{V_{\text{aq}}}{V_{\text{org}}}\right)\%E}{100 - \%E} \quad (50)$$

where V_{aq} and V_{org} represent the volumes in the aqueous and organic phases, respectively. When the volumes of the aqueous and organic phases are equal, the relationship between %*E* and *D* becomes:

$$D = \frac{\%E}{100 - \%E} \quad (51)$$

As %*E* increases in a solvent extraction experiment, *D* increases simultaneously. If the extraction reaches 100%, *D* goes to infinity. When a plot of $\log D$ versus $\log [\text{ligand}]$ is drawn, the slope of the initial set of datapoints are mathematically indicative of the ligand: M^{2+} complex ratio. Following from the general equation for a straight line, $y = mx + c$, the general extraction equation is derived:

$$\log D = a \cdot \log[\text{ligand}] + b \quad (52)$$

where *a* is the slope of the log-log graph (ligand: M^{2+} ratio) and *b* is the extraction (equilibrium) constant, often denoted as K_{ex} .

3.3.7.1 Experimental setup and execution of distribution experiments

The experimental setup was akin to the general procedure previously discussed in **Section 3.2.4**, with a few minor alterations. In an attempt to conserve limited ligand resources, it was agreed to use 2 mL microcentrifuge tubes containing 0.8 mL aqueous phase and 0.8 mL organic phase. The bottom-layered organic phase contained varying concentrations of ligand in chloroform, while the top-layered aqueous phase contained a constant $[M^{2+}]$, [MES/NaOH] buffer (pH ~5.5) and $[NaNO_3]$ to maintain good ionic strength. It was imperative to match the sodium salt's anion with that of the metal salt's anion (nitrates in this case) to avoid competing anionic effects. Ionic strength, *I*, is defined as follows:

$$I = \frac{1}{2} \sum_i^n c_i z_i^2 \quad (53)$$

where *n* is the number of ions in solution, *i* the specific ion in solution, *c* the concentration ($\text{mol}\cdot\text{L}^{-1}$) and *z* the valence or oxidation number. After a set of samples were accurately prepared and mechanically mixed on an overhead shaker/rotator for 24 hours, it was immediately self-analysed via ICP-OES (performed at TU Dresden, Germany).

3.3.7.2 Graphical slope analyses of copper(II) extraction by means of pyrazolyl ligands 5 and 7

The first couple of variable ligand concentration experiments (slope analyses) were performed in a trial and error manner to establish whether the setup was within the experimental boundaries in order to obtain meaningful results. Following an extensive series of experiments within these tentative parameters, it appeared as though both ligands **5** (pentyl) and **7** (heptyl) rapidly plateaued ($> 2.5 \times 10^{-3}$ M), resulting in diagrams that offer very little information of value (**Figure 3.26**). From previous competitive extraction studies, these

ligands' exceptional copper(II) extractive abilities were soon realised, necessitating the modification of one of the following two variables in order to minimise their extractive power: 1) the ligand concentration or 2) the pH of the aqueous phase. The former was only marginally altered since the ligand concentration should ideally be much higher than the metal ion concentration. Should a ligand concentration similar to (or less than) the metal ion concentration be implemented, the extraction system is inherently forced into a 1:1 (ligand:M²⁺) stoichiometric ratio, instead of forming its optimal and most stable stoichiometric complex in the presence of excess ligand. Therefore, the aqueous pH was incrementally lowered to 3 and then to 2, yet ligands **5** and **7** still seemed too effective, yielding similar curves to **Figure 3.26**. Finally, the pH was lowered to 0.72—an extreme acidic environment in which to perform extraction studies.

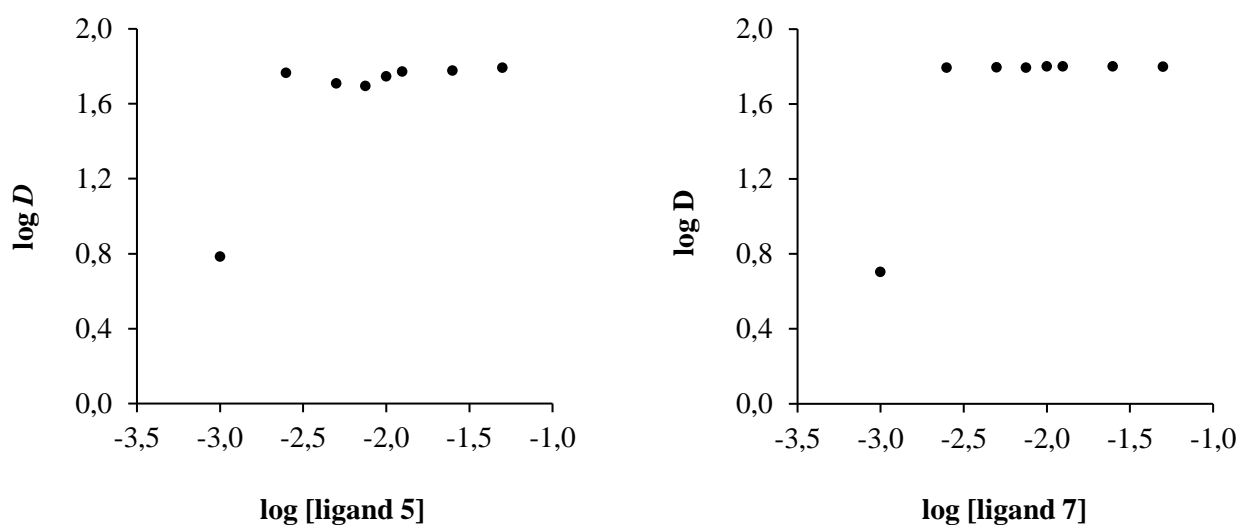


Figure 3.26: Plots for the variable ligand concentration experiments of ligands **5** and **7** with copper(II). [Cu(NO₃)₂] = 1×10⁻³ M; [NaNO₃] = 1×10⁻² M; pH = 5.5 (MES/NaOH buffer); [5] = [7] = 1×10⁻³–5×10⁻² M in CHCl₃. [Error bars omitted for clarity. See data in **Table 16 of Appendix B — DATA TABLES**]

At first, under the new pH conditions it appeared as though the alterations succeeded, with many more data points forming a positive incline instead of a static plateau. However, upon deeper investigation **Figure 3.27** revealed a slope of 2.91 (~3) for ligand **5**, while two distinct slopes of 4.46 (~4) and 1.99 (~2) were noticed for ligand **7**. These results did not make sense, whatsoever. The slopes were expected to be ~1, which would have aligned well with the myriad extraction studies and Job plot analyses already performed. Furthermore, it did not make sense for three or four tridentate pyrazolyl ligands to coordinate to a single copper(II) centre. At most, one would expect a 2:1 (ligand:M²⁺) complex ratio. Undoubtedly, the ultra-acidic conditions created a vastly different extractive environment through which copper(II) was transported from the aqueous to the organic phase by means of a distinct acid-induced mechanism.

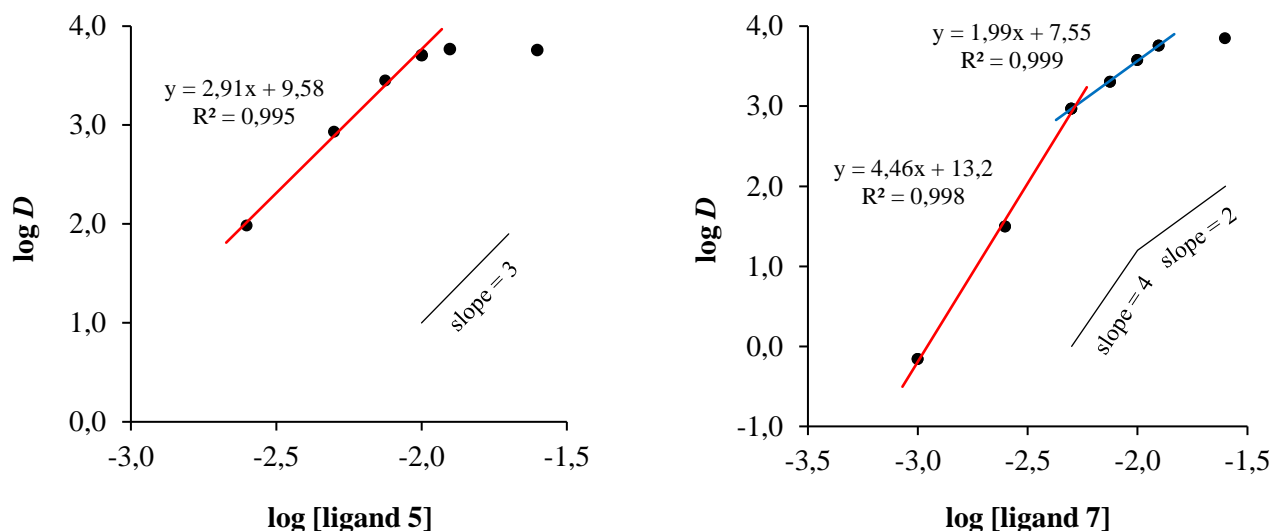


Figure 3.27: Plots for the variable ligand concentration experiments of ligands **5** and **7** with copper(II). $[\text{Cu}(\text{NO}_3)_2] = 1 \times 10^{-3} \text{ M}$; $[\text{NaNO}_3] = 1 \times 10^{-2} \text{ M}$; $\text{pH} = 0.72$ (conc. HNO_3); $[\mathbf{5}] = [\mathbf{7}] = 1 \times 10^{-3} - 2.5 \times 10^{-2} \text{ M}$ in CHCl_3 . [Error bars omitted for clarity. See data in **Table 17** of **Appendix B — DATA TABLES**]

The working theory with regards to this anomaly seemed to be related to micellar-like behaviour. In the case of ligand **7**, four positively charged pyrazolyl moieties face inward to an aqueous core containing one copper(II) ion. The aliphatic *n*-heptyl arms face outward forming a reverse micellar structure (**Figure 3.28**). These “micelles” subsequently carry copper(II) across the interface into the organic phase and remains there due to the presence of eight hydrophobic *n*-alkyl arms. Without a doubt, many experiments and deep investigation are required to solve this conundrum. Subsequently, this theory may need to be adapted and reworked as new information emerges, but for the purposes of this dissertation was not deemed to be within the original scope.

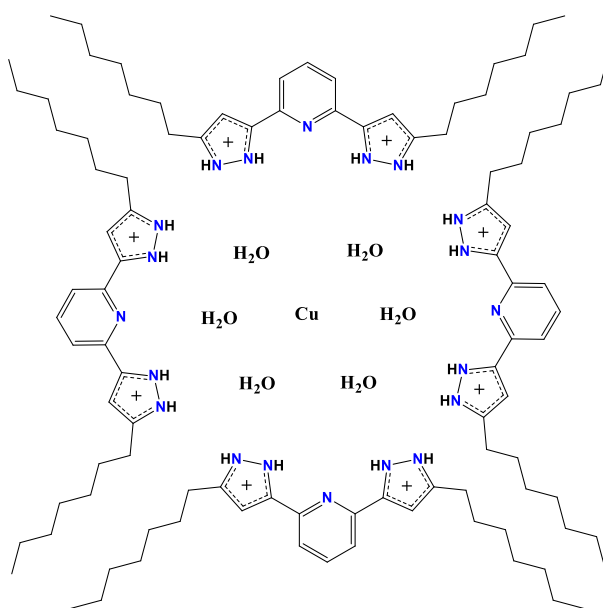


Figure 3.28: Theorised micellar-like structure capable of extracting copper(II) under ultra-acidic conditions.

3.3.7.3 Slope analyses of nickel(II) and cobalt(II) extraction by means of pyrazolyl ligands 5 and 7

After interesting copper(II) variable ligand concentration experiments, nickel(II) and cobalt(II) experiments were conducted as well. Again, ligands **5** and **7** were used to ensure that results are comparable and scientific continuity is sustained. After copper(II) slope analyses were performed under extreme acidic conditions, it was decided to return to a milder pH of 5.5, since both nickel(II) and cobalt(II) were not extracted in the same efficient manner as copper(II). However, the slightly lower ligand concentration was still retained. As expected, slopes of 2.18 (~2) and 2.02 (~2) were revealed once **Figure 3.29** was plotted and studied. This was indicative of 2:1 (ligand:Ni²⁺) complex ratios for both ligands **5** and **7** and is consistent with previously discussed nickel(II) Job plot results. No sudden plateauing at lower ligand concentrations was observed during these experiments, which can be ascribed to the pyrazolyl ligands' weaker affinity toward non-copper(II) base metal ions. Although it might not have been a desired characteristic, it was oddly ideally suited for variable ligand concentration experiments (slope analyses) via ICP-OES.

From **Figure 3.30**, similar cobalt(II) results were obtained and accorded well with previously discussed cobalt(II) Job plots as well. Ligand **5** yielded a slope of 1.89 (~2), with ligand **7** yielding a similar result (2.02, ~2). Previous work done by Zhou and Pesic¹⁵ also revealed 2:1 (ligand:M²⁺) complex ratios for both nickel(II) and cobalt(II) in the presence of 2,6-bis(5-nonyl-1*H*-pyrazol-3-yl)pyridine (given the acronym, BNPP) and the synergist, DNNSA. Of course, no synergist was included in the slope analyses experiments, but evidence seems to suggest that DNNSA (and other sulfonic acids) is most probably involved in the outer coordination sphere via hydrogen bonding (**Section 3.3.8** and **Section 5.7.4, CHAPTER 5**). It is unlikely to coordinate to the metal centre, although one article by Hu and co-workers⁶² demonstrated that a model naphthalene sulfonic acid can coordinate to copper(II) via weak elongated Jahn-Teller axial bonds. To the best of our knowledge, no other literature source reported the presence of sulfonic acid synergists in the inner coordination sphere.

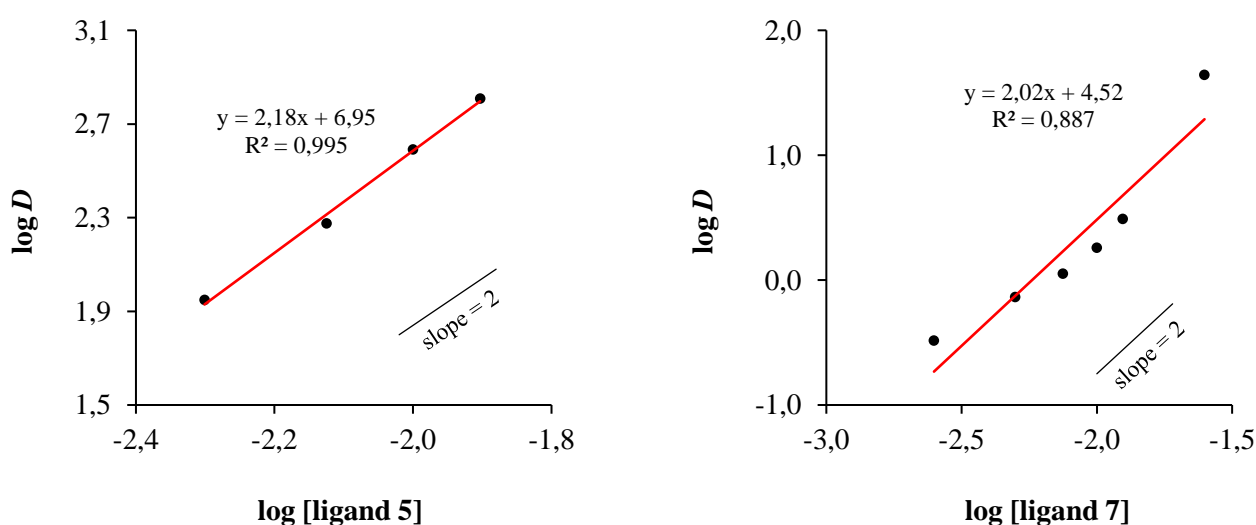


Figure 3.29: Plots for the variable ligand concentration experiments of ligands **5** and **7** with nickel(II). $[\text{Ni}(\text{NO}_3)_2] = 1 \times 10^{-3} \text{ M}$; $[\text{NaNO}_3] = 1 \times 10^{-2} \text{ M}$; pH = 5.5 (MES/NaOH buffer); $[\mathbf{5}] = [\mathbf{7}] = 1 \times 10^{-3} - 2.5 \times 10^{-2} \text{ M}$ in CHCl_3 . [Error bars omitted for clarity. See data in **Table 18 of Appendix B — DATA TABLES**]

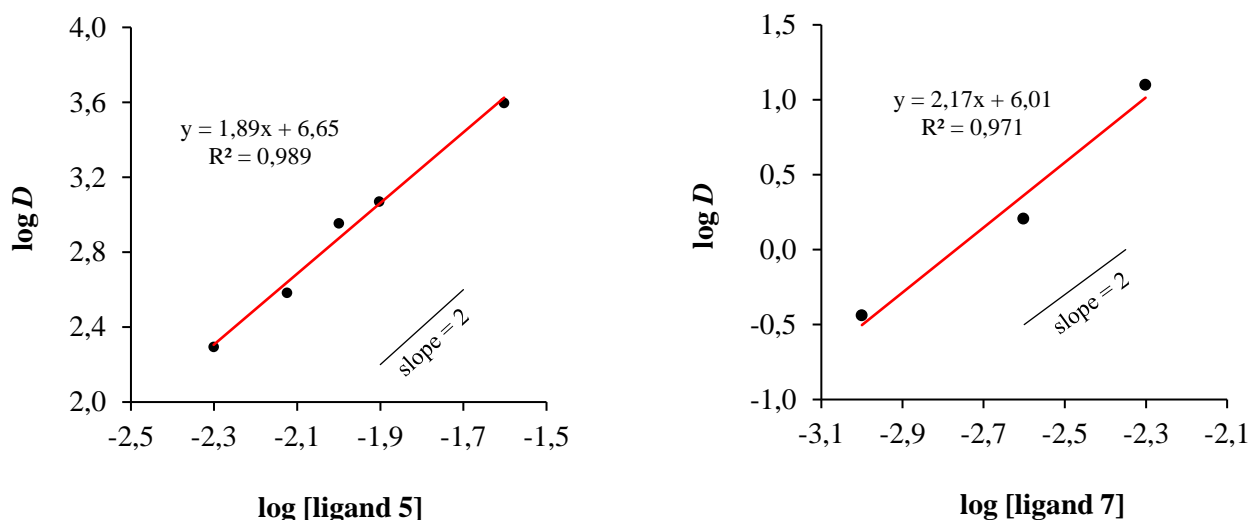


Figure 3.30: Plots for the variable ligand concentration experiments of ligands **5** and **7** with cobalt(II). $[\text{Co}(\text{NO}_3)_2] = 1 \times 10^{-3} \text{ M}$; $[\text{NaNO}_3] = 1 \times 10^{-2} \text{ M}$; $\text{pH} = 5.5$ (MES/NaOH buffer); $[\mathbf{5}] = [\mathbf{7}] = 1 \times 10^{-3} - 2.5 \times 10^{-2} \text{ M}$ in CHCl_3 . [Error bars omitted for clarity. See data in *Table 19 of Appendix B — DATA TABLES*]

3.3.8 Synergistic extraction of nickel(II)

3.3.8.1 Extraction of nickel(II) by means of dodecylbenzenesulfonic acid as synergist

Before any synergistic studies could commence, it was imperative that the optimum synergist concentration first be established. This was a vital piece of information that is often deemed unnecessary or superfluous in modern peer-reviewed solvent extraction articles. The accepted consensus seemed to be that an increase in synergist concentration unequivocally leads to an increase in the percentage extraction (%*E*) of a metal ion.¹⁵ Pearce *et al.*⁶³ have demonstrated that this might not always be the case. Their synergist, sodium dodecylbenzenesulfonate (SDBS), optimally extracted nickel(II) at a 5:1 (SDBS: Ni^{2+}) ratio, while a steady decline was observed from ratios 10:1 to 20:1—an interesting phenomenon that remains unresolved to date. An experiment was undertaken where dodecylbenzenesulfonic acid's (DBSA) concentration was varied, while the nickel(II) concentration was kept constant (**Figure 3.31**). For obvious reasons, all ligands were omitted from this experiment in order to observe the effect of DBSA on the %*E* of nickel(II).

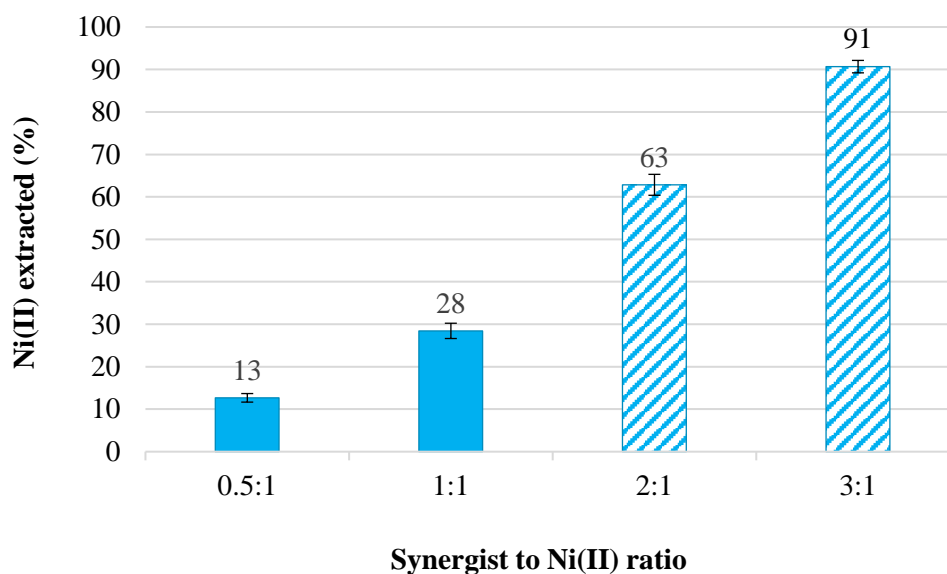


Figure 3.31: Extraction of nickel(II) by means of the synergist, DBSA, at various synergist to Ni²⁺ (S:Ni²⁺) ratios. Diagonally striped bars indicate third phase formation (emulsion). [Ni²⁺] = 8.11 × 10⁻³ M; NaOAc/AcOH buffer; pH 4.93. [Data labels are rounded to two significant figures. See corresponding data in **Table 20** of **Appendix B — DATA TABLES**]

This experiment was complicated, however, due to the formation of cloudy third phase emulsions at DBSA:Ni²⁺ ratios of 2:1 and 3:1. No emulsions were observed for either 0.5:1 or 1:1 DBSA:Ni²⁺ ratios. Therefore, it was decided to forego the use of emulsion forming ratios (2:1 and 3:1) and to focus on the most effective non-emulsion forming nickel(II) extraction ratio, which turned out to be 1:1. The appearance of third phase formations are very common in solvent extraction studies and its impact can be suppressed or even nullified, by the addition of specialised diluents and/or modifiers to extraction setups. Swami *et al.*⁶⁴ showed that their third phase formation—during solvent extraction of trivalent actinides—was overcome with the introduction of high concentrations of polar reagents such as tri-*n*-butyl phosphate (TBP) and *N,N*-dihexyloctanamide (DHOA). In another recent case, Weßling *et al.*⁶⁵ successfully displayed the suppression of third phase formations in the solvent extraction of trivalent actinides and -lanthanides by implementing *N,N,N',N'*-tetra-*n*-octyl-3-oxapentanediamide (TODGA) as modifier. In this study, however, it was decided to exclude all diluents and modifiers to eliminate their possible influences on the base metal ion solvent extraction systems.

DBSA is a well-known surfactant that finds application in many fields of chemistry, some of which include polyaniline-graphene and -zirconium oxide nanocomposites,^{66,67} Brønsted acid-surfactant-combined catalysts⁶⁸ and the fabrication of α-MoO₃ nanobelts⁶⁹. DBSA can be classified as “amphiphilic” or “amphipathic”, due to its dual hydrophilic (sulfonic acid head) and hydrophobic (*n*-alkyl tail) nature. This unique characteristic is ideal for micelle formation, which was shown by Khan and Ali⁷⁰ to occur at the critical micelle concentration (CMC) of 0.0375 mol/L (293 K). It must be noted, however, that these investigators

conducted their conductivity experiments in the presence of polyvinylpyrrolidone (PVP), which might have altered the true CMC of DBSA and be the reason for the discrepancy between our respective findings.

The next step in introducing DBSA as synergist, was the inclusion of pyrazolyl ligands **6–8** and imidazolyl ligands **11–12** as extractants (**Figure 3.32**). These ligands were of particular interest in this study as a result of their poor nickel(II) extraction results previously highlighted in **Figures 3.12** and **3.13**. Pyrazolyl ligands **6–8**, in conjunction with DBSA, exhibited much better nickel(II) extraction results of 69.2 (± 1.8), 71.2 (± 1.5) and 65.3 (± 3.1)%. Their individual synergistic gains were 10.7 (± 1.5), 13.9 (± 1.6) and 16.4 (± 1.9)%, as summarised in **Table 3.5**. Imidazolyl ligands **11** and **12**, in the presence of DBSA as synergist, extracted nickel(II) at 69.0 (± 1.6) and 32.6 (± 1.7)% with synergistic losses (antagonism) in the order of -3.80 (± 1.36) and -1.89 (± 1.54)%, respectively (**Table 3.5**).

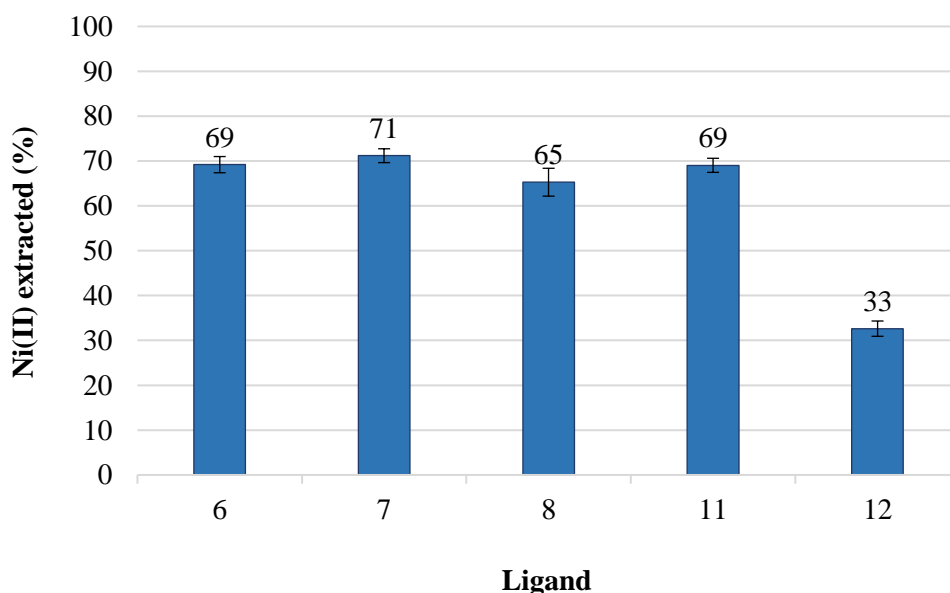


Figure 3.32: Extraction of nickel(II) by means of pyrazolyl ligands **6–8** and imidazolyl ligands **11–12** in the presence of DBSA. [Ligands] $\approx 2 \times 10^{-2}$ M; $[\text{Ni}^{2+}] = 8.11 \times 10^{-3}$ M; [DBSA] = 8.20×10^{-3} M; NaOAc/AcOH buffer; pH 4.93. [Data labels are rounded to two significant figures. See corresponding data in **Table 21** of **Appendix B — DATA TABLES**]

From the nett gain/loss data in **Table 3.5**, it was evident that the $-NH$ moiety present in pyrazolyl ligands **6–8** play a critical role in the stabilisation of the DBSA-ligand- Ni^{2+} assembly. The nitrogenous protons form stabilising hydrogen bonds to DBSA's polar sulfonic head in the outer coordination sphere. The entire conglomerate assembly is subsequently more soluble in the organic phase due to DBSA's long n -alkyl tail. Ultimately, this leads to increased nickel(II) extraction from the aqueous phase, something that is difficult for ligands **11** and **12** to achieve due to their lack of hydrogen bonding moieties. In fact, the imidazolyl ligands in conjunction with DBSA interestingly displayed antisnergistic characteristics. "Antisnergism" can be defined

as the decrease in extraction of a metal ion in the presence of a ligand and synergist, compared to the sum of their individual extractions. Mathematically, this can be expressed as follows:

$$\%E_{LS} < \%E_L + \%E_S \quad (54)$$

where $\%E_{LS}$ is the percentage extraction of the ligand and synergist (DBSA) combined, $\%E_L$ is the percentage extraction of the ligand and $\%E_S$ is the percentage extraction of the synergist (DBSA).

Table 3.5: The synergistic gains (synergism) of pyrazolyl ligands **6–8** and synergistic losses (antisynergism) of imidazolyl ligands **11–12** in the presence of $\sim 1 \times 10^{-2}$ M DBSA.

Ligand	Ni ²⁺ extraction by ligand only (%) [†]	Ni ²⁺ extraction by ligand + DBSA (%) [‡]	Nett gain/loss (%)
6	30.1 (± 0.9)	69.2 (± 1.8)	+10.7 (± 1.5)
7	28.9 (± 1.4)	71.2 (± 1.5)	+13.9 (± 1.6)
8	20.5 (± 0.8)	65.3 (± 3.1)	+16.4 (± 1.9)
11	44.4 (± 0.7)	69.0 (± 1.6)	-3.80 (± 1.36)
12	9.88 (± 1.12)	32.6 (± 1.7)	-1.89 (± 1.54)

Extraction of Ni²⁺ by DBSA alone (**Figure 3.31**): 28.4 (± 1.8)%. [†] Data taken from **Figures 3.12** and **3.13**. [‡] Data taken from **Figure 3.32**.

3.3.8.2 Extraction of nickel(II) by means of *p*-toluenesulfonic acid as synergist

Following the relatively successful extraction of nickel(II) by means of pyrazolyl ligands **6–8** in the presence of DBSA, it was decided to use another molecule to act as synergist. *p*-Toluenesulfonic acid (*p*TSA) was opted for because of its structural resemblances to DBSA, with the only modification being the short methyl tail instead of a long *n*-dodecyl tail. Initially, no significant results from the implementation of *p*TSA as synergist were anticipated due to its excellent solubility in water (~ 67 g/100 mL at 298 K). A thorough study was performed to assess *p*TSA's nickel(II) extractive ability under typical solvent extraction conditions. A wide range of *p*TSA:Ni²⁺ ratios were investigated, but not one particular ratio seemed to be extracting nickel(II) in excess of 3% (**Table 3.6**), something that was not too unexpected after taking *p*TSA's excellent hydrophilicity into account.

Table 3.6: Extraction of nickel(II) by means of the synergist, *p*TSA, at various synergist to Ni²⁺ (S:Ni²⁺) ratios.

<i>p</i> TSA:Ni ²⁺ ratio	Run	[Ni ²⁺] after extraction (mg.L ⁻¹)	Average [Ni ²⁺] after extraction (mg.L ⁻¹)	Average extraction (%)	Standard deviation (σ)
1:1	1	46.8	46.8	1.85	1.62
	2	46.7			
2:1	1	47.0	46.9	1.53	1.00
	2	46.8			
3:1	1	46.5	46.7	2.05	1.16
	2	45.8			
4:1	1	46.6	46.6	2.26	1.00
	2	46.5			
5:1	1	47.4	47.0	1.28	1.53
	2	46.7			
10:1	1	46.5	46.4	2.56	1.27
	2	46.4			
20:1	1	46.6	46.6	2.08	0.914
	2	46.7			

* pH = 4.93 (NaOAc/AcOH buffer); stock concentration: [Ni²⁺] = 8.11×10⁻³ M

The next experimental setup included the addition of 2,6-bis(5-heptyl-1*H*-pyrazol-3-yl)pyridine (**7**) to various *p*TSA:Ni²⁺ ratios to ascertain whether an incremental increase might lead to more efficient extractions of nickel(II). The idea and hope were that the *p*TSA-ligand-Ni²⁺ coordinative assembly might still be largely soluble in the organic phase, whilst knowing full well *p*TSA on its own is poorly soluble in chloroform. This turned out to be a fascinating study, with steady nickel(II) extraction increases observed from a 1:1 to 5:1 *p*TSA:Ni²⁺ ratio (**Figure 3.33**). This, in turn, meant that quite remarkable synergistic gains of -1.15 (± 2.20), 4.17 (± 1.62), 12.9 (± 1.4), 17.0 (± 1.7) and 21.4 (± 1.6)% were obtained for ratios 1:1 through to 5:1. It is postulated, however, the extraction ceiling is more than likely reached from ratio 4:1 (*p*TSA:Ni²⁺) onwards. This is because four available -NH moieties (two coordinating ligands) are theoretically able to form stabilising hydrogen bonds to four *p*TSA molecules in the outer coordination sphere (**Scheme 3.5**).

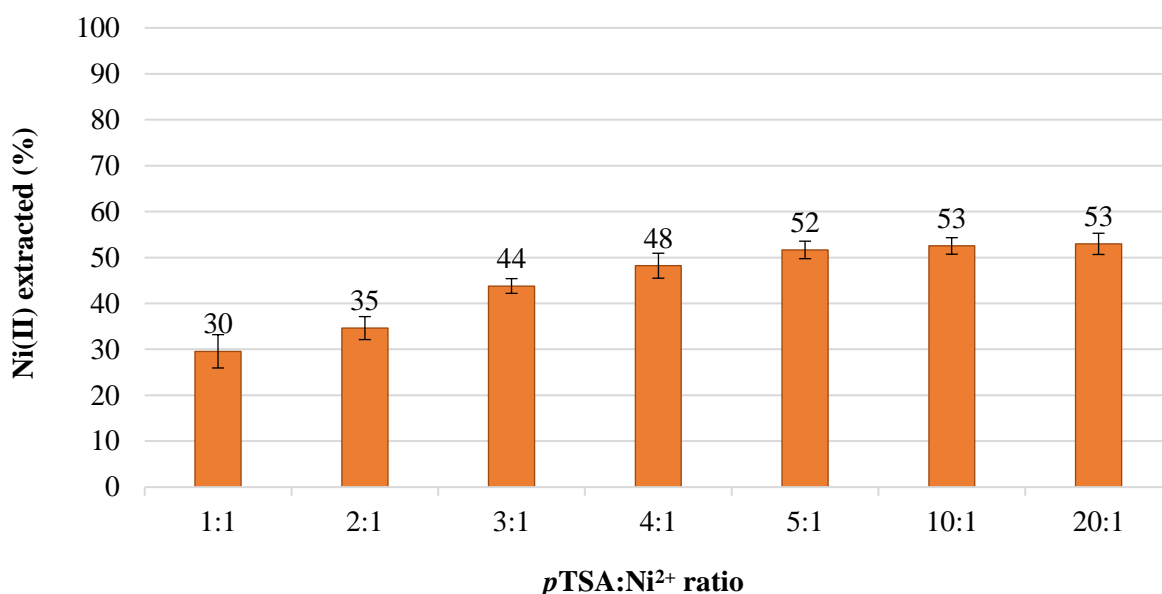
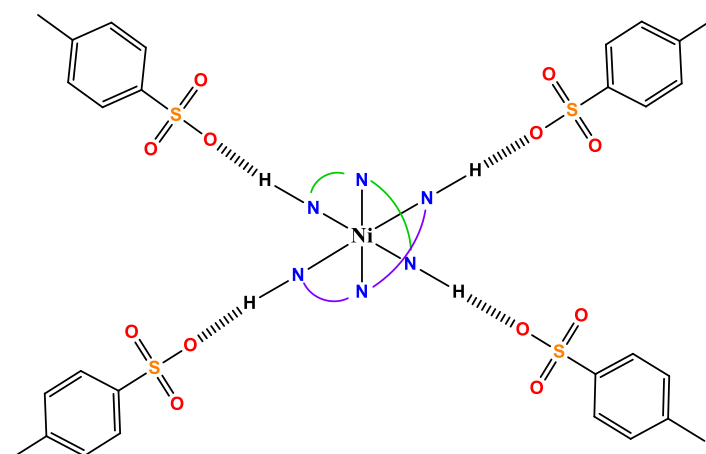


Figure 3.33: Extraction of nickel(II) by means of ligand **7** and *p*TSA with increasing (*p*TSA:Ni²⁺) ratios. [7] = 2×10^{-2} M; [Ni²⁺] = 8.11×10^{-3} M; NaOAc/AcOH buffer; pH 4.93. [Data labels are rounded to two significant figures. See corresponding data in **Table 22 of Appendix B — DATA TABLES**]

Although the overall extractive ability of the *p*TSA assembly was still less than the analogous DBSA assembly, it was strongly believed that the incorporation of an ethyl or propyl tail on the synergist would increase nickel(II) extractions significantly. It should increase the hydrophobicity of the synergist, while also minimising its surfactant-like properties. Unfortunately, this line of study was not pursued any further due to 4-ethylbenzenesulfonic acid's poor chemical purity (technical grade), while 4-propylbenzenesulfonic acid carried an extreme price tag at the time this study was undertaken.



Scheme 3.5: Theorised coordination of two tridentate pyrazolyl ligands to nickel(II) with four *p*TSA molecules stabilising the assembly via hydrogen bonding on the periphery. [Adapted from Roebuck *et al.*¹⁶]

The nickel(II) extraction experiment was repeated, only this time 2,6-bis(1-octylimidazol-2-yl)pyridine (**12**) was implemented as extractant whilst in the presence of *p*TSA at ratios of 1:1 to 5:1 (*p*TSA:Ni²⁺). No real extraction improvements were expected in this case due to previously reported synergistic DBSA results (**Figure 3.32** and **Table 3.5**). This was confirmed upon observing the nickel(II) extraction results in **Table 3.7**. The addition of *p*TSA appeared to have no effect on the extractive ability of ligand **12**. The highest extraction of 10.2 (± 1.0)% occurred at a 4:1 (*p*TSA:Ni²⁺) ratio, which was within experimental error of ligand **12**'s individual nickel(II) extractive performance in the absence of any synergist (**Figure 3.13**). This experiment, along with all aforementioned mini-studies, proved that the presence of -NH moieties are integral components in effective nickel(II) solvent extraction systems.

Table 3.7: Extraction of nickel(II) by means of imidazolyl ligand **12** at increasing *p*TSA:Ni²⁺ ratios.

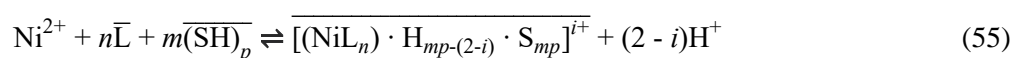
<i>p</i> TSA:Ni ²⁺ ratio	Run	[Ni ²⁺] after extraction (mg.L ⁻¹)	Average [Ni ²⁺] after extraction (mg.L ⁻¹)	Average extraction (%)	Standard deviation (σ)
1:1	1	43.9	43.3	9.08	2.32
	2	42.7			
2:1	1	42.4	42.9	9.86	1.62
	2	43.5			
3:1	1	43.0	43.0	9.75	1.45
	2	43.0			
4:1	1	42.8	42.8	10.2	0.953
	2	42.7			
5:1	1	43.2	42.9	9.93	1.30
	2	42.6			

* pH = 4.93 (NaOAc/AcOH buffer); stock concentration: [Ni²⁺] = 8.11×10⁻³ M; [**12**] = 2×10⁻² M.

3.3.8.3 Proposed synergistic extraction stoichiometry of DBSA and pyrazolyl ligands

Detailed mechanistic studies were by no means the main focus of this dissertation, but rather the syntheses of tridentate pyrazolyl (and imidazolyl) extractants for various applications in base metal solvent extraction setups. However, in order to understand these extractants better, the extraction mechanism should at least be explored to some degree.

The reaction stoichiometry delivers crucial information in understanding the extraction mechanism. For a solvent extraction system with pyrazolyl ligand and DBSA, hydrogen bonding between the two entities is present, with some DBSA molecules aggregating into micelles. The extraction of the nickel(II) system can generally be written as:



where the $\bar{\text{L}}$ symbols denote the organic phase, while the non-barred symbols denote the aqueous phase. L represents a tridentate pyrazolyl ligand, S the sulfonic acid synergist, DBSA, *n* and *m* stoichiometric integers and the subscript, *p*, the aggregation number of DBSA micelles.¹⁵

The equilibrium of the extraction reaction (Eq. 55) can now be derived:

$$K = \frac{[(NiL_n) \cdot H_{mp-(2-i)} \cdot S_{mp}]^{i+} \cdot [H^+]^{2-i}}{[Ni^{2+}] \cdot [L]^n \cdot [SH]_p^m} \quad (56)$$

Taking the logarithm and rearranging, we obtain:

$$\log D = \log K + n \log [L] + m \log [SH]_p + (2 - i) \text{pH} \quad (57)$$

where D is the distribution ratio of nickel(II) and K the equilibrium constant.¹⁵ Since the tridentate pyrazole-pyridinyl ligand is structurally rigid, two molecules can allow their N -donor atoms to find positions very close to the octahedral sites of nickel(II). This inherently offers a great degree of pre-organisation prior to nickel(II) binding.¹⁵ Moreover, due to complexation in an acidic environment, the non-coordinating nitrogen atoms of the pyrazolyl moieties are likely to retain their protons. Following this, the presence of hydrogen bonds between the pyrazolyl ligand and DBSA interfere with the formation of DBSA's micellar structures, as long as the concentration of DBSA never exceeds the concentration of the pyrazolyl ligand. Subsequently, it is anticipated that the monodentate DBSA anion associates with a nickel ionic complex to form an ion pair in the organic phase. But, since a single DBSA anion cannot counterbalance the Ni^{2+} cation, other anions in solution, such as NO_3^- , might also be involved—possibly occupying one coordination site in the cationic complex. Therefore, it is proposed that nickel(II) extraction most likely occurs by means of an ion pair formation mechanism.¹⁵ It should be noted, however, that this extraction mechanism should not be accepted as a universal fact, but merely treated as an educated suggestion.

3.4 Conclusions

Amine extractants are widely used in industry today for the extraction of base metals, precious metals and f -block elements, however, very little work is done on the design, synthesis and optimisation of heterocyclic amine extractants for the sole purpose of extracting base metal ions selectively. Many amine-type extractants are non-selective and therefore co-extract multiple metal ions. This was precisely the gap this study attempted to close, with the implementation of tailored tridentate pyrazole- and imidazole-pyridinyl ligands as extractants.

It was demonstrated that the length of the n -alkyl pendant arms play an important role in effective copper(II) extractions during competitive studies. The longer alkyl arms indirectly allow a higher electron density on the N -donor atoms and inherently improves the extractant's lipophilicity as well. Competitive studies revealed excellent selective extraction of copper(II), with % E generally increasing from ligand **1** (methyl) to **8** (octyl). Imidazolyl ligands **11** and **12**, on the other hand, were mediocre copper(II) extractants at best, yet ligand **11** showed promising selectivity for nickel(II), albeit with a % E in the mid-30% range. Competitive studies, in the absence of copper(II), showed good selectivity for nickel(II) in the cases of ligands **2–5** and **9**, while **6–8** displayed poor selectivity for any metal ion. This was largely ascribed to their lengthy pendant arms sterically impeding on neighbouring molecules and thereby limiting a second incoming molecule's access to the metal

centre. During selectivity studies, ligands **6–8**'s excellent copper(II) extractive abilities were once again on display, even at 10- and 60-fold reduction in copper(II) concentrations. As expected, nickel(II) was the second-most extracted metal ion species.

Copper(II) recovery studies yielded a visually aesthetic graph, with recovery decreasing incrementally from ligand **1** to **8**. The weakest extractant turned out to be the most effective extractant to recover copper(II) from. Conversely, the best extractant appeared to be holding on to its copper(II) more tightly, and therefore did not easily release it back into the aqueous phase. It was suggested that the most efficient extractant for recycling purposes probably lied with an extractant that displayed somewhat efficient performances in both extraction- and recovery processes, *i.e.*, ligand **4** (butyl). Similar trends were observed for the recovery of nickel(II) from loaded organic phases.

Our time-dependent extraction studies of copper(II) and nickel(II) were initially performed to ensure extraction equilibrium was reached before the 24-hour mark. Both pyrazolyl- (**2**, **5** and **7**) and imidazolyl ligands (**11** and **12**) achieved this within the given timeframe, with all three pyrazolyl ligands reaching equilibrium within 8 hours, while both imidazolyl ligands achieved the same within 16 hours. In general though, pyrazolyl ligands exhibited slower nickel(II) extraction rates when compared to the copper(II) results. This was likely due to their slow rate of water substitution in the inner coordination sphere.^{15,42}

Furthermore, we toiled for months on end to determine various ligand: M^{2+} ratios ($M^{2+} = Cu^{2+}$ and Ni^{2+}), often repeating experiments several times to obtain the most accurate and trustworthy results. Via Job's method, a 1:1 (pyrazolyl ligand: Cu^{2+}) complex ratio was demonstrated, with the sole exception of ligand **1**, while imidazolyl ligands appeared to coordinate in a biased 1:1 fashion. Pyrazolyl ligand **2**, formed 2:1 nickel(II)-, cobalt(II)-, cadmium(II)- and zinc(II) complexes, while only one molecule coordinated to lead(II). Two imidazolyl molecules (ligand **12**) evidently coordinated to cobalt(II), nickel(II) and zinc(II), while an even distribution of 1:1 and 2:1 cadmium(II) complexes were observed. Following this, numerous slope analyses by means of ICP-OES were conducted to undergird the Job plot results. Initially, a few problems were encountered during variable ligand concentration experiments (slope analyses) of ligands **5** and **7** with copper(II). These ligands were far too effective in extracting copper(II), even at low concentrations. This was countered by lowering the aqueous phase pH to 0.72. This extreme acidic environment inadvertently altered the mode of extraction by creating favourable reverse micellar conditions in which four pyrazolyl ligands surround an aqueous core containing one copper(II) ion. In the presence of nickel(II) and cobalt(II), however, ligands **5** and **7** did yield slopes of ~ 2 , indicating ligand: Ni^{2+} and ligand: Co^{2+} ratios of 2:1.

Lastly, attention was directed toward nickel(II) synergistic extraction studies. Due to their weak nickel(II) extractive abilities, it was decided to use pyrazolyl ligands **6–8** and imidazolyl ligands **11** and **12** in addition to dodecylbenzenesulfonic acid (DBSA), a synergist akin to DNNSA. It was swiftly realised that DBSA forms third phase emulsions at $\geq 2 \times 10^{-2}$ M. This forced the implementation of the optimum synergist concentration of 1×10^{-2} M. Ligands **6–8** exhibited mammoth synergistic extraction gains of 10.7 (± 1.5), 13.9 (± 1.6) and 16.4 (± 1.9)%, respectively. Imidazolyl ligands **11** and **12** performed poorly, with synergistic extraction losses

of $-3.80 (\pm 1.36)$ and $-1.89 (\pm 1.54)\%$, respectively. These results were vital evidence for the importance of the $-NH$ functional group. Without it, no hydrogen bonds can form on the periphery of the inner coordination sphere complex. Because of this, the use of *p*-toluenesulfonic acid as a synergist was attempted as well. It was known that the absence of a long *n*-alkyl tail on the synergist might compromise its solubility in the organic phase, but since ligand **7** already had two heptyl arms, it was postulated that the extracted assembly (ligand + synergist + Ni^{2+}) would be hydrophobic in nature. The extraction of nickel(II) by means of ligand **7** and *p*TSA, with increasing *p*TSA: Ni^{2+} ratios, delivered tremendous results. From a 1:1 to a 5:1 (*p*TSA: Ni^{2+}) ratio, synergistic gains of $-1.15 (\pm 2.20)$, $4.17 (\pm 1.62)$, $12.9 (\pm 1.4)$, $17.0 (\pm 1.7)$ and $21.4 (\pm 1.6)\%$ were observed, respectively. It is important to emphasise that *p*TSA had no real individual extractive abilities, since it was highly soluble in the aqueous phase and poorly soluble in the organic phase.

3.5 References

- (1) Wang, L.; Lee, M. Solvent Extraction of Cobalt and Nickel from Chloride Solution by Mixtures of Acidic Organophosphorous Extractants and Amines. *Geosystem Eng.* **2016**, *19* (6), 261–265.
- (2) Du Preez, J.; Postma, J.; Ravindran, S.; van Brecht, B. Nitrogen reagents in metal ion separation. PART VI. 2-(1'-Octylthiomethyl)pyridine as extractant for later 3d transition metal ions. *Solvent Extr. Ion Exch.* **1997**, *15* (1), 79–96.
- (3) Du Preez, J.; Sumter, N.; Mattheüs, C.; Ravindran, S.; van Brecht, B. Nitrogen reagents in metal ion separation. Part VII. The development of a novel copper(II) extractant. *Solvent Extr. Ion Exch.* **1997**, *15* (6), 1007–1021.
- (4) Du Preez, J.; Mattheüs, C.; Sumter, N.; Ravindran, S.; Potgieter, C.; van Brecht, B. Nitrogen reagents in metal ion separation. Part VIII. Substituted imidazoles as extractants for Cu^{2+} . *Solvent Extr. Ion Exch.* **1998**, *16* (2), 565–586.
- (5) Du Preez, J.; Mattheüs, C.; Sumter, N.; Edge, W.; Potgieter, C.; van Brecht, B. Nitrogen reagents in metal ion separation. Part IX. Extraction of cobalt and nickel using imidazole derivatives. *Solvent Extr. Ion Exch.* **1998**, *16* (4), 1033–1046.
- (6) Roberts, T.; Little, M.; Kershaw Cook, L.; Halcrow, M. Iron(II) complexes of 2,6-di(1h-pyrazol-3-yl)-pyridine derivatives with hydrogen bonding and sterically bulky substituents. *Dalton Trans.* **2014**, *43* (20), 7577–7588.
- (7) Gal, M.; Tarrago, G.; Steel, P.; Marzin, C. A novel macrocyclic ligand containing 2,6-bis(pyrazol-5-yl)pyridine units. Synthesis and complexation properties. *Nouv. J. Chim.* **1985**, *9* (10), 617–620.
- (8) Yoshinari, A.; Tazawa, A.; Kuwata, S.; Ikariya, T. Synthesis, structures, and reactivities of pincer-type ruthenium complexes bearing two proton-responsive pyrazole arms. *Chem. – An Asian J.* **2012**, *7* (6), 1417–1425.

- (9) Umehara, K.; Kuwata, S.; Ikariya, T. Synthesis, structures, and reactivities of iron, cobalt, and manganese complexes bearing a pincer ligand with two protic pyrazole arms. *Inorg. Chim. Acta* **2014**, *413*, 136–142.
- (10) Li, L.; Luo, Q.; Cui, H.; Li, R.; Zhang, J.; Peng, T. Air-stable ruthenium(II)-NNN pincer complexes for the efficient coupling of aromatic diamines and alcohols to 1*H*-benzo[*d*]imidazoles with the liberation of H₂. *ChemCatChem* **2018**, *10* (7), 1607–1613.
- (11) Polezhaev, A.; Chen, C.; Kinne, A.; Cabelof, A.; Lord, R.; Caulton, K. Ligand design toward multifunctional substrate reductive transformations. *Inorg. Chem.* **2017**, *56* (16), 9505–9514.
- (12) Roberts, T.; Halcrow, M. Supramolecular assembly and transfer hydrogenation catalysis with ruthenium(II) complexes of 2,6-di(1*H*-pyrazol-3-yl)pyridine derivatives. *Polyhedron* **2016**, *103*, 79–86.
- (13) Milutinović, M.; Bogojeski, J.; Klisurić, O.; Scheurer, A.; Elmroth, S.; Bugarčić, Ž. Synthesis and structures of a pincer-type rhodium(III) complex: Reactivity toward biomolecules. *Dalton Trans.* **2016**, *45* (39), 15481–15491.
- (14) Shiga, T.; Matsumoto, T.; Noguchi, M.; Onuki, T.; Hoshino, N.; Newton, G.; Nakano, M.; Oshio, H. Cobalt antiferromagnetic ring and grid single-molecule magnet. *Chem. - An Asian J.* **2009**, *4* (11), 1660-1663+1636.
- (15) Zhou, T.; Pesic, B. A pyridine-based chelating solvent extraction system for selective extraction of nickel and cobalt. *Hydrometallurgy* **1997**, *46* (1), 37–53.
- (16) Roebuck, J.; Bailey, P.; Doidge, E.; Fischmann, A.; Healy, M.; Nichol, G.; O'Toole, N.; Pelsler, M.; Sassi, T.; Sole, K.; *et al.* Strong and selective Ni(II) extractants based on synergistic mixtures of sulfonic acids and bidentate *N*-heterocycles. *Solvent Extr. Ion Exch.* **2018**, *36* (05), 1–22.
- (17) Wilden, A.; Modolo, G.; Kaufholz, P.; Sadowski, F.; Lange, S.; Munzel, D.; Geist, A. Process development and laboratory-scale demonstration of a regular-SANEX process using C5-BPP (2,6-bis(5-(2,2-dimethylpropyl)-1*H*-pyrazol-3-yl)pyridine). *Sep. Sci. Technol. (Philadelphia, PA, United States)* **2015**, *50* (16), 2467–2475.
- (18) Wilden, A.; Modolo, G.; Hupert, M.; Santiago-Schuebel, B.; Loefstroem-Engdahl, E.; Halleroed, J.; Ekberg, C.; Mincher, B.; Mezyk, S. Gamma-radiolytic stability of solvents containing C5-BPP (2,6-bis(5-(2,2-dimethylpropyl)-1*H*-pyrazol-3-yl)pyridine) for actinide(III)/lanthanide(III) separation. *Solvent Extr. Ion Exch.* **2016**, *34* (1), 1–12.
- (19) Kong, X.; Wu, Q.; Lan, J.; Wang, C.; Chai, Z.; Nie, C.; Shi, W. Theoretical insights into preorganized pyridylpyrazole-based ligands toward the separation of Am(III)/Eu(III). *Inorg. Chem.* **2018**, *57* (23), 14810–14820.

- (20) Bremer, A.; Ruff, C.; Girnt, D.; Muellich, U.; Rothe, J.; Roesky, P.; Panak, P.; Karpov, A.; Mueller, T.; Denecke, M.; *et al.* 2,6-Bis(5-(2,2-dimethylpropyl)-1H-pyrazol-3-yl)pyridine as a ligand for efficient actinide(III)/lanthanide(III) separation. *Inorg. Chem.* **2012**, *51* (9), 5199–5207.
- (21) Bremer, A.; Geist, A.; Panak, P. Complexation of Cm(III) and Eu(III) with 2,6-bis(5-(2,2-dimethylpropyl)-1H-pyrazol-3-yl)pyridine and 2-bromohexanoic acid studied by time-resolved laser fluorescence spectroscopy. *Radiochim. Acta* **2013**, *101* (5), 285–291.
- (22) Blake, C.; Baes, C.; Brown, K. Solvent extraction with alkyl phosphoric compounds. *Ind. Eng. Chem.* **1958**, *50* (12), 1763–1767.
- (23) Laing, M. Solvent extraction of metals *Is* coordination chemistry. In *Coordination Chemistry*; ACS Symposium Series; American Chemical Society, 1994; Vol. 565, pp 31–382.
- (24) Joo, S.; Shin, D.; Oh, C.; Wang, J.; Senanayake, G.; Shin, S. Selective extraction and separation of nickel from cobalt, manganese and lithium in pre-treated leach liquors of ternary cathode material of spent lithium-ion batteries using synergism caused by Versatic 10 acid and LIX 84-I. *Hydrometallurgy* **2016**, *159*, 65–74.
- (25) Guimarães, A.; da Silva, P.; Mansur, M. Purification of nickel from multicomponent aqueous sulfuric solutions by synergistic solvent extraction using Cyanex 272 and Versatic 10. *Hydrometallurgy* **2014**, *150*, 173–177.
- (26) Fouad, E. Extraction of nickel by bis(2,4,4-trimethylpentyl) dithiophosphinic acid synergism. *J. Eng. Appl. Sci.* **2009**, *56* (6), 661–677.
- (27) Du Preez, J.; Preston, A. Separation of nickel and cobalt from calcium, magnesium and manganese by solvent extraction with synergistic mixtures of carboxylic acids. *J. South African Inst. Min. Metall.* **2004**, *104* (6), 333–338.
- (28) Flett, D. Solvent extraction. *Chem. Industry* **1977**, No. 6, 223–224.
- (29) Nyman, B.; Hummelstedt, L. Use of liquid cation exchange for separation of nickel(II) and cobalt(II) with simultaneous concentration of nickel sulphate. In *International Solvent Extraction Conference (ISEC)*; SCI: London: Lyon, 1974; pp 669–684.
- (30) Hummelstedt, L.; Lund, H.; Karjaluo, J.; Berts, L.; Nyman, B. Use of extractants mixtures containing Kelex 100 for separation of nickel(II) and cobalt(II). In *International Solvent Extraction Conference (ISEC)*; SCI: London: Lyon, 1974; pp 829–849.
- (31) Osseo-Asare, K.; Keeney, M. Sulfonic acids: Catalysts for the liquid-liquid extraction of metals. *Sep. Sci. Technol.* **1980**, *15* (4), 999–1011.

- (32) Okewole, A.; Magwa, N.; Tshentu, Z. The separation of nickel(II) from base metal ions using 1-octyl-2-(2'-pyridyl)imidazole as extractant in a highly acidic sulfate medium. *Hydrometallurgy* **2012**, 121–124.
- (33) Pearce, B.; Ogutu, H.; Luckay, R. Synthesis of pyrazole-based pyridine ligands and their use as extractants for nickel(II) and copper(II): Crystal structure of a copper(II)–ligand complex. *Eur. J. Inorg. Chem.* **2017**, 2017 (8).
- (34) Gomori, G. Preparation of buffers for use in enzyme studies. In *Methods in Enzymology*; Colowick, S., Kaplan, N., Eds.; Academic Press, Inc., 1955; Vol. 1, pp 138–146.
- (35) Perrin, D.; Dempsey, B. Appendices in: Buffers for pH and metal ion control. In *Buffers for pH and Metal Ion Control*; Perrin, D., Dempsey, B., Eds.; Springer: Dordrecht, 1974; pp 123–166.
- (36) Gottschalk, G. Acetat- und ammonium-puffersysteme. *Fresenius' Zeitschrift für Anal. Chemie* **1959**, 167 (5), 342–351.
- (37) Martell, A.; Smith, R. *Critical Stability Constants*; Plenum Press: New York,.
- (38) Okewole, A.; Antunes, E.; Nyokong, T.; Tshentu, Z. The development of novel nickel selective amine extractants: 2,2'-Pyridylimidazole functionalised chelating resin. *Miner. Eng.* **2013**, 54.
- (39) Ndayambaje, G.; Laatikainen, K.; Laatikainen, M.; Beukes, E.; Fatoba, O.; van der Walt, N.; Petrik, L.; Sainio, T. Adsorption of nickel(II) on polyacrylonitrile nanofiber modified with 2-(2'-pyridyl)imidazole. *Chem. Eng. J.* **2016**, 284.
- (40) Irving, H.; Williams, R. The stability of transition-metal complexes. *J. Chem. Soc.* **1953**, 3192–3210.
- (41) Shannon, R. Revised effective ionic radii and systematic studies of interatomic distances in halides and chalcogenides. *Acta Crystallogr. Sect. A* **1976**, 32 (5), 751–767.
- (42) Eigen, M. Fast elementary steps in chemical reaction mechanisms. *Pure Appl. Chem.* **1963**, 6 (1), 97–116.
- (43) Ostromisslensky, I. Über eine neue, auf dem massenwirkungsgesetz fußende analysenmethode einiger binären verbindungen. *Berichte der Dtsch. Chem. Gesellschaft* **1911**, 44 (1), 268–273.
- (44) Denison, R. Contributions to the knowledge of liquid mixtures - I. Property-composition curves and the molecular changes which take place on forming binary liquid mixtures. *Trans. Faraday Soc.* **1912**, 8 (OCTOBER), 20–34.
- (45) Job, P. Formation and stability of inorganic complexes in solution. *Ann. Chim. (Cachan, Fr.)* **1928**, 9, 113–203.

- (46) Rydberg, J. *Solvent Extraction Principles and Practice*, 2nd Edition; Taylor & Francis Group, LLC: New York, 2004.
- (47) Stephan, H.; Juran, S.; Antonioli, B.; Gloe, K.; Gloe, K. Extraction methods. *Analytical Methods in Supramolecular Chemistry*. December 15, 2006, pp 79–103.
- (48) Yoe, J.; Jones, A. Colorimetric determination of iron with disodium-1,2-dihydroxybenzene-3,5-disulfonate. *Ind. Eng. Chem. - Anal. Ed.* **1944**, *16* (2), 111–115.
- (49) Harvey Jr., A.; Manning, D. Spectrophotometric methods of establishing empirical formulas of colored complexes in solution. *J. Am. Chem. Soc.* **1950**, *72* (10), 4488–4493.
- (50) Connors, K. *Binding constants: The Measurement of Molecular Complex Stability*; Wiley interscience publication; Wiley, 1987.
- (51) Hirose, K. A practical guide for the determination of binding constants. *J. Incl. Phenom.* **2001**, *39* (3–4), 193–209.
- (52) Sayago, A.; Boccio, M.; Asuero, A. Continuous variation data: 1:1 or 2:2 weak complexes? *Int. J. Pharm.* **2005**, *295* (1–2), 29–34.
- (53) Sayago, A.; Asuero, A. Spectrophotometric evaluation of stability constants of 1:1 weak complexes from continuous variation data. *Int. J. Pharm.* **2006**, *321* (1–2), 94–100.
- (54) Facchiano, A.; Ragone, R. Modification of Job's method for determining the stoichiometry of protein-protein complexes. *Anal. Biochem.* **2003**, *313* (1), 170–172.
- (55) Likussar, W.; Boltz, D. Theory of continuous variations plots and a new method for spectrophotometric determination of extraction and formation constants. *Anal. Chem.* **1971**, *43* (10), 1265–1272.
- (56) Purohit, D.; Goswami, A.; Chauhan, R.; Ressalan, S. Purohit's spectrophotometric method for determination of stability constants of complexes using Job's curves. *Asian J. Chem.* **1999**, *11* (1), 123–129.
- (57) Gil, V.; Oliveira, N. On the use of the method of continuous variations. *J. Chem. Educ.* **1990**, *67* (6), 473–478.
- (58) Liou, L.; McNeil, A.; Ramirez, A.; Toombes, G.; Gruver, J.; Collum, D. Lithium enolates of simple ketones: Structure determination using the method of continuous variation. *J. Am. Chem. Soc.* **2008**, *130* (14), 4859–4868.
- (59) Olson, E.; Bühlmann, P. Getting more out of a Job plot: Determination of reactant to product stoichiometry in cases of displacement reactions and n:n complex formation. *J. Org. Chem.* **2011**, *76* (20), 8406–8412.

- (60) Renny, J.; Tomasevich, L.; Tallmadge, E.; Collum, D. Method of continuous variations: Applications of Job plots to the study of molecular associations in organometallic chemistry. *Angew. Chemie - Int. Ed.* **2013**, *52* (46), 11998–12013.
- (61) Miessler, G.; Tarr, D. *Inorganic Chemistry*, 4th Edition; Pearson Prentice Hall, Upper Saddle River, NJ, USA; Boston; London, 2011.
- (62) Hu, F.; Hu, H.; Hu, J.; Zhu, S.; Yang, J.; Wang, Y. Improving selective separation of Cu(II) from acidic polymetallic media with 2-ethylhexyl 4-pyridinecarboxylate ester: Extraction behaviors, coordination structure and microscopic mechanism. *J. Mol. Liq.* **2017**, *248*, 1050–1058.
- (63) Pearce, B.; Ogutu, H.; Saban, W.; Luckay, R. Synthesis, characterization and use of imidazole and methyl-pyrazole based pyridine ligands as extractants for nickel(II) and copper(II). *Inorg. Chim. Acta* **2019**, *490*, 57–67.
- (64) Swami, K.; Venkatesan, K.; Antony, M. Role of phase modifiers in controlling the third-phase formation during the solvent extraction of trivalent actinides. *Solvent Extr. Ion Exch.* **2019**, *37* (7), 500–517.
- (65) Weßling, P.; Müllich, U.; Guerinoni, E.; Geist, A.; Panak, P. Solvent extraction of An(III) and Ln(III) using TODGA in aromatic diluents to suppress third phase formation. *Hydrometallurgy* **2020**, *192*.
- (66) Anwer, T.; Ansari, M.; Mohammad, F. Dodecylbenzenesulfonic acid micelles assisted in situ preparation and enhanced thermoelectric performance of semiconducting polyaniline-zirconium oxide nanocomposites. *J. Ind. Eng. Chem.* **2013**, *19* (5), 1653–1658.
- (67) Adrian, L.; Mariatti, M.; Lockman, Z. Effect of dodecylbenzenesulfonic acid as a surfactant on the properties of polyaniline/graphene nanocomposites. In *Materials Today: Proceedings*; 2019; Vol. 17, pp 864–870.
- (68) Kaur, G.; Thakur, S.; Kaundal, P.; Chandel, K.; Banerjee, B. *p*-Dodecylbenzenesulfonic acid: An efficient Brønsted acid-surfactant-combined catalyst to carry out diverse organic transformations in aqueous medium. *ChemistrySelect* **2018**, *3* (45), 12918–12936.
- (69) Li, J.; Liu, X. Fabrication and enhanced electrochemical properties of α -MoO₃ nanobelts using dodecylbenzenesulfonic acid as both reactant and surfactant. *CrystEngComm* **2014**, *16* (2), 184–190.
- (70) Khan, M.; Ali, Z. Micellization studies of dodecyl benzenesulfonic acid and its interaction with polyvinylpyrrolidone. *Chinese J. Polym. Sci.* **2005**, *23* (01), 29–35.

CHAPTER 4

SYNTHESIS AND CHARACTERISATION OF VARIOUS BASE METAL COMPLEXES IN ADDITION TO CRYSTAL AND MOLECULAR STRUCTURES OF TWO COPPER(II) COMPLEXES

4.1 Introduction

The formation of metal complexes with tridentate aromatic amine ligands is an area of study that is widely regarded to be in its blooming years, with major advancements made in the past decade. Interest in this research area originates from the idea that supramolecular architectures can be designed and tailored to satisfy specific needs. From this idea the field of crystal engineering was born. The term “crystal engineering” was first coined by Schmidt¹ in 1971, when he studied photodimerisation reactions in crystalline cinnamic acids. In 1989, Desiraju² defined “crystal engineering” as follows:

“It is the understanding of intermolecular interactions in the context of crystal packing and the utilization of such understanding in the design of new solids with desired physical and chemical properties.”

Systems that are self-assembled by weak intermolecular forces are vital in crystal engineering. One such example includes molecular materials assembled by means of hydrogen bond interactions.³ The objective to design new materials with an array of different physical and chemical properties, however, can solely be achieved once the properties of the individual units, their response to chemical substitutions, as well as their interactions are quantitatively understood.⁴

For synthetic chemists, it can be a significant challenge in trying to understand the main factors that govern the wide variety of supramolecular crystal packing organisations. The study of single-crystal structures of metal ion complexes greatly increases the level of understanding of these factors.⁴ This has allowed synthetic chemists to design ligands that exhibit unique complexing properties in a much improved manner. The cavity (bite-size) of tridentate aromatic *N*-donor ligands is of prime interest in understanding their selectivity for certain metal ions. This, in addition to bond lengths, bond angles, torsion angles, overall geometry, packing efficiency, *etc.*, can be visualized with crystal and molecular structure determinations. Naturally, an account of deformed bond angles and bond lengths are also given, of which Jahn-Teller compression and elongation of axial bonds are the most common.⁵

In this study, crystal structures were mainly derived to give insight regarding solution-based coordination chemistry of tridentate aromatic *N*-donor ligands to base metal ions. Although some might consider it a stretch too far to compare solid state with solution-based studies, it is merely ground-level information that is sought

after. Moreover, solid state studies must not be treated as an isolated analytical technique, but rather in combination with rigorous computational and solution-based studies.

4.2 Materials and methods

4.2.1 Chemicals and reagents

The chemicals listed in **Table 4.1** were bought from reputable chemical suppliers and used without additional purification. In addition to these, 2,6-bis(5-ethyl-1*H*-pyrazol-3-yl)pyridine (**2**) and 2,6-bis(5-(*tert*-butyl)-1*H*-pyrazol-3-yl)pyridine (**9**) was also used as synthetically prepared in **Sections 2.3.3** and **2.3.10** of **CHAPTER 2**.

Table 4.1: List of chemicals used in alphanumeric order.

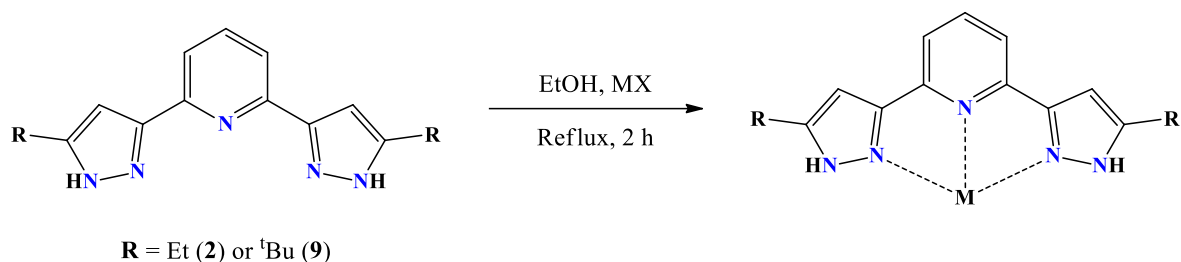
Chemical/Reagent	Purity (%)	Commercial Supplier
Copper(II) bromide (anhydrous)	99	Sigma-Aldrich (Pty) Ltd.
Copper(II) chloride dihydrate	> 99	Sigma-Aldrich (Pty) Ltd.
Copper(II) nitrate trihydrate	≥ 99	Sigma-Aldrich (Pty) Ltd.
Copper(II) perchlorate hexahydrate	98	Sigma-Aldrich (Pty) Ltd.
Copper(II) sulfate pentahydrate	≥ 98	Sigma-Aldrich (Pty) Ltd.
Diethyl ether	≥ 98	Merck (Pty) Ltd.
Ethanol (absolute)	≥ 99	KIMIX Chemical and Lab Supplies (CC)
Ethyl acetate	≥ 98	KIMIX Chemical and Lab Supplies (CC)
Methanol	≥ 97	KIMIX Chemical and Lab Supplies (CC)
Nickel(II) chloride hexahydrate	≥ 98	Sigma-Aldrich (Pty) Ltd.
Nickel(II) sulfate hexahydrate	≥ 98	Sigma-Aldrich (Pty) Ltd.
Zinc(II) bromide (anhydrous)	> 99	Sigma-Aldrich (Pty) Ltd.

4.2.2 Instrumentation

The various characterisation techniques, along with their respective technical instruments, were generally akin to those reported in **Sections 2.2.2** of **CHAPTER 2** and **3.2.2** of **CHAPTER 3**. The only exceptions were the use of a *Bruker VERTEX 70* spectrometer for infrared (IR) analyses (4000–500 cm⁻¹) and a *BÜCHI Melting Point M-560* apparatus (maximum temperature 400 °C). These instruments were operated at Technische Universität Dresden, Germany.

4.3 Experimental

4.3.1 General syntheses of various divalent base metal complexes



Scheme 4.1: Synthetic route to a variety of base metal complexes by using either 2,6-bis(5-ethyl-1*H*-pyrazol-3-yl)pyridine (**2**) or 2,6-bis(5-(*tert*-butyl)-1*H*-pyrazol-3-yl)pyridine (**9**) as ligand. MX represents the following hydrated salts: CuCl₂, CuBr₂ (anhydrous), Cu(ClO₄)₂, CuSO₄, NiSO₄, NiCl₂ or ZnBr₂ (anhydrous).

Either ligand **2** (60 mg, 0.224 mmol) or **9** (70 mg, 0.216 mmol) was dissolved in 5 mL absolute ethanol and added to MX (~0.220 mmol) in ethanol (5 mL). The mixture was stirred under refluxing conditions for 2 hours, whereafter it was allowed to cool to room temperature. The solvent was removed *in vacuo*, yielding a solid material, which was often brightly coloured due to complexation. The solid was quantitatively transferred onto filter paper and washed with ice-cold diethyl ether and ethyl acetate whilst running the suction pump. The remaining shiny solid material was collected and stored in glass vials.

4.3.1.1 [CuCl(L2)]Cl complex

Analogous to the general synthetic procedure, the [CuCl(L2)]Cl complex was obtained as a green solid (52 mg, 0.129 mmol) in a yield of 57.8%. **IR (KBr, cm⁻¹)** 3424 (N–H str), 3059 (aromatic C–H str), 2963/2933 (aliphatic C–H str), 1611 (pyridine C=N str), 1575 (pyrazole C=N str), 1461 (–CH₂– bend). **ESI-MS (*m/z*)** 268.16 (C₁₅H₁₇N₅ + H)⁺, 298.61 [Cu(C₁₅H₁₇N₅)₂]²⁺, 330.08 [Cu(C₁₅H₁₆N₅) + H]⁺, 347.08 [Cu(C₁₅H₁₆N₅)(H₂O)]⁺, 365.05 [CuCl(C₁₅H₁₇N₅)]⁺, 375.08 [Cu(C₂H₅O)(C₁₅H₁₇N₅)]⁺, 596.22 [Cu(C₁₅H₁₆N₅)₂ + H]⁺, 695.11 [Cu₂Cl(C₁₅H₁₆N₅)₂]⁺. **m.p.** 299–300 °C. *See spectra on pages 79 and 80 of Appendix A — SPECTRA.*

4.3.1.2 [Ni(L2)₂]SO₄ complex

Analogous to the general synthetic procedure, the [Ni(L2)₂]SO₄ complex was obtained as a shiny yellow-brown solid (45 mg, 0.0653 mmol) in a yield of 58.4%. **IR (KBr, cm⁻¹)** 3188 (N–H str), 2970/2933 (aliphatic C–H str), 1613 (pyridine C=N str), 1577 (pyrazole C=N str), 1462 (–CH₂– bend). **ESI-MS (*m/z*)** 296.11 [Ni(C₁₅H₁₇N₅)₂]²⁺, 326.09 [Ni(C₁₅H₁₇N₅) + H]⁺, 370.08 [Ni(C₂H₅O)(C₁₅H₁₇N₅)]⁺, 422.05 [NiSO₄(C₁₅H₁₇N₅) + H]⁺, 591.22 [Ni(C₁₅H₁₆N₅)₂ + H]⁺. **m.p.** 310–311 °C. *See spectra on pages 81 and 82 of Appendix A — SPECTRA.*

4.3.1.3 [Ni(L2)₂]Cl₂ complex

Analogous to the general synthetic procedure, the [Ni(L2)₂]Cl₂ complex was obtained as a brown solid (34 mg, 0.0512 mmol) in a yield of 45.9%. **IR (KBr, cm⁻¹)** 3274 (N–H str), 3065 (aromatic C–H str), 2966/2938 (aliphatic C–H str), 1611 (pyridine C=N str), 1576 (pyrazole C=N str), 1457 (–CH₂– bend). **ESI-MS (m/z)** 268.15 (C₁₅H₁₇N₅ + H)⁺, 296.11 [Ni(C₁₅H₁₇N₅)₂]²⁺, 342.07 [Ni(C₁₅H₁₆N₅)(H₂O)]⁺, 370.07 [Ni(C₂H₅O)(C₁₅H₁₇N₅)]⁺, 591.20 [Ni(C₁₅H₁₆N₅)₂ + H]⁺. **m.p.** > 400 °C. *See spectra on pages 83 and 84 of Appendix A — SPECTRA.*

4.3.1.4 [Cu(L2)₂]Br₂ complex

Analogous to the general synthetic procedure, the [Cu(L2)₂]Br₂ complex was obtained as a light green solid (36 mg, 0.0475 mmol) in a yield of 42.4%. **IR (KBr, cm⁻¹)** 3115 (N–H str), 3052 (aromatic C–H str), 2970/2934 (aliphatic C–H str), 1610 (pyridine C=N str), 1576 (pyrazole C=N str), 1465 (–CH₂– bend). **ESI-MS (m/z)** 268.16 (C₁₅H₁₇N₅ + H)⁺, 298.61 [Cu(C₁₅H₁₇N₅)₂]²⁺, 330.08 [Cu(C₁₅H₁₆N₅) + H]⁺, 375.08 [Cu(C₂H₅O)(C₁₅H₁₇N₅)]⁺, 410.99 [CuBr(C₁₅H₁₇N₅)]⁺, 596.22 [Cu(C₁₅H₁₆N₅)₂ + H]⁺. **m.p.** 288–289 °C. *See spectra on pages 85 and 86 of Appendix A — SPECTRA.*

4.3.1.5 [Zn(L2)₂]Br₂ complex

Analogous to the general synthetic procedure, the [Zn(L2)₂]Br₂ complex was obtained as a beige solid (33 mg, 0.0434 mmol) in a yield of 38.8%. **IR (KBr, cm⁻¹)** 3329 (N–H str), 3075 (aromatic C–H str), 2970/2935 (aliphatic C–H str), 1614 (pyridine C=N str), 1577 (pyrazole C=N str), 1465 (–CH₂– bend). **ESI-MS (m/z)** 268.16 (C₁₅H₁₇N₅ + H)⁺, 299.12 [Zn(C₁₅H₁₇N₅)₂]²⁺, 347.08 [Zn(C₁₅H₁₆N₅)(H₂O)]⁺, 376.07 [Zn(C₂H₅O)(C₁₅H₁₇N₅)]⁺, 597.22 [Zn(C₁₅H₁₆N₅)₂ + H]⁺. **m.p.** 370–371 °C. *See spectra on pages 87 and 88 of Appendix A — SPECTRA.*

4.3.1.6 [Cu(L2)₂](ClO₄)₂ complex

Analogous to the general synthetic procedure, the [Cu(L2)₂](ClO₄)₂ complex was obtained as a light green solid (51 mg, 0.0640 mmol) in a yield of 57.3%. **IR (KBr, cm⁻¹)** 3219 (N–H str), 3086 (aromatic C–H str), 2982 (aliphatic C–H str), 1619 (pyridine C=N str), 1571 (pyrazole C=N str), 1472 (–CH₂– bend). **ESI-MS (m/z)** 268.16 (C₁₅H₁₇N₅ + H)⁺, 298.61 [Cu(C₁₅H₁₇N₅)₂]²⁺, 330.08 [Cu(C₁₅H₁₆N₅) + H]⁺, 375.08 [Cu(C₂H₅O)(C₁₅H₁₇N₅)]⁺, 429.03 [Cu(ClO₄)(C₁₅H₁₇N₅)]⁺, 596.22 [Cu(C₁₅H₁₆N₅)₂ + H]⁺. **m.p.** 254–255 °C. *See spectra on pages 89 and 90 of Appendix A — SPECTRA.*

4.3.1.7 [Cu(L9)₂]SO₄ complex

Analogous to the general synthetic procedure, the [Cu(L9)₂]SO₄ complex was obtained as a light green solid (73 mg, 0.0905 mmol) in a yield of 81.1%. **IR (KBr, cm⁻¹)** 3127 (N–H str), 3056 (aromatic C–H str), 2963 (aliphatic C–H str), 1615 (pyridine C=N str), 1577 (pyrazole C=N str). **ESI-MS (m/z)** 315.63 [Ni(C₂H₅O)₂(C₁₃H₁₃N₅)₂]²⁺, 354.68 [Cu(C₁₉H₂₅N₅)₂]²⁺, 403.13 [Cu(C₁₉H₂₃N₅)(H₂O)]⁺, 431.14 [Cu(C₂H₅O)(C₁₉H₂₅N₅)]⁺, 630.24 [Ni(C₂H₅O)₂(C₁₃H₁₂N₅)₂ + H]⁺, 708.34 [Cu(C₁₉H₂₄N₅)₂ + H]⁺. **m.p.** 303–304 °C. *See spectra on pages 91 and 92 of Appendix A — SPECTRA.*

4.3.1.8 [Cu(L9)₂](ClO₄)₂ complex

Analogous to the general synthetic procedure, the [Cu(L9)₂](ClO₄)₂ complex was obtained as a shiny green solid (59 mg, 0.0649 mmol) in a yield of 57.8%. **IR (KBr, cm⁻¹)** 3251 (N–H str), 3080 (aromatic C–H str), 2968 (aliphatic C–H str), 1616 (pyridine C=N str), 1580 (pyrazole C=N str). **ESI-MS (m/z)** 315.63 [Ni(C₂H₅O)₂(C₁₃H₁₃N₅)₂]²⁺, 324.22 (C₁₉H₂₅N₅ + H)⁺, 354.68 [Cu(C₁₉H₂₅N₅)₂]²⁺, 386.14 [Cu(C₁₉H₂₄N₅) + H]⁺, 403.14 [Cu(C₁₉H₂₃N₅)(H₂O)]⁺, 421.11 [Cu(C₁₉H₂₄N₅)(H₂O)₂]⁺, 431.14 [Cu(C₂H₅O)(C₁₉H₂₅N₅)]⁺, 485.09 [Cu(ClO₄)(C₁₉H₂₅N₅)]⁺, 709.35 [Cu(C₁₉H₂₄N₅)₂ + H]⁺. **m.p.** 230–231 °C. *See spectra on pages 93 and 94 of Appendix A — SPECTRA.*

4.4 Crystal and molecular structures of two copper(II) complexes

4.4.1 Techniques for growing quality crystals

There are myriad techniques for growing crystals for X-ray diffraction analyses. It is vital, however, that time and effort be spent in growing high-quality crystals to ensure that accurate molecular determinations can be made. The following crystallisation techniques were implemented during this study:

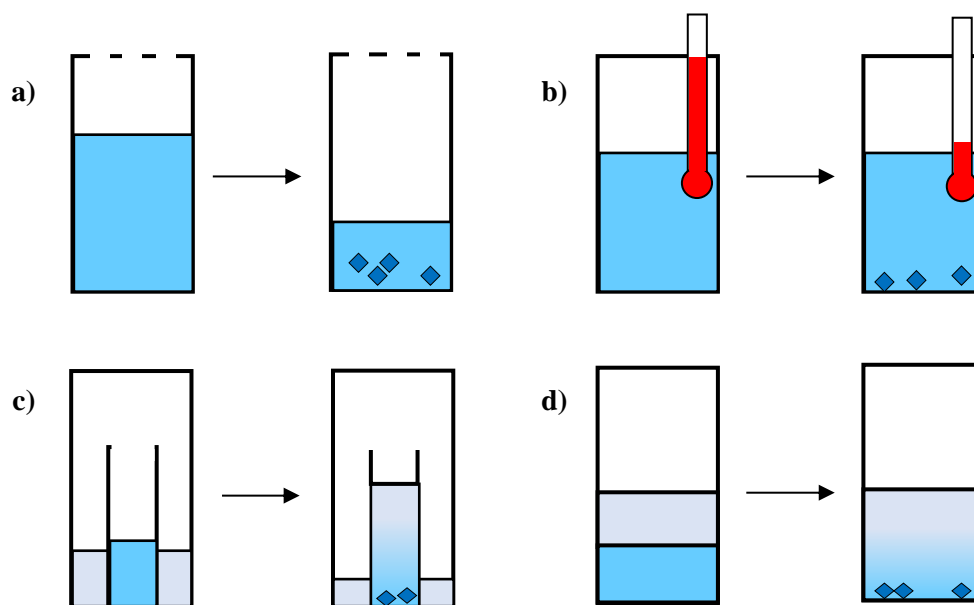


Figure 4.1: Schematic diagram representing various crystal growth techniques: **a)** slow evaporation, **b)** slow cooling, **c)** vapour diffusion and **d)** liquid-liquid diffusion.

4.4.1.1 Slow evaporation method

This crystal growing method is probably the simplest to execute, yet often the most time-consuming depending on the solvent used (**Figure 4.1a**). A near-saturated solution of the applicable compound in a suitable solvent is placed into a clean container with a large surface area. The container can be covered in aluminium foil or parafilm and punched with tiny holes to allow the solvent to evaporate gradually over a few days. Set the container to one side and prevent stirring or swirling the solution. On the downside, this method might require large amounts of material to ensure the solution is near its saturation point.

4.4.1.2 Slow cooling method

A near-saturated solution of the compound should be prepared at the boiling point of the solvent. The hot solution is subsequently transferred to a clean container and allowed to cool to room temperature (**Figure 4.1b**). Alternatively, a near-saturated solution can be prepared at room temperature and placed in a fridge or freezer to encourage slow crystal growth.

4.4.1.3 Vapour diffusion method

This method requires a dual solvent system that mixes well (**Figure 4.1c**). The compound should ideally be highly soluble in the solvent with the highest boiling point and nearly insoluble in the solvent with the lower boiling point. A solution of the compound is prepared in a small open-top container and placed in a slightly larger container containing the low boiling solvent. The outer container must be tightly sealed to avoid solvent vapour from escaping. Over time, the low boiling solvent will vaporise and diffuse into the higher boiling solvent, leading to oversaturation, nucleation and crystallisation. If need be, the speed of vaporisation can be regulated by adjusting the temperature.

4.4.1.4 Liquid-liquid diffusion method

As with the vapour diffusion method, this method also requires a dual solvent system (**Figure 4.1d**). In this case, the solvent boiling points do not really matter, but their respective densities do. A saturated solution of the compound is prepared and the solvent with the highest specific density is placed in a small container, such as a glass vial. Use a syringe and hypodermic needle to layer the remaining liquid in the vial. Over time, the liquids will gradually mix and yield crystals. A variation to this method is to freeze the lower layer before adding the remaining liquid. This will ensure distinct separation, while the lower frozen layer gently thaws.

4.4.2 Instrumentation and determination of crystal structures

4.4.2.1 Analysis of the $[\text{Cu}(\text{L}2)_2](\text{NO}_3)_2$ complex

A suitable crystal was mounted on a thin glass fiber, while data was collected using a *Bruker APEX II Duo CCD* diffractometer with graphite monochromated $\text{Mo-K}\alpha$ radiation ($\lambda = 0.71073 \text{ \AA}$). Data reduction was performed using *SAINTE V8.38A*.⁶ A cryostat: *Oxford Cryogenics (700 Series Cryostream Plus)* was used to cool the crystal to 100 K. Empirical corrections were performed with *SADABS-2016/2*.⁷ The structure was solved by direct methods, while the remainder of the atomic positions were found using difference Fourier methods. All non-hydrogen atoms were refined anisotropically (with appropriate restraints using *SIMU* and *ISOR*) by blocked full-matrix least squares calculations on F^2 using *SHELXL-2018/3* within the *X-Seed* environment.⁸⁻¹⁰ Hydrogen atoms were added to the structure model on calculated positions and were refined as rigid atoms. *Mercury 2020.1* for Windows was used to generate figures.

4.4.2.2 Analysis of the $[\text{Cu}(\text{H}_2\text{O})_2(\text{L}2)]\text{SO}_4$ complex

A suitable crystal was mounted on a thin glass fiber, while data was collected using a *SuperNova, Dual, Cu at zero, Atlas S2* diffractometer with mirror monochromated $\text{Cu-K}\alpha$ radiation ($\lambda = 1.54184 \text{ \AA}$). Data reduction and empirical corrections were performed using *CrysAlisPro 1.171.38.41*.¹¹ A cryostat: *Oxford Cryogenics (700 Series Cryostream Plus)* was used to cool the crystal to 100 K. The structure was solved by direct

methods, while the remainder of the atomic positions were found using difference Fourier methods. All non-hydrogen atoms were refined anisotropically by blocked full-matrix least squares calculations on F^2 using *SHELXL-2018/3* within the *Olex2 1.3* environment.^{8,12} Hydrogen atoms were added to the structure model on calculated positions and were refined as rigid atoms. *Mercury 2020.1* for *Windows* was used to generate figures.

4.4.3 Preparation of the crystalline [Cu(L2)₂](NO₃)₂ complex

A mixture of Cu(NO₃)₂·3H₂O (135 mg, 0.559 mmol) and 2,6-bis(5-ethyl-1*H*-pyrazol-3-yl)pyridine (**2**) (150 mg, 0.561 mmol) in absolute ethanol (5.00 mL) was refluxed for 2 hours. After the resulting bottle green solution was allowed to cool to room temperature it was filtered to remove specks of black impurities. The solution was reduced to ~2 mL *in vacuo*, transferred to a clean glass vial and loosely fitted with a plastic stopper. The container was placed in a locker, allowing the solvent to evaporate over a period of 3 days under ambient conditions, whereafter bright green crystal shards had formed. **IR (KBr, cm⁻¹)** 3170 (N–H str), 3069 (aromatic C–H str), 2972/2936 (aliphatic C–H str), 1615 (pyridine C=N str), 1576 (pyrazole C=N str), 1375 (–CH₃ bend). **ESI-MS (*m/z*)** 268.16 (C₁₅H₁₇N₅ + H)⁺, 298.61 [Cu(C₁₅H₁₇N₅)₂]²⁺, 375.08 [Cu(C₂H₅O)(C₁₅H₁₇N₅)]⁺, 596.22 [Cu(C₁₅H₁₆N₅)₂ + H]⁺. **m.p.** 240–241 °C. *See full range of spectra on pages 95 and 96 of Appendix A — SPECTRA.*

4.4.4 Preparation of the crystalline [Cu(H₂O)₂(L2)]SO₄ complex

A 25 mL round-bottom flask was charged with CuSO₄·5H₂O (95.0 mg, 0.380 mmol) and 2,6-bis(5-ethyl-1*H*-pyrazol-3-yl)pyridine (**2**) (100 mg, 0.374 mmol) in absolute ethanol (5.00 mL). This mixture was stirred under refluxing conditions for 3 hours, followed by filtration to remove all unreacted solid material and impurities. The solvent of the green filtrate was removed under reduced pressure to yield a dark green solid. The crude solid material was washed with cold diethyl ether over a filtration system, yielding a light green solid material. Approximately 30 mg of this product was transferred to a clean glass vial and redissolved in methanol. Crystals were grown via the vapour diffusion method with diethyl ether as the external high-vaporising solvent. After 5 days, cubic colourless crystals were observed on the side walls of the internal vial. **IR (KBr, cm⁻¹)** 3069 (aromatic C–H str), 2973/2938 (aliphatic C–H str), 1613 (pyridine C=N str), 1575 (pyrazole C=N str), 1468 (–CH₂– bend). **ESI-MS (*m/z*)** 268.16 (C₁₅H₁₇N₅ + H)⁺, 298.61 [Cu(C₁₅H₁₇N₅)₂]²⁺, 330.08 [Cu(C₁₅H₁₆N₅) + H]⁺, 375.08 [Cu(C₂H₅O)(C₁₅H₁₇N₅)]⁺, 596.22 [Cu(C₁₅H₁₆N₅)₂ + H]⁺. **m.p.** 278–279 °C. *See full range of spectra on pages 97 and 98 of Appendix A — SPECTRA.*

4.5 Results and discussion

Crystal and molecular structure analyses provide valuable information regarding the interaction of tridentate aromatic *N*-donor ligands with base metal ions. In total, eight various base metal complexes, with either ligands **2** (ethyl) or **9** (*tert*-butyl), were prepared in an attempt to grow quality single crystals for X-ray diffraction analyses (**Section 4.3.1.1–4.3.1.8**). Unfortunately, none of these yielded satisfactory results. In their powdered form, however, they still provided some insight regarding the ligand-to-metal (L:M²⁺) stoichiometry. All of these examples, as revealed through MS analyses, showed the presence of numerous L:M²⁺

stoichiometries. The 2:1 (L:M²⁺) complexes, in addition to its doubly charged fragments, were the easiest to identify, followed by the 1:1 (L:M²⁺) complexes. Upon closer investigation, many other metal species were also detected. These typically include 1:1 complexes with various combinations of solvent and/or anions that occupy the remaining coordination sites. On occasion, 2:1 complexes were also encountered with solvent molecules present in the outer coordination sphere. In other instances, anion-bridged complexes were also identified, making it near impossible to pinpoint the predominant complex species. For this reason, EA analysis was not deemed a sensible characterisation technique since the bulk of the samples was not a single complex species, but rather multiple complex species.

Following this, two crystals suitable for X-ray diffraction were grown by means of the slow evaporation and vapour diffusion methods. Various ligand (**1–12**) and base metal ion (Co²⁺, Ni²⁺, Cu²⁺, Zn²⁺, Cd²⁺ and Pb²⁺) complexes were synthesised in an attempt to grow quality crystals, but all attempts were futile. It was always going to be difficult to grow crystals with ligands that have extended *n*-alkyl arms (ligands **5–8** and **12**) due to inefficient packing and considerable disorder. Eventually, two quality crystals were grown after reacting 2,6-bis(5-ethyl-1*H*-pyrazol-3-yl)pyridine (**2**) with hydrated Cu(NO₃)₂ and CuSO₄, respectively.

The IR spectra of both the bis[2,6-bis(5-ethyl-1*H*-pyrazol-3-yl)pyridine]copper(II) nitrate and diaqua[2,6-bis(5-ethyl-1*H*-pyrazol-3-yl)pyridine]copper(II) sulfate complexes clearly show shifts in the pyridyl- and pyrazolyl N–H stretching frequencies to higher wavenumbers. This is a powerful tool that indicates successful coordination.

4.5.1 Crystal and molecular structure of the [Cu(L2)₂](NO₃)₂ complex

The asymmetric unit cell contains one quarter of the [Cu(L2)₂](NO₃)₂ complex (**Figure 4.2**). The complex crystallised in the tetragonal crystal system, space group P $\bar{4}$. Crystallographic data and structure refinement details are summarised in **Table 4.3**.

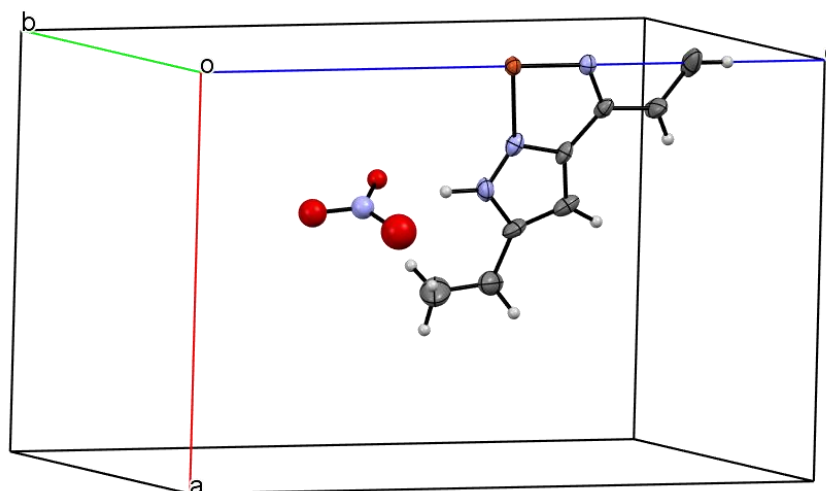


Figure 4.2: Asymmetric unit cell diagram of the [Cu(L2)₂](NO₃)₂ complex (50% thermal ellipsoids).

The ORTEP diagram of one full complexing unit is shown in **Figure 4.3**, indicating an octahedral geometry as one would expect with two coordinating tridentate aromatic *N*-donor ligands. The dimeridionally organised structure ensures the ethyl pendant arms are optimally distanced from one another in order to occupy coordination sites in the most energetically favoured configuration.

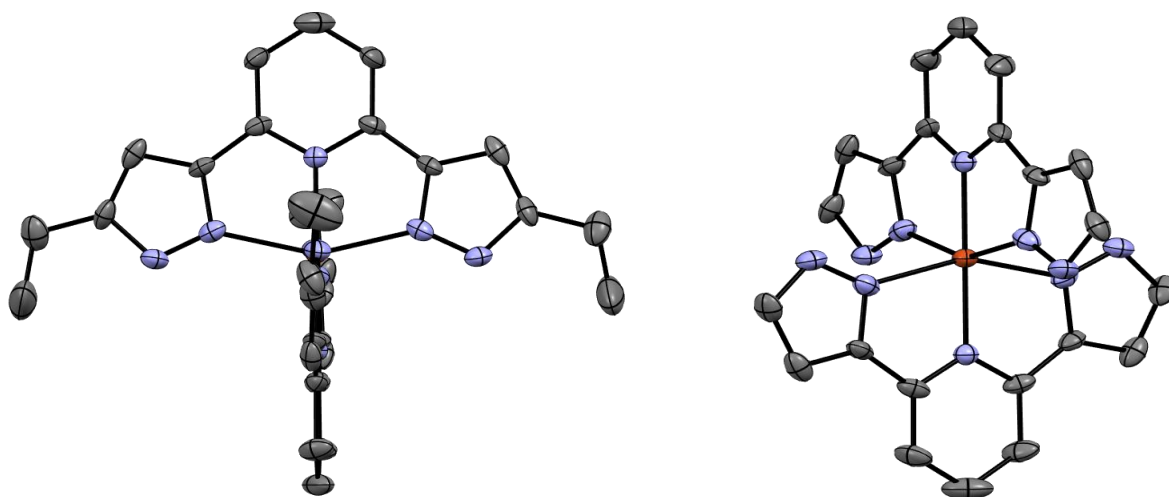


Figure 4.3: ORTEP diagrams of the full $[\text{Cu}(\text{L}2)_2](\text{NO}_3)_2$ complexing unit. (50% thermal ellipsoids). NO_3^- counter ion and H-atoms omitted for clarity, while ethyl-tethered arms are omitted in right-hand example as well.

Figure 4.4 shows the $[\text{Cu}(\text{L}2)_2](\text{NO}_3)_2$ complex with appropriate atom numbering and reveals extended equatorial coordination bonds from Cu1 to N1/3/4/6 at 2.191(6) Å. The axial Cu1–N2 and Cu1–N5 bonds are somewhat shorter [1.987(7) Å] than the equatorial bonds and reveal slight Jahn-Teller contraction (**Table 4.2**). The axial N2–Cu1–N5 bond angle is 180.0(2)°, while the N1–Cu1–N4 and N3–Cu1–N6 bond angles are less ideal at 155.0(3)°. This is due to the internal equatorial N–Cu–N bond angles being fixed at 92.69(7)°, instead of exactly 90°. Moreover, these equatorial *N*-donor atoms do not sit perfectly in plane, thereby significantly contributing to the overall distorted octahedral geometry.

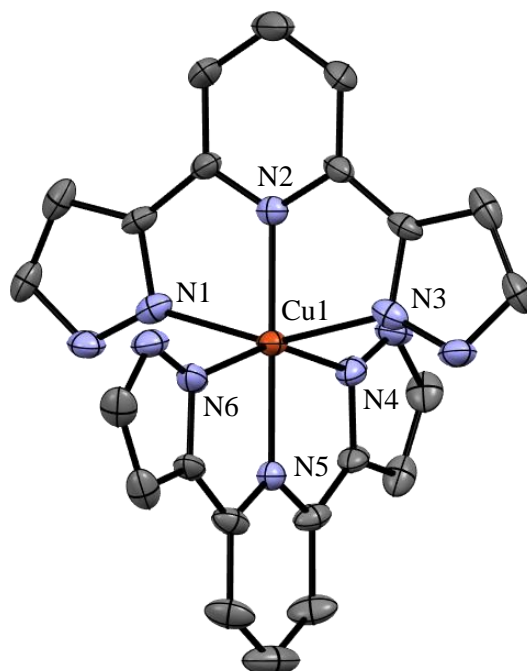


Figure 4.4: ORTEP diagram with selected labels of the $[\text{Cu}(\text{L}2)_2](\text{NO}_3)_2$ complex (50% thermal ellipsoids). H-atoms and ethyl-tethered arms omitted for clarity.

Table 4.2: Selected bond lengths and angles of the $[\text{Cu}(\text{L}2)_2](\text{NO}_3)_2$ complex.

Bond lengths (Å)		Bond angles (°)	
Cu1–N1	2.191(6)	N1–Cu1–N2	77.49(16)
Cu1–N2	1.987(7)	N1–Cu1–N3	155.0(3)
Cu1–N3	2.191(6)	N1–Cu1–N4	92.69(7)
Cu1–N4	2.191(6)	N1–Cu1–N5	102.51(16)
Cu1–N5	1.987(7)	N1–Cu1–N6	92.69(7)
Cu1–N6	2.191(6)	N2–Cu1–N3	77.49(16)
		N2–Cu1–N4	102.51(16)
		N2–Cu1–N5	180.0(2)
		N2–Cu1–N6	102.51(16)
		N3–Cu1–N4	92.69(7)
		N3–Cu1–N5	102.51(16)
		N3–Cu1–N6	92.69(7)
		N4–Cu1–N5	77.49(16)
		N4–Cu1–N6	155.0(3)
		N5–Cu1–N6	77.49(16)

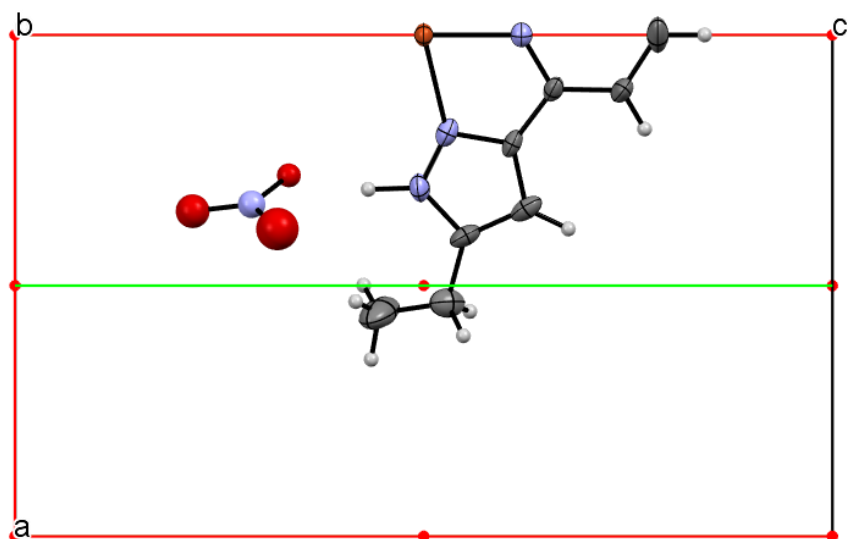


Figure 4.5: Symmetry elements present in an asymmetric unit cell of the $[\text{Cu}(\text{L}2)_2](\text{NO}_3)_2$ complex along the b-axis (50% thermal ellipsoids). [Complementary to **Table 4.3**]

Table 4.3: Symmetry elements and operators of the crystalline $[\text{Cu}(\text{L}2)_2](\text{NO}_3)_2$ complex. [Complementary to **Figure 4.5**]

#	Colour	Symmetry operation	Description	Order	Type
1	–	x, y, z	Identity	1	1
2	Red	$y, -x, -z$	Rotoinversion axis (4-fold)	4	-4
3	Green	$-x, -y, z$	Rotation axis (2-fold)	2	2
4	Red	$-y, x, -z$	Rotoinversion axis (4-fold)	4	-4

From **Figure 4.6**, it is clear that H-bonding is an integral part of the stabilisation of this copper(II) complex assembly, as purported throughout **CHAPTER 3**. These pyrazolyl N–H moieties are significant inclusions in tridentate extractants and largely explains the discrepancy in the pyrazole- (**1–10**) and imidazole-pyridinyl ligands' (**11** and **12**) extraction power.

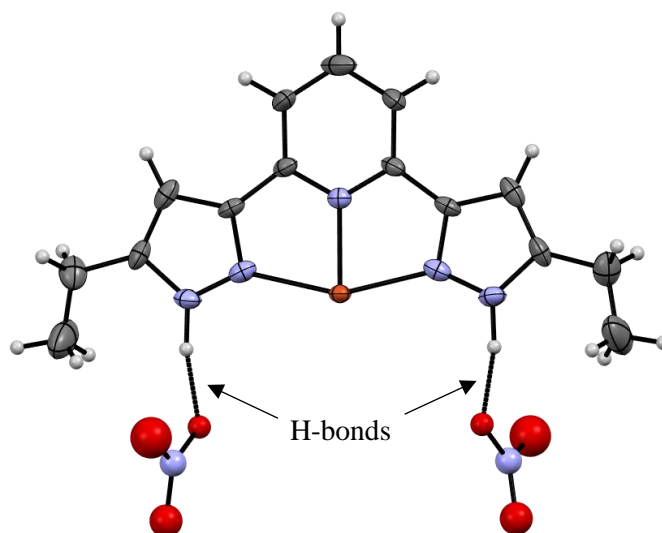


Figure 4.6: ORTEP diagram of the $[\text{Cu}(\text{L2})_2](\text{NO}_3)_2$ complex revealing H-bonding from pyrazolyl NH atoms to neighbouring NO_3^- ions (50% thermal ellipsoids). Only half the complex shown.

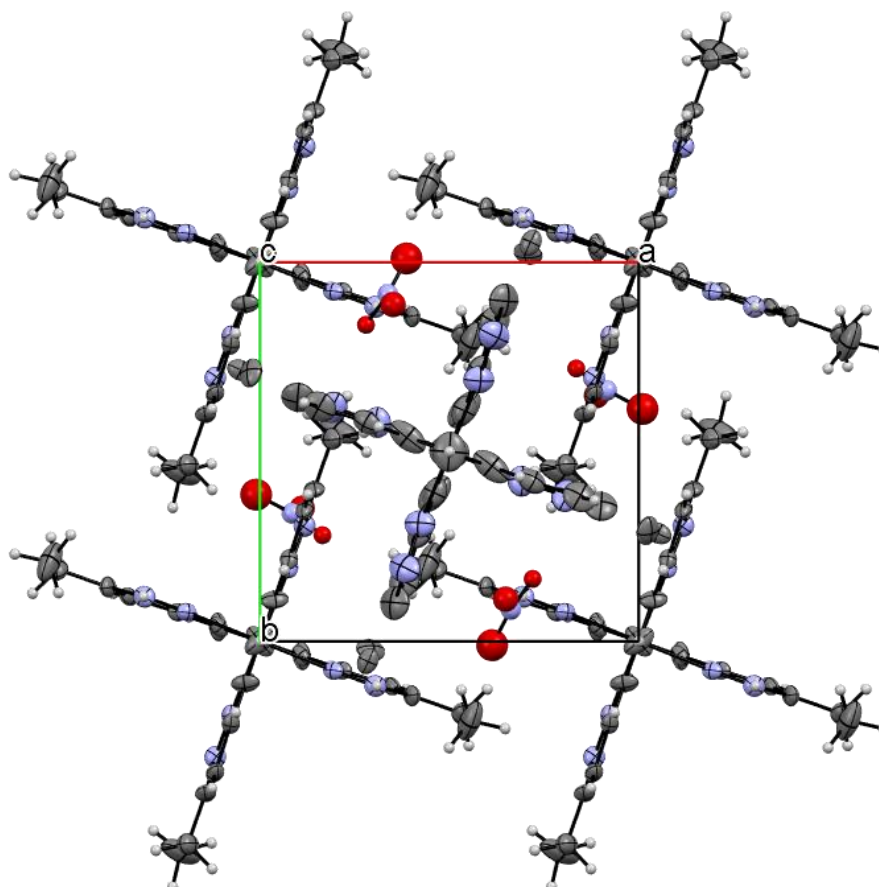


Figure 4.7: Packing diagram of the $[\text{Cu}(\text{L2})_2](\text{NO}_3)_2$ complex along the c -axis (50% thermal ellipsoids).

Table 4.4: Crystallographic data and structure refinement of the [Cu(L2)₂](NO₃)₂ complex.

Compound	[Cu(C ₁₅ H ₁₇ N ₅) ₂](NO ₃) ₂
Empirical formula	C ₁₅ H ₁₆ Cu _{0.5} N _{6.5} O _{4.5}
M _r (g.mol ⁻¹)	391.42
Temperature (K)	100(2)
Instrument	<i>Bruker APEX II DUO CCD</i>
Crystal habit	Shard
Crystal dimensions (mm)	0.287 × 0.179 × 0.114
Crystal system	Tetragonal
Space group (number)	P $\bar{4}$
a (Å)	10.2009(12)
b (Å)	10.2009(12)
c (Å)	16.609(2)
α (°)	90
β (°)	90
γ (°)	90
μ (MoKα) (mm ⁻¹)	0.705
V (Å ³)	1728.3(5)
Z, D _c (M, g.m ⁻³)	4, 1.504
Index ranges	-13 ≤ h ≤ 13, -13 ≤ k ≤ 13, -21 ≤ l ≤ 21
Reflections collected	19363
Independent reflections	6757
Absorption correction	Multi-scan
Refinement method	Full matrix least squares on F ²
Data/restraints/parameters	3975/19/267
F(000)	809
R (reflections) R1, wR2	0.0704, 0.1892
Goodness of fit on F ²	1.049

4.5.2 Crystal and molecular structure of the [Cu(H₂O)₂(L2)]SO₄ complex

The asymmetric unit cell contains a complete complex assembly, with 2,6-bis(5-ethyl-1*H*-pyrazol-3-yl)pyridine (**2**), two coordinated H₂O molecules and one uncoordinated SO₄²⁻ counter ion (**Figure 4.8**). The system crystallised in the triclinic crystal system, space group P $\bar{1}$. Complete crystallographic data and structure refinement details are summarised in **Table 4.7**.

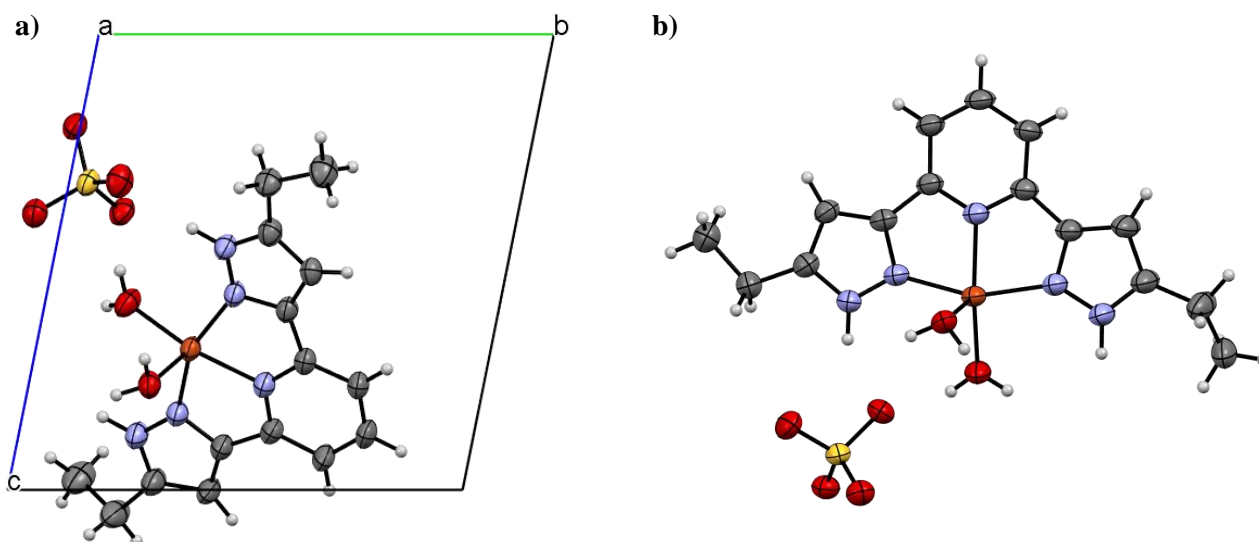


Figure 4.8: The **a)** asymmetric unit cell diagram along the *a*-axis and the **b)** full representation of the $[\text{Cu}(\text{H}_2\text{O})_2(\text{L}2)]\text{SO}_4$ complex (50% thermal ellipsoids).

The molecular structure of the $[\text{Cu}(\text{H}_2\text{O})_2(\text{L}2)]\text{SO}_4$ complex with appropriate atom numbering is shown in **Figure 4.9**, with selected bond lengths and angles listed in **Table 4.5**. According to Miessler and Tarr,¹³ very little energy is needed to convert between trigonal bipyramidal and square pyramidal geometries, which often leads to incorrect geometry assignments of 5-coordinate complexes. Trigonal bipyramidal complexes can also undergo Berry pseudorotation, whereby axial monodentate ligands rotate toward the equatorial positions and two equatorial monodentate ligands rotate toward the axial positions.¹⁴ Conventional NMR studies cannot distinguish between the axial and equatorial ligands due to rapid pseudorotations, thereby rendering the ligands chemically equivalent. Therefore, low-temperature NMR studies are required to slow down the rate of pseudorotation, whereafter distinct axial and equatorial signals appear. In this study, however, rapid pseudorotation was restricted due to the presence of a tridentate aromatic amine ligand. To determine whether a complex is either trigonal bipyramidal or square pyramidal, one must evaluate the geometric parameter, tau (τ), which is calculated as follows:¹⁵

$$\tau = (\beta - \alpha) / 60 \quad (58)$$

where β is the largest angle ($^\circ$) between any of the five ligand coordinates and α is the second largest angle ($^\circ$). When $\tau = 1$, an ideal trigonal bipyramidal geometry is implied, while $\tau = 0$ implies an ideal square pyramidal structure. In the case of $0 < \tau < 0.5$, a pseudo square pyramidal is implied, while $0.5 < \tau < 1$ signifies a pseudo trigonal bipyramidal geometry.¹⁵ In this study, τ was found to be:

$$\tau = (163.64 - 157.08) / 60 \approx 0.109 \quad (59)$$

This τ -value suggests the $[\text{Cu}(\text{H}_2\text{O})_2(\text{L}2)]\text{SO}_4$ complex possesses ample square pyramidal character. One of the characteristic features is the elongated Cu1–O2 bond of 2.205(3) Å, which is significantly longer than any of the remaining bonds due to Jahn-Teller elongation. The O2 atom evidently occupies the sole axial position,

while the remaining O1 atom and three *N*-donor atoms occupy the equatorial positions, forming the base of the pyramidal structure.

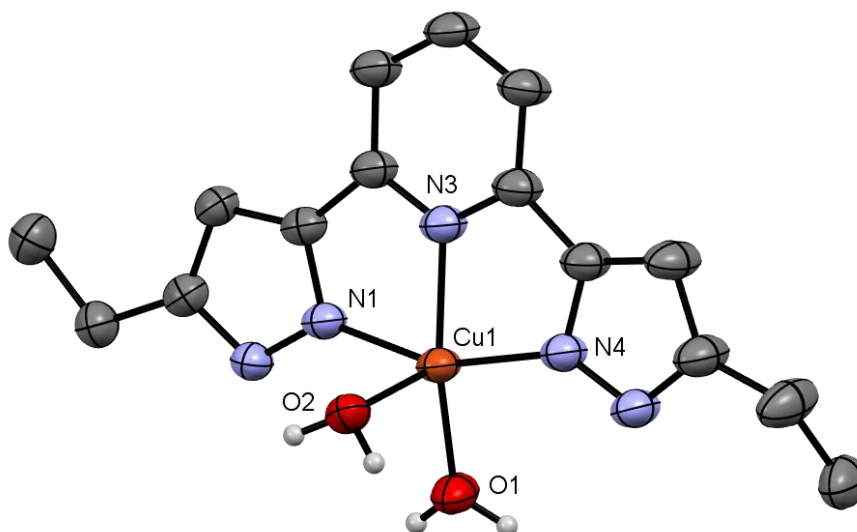


Figure 4.9: ORTEP diagram with selected labels of the $[\text{Cu}(\text{H}_2\text{O})_2(\text{L}2)]\text{SO}_4$ complex (50% thermal ellipsoids). Selected H-atoms and SO_4^{2-} counter ion omitted for clarity.

Table 4.5: Selected bond lengths and angles of the $[\text{Cu}(\text{H}_2\text{O})_2(\text{L}2)]\text{SO}_4$ complex.

Bond lengths (Å)		Bond angles (°)	
Cu1–N1	2.009(4)	N1–Cu1–N3	78.45(15)
Cu1–N3	1.969(3)	N1–Cu1–N4	157.08(14)
Cu1–N4	2.015(4)	N1–Cu1–O1	100.01(14)
Cu1–O1	1.928(3)	N1–Cu1–O2	92.99(14)
Cu1–O2	2.205(3)	N3–Cu1–N4	79.40(15)
		N3–Cu1–O1	163.64(17)
		N3–Cu1–O2	102.35(14)
		N4–Cu1–O1	99.57(14)
		N4–Cu1–O2	97.41(14)
		O1–Cu1–O2	93.99(15)

Once again, H-bonds appear to be vital components that stabilises this copper(II) complex through the N–H moieties of the aromatic tridentate ligand (**2**). However, two SO_4^{2-} ions facilitate this stabilisation not only through the N–H moieties, but through one coordinated H_2O molecule as well (**Figure 4.11**).

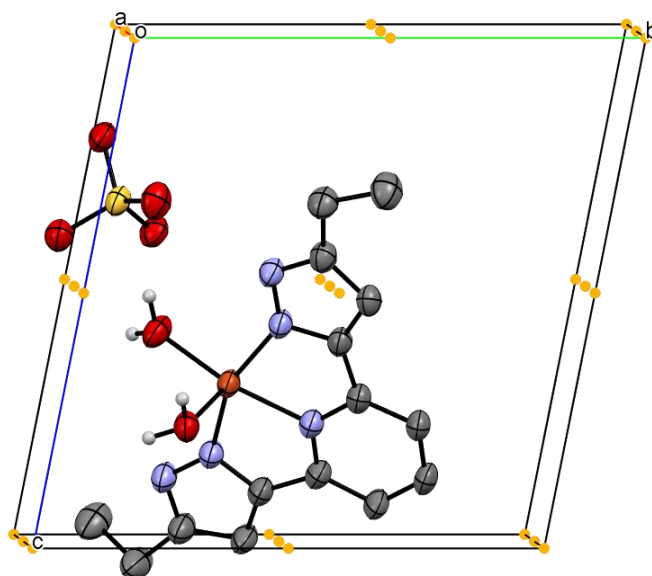


Figure 4.10: Symmetry elements present in an asymmetric unit cell of the $[\text{Cu}(\text{H}_2\text{O})_2(\text{L}2)]\text{SO}_4$ complex along the a^* -axis (50% thermal ellipsoids). [Complementary to **Table 4.6**]

Table 4.6: Symmetry elements and operators of the crystalline $[\text{Cu}(\text{H}_2\text{O})_2(\text{L}2)]\text{SO}_4$ complex. [Complementary to **Figure 4.10**]

#	Colour	Symmetry operation	Description	Order	Type
1	–	x, y, z	Identity	1	1
2	Yellow	$-x, -y, -z$	Inversion centre	2	-1

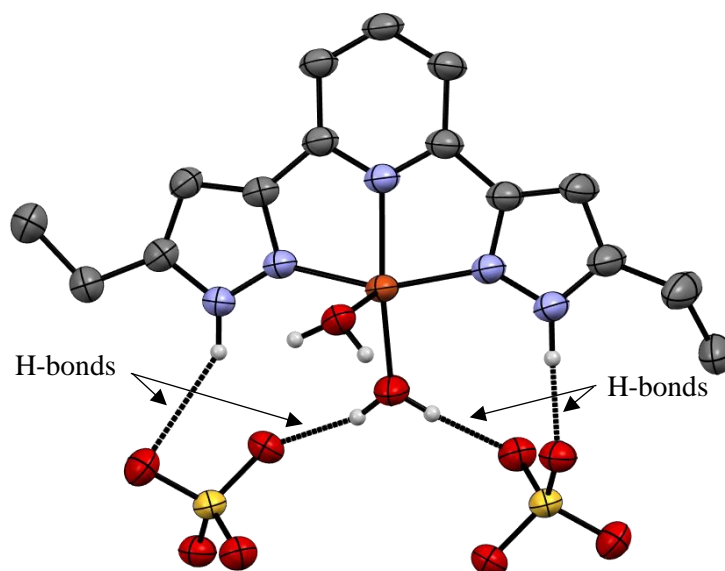


Figure 4.11: ORTEP diagram of the $[\text{Cu}(\text{H}_2\text{O})_2(\text{L}2)]\text{SO}_4$ complex revealing H-bonding from pyrazolyl NH atoms and coordinated H_2O molecules to neighbouring SO_4^{2-} counter ions (50% thermal ellipsoids). Selected H-atoms omitted for clarity.

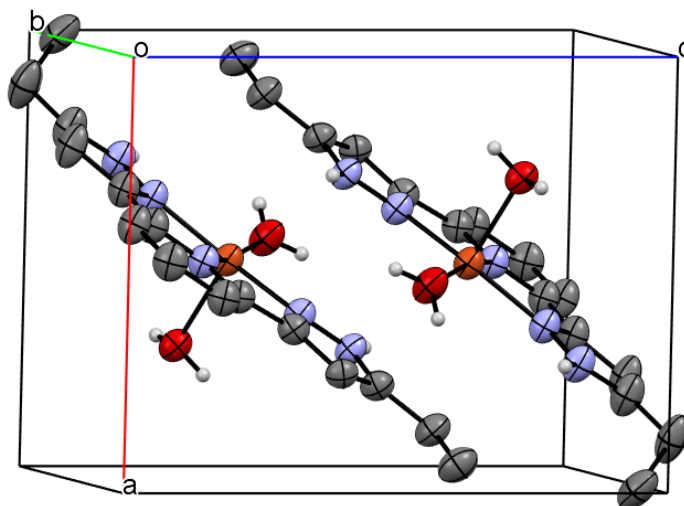


Figure 4.12: Packing diagram of the $[\text{Cu}(\text{H}_2\text{O})_2(\text{L}2)]\text{SO}_4$ complex along the b^* -axis (50% thermal ellipsoids). Selected H-atoms and SO_4^{2-} counter ion omitted for the sake of clarity.

Table 4.7: Crystallographic data and structure refinement of the $[\text{Cu}(\text{H}_2\text{O})_2(\text{L}2)]\text{SO}_4$ complex.

Compound	$[\text{Cu}(\text{H}_2\text{O})_2(\text{C}_{15}\text{H}_{17}\text{N}_5)]\text{SO}_4$
Empirical formula	$\text{C}_{15}\text{H}_{21}\text{CuN}_5\text{O}_2, \text{O}_4\text{S}, 3\text{H}_2\text{O}$
M_r ($\text{g}\cdot\text{mol}^{-1}$)	517.01
Temperature (K)	100.01(10)
Instrument	<i>SuperNova, Dual, Cu at zero, AtlasS2</i>
Crystal habit	Block
Crystal dimensions (mm)	$0.164 \times 0.102 \times 0.065$
Crystal system	Triclinic
Space group (number)	$P\bar{1}$
a (\AA)	8.9349(12)
b (\AA)	10.9312(9)
c (\AA)	11.1415(11)
α ($^\circ$)	101.265(8)
β ($^\circ$)	91.346(10)
γ ($^\circ$)	92.643(8)
μ ($\text{CuK}\alpha$) (mm^{-1})	2.892
V (\AA^3)	1065.5(2)
Z, D_c ($M, \text{g}\cdot\text{m}^{-3}$)	2, 1.612
Index ranges	$-11 \leq h \leq 11, -13 \leq k \leq 10, -11 \leq l \leq 14$
Reflections collected	9464
Independent reflections	4396

Table continues...

Compound	[Cu(H ₂ O) ₂ (C ₁₅ H ₁₇ N ₅)]SO ₄
Absorption correction	Gaussian
Refinement method	Full matrix least squares on F^2
Data/restraints/parameters	4396/7/319
F(000)	538
R (reflections) R1, wR2	0.0642, 0.1902
Goodness of fit on F^2	1.060

4.6 Concluding remarks and making sense of seemingly contradictory results

It is quite obvious that the [Cu(L2)₂](NO₃)₂ complex in **Section 4.3.1** and the [Cu(H₂O)₂(L2)]SO₄ complex in **Section 4.3.2** reveal very different ligand-to-metal (L:M²⁺) ratios. This is significant since this study focuses on base metal solvent extraction systems and the ratio at which these ligands are required to effectively transport one metal ion across the aqueous/organic phase interface. Both the Job plot studies and slope analyses, as reported in **CHAPTER 3**, seemed to suggest that copper(II) is primarily coordinated by one tridentate pyrazolyl ligand in solution. This aligns well with the [Cu(H₂O)₂(L2)]SO₄ complex, but not necessarily with the [Cu(L2)₂](NO₃)₂ complex or any of the eight complexes described in **Sections 4.3.1.1–4.3.1.8**. The fact that the aforementioned solution-based studies are exactly that—solution-based—must carry more gravitas than solid state studies, since solvent extraction systems are naturally the distribution of metal ions between two immiscible liquids. As alluded to in the introduction of this chapter, solid state studies must be understood in light of solution-based studies and comprehensive computational modelling. Only then clear and comprehensive conclusions can be drawn. Unfortunately, throughout this dissertation computational studies were not performed, but should undoubtedly be considered in future studies.

With that being said, three distinct theoretical conjectures are put forth with regards to the “solution vs. solid state” debate in the solvent extraction community:

- (1) *Packing of NO₃⁻ vs. SO₄²⁻ counterions:* NO₃⁻ is a slightly smaller anion with lower charge and could force the 2:1 (L:Cu²⁺) stoichiometry, while the SO₄²⁻ anionic species produces the 1:1 (L:Cu²⁺) stoichiometry.
- (2) *Presence of both 1:1 and 2:1 (L:Cu²⁺) stoichiometries:* In solution, both stoichiometries are present and by happenstance the 2:1 crystal was picked for single crystal X-ray diffraction analysis. This viewpoint seems to be supported by MS results in **Sections 4.3.1.1–4.3.1.8**.
- (3) *Solution vs. solid state thermodynamics:* The thermodynamics of the 1:1 and 2:1 (L:Cu²⁺) complexes might be vastly different in solution compared to the solid state. The 2:1 complex might be occupying lower energy states once it crystallises, while the 1:1 complex maintains its higher overall energy, making crystallisation of this complex less favourable.

4.7 References

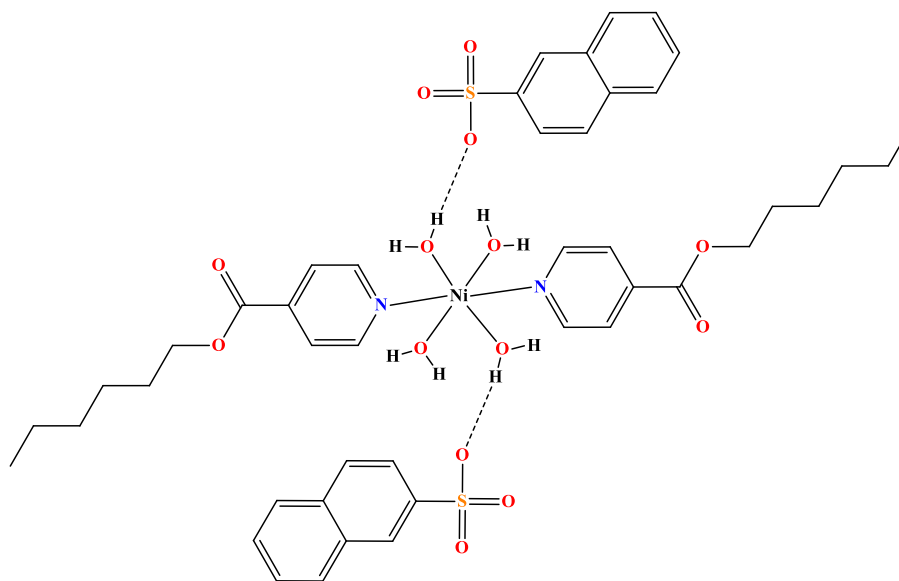
- (1) Schmidt, G. Photodimerization in the solid state. *Pure Appl. Chem.* **1971**, *27* (4), 647–678.
- (2) Desiraju, G. *Crystal engineering: The design of organic solids*; Elsevier: Amsterdam, 1989, pp 312.
- (3) Wang, Q.; Yan, S.; Liao, D.; Jiang, Z.; Cheng, P.; Leng, X.; Wang, H. A novel three-dimensional cobalt(III) complex via hydrogen bonds: [Co(tacn)₂](ClO₄)₃ (tacn = 1,4,7-triazacyclononane). *J. Mol. Struct.* **2002**, *608* (1), 49–53.
- (4) Sumani, J. Synthesis and characterisation of macrocyclic ligands with hydroxyalkyl and thiol pendant arms tethered on 1,5,9-triazacyclododecane and their complex formation chemistry, Stellenbosch University (MSc thesis), Stellenbosch, South Africa, 2010.
- (5) Jahn, H.; Teller, E. Stability of polyatomic molecules in degenerate electronic states. I. Orbital degeneracy. *Proc. R. Soc. London. Ser. A - Math. Phys. Sci.* **1937**, *161* (905), 220–235.
- (6) SAINT V8.38A. Bruker AXS Inc.: Madison (WI), USA 2018.
- (7) Krause, L.; Herbst-Irmer, R.; Sheldrick, G.; Stalke, D. Comparison of silver and molybdenum microfocus X-ray sources for single-crystal structure determination. *J. Appl. Crystallogr.* **2015**, *48*, 3.
- (8) Sheldrick, G. Crystal structure refinement with *SHELXL*. *Acta Crystallogr. Sect. C* **2015**, *71* (1), 3–8.
- (9) Barbour, L. X-Seed — A software tool for supramolecular crystallography. *J. Supramol. Chem.* **2001**, *1* (4), 189–191.
- (10) Atwood, J.; Barbour, L. Molecular graphics: From science to art. *Cryst. Growth Des.* **2003**, *3* (1), 3–8.
- (11) Rigaku Oxford Diffraction, *CrysAlisPro* software V1.171.38.41, Rigaku Corporation: Oxford, UK 2015.
- (12) Dolomanov, O.; Bourhis, L.; Gildea, R.; Howard, J.; Puschmann, H. *OLEX2*: A complete structure solution, refinement and analysis program. *J. Appl. Crystallogr.* **2009**, *42* (2), 339–341.
- (13) Miessler, G.; Tarr, D. *Inorganic Chemistry*, 4th Edition; Pearson Prentice Hall, Upper Saddle River, NJ, USA; Boston; London, 2011.
- (14) Berry, R. Correlation of rates of intramolecular tunneling processes, with application to some group V compounds. *J. Chem. Phys.* **1960**, *32* (3), 933–938.
- (15) Addison, A.; Rao, T.; Reedijk, J.; van Rijn, J.; Verschoor, G. Synthesis, structure, and spectroscopic properties of copper(II) compounds containing nitrogen–sulphur donor ligands; the crystal and molecular structure of aqua[1,7-bis(*N*-methylbenzimidazol-2'-yl)-2,6-dithiaheptane]copper(II) perchlorate. *J. Chem. Soc. Dalton Trans.* **1984**, No. 7, 1349–1356.

CHAPTER 5

**EXTRACTION OF NICKEL(II) BY MEANS OF AROMATIC
OXIMES AND BIDENTATE PYRAZOLYL LIGANDS IN
THE PRESENCE OF SULFONIC-, CARBOXYLIC-
AND PHOSPHINIC ACID SYNERGISTS**

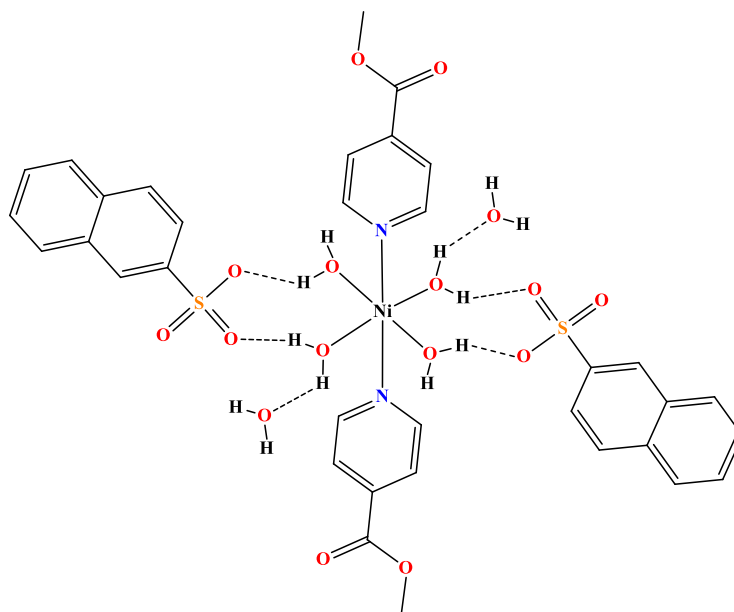
5.1 Introduction

There are only a handful of examples in the literature of synergistic sulfonic acid-nickel(II) mechanisms.¹⁻³ These publications derived their mechanisms either by means of X-ray crystallography, FT-IR or ESI-MS. Li *et al.*² demonstrated the coordination of two hexyl isonicotinate molecules and four water molecules in a distorted octahedral fashion. Two additional naphthalenesulfonic acid molecules on the periphery (outer coordination sphere) of the complex stabilised the assembly via hydrogen bonds to the coordinated water molecules (**Scheme 5.1**).



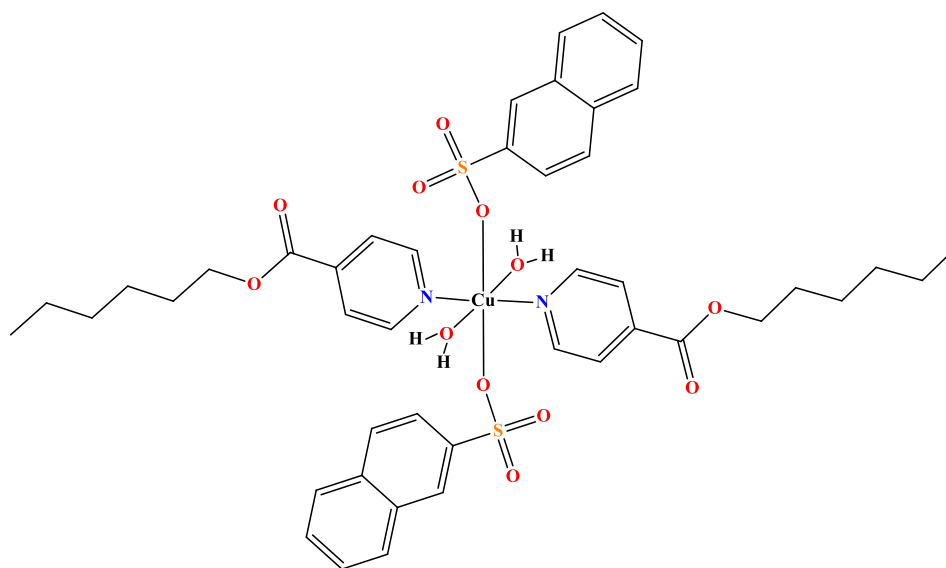
Scheme 5.1: Nickel synergist complex with two naphthalenesulfonic acid molecules providing stabilisation via hydrogen bonds. [Adapted from Li *et al.*²]

Another similar case was reported by Zhu *et al.*,¹ where these co-workers successfully grew a crystal of their nickel synergist complex (**Scheme 5.2**). They too reported the use of naphthalenesulfonic acid (model synergist) and an abbreviated isonicotinate molecule in their attempt to determine the role of the sulfonic acid synergist. This article was later followed by a related article by Hu *et al.*,³ revealing much the same result by implementing naphthalenedisulfonic acid as synergist.



Scheme 5.2: Nickel synergist complex with two naphthalenesulfonic acid molecules and two water molecules providing ample stabilisation through hydrogen bonds. [Adapted from Zhu *et al.*¹]

In 2017, Hu and co-workers⁴ published yet another interesting paper, in which they demonstrated via X-ray crystallography that naphthalenesulfonic acid is not merely restricted to outer-sphere coordination chemistry, but possibly inner-sphere coordination chemistry as well. Two naphthalenesulfonic acid molecules were shown to coordinate to copper(II) in extended axial positions, with two hexyl isonicotinate molecules and two water molecules occupying the remaining coordination sites (**Scheme 5.3**). Of course, this example was copper-based and may not be directly relatable to nickel complexes of the same type, but this does give one an inkling as to what mechanistic role the sulfonic acid synergist might play in similar nickel complexes.



Scheme 5.3: Nickel synergist complex with two naphthalenesulfonic acid molecules coordinated directly to the copper centre. [Adapted from Hu *et al.*⁴]

One could argue, however, that the elongated Jahn-Teller distorted Cu-O bonds [2.358(3) Å] to the two SO_3^- moieties should be considered as “pseudo-bonds”.⁴ Whether these extended axial bonds are true bonds or not, the fact that naphthalene sulfonic acid is involved in the inner coordination sphere and not merely peripherally, should be acknowledged and not simply discarded as an one-off anomalous occurrence.

Roebuck *et al.*⁵ published a fascinating in-depth article in which they reported the crystal structures of two bidentate pyrazolyl ligands coordinated to nickel with peripheral H-bonded naphthalenesulfonic acid synergists (**Figures 5.1** and **5.2**). Both cases clearly show naphthalenesulfonic acid as an outer-sphere “stabiliser”. These acid stabilising molecules not only assists in this manner, but provides additional lipophilicity to the assembly as well, thereby facilitating the transport of the assembly across the aqueous-organic interface.

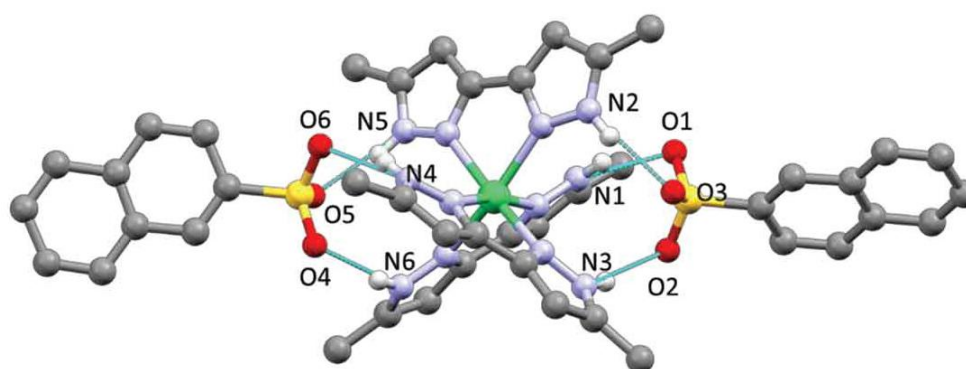


Figure 5.1: X-ray crystal structure of three bipyrazolyl ligands coordinated to nickel (octahedral geometry) with H-bonded sulfonic acid moieties acting as stabilisers. [Taken without alteration from Roebuck *et al.*⁵]

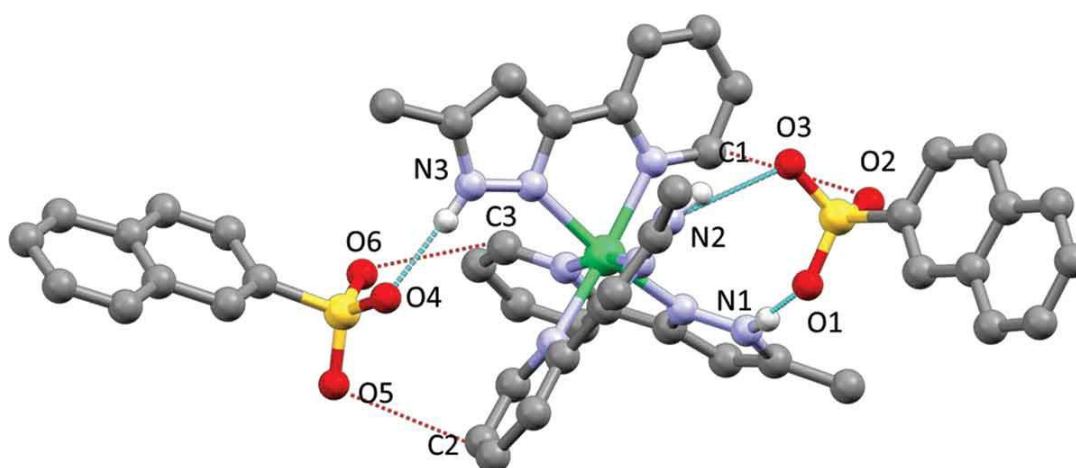


Figure 5.2: X-ray crystal structure of three bidentate pyrazole-pyridinyl ligands coordinated to nickel (octahedral geometry) with H-bonded naphthalenesulfonic acid acting as stabilisers on the periphery (outer coordination sphere). [Taken without alteration from Roebuck *et al.*⁵]

5.2 Materials and methods

5.2.1 Chemicals and reagents

The chemicals listed in **Table 5.1** were bought and used without additional purification.

Table 5.1: List of chemicals used in alphanumeric order.

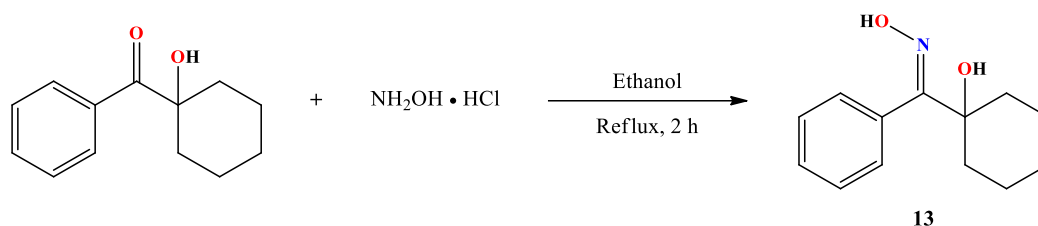
Chemical/Reagent	Purity (%)	Commercial Supplier
1-Hydroxycyclohexyl phenyl ketone	99	Sigma-Aldrich (Pty) Ltd.
2-Naphthalenesulfonic acid	98	Alfa-Aesar
3,3-dimethyl-2-butanone	97	Sigma-Aldrich (Pty) Ltd.
3,5,5-Trimethylhexanoic acid	97	Alfa-Aesar
Bis(2,4,4-trimethylpentyl)phosphinic acid (Cyanex [®] 272)	85	Cytec Industries Inc.
Chloroform	≥ 98	KIMIX Chemical and Lab Supplies (CC)
Dichloromethane	≥ 98	KIMIX Chemical and Lab Supplies (CC)
Diethyl ether	≥ 98	KIMIX Chemical and Lab Supplies (CC)
Diethyl oxalate	≥ 99	Sigma-Aldrich (Pty) Ltd.
Dinonylnaphthalenesulfonic acid (Nacure [®] 1051)	62% in 2-butoxyethanol	King Industries, Inc.
Ethanol (absolute)	≥ 99	KIMIX Chemical and Lab Supplies (CC)
Ethyl 2-picolinate	99	Sigma-Aldrich (Pty) Ltd.
Ethyl acetate	≥ 98	KIMIX Chemical and Lab Supplies (CC)
Hexane	≥ 99	KIMIX Chemical and Lab Supplies (CC)
Hydrazine monohydrate	98 (64–65% N ₂ H ₄)	Sigma-Aldrich (Pty) Ltd.
Hydrochloric acid solution	32 wt.% in H ₂ O	KIMIX Chemical and Lab Supplies (CC)
Hydroxylamine hydrochloride	98	Sigma-Aldrich (Pty) Ltd.
Methanol	≥ 97	KIMIX Chemical and Lab Supplies (CC)
Nickel(II) sulfate hexahydrate	≥ 98	Sigma-Aldrich (Pty) Ltd.
Phenyl 2-pyridyl ketoxime	98	Sigma-Aldrich (Pty) Ltd.
Potassium bromide (FT-IR grade)	≥ 99	Merck (Pty) Ltd.
Sodium acetate	≥ 99	KIMIX Chemical and Lab Supplies (CC)
Sodium ethoxide (powder)	≥ 95	Alfa-Aesar
Sodium hydride	60 wt.% in mineral oil	Sigma-Aldrich (Pty) Ltd.
Sodium sulfate (anhydrous)	≥ 99	Merck (Pty) Ltd.
Sulfuric acid	95–98	Protea Chemicals (Pty) Ltd.
Toluene	99	KIMIX Chemical and Lab Supplies (CC)

5.2.2 Instrumentation

The various characterisation techniques used, along with their respective technical instruments, were the same as previously reported in Sections 2.2.2 of CHAPTER 2 and 3.2.2 of CHAPTER 3.

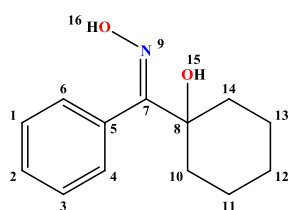
5.3 Experimental

5.3.1 Synthesis of (1-hydroxycyclohexyl)-phenyl ketone oxime (13)



Scheme 5.4: Synthetic route to (1-hydroxycyclohexyl)-phenyl ketone oxime (**13**). [Adapted from Barnard *et al.*⁶]

1-Hydroxycyclohexyl phenyl ketone (5.00 g, 24.5 mmol), sodium acetate (2.05 g, 25.1 mmol) and hydroxylamine hydrochloride (1.87 g, 26.9 mmol) were simultaneously dissolved in absolute ethanol (30 mL). After the mixture refluxed for 2 hours and allowed to cool to room temperature, it was filtered to remove minor solid impurities. Dichloromethane (30 mL) was added to the clear colourless filtrate, which immediately became cloudy. To the solution was added deionised water (3×25 mL) in order to remove inorganic impurities, after which the separated organic layer was dried overnight over anhydrous Na_2SO_4 . After filtering off the drying agent, the solvent was removed under reduced pressure, yielding ligand **13** as an off-white solid (5.18 g, 96.4%).



FT-IR (KBr pellet, cm^{-1}) 3527 (free O–H str), 3262 (H-bonded O–H str), 3059 (aromatic C–H str), 2937 (aliphatic C–H str), 1651 (C=N str), 1440 ($-\text{CH}_2$ bend).

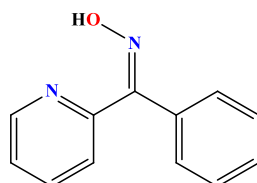
^1H NMR (400 MHz, CDCl_3) δ 7.47–7.37 (m, H_{1-6} , 3H), 7.24–7.19 (m, H_{1-6} , 2H), 1.73–1.51 (m, H_{10-14} , 9H), 1.20–1.06 (m, H_{10-14} , 1H).

$^{13}\text{C}\{^1\text{H}\}$ NMR (100 MHz, CDCl_3) δ 164.3 (C7), 132.1 (C5), 128.7 (C2), 128.3 (C4/6), 128.1 (C1/3), 74.1 (C8),

35.7 (C10/14), 25.3 (C12), 21.6 (C11/13). **Calculated exact mass (μ)** 219.13. **ESI-MS (m/z)** 202.12 ($M - \text{OH}$), 220.13 ($M + \text{H}^+$), 242.12 ($M + \text{Na}^+$). **EA calculated (%)** C, 71.21; H, 7.81; N, 6.39. **EA found (%)** C, 71.51; H, 7.72; N, 6.22. **m.p.** 91–92 °C. See full range of spectra on pages 59–62 of Appendix A — SPECTRA.

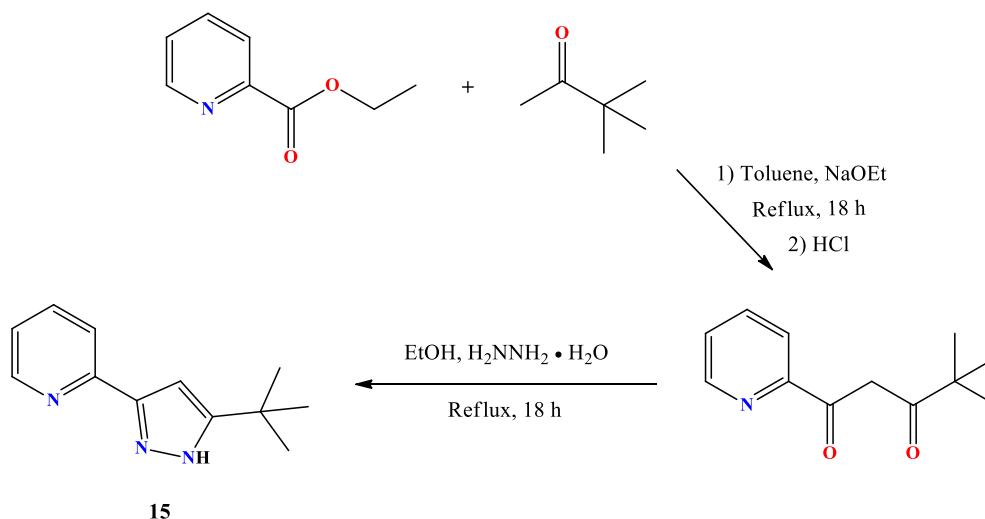
5.3.2 Phenyl 2-pyridyl ketoxime (14)

This ligand was not synthesised, but rather purchased directly from Sigma-Aldrich (Pty) Ltd. and used without any additional purification.



Scheme 5.5: Chemical structure of phenyl 2-pyridyl ketoxime (14).

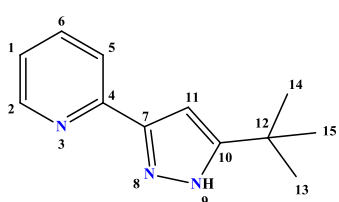
5.3.3 Synthesis of 2-(5-(*tert*-butyl)-1*H*-pyrazol-3-yl)pyridine (15)



Scheme 5.6: Synthetic route to 2-(5-(*tert*-butyl)-1*H*-pyrazol-3-yl)pyridine (15). [Adapted from Roebuck *et al.*⁵ and Satake & Nakata⁷]

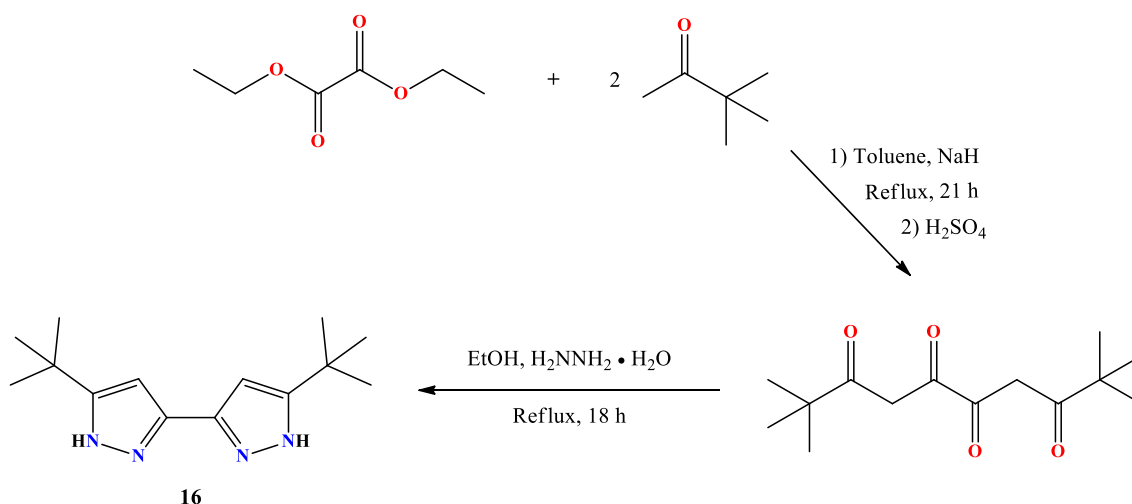
Sodium ethoxide (3.02 g, 44.4 mmol) was added to 100 mL toluene, resulting in an orange suspension. To this suspension was added 3,3-dimethyl-2-butanone (5.09 mL, 40.7 mmol) followed by the dropwise addition of ethyl 2-picolinate. The mixture was stirred under refluxing conditions for 18 hours, resulting in a dark brown solution. After the solution was allowed to cool to room temperature, 100 mL deionised water was added, which drained most of the colour from the organic layer. Hydrochloric acid was slowly added while stirring until pH ~5. The top-layered organic layer became bright orange, indicating that the enol formation went to completion [enolate (water-soluble) to enol (organic-soluble)]. The organic layer was separated and dried over anhydrous Na₂SO₄. Following this, the drying agent was filtered off, resulting in a bright yellow-orange solution that was concentrated *in vacuo*. A crude dark orange intermediary oil was obtained and used without additional purification.

The crude intermediate was dissolved in 50 mL absolute ethanol, followed by hydrazine monohydrate (4.00 mL, 81.7 mmol). The solution was heated to a refluxing temperature and stirred for 18 hours, during which the solution became golden yellow. The solvent was removed under reduced pressure to afford an auburn-coloured viscous oil. This oil was subsequently redissolved in chloroform and washed with deionised water (3×30 mL) to rid the mixture of any unwanted impurities. The organic layer was separated and dried over anhydrous Na_2SO_4 overnight. Thereafter, the drying agent was filtered off and the solvent removed *in vacuo*, yielding a brown toffee-like substance. The product was purified via gravitational column chromatography on silica gel by first using toluene ($R_f = 0.202$) as eluent, followed by ethyl acetate ($R_f = 0.798$). The product-containing fractions were collected and the solvent subsequently removed under reduced pressure. Finally, ligand **15** (3.33 g, 44.7 %) was obtained as a pale yellow viscous oil that ultimately crystallised over 2–3 days.



FT-IR (ATR, cm^{-1}) 3186 (aromatic C–H str), 2956 (aliphatic C–H str), 1595 (pyridine C=N str), 1566 (pyrazole C=N str), 1458 ($-\text{CH}_3$ bend). **^1H NMR (400 MHz, CDCl_3)** δ 8.60 (d, $J = 4.6$ Hz, H_2 , 1H), 7.82 (d, $J = 7.9$ Hz, H_5 , 1H), 7.68 (td, $J = 7.7, 1.8$ Hz, H_1 , 1H), 7.16 (ddd, $J = 7.4, 4.9, 1.0$ Hz, H_6 , 1H), 6.67 (s, H_{11} , 1H), 1.36 (s, H_{13-15} , 9H). **$^{13}\text{C}\{^1\text{H}\}$ NMR (100 MHz, CDCl_3)** δ 159.2 (C_4), 150.5 (C_7), 149.4 (C_2), 146.9 (C_{10}), 136.8 (C_6), 122.5 (C_1), 120.1 (C_5), 99.9 (C_{11}), 31.7 (C_{12}), 30.5 (C_{13-15}). **Calculated exact mass (μ)** 201.13. **ESI-MS (m/z)** 202.13 ($M + \text{H}^+$), 224.12 ($M + \text{Na}^+$). **EA calculated for $\text{C}_{12}\text{H}_{15}\text{N}_3 \cdot 0.25\text{C}_7\text{H}_8$ (%)** C, 73.63; H, 7.64; N, 18.73. **EA found (%)** C, 73.69; H, 7.49; N, 18.89. **m.p.** 104–105 °C. See full range of spectra on pages 63–66 of *Appendix A — SPECTRA*.

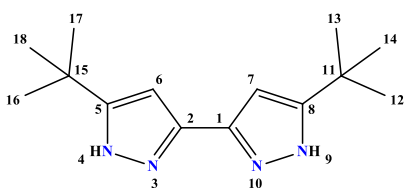
5.3.4 Synthesis of 5,5'-di-*tert*-butyl-1*H*,1'*H*-3,3'-bipyrazole (**16**)



Scheme 5.7: Synthetic route to 5,5'-di-*tert*-butyl-1*H*,1'*H*-3,3'-bipyrazole (**16**). [Adapted from Roebuck *et al.*,⁵ Satake & Nakata,⁷ Bouabdallah *et al.*⁸ and Shironina *et al.*⁹]

Sodium hydride (2.74 g, 68.4 mmol) was added to toluene (50 mL) after being washed with hexane. To this grey suspension, was added 3,3-dimethyl-2-butanone (7.13 mL, 57.5 mmol) and diethyl oxalate (3.70 mL, 27.4 mmol) in a dropwise manner. The mixture was heated to a refluxing temperature and stirred for 21 hours. After 2 hours the mixture had become bright orange and after 6 hours, bright yellow. After the 21-hour period expired, the mixture had become a thick yellow sludge (most probably due to salt formation). After allowing the reaction flask to cool to room temperature, 100 mL deionised water was added, which immediately drained all colour from the organic phase. Sulfuric acid was slowly added to the stirring mixture until pH ~5. This resulted in the organic layer regaining its yellow hue, while the aqueous layer held a pink-orange hue. The organic layer was separated, dried over anhydrous Na₂SO₄ and filtered to yield a clear yellow solution. The product was subsequently concentrated *in vacuo* to yield a crude brown intermediate solid (4.32 g).

The crude intermediate was redissolved in absolute ethanol (100 mL), followed by the addition of hydrazine monohydrate (2.04 mL, 24.1 mmol) and 3 drops of HCl. The intense yellow solution was refluxed for 18 hours, after which the solution became yellow-orange with a white precipitation present at the bottom of the reaction flask. The white precipitate was collected and dried in an oven at 50 °C overnight, ultimately yielding ligand **16** (2.16 g, 23.5%) as shiny white granules.



FT-IR (KBr pellet, cm⁻¹) 3426 (N–H stretch), 3075 (heterocyclic C–H str), 2965 (aliphatic C–H str), 1564 (C=N str), 1362 (–CH₃ bend). **¹H NMR (400 MHz, DMSO-*d*₆)** δ 12.22 (s, *H*_{4/9}, 2H), 6.29 (s, *H*_{6/7}, 2H), 1.31 (s, *H*_{12–14/16–18}, 18H). **¹³C{¹H} NMR (100 MHz, DMSO-*d*₆)**

δ 156.0 (*C*_{1/2}), 141.3 (*C*_{5/8}), 97.7 (*C*_{6/7}), 30.5 (*C*_{11/15}), 29.8 (*C*_{12–14/16–18}). **Calculated exact mass (μ).**

ESI-MS (*m/z*) 247.19 (*M* + *H*)⁺, 269.17 (*M* + *Na*)⁺. **EA calculated (%)** C, 68.26; H, 9.00; N, 22.74. **EA found (%)** C, 67.95; H, 9.34; N, 23.23. **m.p.** > 250 °C. See full range of spectra on pages 67–71 of *Appendix A — SPECTRA*.

5.4 Synthetic results and discussion

5.4.1 (1-Hydroxycyclohexyl)-phenyl ketone oxime

The synthesis of (1-hydroxycyclohexyl)-phenyl ketone oxime (**13**) was fairly straightforward and rather uneventful. The only minor difficulty was in the process of discerning whether ligand **13** had successfully been synthesised or not, since its ¹H and ¹³C NMR spectra were expectantly similar to that of the ketone starting material. From the IR spectrum, however, it was clear that the disappearance of the carbonyl stretching frequency (~1710 cm⁻¹) and the subsequent appearance of the imine stretching frequency (1652 cm⁻¹) was solid evidence for the successful synthesis of ligand **13**. To compliment this analytical result, both the MS and EA results indicated the reaction did in fact go to completion, which afforded the oxime ligand in an excellent yield of 96.4%.

5.4.2 2-(5-(*Tert*-butyl)-1*H*-pyrazol-3-yl)pyridine

The synthesis of 2-(5-(*tert*-butyl)-1*H*-pyrazol-3-yl)pyridine (**15**) was a far more cumbersome procedure, with numerous workups and purification processes involved. This ligand, however, has previously been synthesised in our laboratory and was subsequently reported by Pearce *et al.*¹⁰ in 2017. On that occasion, a meagre overall yield of 26.1% was obtained. This time round, a concerted effort was launched to increase the yield of this ligand, resulting in fewer chemical resources used and financial resources spent.

After successfully synthesising tridentate ligands **1–10** (Sections 2.3.2–2.3.11, CHAPTER 2) by implementing sodium ethoxide as base, it was decided to use this base for the synthesis of ligand **15** as well, instead of sodium hydride as reported by Pearce *et al.*¹⁰ Sodium ethoxide is a much milder base, which inevitably requires longer reaction times to deprotonate the α -carbon of 3,3-dimethyl-2-butanone. Therefore, the reaction mixture was stirred under refluxing conditions for 18 hours (compared to the mere 20 minutes as reported by the aforementioned authors), after which the crude diketone (or di-enol) intermediary species was obtained post workup. Additionally, ample time (18 hours) was allowed for the cyclisation reaction to go to completion, compared to the 90 minutes of the 2017 publication. The final purification procedure via gravitational column chromatography, however, remained unchanged. All-in-all, the yield of ligand **15** was successfully improved from 26.1% to 44.7%. The chemical structure was subsequently confirmed via ¹H and ¹³C NMR, IR, MS and EA.

5.4.3 5,5'-Di-*tert*-butyl-1*H*,1'*H*-3,3'-bipyrazole

The synthesis of 5,5'-di-*tert*-butyl-1*H*,1'*H*-3,3'-bipyrazole (**16**) was in essence very similar to that of ligand **15**, but on this occasion the use of sodium ethoxide—even at reaction times in excess of 24 hours—did not proceed forward. This necessitated the implementation of sodium hydride as base once again. After washing the base with dry hexane, it appeared as though the reaction was successful with 4.32 g of a crude brown intermediate solid being obtained. It was interesting to note, however, that relatively long reaction times (21 hours) were still required, even in the presence of a far stronger base. This, as expected, resulted in the formation of unwanted side-products, lowering the overall yield considerably. After the cyclisation step employing hydrazine, a white grainy precipitate was noticed at the bottom of the reaction flask. At first, this precipitate was considered to be a salt that formed as a result of reacting hydrazine with the aforementioned side-products. This was an encouraging result since this “impurity” could simply be filtered off. As it turned out, this white precipitate was in fact the desired bipyrazolyl ligand, 5,5'-di-*tert*-butyl-1*H*,1'*H*-3,3' bipyrazole (**16**), after analysing it via infrared spectroscopy. From the IR spectrum (Figure 5.3), it was evident that organic moieties were present in the white grainy “impurity”.

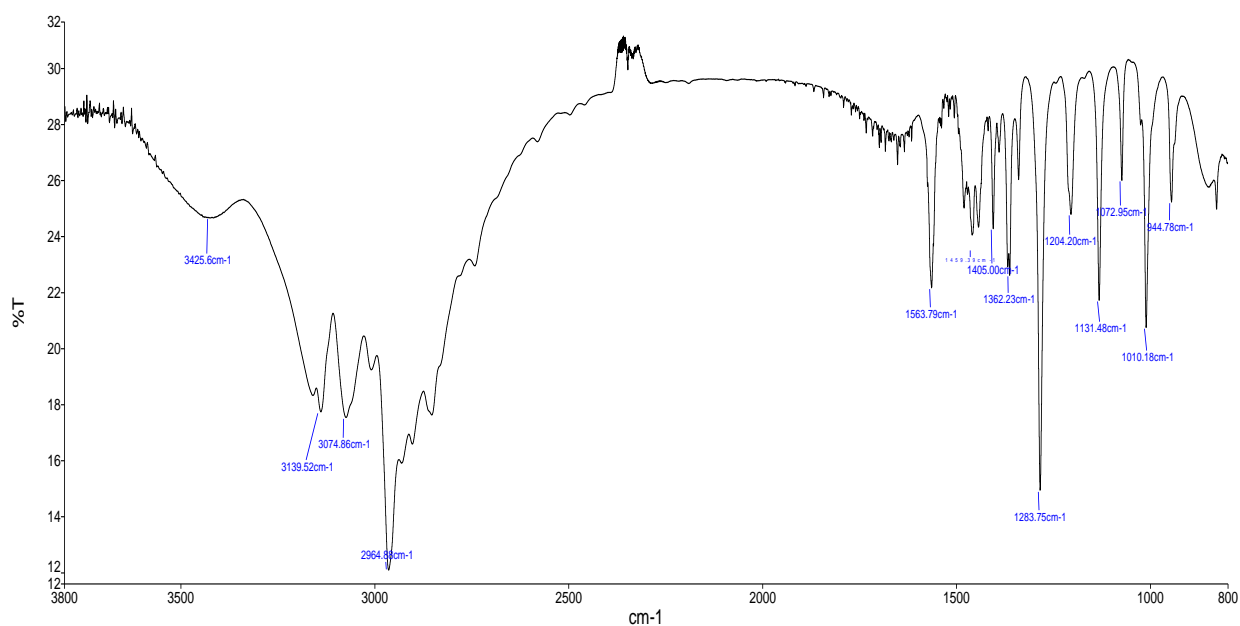


Figure 5.3: FT-IR (KBr pellet) spectrum of 5,5'-di-*tert*-butyl-1*H*,1'*H*-3,3'-bipyrazole (**16**).

This result necessitated further investigation via other characterisation techniques. Both MS and EA results indicated that the white “impurity” was in fact ligand **16**. The NMR analyses, however, were by far the most challenging characterisation technique to perform since the product was insoluble in most common organic solvents. A myriad of polar and non-polar organic solvents were tested to no avail. This was most probably due to either strong inter- or intramolecular hydrogen bonding—akin to that of 2,6-bis(1*H*-imidazol-2-yl)pyridine previously highlighted in **Scheme 2.26** of **CHAPTER 2**. The only glimmer of success appeared to be dimethyl sulfoxide at elevated temperatures. Eventually, ^1H and ^{13}C NMR analyses were performed in DMSO- d_6 at 100 °C. This forced a miniscule amount of product into solution, allowing the operator to record usable spectra. From the ^1H NMR spectrum (**Figure 5.4**), the 18 *tert*-butyl protons were identified by the resonance at 1.31 ppm, while the 2 *NH* protons and 2 pyrazolyl protons were assigned to the signals at 12.22 and 6.29 ppm, respectively.

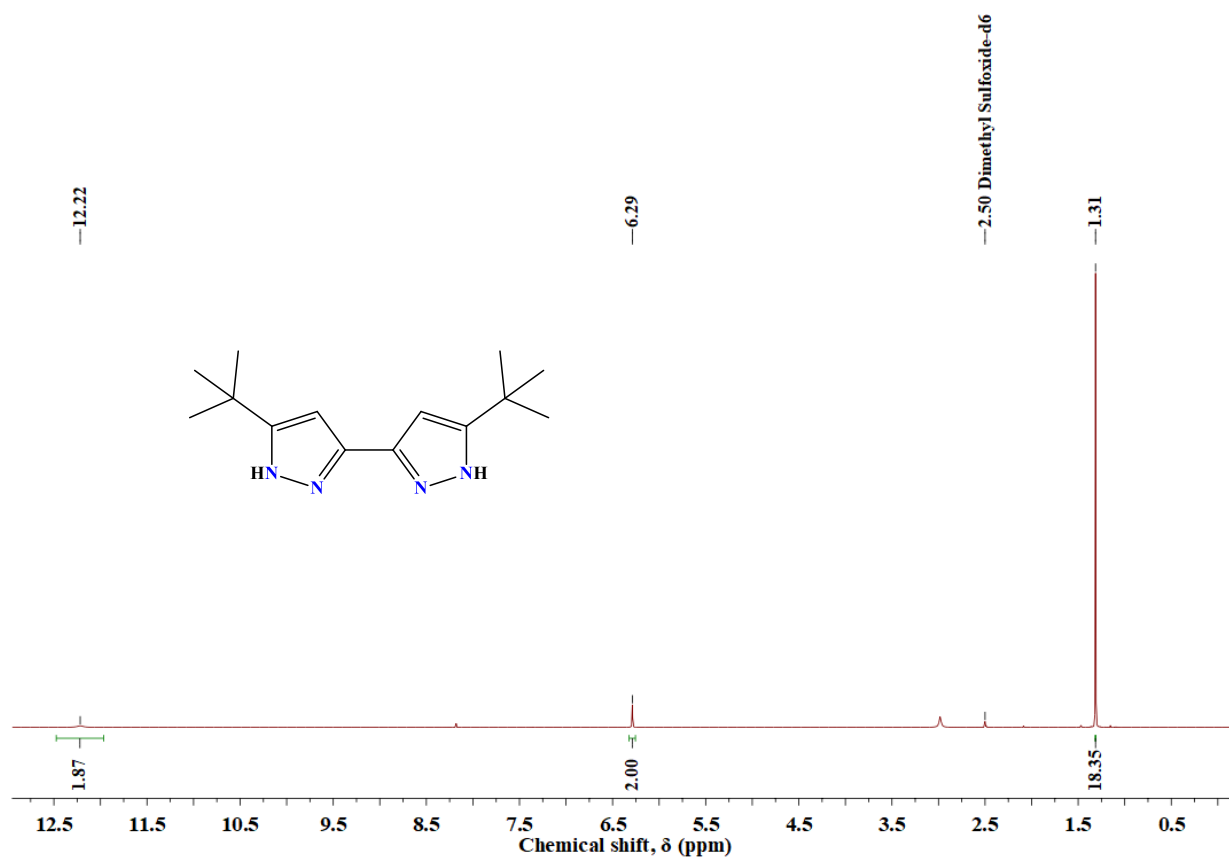


Figure 5.4: ¹H NMR spectrum of 5,5'-di-*tert*-butyl-1*H*,1'*H*-3,3'-bipyrazole (**16**) [400 MHz, DMSO-d₆, 100 °C].

The ¹³C NMR spectrum (**Figure 5.5**), on the other hand, was more intricate and difficult to resolve. Two upfield signals were noticed at 29.8 and 30.5 ppm, which were linked to the primary (1°) and quaternary (4°) carbons of the *tert*-butyl moieties, respectively. The CH pyrazolyl carbon signals were also evident at 97.7 ppm, but the four protonless pyrazolyl carbon signals (adjacent to the nitrogen atoms) were ostensibly absent from the spectrum. Upon further investigation, it was realised that yet another case of tautomerism was present. This resulted in poorly defined resonance signals at 156.0 and 141.3 ppm (**Figure 5.6**), which was assigned to the four protonless pyrazolyl carbons (two chemical environments due to symmetry).

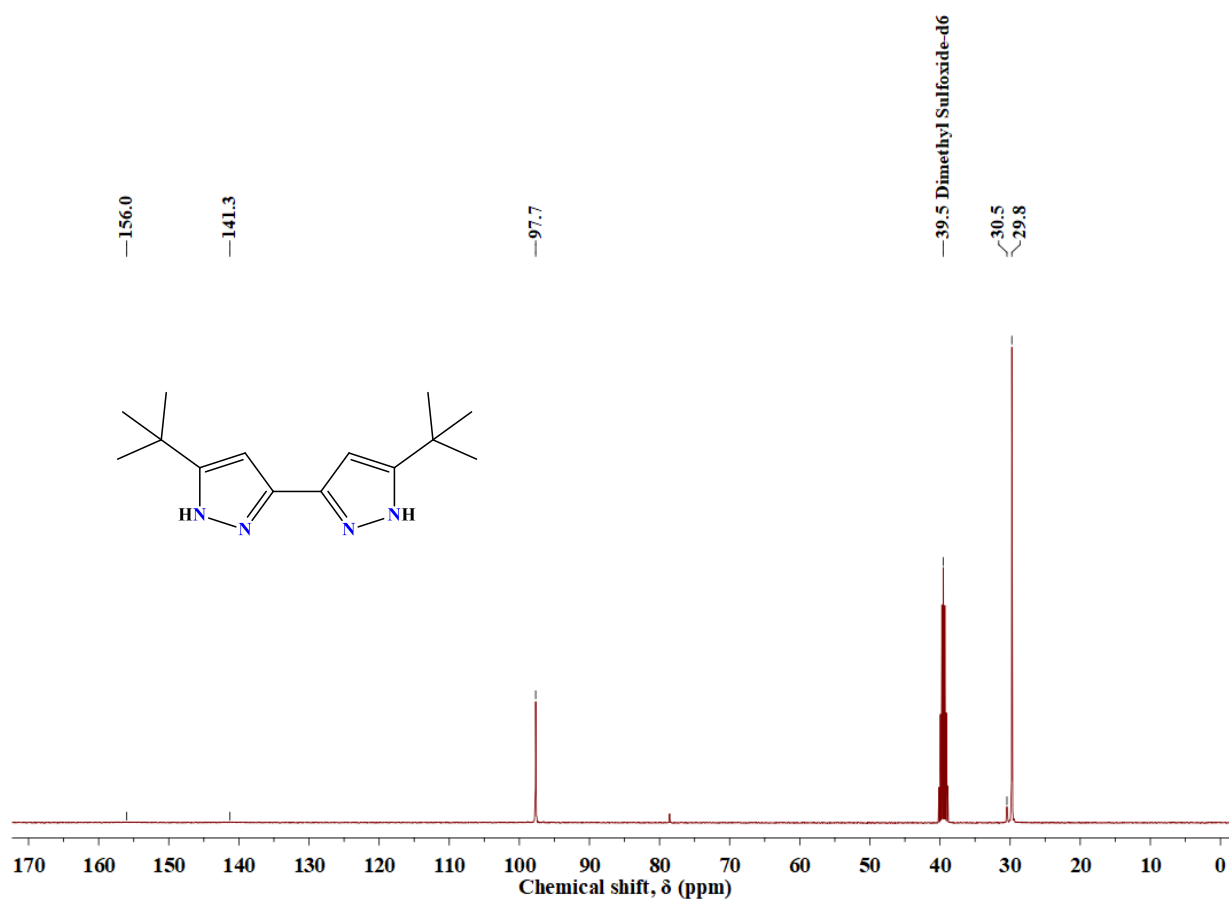


Figure 5.5: ^{13}C NMR spectrum of 5,5'-di-tert-butyl-1H,1'H-3,3'-bipyrazole (**16**) [100 MHz, DMSO- d_6 , 100 °C].

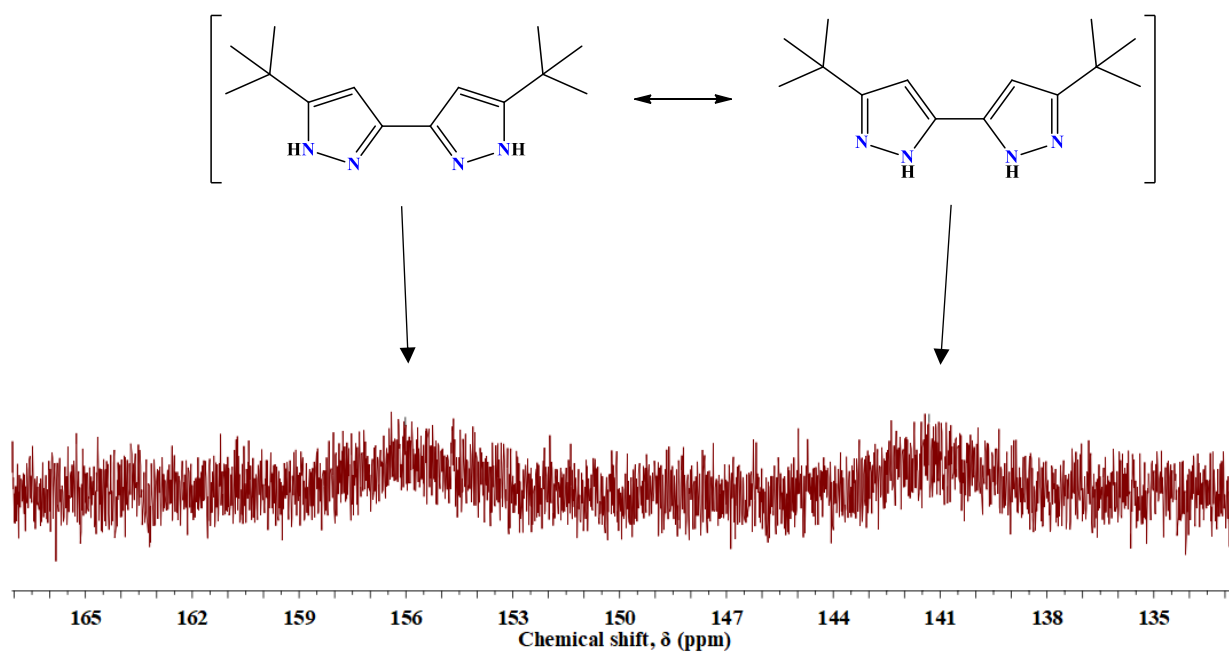


Figure 5.6: Zoomed-in ^{13}C NMR spectrum of 5,5'-di-tert-butyl-1H,1'H-3,3'-bipyrazole (**16**), indicating the presence of two broadened resonances [100 MHz, DMSO- d_6 , 100 °C].

5.5 Solvent extraction of nickel(II)

5.5.1 General solvent extraction procedure, conditions and synergists

All-in-all, the extraction setup was fairly similar to that previously reported in **Section 3.2.4** of **CHAPTER 3**. One of the differences, however, were the use of $\text{NiSO}_4 \cdot 6\text{H}_2\text{O}$ instead of its nitrate analogue. Of course, this also meant that sulfuric acid was needed to adjust the pH to ~ 6 in order to maintain the same anionic species in solution. Furthermore, instead of using chloroform as organic solvent, toluene was used instead due to its less polar nature and lower dielectric constant [C_7H_8 : $\epsilon = 2.379$ (25°C); CHCl_3 : $\epsilon = 4.806$ (20°C)].¹¹ According to the Hofmeister series, metals with larger and more charge-diffuse anions, such as sulfates, are more readily extracted into non-polar solvents than smaller and charge-localised anions, such as nitrates. Therefore, one would expect greater extraction efficiencies of nickel(II) into toluene compared to chloroform when sulfate salts are used.

Furthermore, it is important to note that due to toluene's lower density, the aqueous- and organic phases are reversed within the glass vial (**Figure 5.7**), *i.e.*, the organic phase is now represented by the top-layered band, while the bottom band represents the metal-rich aqueous phase.

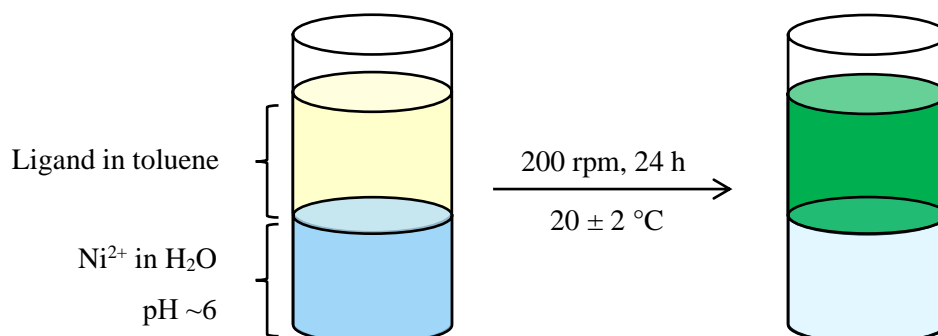
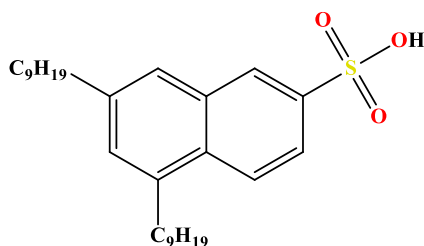
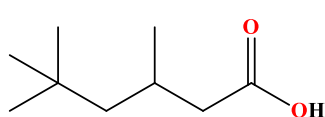


Figure 5.7: General experimental setup and execution of the nickel(II) solvent extraction process.

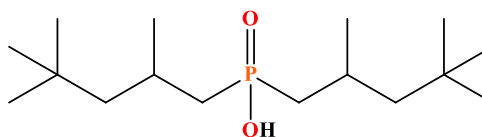
Nota bene: No other metal ions were used or investigated in this chapter. This chapter purely focused on the extraction of nickel(II) by means of ligands **13–16** in the presence of three acid synergists: DNNSA (**SA**), Versatic[®] 9 (**CA**) and CYANEX[®] 272 (**PA**) (**Scheme 5.8**). All experiments were conducted in duplicate to ensure results were accurate and reliable.



5,7-dinonylnaphthalene-2-sulfonic acid (SA)



3,5,5-trimethylhexanoic acid (CA)



bis(2,4,4-trimethylpentyl)phosphinic acid (PA)

Scheme 5.8: Three common acid synergists implemented for the extraction of nickel(II).

5.6 Solvent extraction results and discussion

5.6.1 Nickel(II) extractive ability of ligands and synergists

Before any solvent extraction experiments could commence, it was imperative to select a sensible ligand-to-Ni²⁺ (L:Ni²⁺) experimental ratio. Since ligands **13–16** were bidentate ligands known to form octahedral complexes with nickel(II), it was decided to employ a 3:1 (L:Ni²⁺) experimental extraction ratio. By the same logic a suitable synergist-to-Ni²⁺ (S:Ni²⁺) ratio was employed for the acid synergists as well. Since all three synergists [sulfonic- (SA), carboxylic- (CA) and phosphinic acid (PA)] were monodentate in nature, it was decided to implement a 6:1 (S:Ni²⁺) ratio.

Before the onset of extraction experiments with various combinations of ligands and synergists, it was first necessary to establish the extractive power of the ligands and synergists on their own. As solo extractants, ligands **13–15** meagerly extracted nickel(II) at 3.1 (± 0.3), 1.3 (± 0.5) and 1.4 (± 0.2)%, respectively. These were extraordinarily poor extraction results, yet were somewhat expected. Hence, the need for a synergist to assist in the extraction of nickel(II). According to Du Preez *et al.*¹² and Okewole *et al.*,¹³ the presence of the harder *O*-donor atoms of oxime ligands **13** and **14**, reduces their selectivity for nickel(II) over cobalt(II) and iron(III). In this study, however, the selective nature of these ligands was not of interest, but rather the nickel(II) extractive ability of these ligands in conjunction with various acid synergists. It should be highlighted, however, that ligand **16** (bipyrazole) was not included in this preliminary experiment due to its poor solubility in most known organic solvents, as previously alluded to in **Section 5.4.3**.

Acid synergists SA, CA and PA extracted nickel(II) at 99 (± 0.7), 0.32 (± 0.28) and 1.4 (± 0.4)%, respectively. Only SA showed significant extractive abilities and can likely be attributed to its lower pK_a value of 0.68.¹⁴ Compared to CA (pK_a = 4.8)¹⁴ and PA (pK_a = 5.22),¹⁵ only SA is deprotonated at lower pH values and able to coordinate to nickel(II) and transport it across the biphasic interface. The aromaticity of these synergists

certainly plays an important role in their extraction efficacies too. Only **SA** consists of an aromatic torso that forces electron density onto the SO_3^- moiety,¹⁶ rendering its donor atoms more effective in their coordination to nickel(II). With that being said, all three synergists have two essential traits: 1) polar donor moieties, which assists in the coordination process, as well as 2) hydrophobic non-polar tails, which assists in carrying complex species into the organic phase.

5.6.2 Combinative (synergistic) extraction of nickel(II)

The extraction of nickel(II) by means of a combination of ligand and acid synergist was investigated by enriching the aqueous phase with $\text{NiSO}_4 \cdot 6\text{H}_2\text{O}$. **Figure 5.8** revealed that ligand **13**'s %*E* increased from 2.7 (± 0.1)% (no synergist involved) to 83 (± 0.3), 3.7 (± 0.5) and 6.2 (± 4.2)% in the presence of **SA**, **CA** and **PA**, respectively. Ligand **14** showed synergistic gains from 1.1 (± 0.3)% (no synergist involved) to 44 (± 0.2) [**SA**], 17 (± 0.1) [**CA**] and 12 (± 0.2)% [**PA**], while ligand **15** exhibited gains from 0.82 (± 0.09)% to 92 (± 0.5) [**SA**], 1.5 (± 0.1) [**CA**] and 5.6 (± 0.1)% [**PA**], respectively.

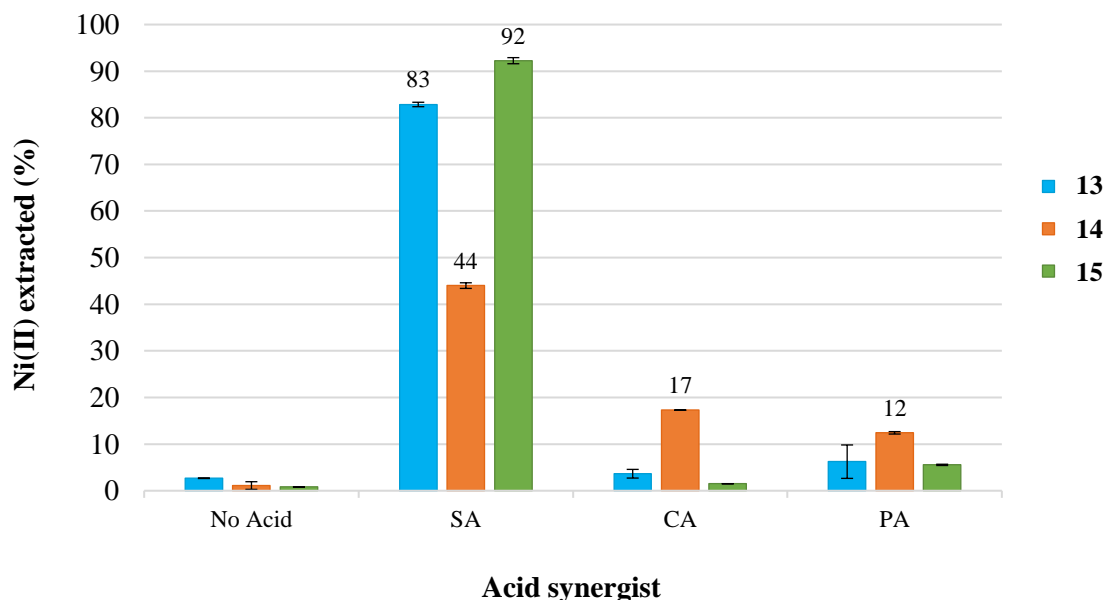


Figure 5.8: Nickel(II) extraction by means of ligands **13–15** in the presence of **SA**, **CA** and **PA** synergists. [Ligands] = 3×10^{-2} M; [synergists] = 2×10^{-2} M; $[\text{Ni}^{2+}] = 1.1 \times 10^{-2}$ M; pH 6.11.

Further investigation was required to ascertain the impact of the **SA**-to-nickel(II) (**SA**: Ni^{2+}) ratio, since it showed the most promising results. The %*E* remained above 95% when the **SA** equivalent was reduced from 6 to 4. The %*E* values only dropped to 88 (± 0.3)% upon the implementation of 3 equivalents, and decreased even further to 72 (± 0.3), 37 (± 0.4) and 19 (± 0.5)% in the presence of 2, 1 and 0.5 equivalents of **SA**, respectively (**Figure 5.9**).

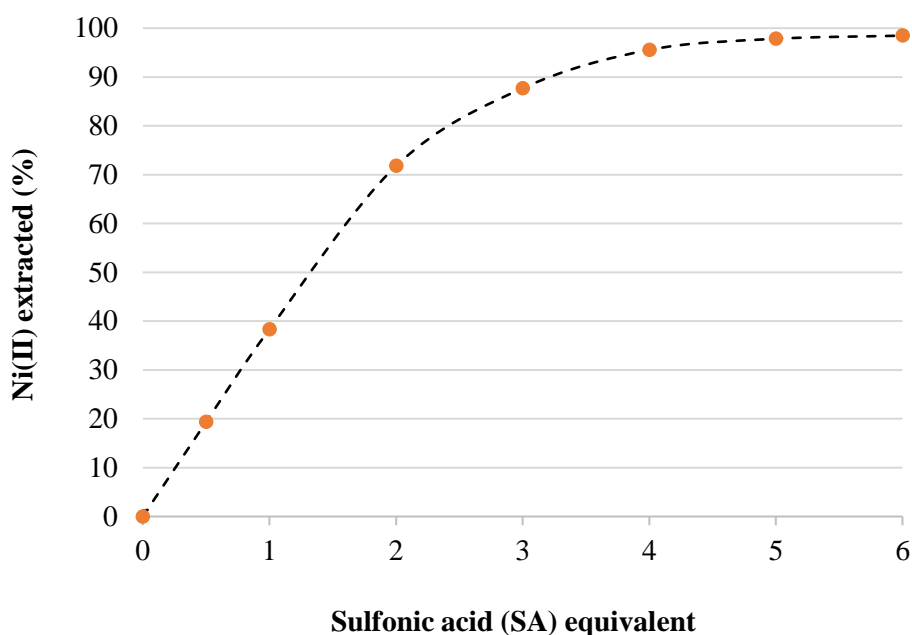


Figure 5.9: Extraction of nickel(II) at increasing sulfonic acid synergist ratios. $[\text{Ni}^{2+}] = 1 \times 10^{-2} \text{ M}$; $[\text{SA}] = 1 \times 10^{-2} - 6 \times 10^{-2} \text{ M}$; pH 5.92

This result shows that only three **SA** molecules are needed to extract nickel(II) efficiently. The SO_3^- moiety might coordinate to nickel(II) through two of its *O*-donor atoms in a bidentate fashion. This theory is substantiated by Zhu *et al.*¹ and Hu *et al.*³ Another possible mechanism of extraction might be micellar in nature, as previously alluded to in **Section 3.3.8** of **CHAPTER 3**.

5.6.3 pH isotherm studies

Nickel(II) extraction studies at varying pH values were conducted to determine the ligands' extractive abilities at low pH values for potential industrial applications. This was done by fixing the ligand-synergist-nickel (L:S: Ni^{2+}) ratio at 3:2:1.1, while varying the nickel-rich aqueous phase pH from 1–6 (**Figure 5.10**). In the mining industry, metal ions are leached from the ore by using concentrated sulfuric acid, resulting in extremely acidic aqueous solutions from which the metals must be recovered. Therefore, it is imperative that ligands and/or synergists are able to operate efficiently in such extreme environments. From **Figure 5.10**, it was evident that extraction abilities of ligands **13–15**, in conjunction with **SA**, remained high throughout the whole experimental pH range. These were encouraging results and warrants further investigation.

The ligand **15-SA** combination exhibited significantly higher %*E* values compared to ligands **13** and **14** with the same synergist. This clearly illustrates the importance of two *N*-donor atoms (*O*-donor atoms are slightly too hard) and a ligand that is highly soluble in the organic phase (ligands **13** and **14** were weakly soluble in toluene). The large ligand **15-SA** extractive assembly clearly promotes more effective binding of nickel(II) and allows for better solubility in the organic phase. This was an exciting result, since Pearce *et al.*¹⁰ already demonstrated the selectivity of ligand **15** for nickel(II). It should be mentioned, however, that copper(II) ought

to be extracted first by means of another ligand/synergist combination (perhaps one of our tridentate pyrazolyl ligands mentioned in **CHAPTER 3**?) in order to extract nickel(II) without any copper(II) interferences.

Ligand **13** and **14** in combination with **CA** and **PA** yielded very disappointing results. It would seem from **Figure 5.10** that neither combination effectively extracted nickel(II), with their %*E* values remaining below 20% throughout. Due to these ligands' poor solubility in toluene, it was decided to redo the pH isotherm study in chloroform instead. This did affect their %*E* somewhat positively, yet these ligands never achieved the exceptional efficiencies of the ligand **15-SA** combination.

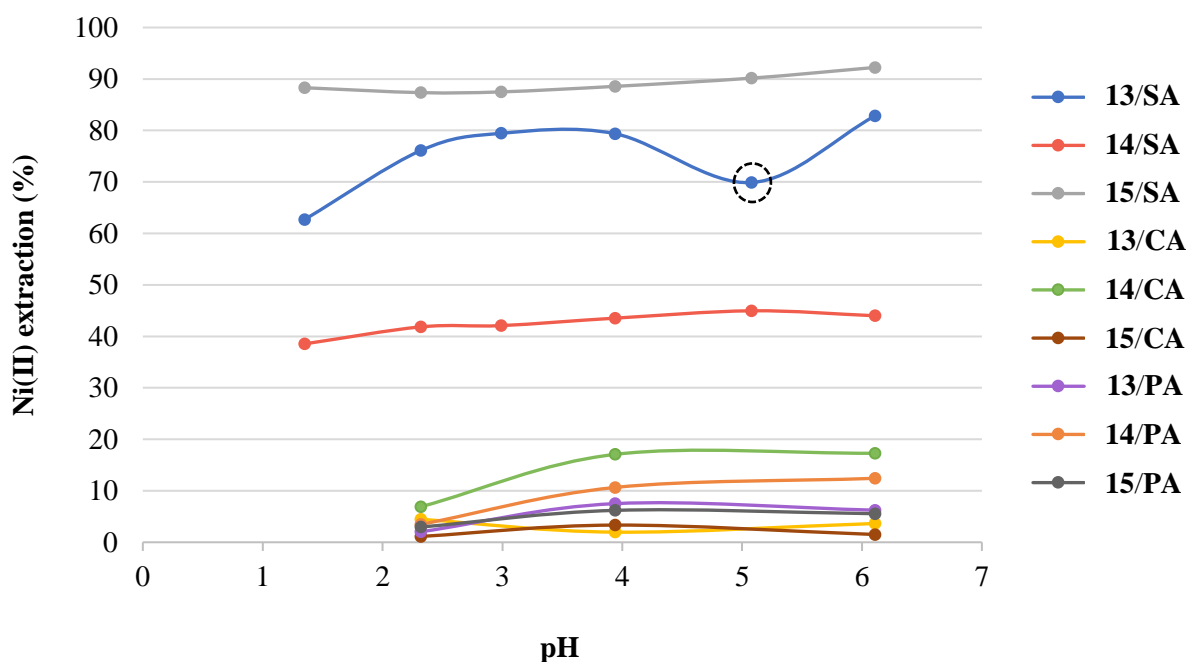


Figure 5.10: Nickel(II) extraction by means of ligands **13–15** in combination with **SA**, **CA** and **PA** at various pH values. Encircled data point considered an “outlier”. [Ligands] = 3×10^{-2} M; [synergists] = 2×10^{-2} M; $[\text{Ni}^{2+}] = 1.1 \times 10^{-2}$ M; pH 1–6.

Following this, another pH isotherm study was performed with bipyrazolyl ligand **16**. Numerous solubility tests were done to ascertain this ligand's solubility in the presence of acid synergists **SA**, **CA** and **PA**. Surprisingly, ligand **16** became soluble in toluene when a 2:1 (S:L) ratio was employed. This was most likely due to **SA** “disturbing” the intra- and/or intermolecular H-bonds of ligand **16**, allowing the assembly to go into solution. However, the same cannot be said of **CA** and **PA**, yet these combinations' extractive abilities were still probed, even in solid form. **Figure 5.11** shows remarkable nickel(II) extractive ability with ligand **16** in combination with **SA**. It seems that only at pH 1–2, the %*E* starts to decrease significantly, yet still maintaining extraction above 50%. The synergistic assemblies of **CA** and **PA** yielded no extraction whatsoever, which can undoubtedly be ascribed to ligand **16**'s poor solubility in toluene. Initially, it was anticipated that the ligand would become soluble in the presence of **CA** and **PA** over an extended period of time, but this turned out not to be the case. For future studies, one should look at disrupting the aforementioned H-bonds or by substituting

the *tert*-butyl moieties with longer *n*-alkyl tethers, thereby forcing the ligand to be more soluble in the organic phase.

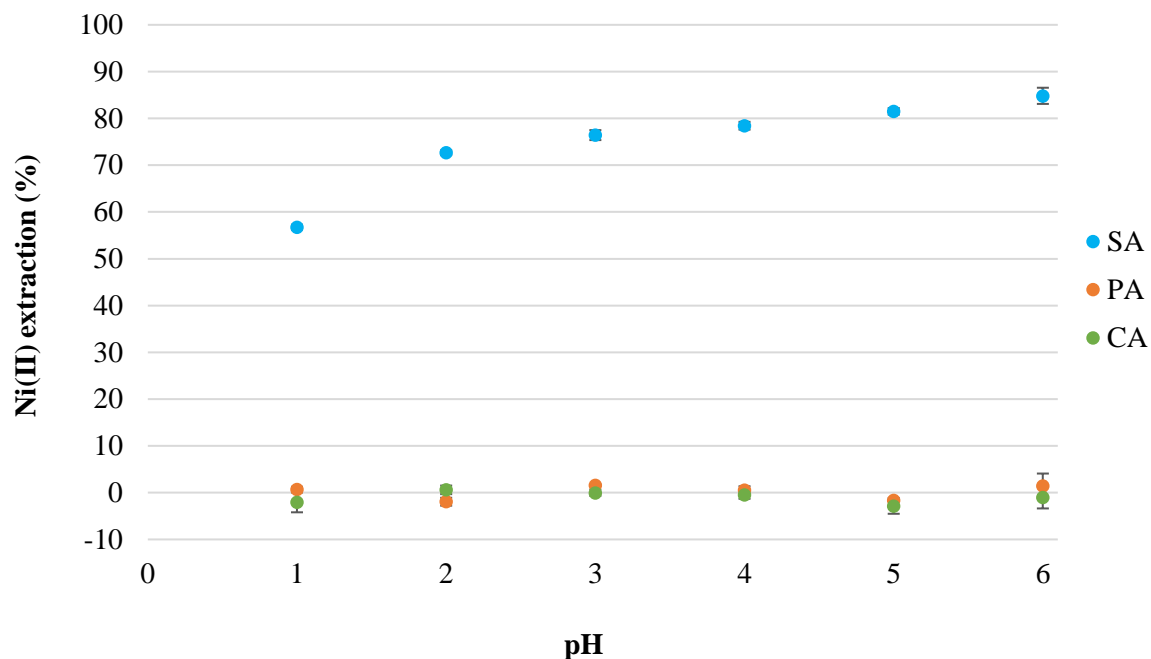


Figure 5.11: Nickel(II) extraction by means of ligand **16** in combination with SA, CA and PA at various pH values. [Ligand **16**] in toluene = 1.5×10^{-2} M; [synergists] = 3×10^{-2} M; $[\text{Ni}^{2+}] = 5.5 \times 10^{-3}$ M; pH 1–6.

5.7 Crystallographic results and discussion

Crystal preparation techniques, instrumentation and software were akin to those previously reported in Sections 4.4.1.1 and 4.4.2.1 of CHAPTER 4.

5.7.1 Preparation of free ligand 5,5'-di-*tert*-butyl-1*H*,1'*H*-3,3'-bipyrazole (**16**)

Ligand **16** (205 mg, 0.832 mmol), as synthesised in Section 5.3.4, was quantitatively transferred to a 25 mL glass vial (polytop) and dissolved with 10 mL hot absolute ethanol that contained 10 drops of DMSO as well. The vial was closed with a perforated plastic stopper, safely placed on the workbench and allowed to undergo slow evaporation. After two weeks, colourless cubic crystals were observed at the bottom of the glass vial. A suitable crystal was selected and submitted for X-ray analysis. **FT-IR (ATR, cm^{-1})** 3426 (N–H stretch), 3075 (heterocyclic C–H str), 2965 (aliphatic C–H str), 1564 (C=N str), 1362 ($-\text{CH}_3$ bend). **ESI-MS (m/z)** 247.19 ($\text{M} + \text{H}^+$), 269.17 ($\text{M} + \text{Na}^+$). **EA calculated for $\text{C}_{14}\text{H}_{22}\text{N}_4$ (%)** C, 68.26; H, 9.00; N, 22.74. **EA Found (%)** C, 68.33; H, 9.10; N, 22.52. See spectra on pages 70 and 71 of Appendix A — SPECTRA.

5.7.2 Crystal and molecular structure of free 5,5'-di-*tert*-butyl-1*H*,1'*H*-3,3'-bipyrazole (**16**)

The asymmetric unit cell contains one half of ligand **16** (Figure 5.12). The ligand crystallised in the tetragonal crystal system, space group $I4_1/a$. The crystallographic data and structure refinement details are summarised in Table 5.3 at the end of this sub-section. The complete molecular structure of free 5,5'-di-*tert*-butyl-1*H*,1'*H*-3,3'-bipyrazole (**16**) is shown in Figure 5.13. It was interesting to note that the two pyrazolyl moieties of

ligand **16** were arranged in a “trans” fashion, ensuring the inner *N*-atoms are at their maximum distances from each other, which energetically-speaking, is its most stable and preferred conformation.

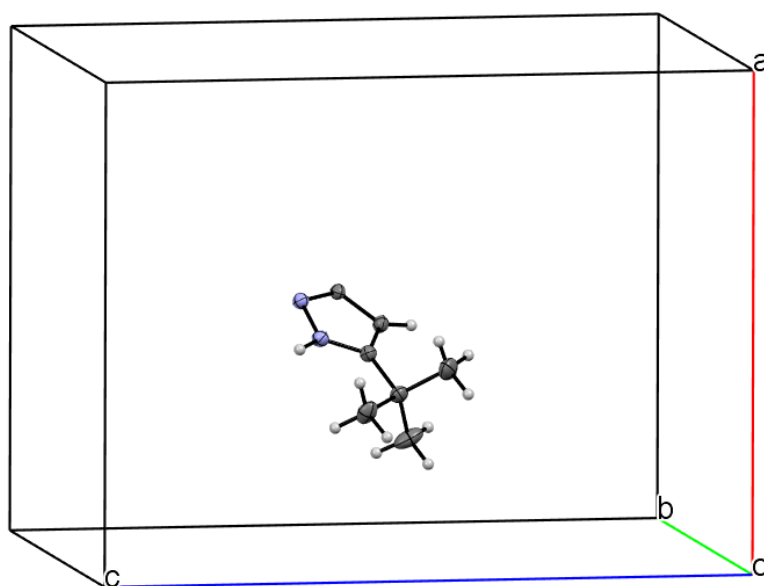


Figure 5.12: Asymmetric unit cell diagram of free 5,5'-di-*tert*-butyl-1*H*,1'*H*-3,3'-bipyrazole (50% thermal ellipsoids).

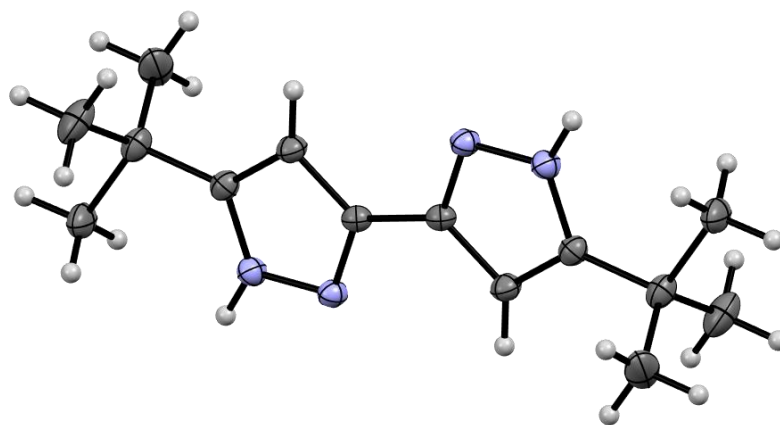


Figure 5.13: ORTEP diagram of free 5,5'-di-*tert*-butyl-1*H*,1'*H*-3,3'-bipyrazole (50% thermal ellipsoids).

A total of sixteen symmetry elements were present in the packing of this crystal lattice (**Figure 5.14**): an identity, a two-fold screw axis (green), four four-fold screw axes (red), a two-fold rotation axis (green), two inversion centres (yellow), four four-fold rotoinversion axes (red), a centring vector and two glide planes (purple). See **Table 5.2** for more detailed information regarding the symmetry elements and operators.

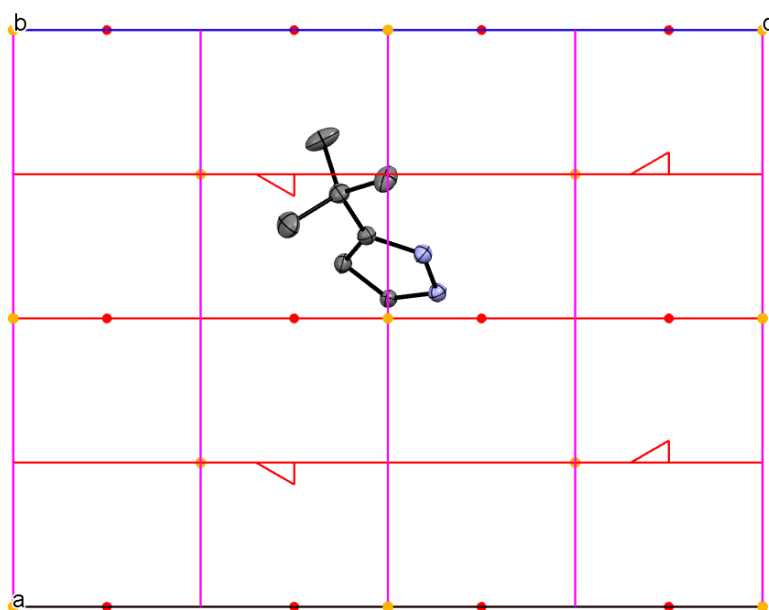


Figure 5.14: Symmetry elements present in the asymmetric unit cell along the b-axis. Hydrogen atoms omitted for clarity. [Complimentary to **Table 5.2** below]

Table 5.2: Crystallographic symmetry elements and operators of free 5,5'-di-*tert*-butyl-1*H*,1'*H*-3,3'-bipyrazole (16). [Complimentary to **Figure 5.14** above]

#	Colour	Symmetry operation	Description	Order	Type
1	–	x, y, z	Identity	1	1
2	Red	$\frac{3}{4}-y, \frac{1}{4}+x, \frac{1}{4}+z$	Screw axis (4-fold)	4	4
3	Green	$-x, \frac{1}{2}-y, z$	Rotation axis (2-fold)	2	2
4	Red	$\frac{1}{4}+y, \frac{1}{4}-x, \frac{1}{4}+z$	Screw axis (4-fold)	4	4
5	–	$\frac{1}{2}+x, \frac{1}{2}+y, \frac{1}{2}+z$	Centring vector	1	1
6	Red	$\frac{1}{4}-y, \frac{3}{4}+x, \frac{3}{4}+z$	Screw axis (4-fold)	4	4
7	Green	$\frac{1}{2}-x, -y, \frac{1}{2}+z$	Screw axis (2-fold)	2	2
8	Red	$\frac{3}{4}+y, \frac{3}{4}-x, \frac{3}{4}+z$	Screw axis (4-fold)	4	4
9	Yellow	$-x, -y, -z$	Inversion centre	2	-1
10	Red	$\frac{1}{4}+y, \frac{3}{4}-x, \frac{3}{4}-z$	Rotoinversion axis (4-fold)	4	-4
11	Purple	$x, \frac{1}{2}+y, -z$	Glide plane	2	-2
12	Red	$\frac{3}{4}-y, \frac{3}{4}+x, \frac{3}{4}-z$	Rotoinversion axis (4-fold)	4	-4
13	Yellow	$\frac{1}{2}-x, \frac{1}{2}-y, \frac{1}{2}-z$	Inversion centre	2	-1
14	Red	$\frac{3}{4}+y, \frac{1}{4}-x, \frac{1}{4}-z$	Rotoinversion axis (4-fold)	4	-4
15	Purple	$\frac{1}{2}+x, y, \frac{1}{2}-z$	Glide plane	2	-2
16	Red	$\frac{1}{4}-y, \frac{1}{4}+x, \frac{1}{4}-z$	Rotoinversion axis (4-fold)	4	-4

The fact that this ligand was incredibly difficult to dissolve by means of common laboratory solvents only became clear now, with the presence of intermolecular hydrogen bonds in the free ligand crystal structure (**Figure 5.15**). This finding confirmed our speculation in **Section 5.4.3** (see **Scheme 2.26** in **CHAPTER 2** as well).

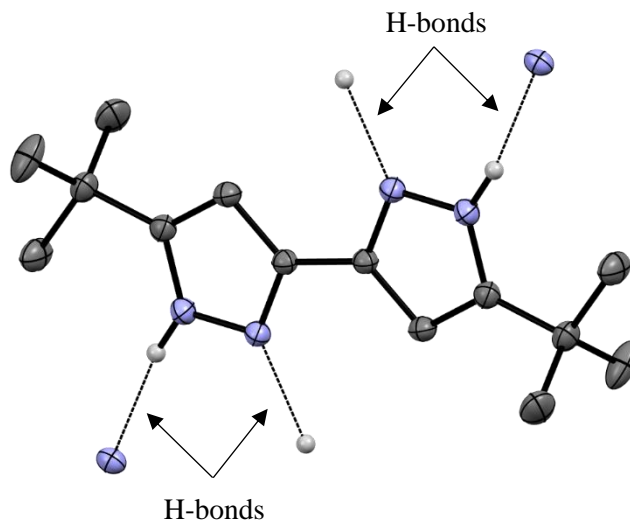


Figure 5.15: ORTEP diagram of free 5,5'-di-*tert*-butyl-1*H*,1'*H*-3,3'-bipyrazole (**16**) revealing a network of intermolecular hydrogen bonds (50% thermal ellipsoids). Only relevant hydrogens shown for clarity.

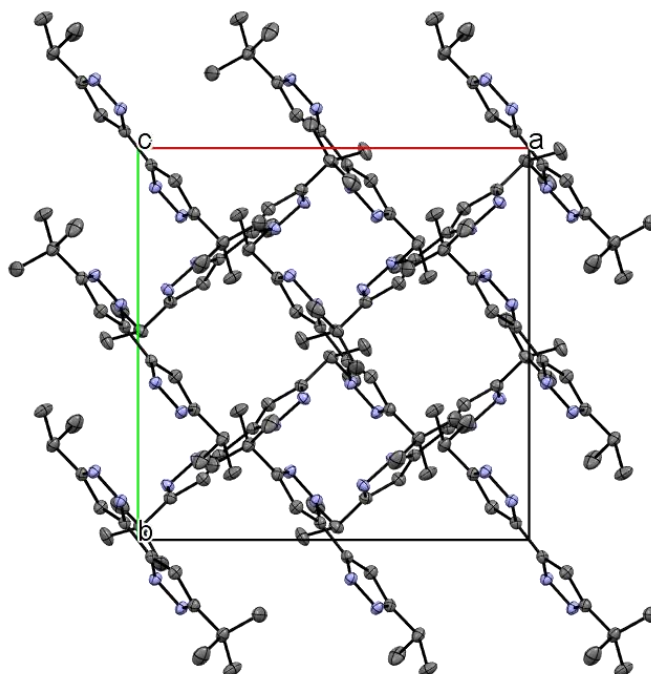


Figure 5.16: Packing diagram of free 5,5'-di-*tert*-butyl-1*H*,1'*H*-3,3'-bipyrazole (**16**) along the *c*-axis (50% thermal ellipsoids). Hydrogen atoms omitted for clarity.

Table 5.3: Crystallographic data and structure refinement of 5,5'-di-*tert*-butyl-1*H*,1'*H*-3,3'-bipyrazole (**16**).

Compound	5,5'-di- <i>tert</i> -butyl-1 <i>H</i> ,1' <i>H</i> -3,3'-bipyrazole
Empirical formula	C ₁₄ H ₂₂ N ₄
M _r (g.mol ⁻¹)	246.35
Temperature (K)	100(2)
Instrument	<i>Bruker APEX II DUO CCD</i>
Crystal habit	Block
Crystal dimensions (mm)	0.194 × 0.183 × 0.173
Crystal system	Tetragonal
Space group (number)	I 4 ₁ /a (88)
a (Å)	13.1226(9)
b (Å)	13.1226(9)
c (Å)	17.0412(12)
α (°)	90
β (°)	90
γ (°)	90
μ (MoKα) (mm ⁻¹)	0.069
V (Å ³)	2934.54
Z, D _c (M, g.m ⁻³)	8, 1.115
Index ranges	-17 ≤ h ≤ 17, -17 ≤ k ≤ 15, -22 ≤ l ≤ 22
Reflections collected	17535
Independent reflections	3324
Absorption correction	Multi-scan
Refinement method	Full matrix least squares on <i>F</i> ²
Data/restraints/parameters	1830/0/120
F(000)	1072
R (reflections) R ₁ , wR ₂	0.0465, 0.1386
Goodness of fit on <i>F</i> ²	1.062

5.7.3 Preparation of the crystalline [Ni₂(H₂O)₂(L15)₄(SO₄)·(naphth-SO₃)₂] assembly

A 25 mL round-bottom flask was charged with 2-naphthalenesulfonic acid (83.6 mg, 401 μmol), NiSO₄·6H₂O (35.0 mg, 133 μmol) and previously synthesised 2-(5-(*tert*-butyl)-1*H*-pyrazol-3-yl)pyridine (**15**) (80.5 mg, 400 μmol). These combined solids were subsequently dissolved in 10 mL absolute ethanol and refluxed for 2 hours. The hot ethanolic solution was filtered to rid the light blue solution of any remaining solid impurities. Thereafter, the filtrate was quantitatively transferred to a 25 mL glass vial (with perforated plastic stopper) and allowed to undergo slow evaporation under ambient conditions. After 4 days, royal blue crystals were noticed on the sides of the glass vial. A suitable crystal was selected and submitted for X-ray analysis.

FT-IR (ATR, cm^{-1}) 3066 (aromatic C–H str), 2960 (aliphatic C–H str), 1608 (pyridine C=N str), 1576 (pyrazole C=N str), 1367 (asymmetric S=O str), 1153 (symmetric S=O str). **ESI-MS (m/z)** 202.13 ($\text{C}_{12}\text{H}_{15}\text{N}_3 + \text{H}$)⁺, 230.09 $[\text{Ni}(\text{C}_{12}\text{H}_{15}\text{N}_3)_2]^{2+}$, 330.66 $[\text{Ni}(\text{C}_{12}\text{H}_{15}\text{N}_3)_3]^{2+}$, 459.18 $\{[\text{Ni}(\text{C}_{24}\text{H}_{29}\text{N}_6)]_2\}^{2+}$, 660.31 $[\text{Ni}(\text{C}_{12}\text{H}_{14}\text{N}_3)(\text{C}_{12}\text{H}_{15}\text{N}_3)_2]^+$, 667.20 $[\text{Ni}(\text{C}_{12}\text{H}_{15}\text{N}_3)_2\cdot\text{naphth-SO}_3^-]^+$, 868.33 $[\text{Ni}(\text{C}_{12}\text{H}_{15}\text{N}_3)_3\cdot\text{naphth-SO}_3^-]^+$. **EA calculated for $\text{C}_{68}\text{H}_{78}\text{N}_{12}\text{Ni}_2\text{O}_{12}\text{S}_3$ (%)** C, 55.60; H, 5.35; N, 11.44; S, 6.55. **EA Found (%)** C, 55.91; H, 5.50; N, 11.23; S, 7.02. See spectra on pages 99 and 100 of *Appendix A — SPECTRA*.

5.7.4 Crystal and molecular structure of the $[\text{Ni}_2(\text{H}_2\text{O})_2(\text{L15})_4(\text{SO}_4)\cdot(\text{naphth-SO}_3)_2]$ assembly

The asymmetric unit cell contains a complete complex assembly (**Figure 5.17**). The complex crystallised in the monoclinic crystal system, space group $\text{P}2_1/\text{c}$. The crystallographic data and structure refinement details are summarised in **Table 5.6** at the end of this sub-section. The ORTEP diagram (in “depth cue” mode) of the complete complex assembly is shown in **Figure 5.18**, with two naphthalene sulfonic acid molecules clearly part of the outer coordination sphere, *i.e.*, they are not directly bonded to nickel(II). This interesting sulfate-bridged complex contains two nickel “sub-complexes” on opposite ends of the SO_4^{2-} anion. Each nickel “sub-complex” consists of two ligand **15** molecules, one water molecule and the centralised sulfate anion.

The molecular structure of one half of the complex assembly with appropriate atom numbering is shown in **Figure 5.19**, with selected bond lengths and angles listed in **Table 5.4**. The ligands of each “sub-complex” are coordinated in a distorted octahedral fashion.

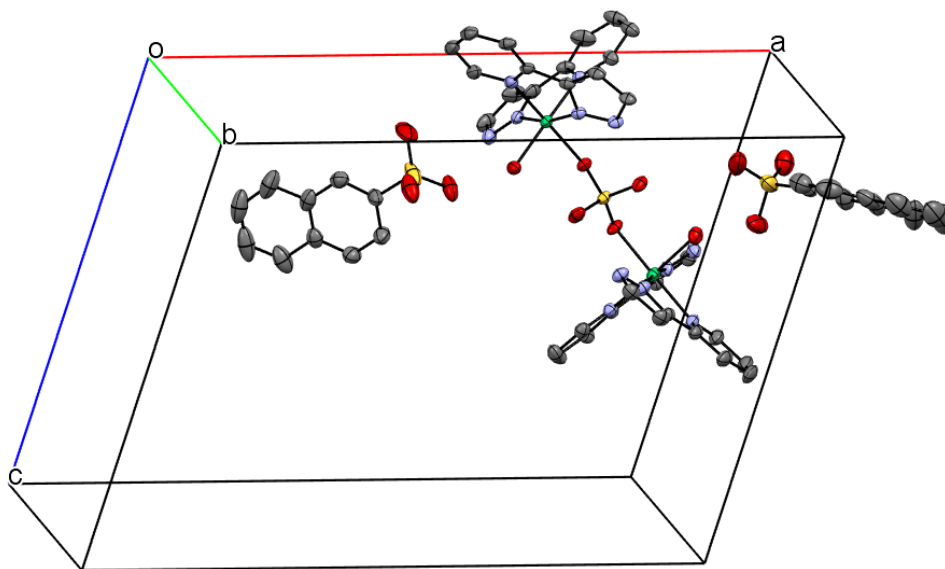


Figure 5.17: Asymmetric unit cell diagram of the $[\text{Ni}_2(\text{H}_2\text{O})_2(\text{L15})_4(\text{SO}_4)\cdot(\text{naphth-SO}_3)_2]$ complex (50% thermal ellipsoids). Hydrogen atoms and *tert*-butyl moieties omitted for clarity.

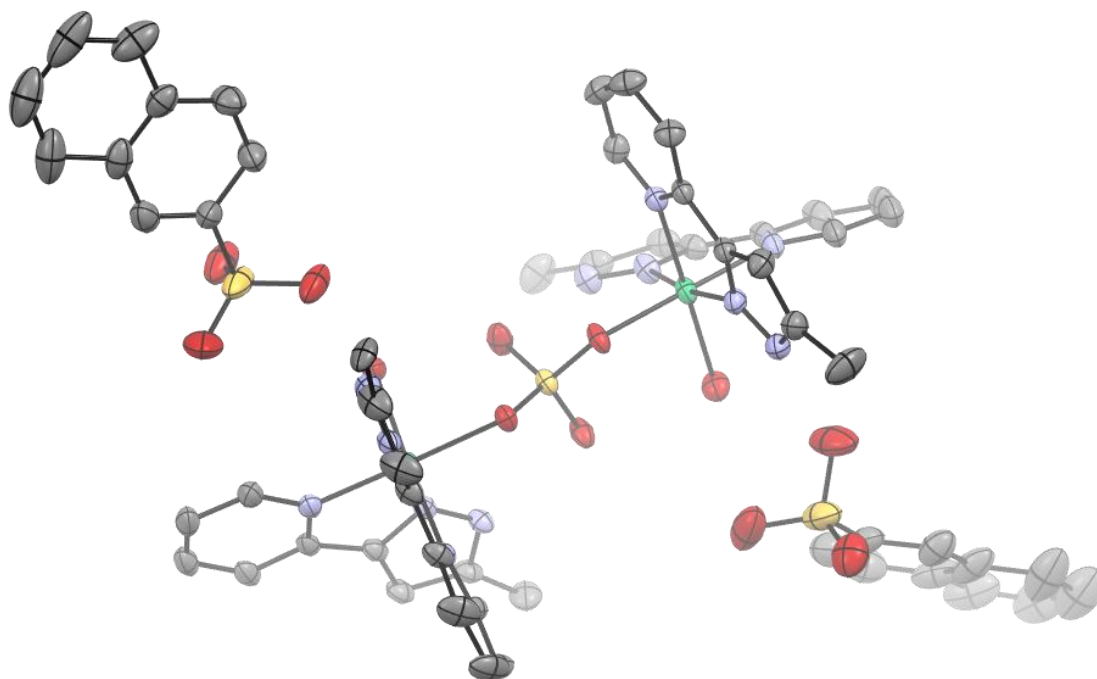


Figure 5.18: ORTEP diagram of the $[\text{Ni}_2(\text{H}_2\text{O})_2(\text{L15})_4(\text{SO}_4)\cdot(\text{naphth-SO}_3)_2]$ complex in “depth cue” mode (50% thermal ellipsoids). Hydrogen atoms and *tert*-butyl moieties omitted for clarity.

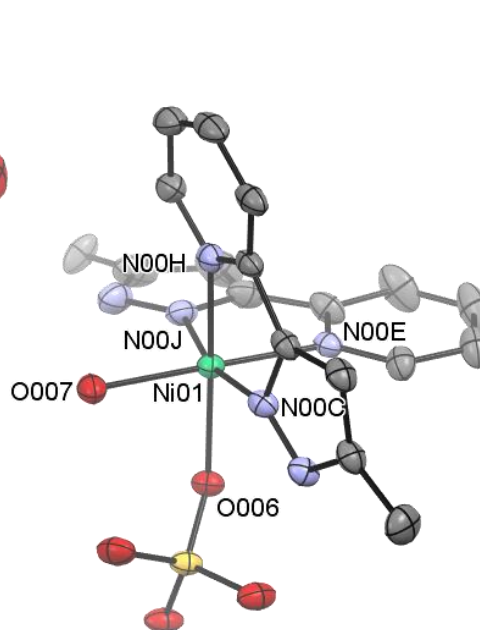


Figure 5.19: ORTEP diagram with selected labels of one half of the $[\text{Ni}_2(\text{H}_2\text{O})_2(\text{L15})_4(\text{SO}_4)\cdot(\text{naphth-SO}_3)_2]$ complex in “depth cue” mode (50% thermal ellipsoids). H-atoms and *tert*-butyl moieties omitted for clarity.

Table 5.4: Selected bond lengths and angles for the $[\text{Ni}_2(\text{H}_2\text{O})_2(\text{L15})_4(\text{SO}_4)\cdot(\text{naphth-SO}_3)_2]$ complex.

Bond lengths (Å)		Bond angles (°)	
Ni01–N00C	2.041(3)	O006–Ni01–O007	86.6(1)
Ni01–N00E	2.120(3)	O006–Ni01–N00C	94.7(1)
Ni01–N00H	2.105(3)	O006–Ni01–N00E	90.6(1)
Ni01–N00J	2.063(4)	O006–Ni01–N00J	91.1(1)
Ni01–O006	2.094(2)	O006–Ni01–N00H	170.7(1)
Ni01–O007	2.077(3)	O007–Ni01–N00C	94.2(1)
		O007–Ni01–N00E	174.7(1)
		O007–Ni01–N00H	88.9(1)
		O007–Ni01–N00J	97.6(1)
		N00C–Ni01–N00E	90.4(1)
		N00C–Ni01–N00H	77.6(1)
		N00C–Ni01–N00J	167.1(1)
		N00E–Ni01–N00H	94.5(1)
		N00E–Ni01–N00J	78.0(1)
		N00H–Ni01–N00J	97.5(1)

The pyridyl and pyrazolyl *N*-donor atoms (N00H and N00C), along with atoms C00P, C00T and Ni01 formed a 5-membered chelate ring. The bond lengths and angles were compared to those of ethylenediamine (EN) in its least strained conformation when coordinated to a large metal ion (**Figure 5.20**).

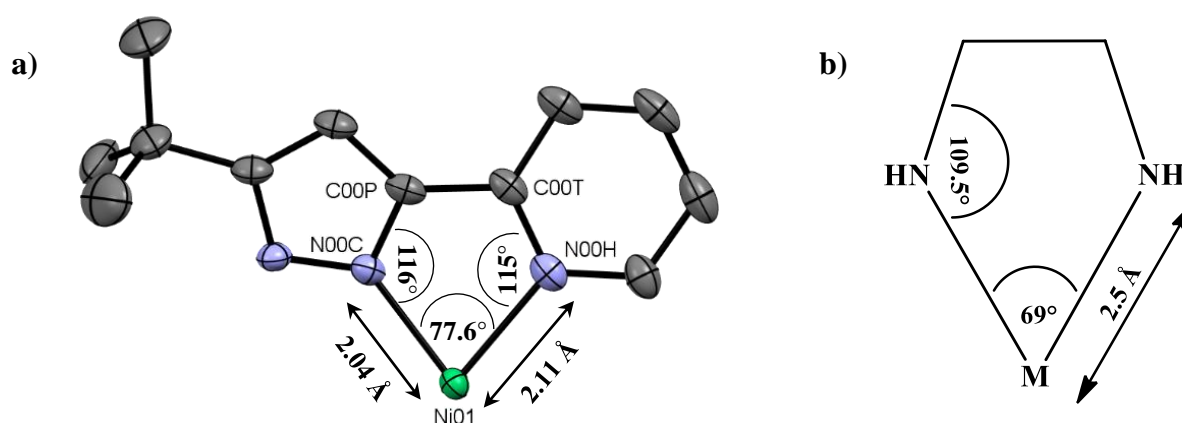


Figure 5.20: Bond lengths and angles of the 5-membered chelate ring present in a) $[\text{Ni}_2(\text{H}_2\text{O})_2(\text{L15})_4(\text{SO}_4)\cdot(\text{naphth-SO}_3)_2]$ and b) the minimum strain conformation of ethylenediamine (EN). [Redrawn from Hancock¹⁷]

The C–N–Ni bond angles of the pyridine-pyrazolyl complex (**Figure 5.20a**) are slightly larger (115 and 116°) than the idealised bond angles of ethylenediamine (109.5°), which was surprising since the N–Ni–N bond angle enlarged to 77.6°.¹⁸ Additionally, the Ni–N bond lengths were much shorter (2.04 and 2.11 Å) than the M–N bond length of ethylenediamine (2.5 Å).¹⁸ This indicates that strong coordination bonds have formed between the pyridyl and pyrazolyl *N*-donor atoms and Ni01, which in turn forced the bond angles to be slightly larger compared to the idealised bond angles of ethylenediamine. Moreover, the bond angles and lengths of the pyridine-pyrazolyl complex accommodates a smaller nickel(II) ion more efficiently, while the bond lengths and angles of ethylenediamine are better suited to fit larger metal ions. It should be noted, however, that the C–N bonds of the pyridine-pyrazolyl complex have double bond character, while the C–N bonds of ethylenediamine merely have single bond character.

In this investigation, the average Ni–N bond distance was 2.08 Å. The average Ni–N bond distances reported by Roebuck *et al.*,⁵ Zhilina *et al.*¹⁹ and Henkelis *et al.*²⁰ for similar complexes were 2.09, 1.98 and 2.04 Å, respectively. In this study, the N–Ni–N bond angle—also referred to as the “bite angle”—was 77.6° and accords well with the average bond angles of 78.31, 79.35 and 78.52° as reported by the aforementioned authors, respectively. This shows these findings to be in the same “ballpark” as those found in the literature.

A total of four symmetry elements are present in the packing of this crystal lattice (**Figure 5.21**): an identity, a two-fold screw axis (green), an inversion centre (yellow) and a glide plane (purple). See **Table 5.5** for more detailed information regarding the symmetry elements and operators.

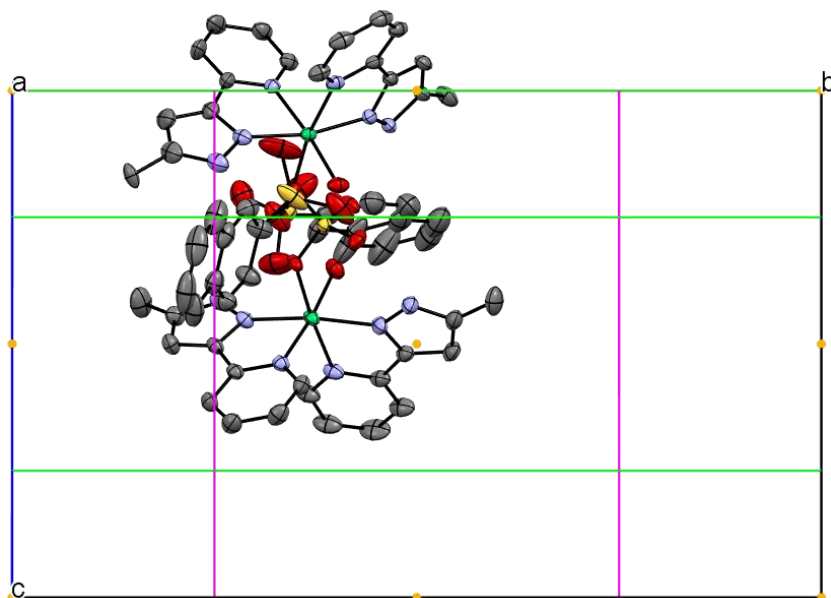


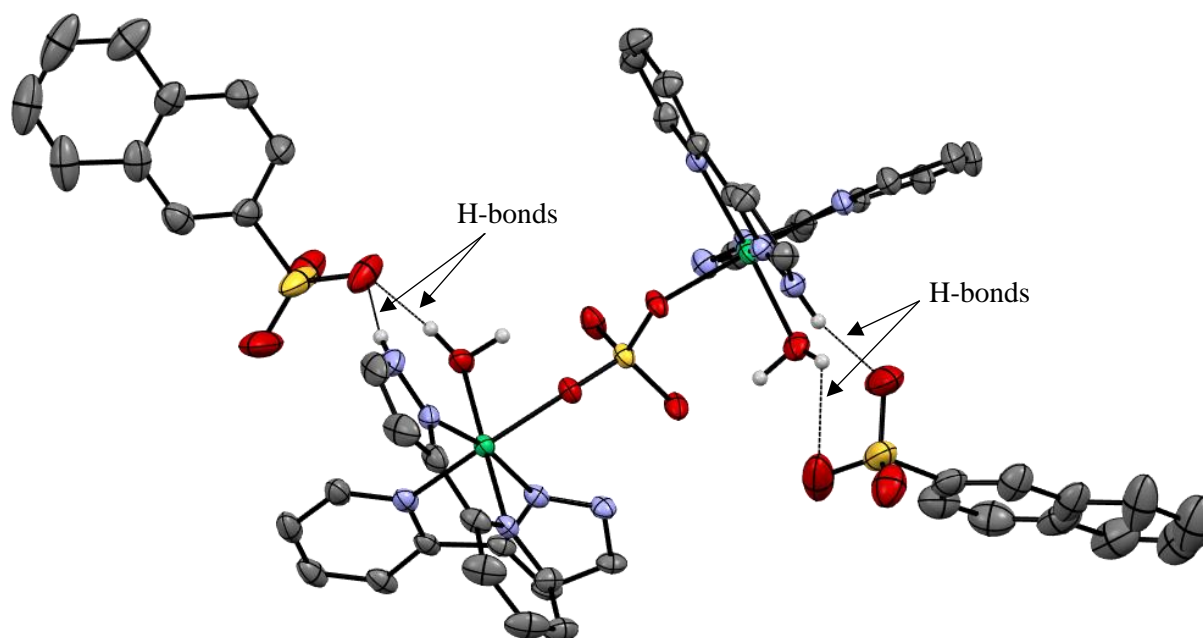
Figure 5.21: Symmetry elements present in an asymmetric unit cell along the a-axis. Hydrogen atoms and *tert*-butyl moieties omitted for clarity. [Complimentary to **Table 5.5**]

Table 5.5: Crystallographic symmetry elements and operators of the complex, $[\text{Ni}_2(\text{H}_2\text{O})_2(\text{L15})_4(\text{SO}_4)\cdot(\text{naphth-SO}_3)_2]$. [Complimentary to **Figure 5.21**]

#	Colour	Symmetry operation	Description	Order	Type
1	–	x, y, z	Identity	1	1
2	Green	$-x, \frac{1}{2}+y, \frac{1}{2}-z$	Screw axis (2-fold)	2	2
3	Yellow	$-x, -y, -z$	Inversion centre	2	-1
4	Purple	$x, \frac{1}{2}-y, \frac{1}{2}+z$	Glide plane	2	-2

The crystal assembly is stabilised by a network of outer coordination sphere hydrogen bonds (**Figure 5.22**). This involves two peripheral naphth-SO₃ molecules, two coordinated water molecules and two pyrazole-pyridinyl ligands (**15**). This result accords well with work done by Roebuck *et al.*,⁵ showing that the naphth-SO₃ molecules do not coordinate directly to nickel(II) (inner coordination sphere), but rather stabilises the assembly peripherally (see **Figure 5.2**). Interestingly, in stark contrast to Roebuck and co-worker's⁵ result, this crystal assembly does not display hydrogen bonds to every available pyrazolyl N–H moiety, but merely displays the presence of a hydrogen bond to one pyrazolyl N–H moiety per “sub-complex”.

This is a tremendous result that strengthens the case for outer-sphere synergistic stabilisers, something that has been blindly accepted by the academic fraternity over the past few decades. Now, mounting evidence suggests that this “blind faith” has duly been justified.

**Figure 5.22:** ORTEP diagram of the $[\text{Ni}_2(\text{H}_2\text{O})_2(\text{L15})_4(\text{SO}_4)\cdot(\text{naphth-SO}_3)_2]$ complex revealing intermolecular hydrogen bonds (50% thermal ellipsoids). Only relevant hydrogens shown for clarity.

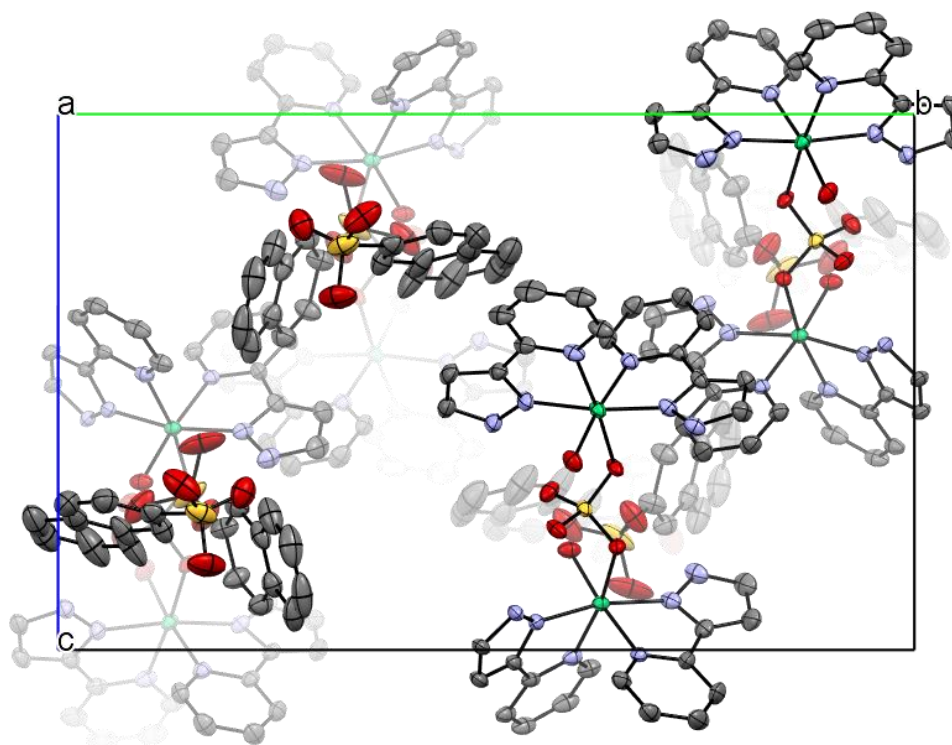


Figure 5.23: Packing diagram of the $[\text{Ni}_2(\text{H}_2\text{O})_2(\text{L15})_4(\text{SO}_4)\cdot(\text{naphth-SO}_3)_2]$ complex along the a-axis in “depth cue” mode (50% thermal ellipsoids). Hydrogen atoms and *tert*-butyl moieties omitted for clarity.

Table 5.6: Crystallographic data and structure refinement of the $[\text{Ni}_2(\text{H}_2\text{O})_2(\text{L15})_4(\text{SO}_4)\cdot(\text{naphth-SO}_3)_2]$ complex.

Compound	$[\text{Ni}_2(\text{H}_2\text{O})_2(\text{C}_{12}\text{H}_{15}\text{N}_3)_4(\text{SO}_4)\cdot(\text{naphth-SO}_3)_2]$
Empirical formula	$\text{C}_{68}\text{H}_{78}\text{N}_{12}\text{Ni}_2\text{O}_{12}\text{S}_3$
M_r ($\text{g}\cdot\text{mol}^{-1}$)	1469.02
Temperature (K)	100(2)
Instrument	<i>Bruker APEX II DUO CCD</i>
Crystal habit	Shard
Crystal dimensions (mm)	$0.30 \times 0.174 \times 0.088$
Crystal system	Monoclinic
Space group (number)	$P 2_1/c$ (14)
a (Å)	21.2817(17)
b (Å)	23.2855(19)
c (Å)	15.3060(12)
α (°)	90
β (°)	108.0430(10)
γ (°)	90

Table continues...

Compound	[Ni ₂ (H ₂ O) ₂ (C ₁₂ H ₁₅ N ₃) ₄ (SO ₄)·(naphth-SO ₃) ₂]
μ (MoK α) (mm ⁻¹)	0.676
V (Å ³)	7212.0(10)
Z, Dc (M, g.m ⁻³)	4, 1.353
Index ranges	-28 ≤ h ≤ 28, -31 ≤ k ≤ 31, -20 ≤ l ≤ 20
Reflections collected	17968
Independent reflections	9318
Absorption correction	Multi-scan
Refinement method	Full matrix least squares on F ²
Data/restraints/parameters	17968/64/958
F(000)	3080
R (reflections) R1, wR2	0.0761, 0.1798
Goodness of fit on F ²	1.119

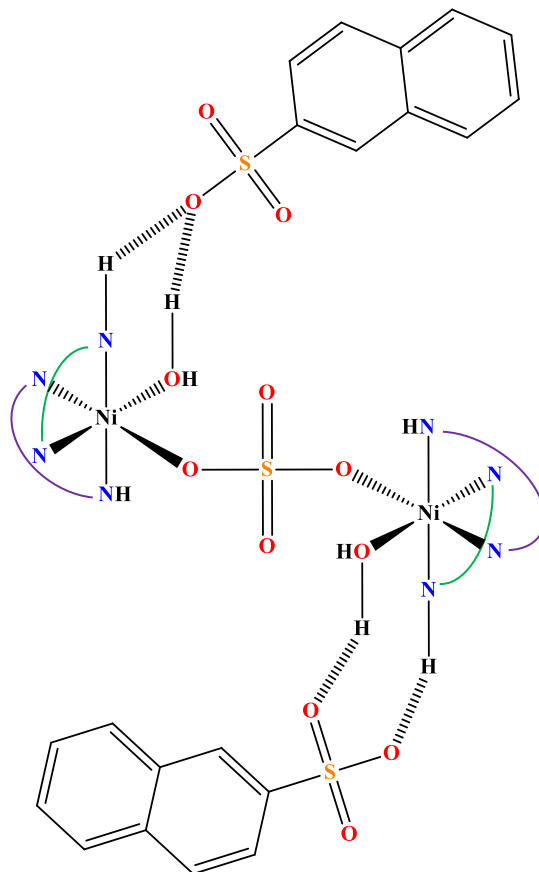
5.8 Conclusions

The syntheses of ligands **13–16** were generally straightforward and resulted in pure product. The yields of *N*-heterocyclic ligands **15** and **16** were particularly low and forced multiple small-scale syntheses—often taking weeks to obtain enough product to execute numerous solvent extraction and crystallographic experiments. The most challenging aspect, by far, turned out to be the exceptionally poor solubility of bipyrazolyl ligand **16**. This was partially overcome by running ¹H and ¹³C NMR experiments in DMSO-d₆ at 100 °C. However, due to miscibility reasons, solvent extraction studies were not possible in a monophasic aqueous/DMSO system, since the very nature of such studies require, at the very least, an immiscible biphasic system. Therefore, ligand **16**'s extraction ability was only probed in the presence of the sulfonic acid synergist (**SA**). Only this synergist was able to disturb the strong intermolecular hydrogen bonds, allowing it to go into solution.

All-in-all, it seemed as if only **SA** managed to complement ligands **13–16** in their nickel(II) extractive abilities. Both the carboxylic acid (**CA**) and phosphinic acid (**PA**) synergists performed poorly in the presence of ligands **13–16**, which can partly be attributed to the lack of an aromatic torso in their structural makeup. This naphthalene moiety present in **SA** somehow compliments the aromatic and *N*-heterocyclic ligands. This can similarly be explained by the way in which polar solvents effectively dissolve analogous polar solid materials (“like dissolves like”). The synergistic combination of ligand **15** and **SA** yielded the most effective extraction of nickel(II), with 92 (± 0.5)%. This was a remarkable result and deserves additional investigation regarding its metal ion recovery ability (not performed in this study). It will reveal whether this synergistic combination is both an effective and efficient nickel(II) extraction system.

Lastly, two quality crystals for X-ray diffraction analyses were grown via slow evaporation. First, a colourless crystal of free 5,5'-di-*tert*-butyl-1*H*,1'*H*-3,3'-bipyrazole (**16**), which revealed a network of hydrogen bonds that

experimentally explained this ligand's poor solubility. Secondly, an exciting sulfate-bridged (Ni–SO₄–Ni) complex was obtained, clearly showing two naphtha-SO₃ molecules present in the outer coordination sphere. These molecules provided stabilisation in the form of hydrogen bonds to either coordinated water molecules or N–H moieties present in ligand **15**. Schematically-speaking, this complex can be illustrated as follows:



Scheme 5.9: Schematic representation of the $[\text{Ni}_2(\text{H}_2\text{O})_2(\text{L15})_4(\text{SO}_4)\cdot(\text{naphth-SO}_3)_2]$ complex.

Although similar starting materials to that of Roebuck *et al.*⁵ were implemented in the synthesis of this unique complex, a very different result was obtained. These authors reported a solitary nickel(II) centre coordinated by three 2-(5-(*tert*-butyl)-1*H*-pyrazol-3-yl)pyridine (**15**) molecules, yet they too reported naphtha-SO₃ molecules acting as H-bond stabilisers in the outer coordination sphere.

Finally, a statement by Roebuck *et al.*⁵ revealed the importance and relevance of solid vs. liquid state studies, something one should continually be mindful of:

“The structural information on the model synergistic assembly discussed above, despite being obtained in the solid state, provides some relevant insight into the factors that might influence the stability of assemblies formed in water-immiscible solvents during extraction experiments. However, the utmost of care must be taken when relating this data to that of solution-based extraction studies.”

5.9 References

- (1) Zhu, S.; Hu, H.; Hu, J.; Li, J.; Hu, F.; Wang, Y. Structural insights into the coordination and extraction mechanism of nickel(II) with dinonylnaphthalene sulfonic acid and *n*-hexyl 3-pyridinecarboxylate ester as extractants. *J. Chinese Chem. Soc.* **2017**, *64* (11), 1294–1302.
- (2) Li, J.; Hu, H.; Zhu, S.; Hu, F.; Wang, Y. The coordination structure of the extracted nickel(II) complex with a synergistic mixture containing dinonylnaphthalene sulfonic acid and 2-ethylhexyl 4-pyridinecarboxylate ester. *Dalton Trans.* **2017**, *46* (4), 1075–1082.
- (3) Hu, F.; Hu, H.; Luo, Y.; Wang, Y.; Yang, J.; Hu, J. The separation of Ni(II) over base metal ions in acidic polymetallic medium: Synergistic extraction and structural evidence. *Hydrometallurgy* **2018**, *181*, 240–247.
- (4) Hu, F.; Hu, H.; Hu, J.; Zhu, S.; Yang, J.; Wang, Y. Improving selective separation of Cu(II) from acidic polymetallic media with 2-ethylhexyl 4-pyridinecarboxylate ester: Extraction behaviors, coordination structure and microscopic mechanism. *J. Mol. Liq.* **2017**, *248*, 1050–1058.
- (5) Roebuck, J.; Bailey, P.; Doidge, E.; Fischmann, A.; Healy, M.; Nichol, G.; O'Toole, N.; Pelsler, M.; Sassi, T.; Sole, K.; *et al.* Strong and selective Ni(II) extractants based on synergistic mixtures of sulfonic acids and bidentate *N*-heterocycles. *Solvent Extr. Ion Exch.* **2018**, *36* (05), 1–22.
- (6) Barnard, K.; Shiers, D.; Kelly, N.; Lombardo, D. Synthesis of a *t*- α -hydroxy oxime and its synergistic behavior with Versatic 10. *Solvent Extr. Ion Exch.* **2015**, *33* (2), 166–182.
- (7) Satake, A.; Nakata, T. Novel η^3 -allylpalladium-pyridinylpyrazole complex: Synthesis, reactivity, and catalytic activity for cyclopropanation of ketene silyl acetal with allylic acetates. *J. Am. Chem. Soc.* **1998**, *120* (40).
- (8) Bouabdallah, I.; Ramdani, A.; Zidane, I.; Touzani, R.; Eddike, D.; Radi, S.; Haidoux, A. Regioselective synthesis and crystal structure of 1,1'-dibenzyl-5,5'-diisopropyl-3,3'-bipyrazole. *Moroccan J. Heterocycl. Chem.* **2004**, *3* (1), 39–44.
- (9) Shironina, T.; Igidov, N.; Koz'minykh, E.; Kon'shina, L.; Kasatkina, Y.; Koz'minykh, V. 1,3,4,6-Tetracarbonyl compounds: IV. Reaction of 3,4-dihydroxy-2,4-hexadiene-1,6-diones with hydrazine and arylhydrazines. *Russ. J. Org. Chem.* **2001**, *37* (10), 1486–1494.
- (10) Pearce, B.; Ogutu, H.; Luckay, R. Synthesis of pyrazole-based pyridine ligands and their use as extractants for nickel(II) and copper(II): Crystal structure of a copper(II)–ligand complex. *Eur. J. Inorg. Chem.* **2017**, *2017* (8).
- (11) Maryott, A.; Smith, E. *Table of Dielectric Constants of Pure Liquids*; U.S. Dept. Commerce, Natl. Bur. Standards Circ. 514: Washington, D.C., 1951.

- (12) Du Preez, J.; Postma, J.; Ravindran, S.; van Brecht, B. Nitrogen reagents in metal ion separation. Part 6. 2-(1'-Octylthiomethyl)pyridine as extractant for later 3d transition metal ions. *Solvent Extr. Ion Exch.* **1997**, *15* (1), 79–96.
- (13) Okewole, A.; Magwa, N.; Tshentu, Z. The separation of nickel(II) from base metal ions using 1-octyl-2-(2'-pyridyl)imidazole as extractant in a highly acidic sulfate medium. *Hydrometallurgy* **2012**, *121–124*.
- (14) Rydberg, J. *Solvent Extraction Principles and Practice*, 2nd Edition; Taylor & Francis Group, LLC: New York, 2004.
- (15) Zhang, P.; Inoue, K.; Tsuyama, H. Recovery of metal values from spent hydrodesulfurization catalysts by liquid-liquid extraction. *Energy & Fuels* **1995**, *9* (2), 231–239.
- (16) Du Preez, J. Recent advances in amines as separating agents for metal ions. *Solvent Extr. Ion Exch.* **2000**, *18* (4), 679.
- (17) Hancock, R. Molecular mechanics calculations and metal ion recognition. *Acc. Chem. Res.* **1990**, *23* (8), 253–257.
- (18) Martell, A.; Hancock, R. *Metal Complexes in Aqueous Solutions*; Fackler, J., Ed.; Plenum Press: New York, 1996.
- (19) Zhilina, E.; Chizhov, D.; Sidorov, A.; Aleksandrov, G.; Kiskin, M.; Slepukhin, P.; Fedin, M.; Starichenko, D.; Korolev, A.; Shvachko, Y.; *et al.* Neutral tetranuclear Cu(II) complex of 2,6-di(5-trifluoromethylpyrazol-3-yl)pyridine: Synthesis, characterization and its transformation with selected aza-ligands. *Polyhedron* **2013**, *53*, 122–131.
- (20) Henkelis, J.; Jones, L.; de Miranda, M.; Kilner, C.; Halcrow, M. Two heptacopper(II) disk complexes with a $[\text{Cu}_7(\mu_3\text{-OH})_4(\mu\text{-OR})_2]^{8+}$ core. *Inorg. Chem.* **2010**, *49* (23), 11127–11132.

CHAPTER 6

CHAPTER SUMMARIES, CONCLUDING REMARKS AND FUTURE WORK

6.1 Chapter summaries

CHAPTER 1 initially informed the reader of the historic provenance of extractive metallurgy, which involves the scientific disciplines of pyro-, electro- and hydrometallurgy. Important historical hydrometallurgical processes, such as the cyanidation- and Bayer processes, were mentioned with the focus on modern hydrometallurgical means of separating base metal ions. Strong emphases were placed on various cationic, anionic and solvating extractants and the roles they play within solvent extraction systems. This was followed by a detailed study on the design of ligands for the sole purpose of optimising ligand-metal compatibility. Numerous factors, such as the chelate effect and donor atom selection, were considered and investigated. This ultimately led to the core aim of this study—the selective separation of six base metal ions (Co^{2+} , Ni^{2+} , Cu^{2+} , Zn^{2+} , Cd^{2+} and Pb^{2+}) by means of pyrazole- and imidazole-pyridinyl ligands within a solvent extraction context.

CHAPTER 2 gave a comprehensive synthetic account of pyrazole- (**1–10**) and imidazole-pyridinyl (**11** and **12**) ligands, complete with appropriate IR, MS, EA, ^1H and ^{13}C NMR characterisations. The classic Claisen-Schmidt condensation and Knorr mechanisms were studied in an attempt to explain the formation of unwanted side-products, whereafter certain reaction conditions were modified to maximise yields. However, tedious and cumbersome purification techniques, such as silica-based gravitational column chromatography, were still necessary to obtain pure products. The imidazolyl ligands (**11** and **12**) were especially difficult to synthesise due to the parent ligand's poor solubility in most common laboratory solvents. This was eventually overcome by implementing a biphasic (H_2O /toluene) reaction setup containing either Et_3N or KOH as base in the presence of the phase-transfer catalyst, TBAB. Finally, for the first time the syntheses of 2,6-bis(5-pentyl-1*H*-pyrazol-3-yl)pyridine (**5**), 2,6-bis(5-heptyl-1*H*-pyrazol-3-yl)pyridine (**7**) and 2,6-bis(1-octylimidazol-2-yl)pyridine (**12**) were reported, which to the best of our knowledge are novel. The following ligands have been mentioned in the literature,^{1,2} yet no synthetic conditions or parameters were expounded on in any way. Therefore, these ligands are considered to be “pseudo-novel”: 2,6-bis(5-hexyl-1*H*pyrazol-3-yl)pyridine (**6**), 2,6-bis(5-octyl-1*H*-pyrazol-3-yl)pyridine (**8**) and 2,6-bis(1-butylimidazol-2-yl)pyridine (**11**).

CHAPTER 3 represented the bulk of the laboratory work done for this dissertation. First, the reader was introduced to tridentate aromatic *N*-donor ligands (**1–12**) for the sole purpose of selectively extracting base metal ions. The term “synergism” was also introduced and its significance in modern-day hydrometallurgy was explained. This led to the justification of the use of the sulfonic acid synergist, DBSA, in this investigation by referring to studies done by Flett,³ Okewole *et al.*,⁴ Osseo-Asare & Keeney⁵ and Roebuck *et al.*⁶ The general solvent extraction setup was described in great detail, followed by competitive extraction studies (Cu^{2+}

included). The data showed an obvious trend for the selective extraction of copper(II) by means of pyrazolyl-pyridine ligands, **1–8**, where the general percentage extraction (%*E*) of copper(II) was arranged in the following order:

$$\text{ligand } \mathbf{1} < \text{ligand } \mathbf{2} < \text{ligand } \mathbf{3} < \text{ligand } \mathbf{4} < \text{ligand } \mathbf{5} < \text{ligand } \mathbf{6} \approx \text{Ligand } \mathbf{7} \approx \text{ligand } \mathbf{8}$$

This trend was primarily attributed to the increase in alkyl chain length from ligand **1** (methyl) to ligand **8** (octyl). Another set of competitive extractions were executed in the absence of copper(II) and revealed nickel(II) to be the predominant second-most extractable species in solution. Selectivity studies showed that copper(II) was extracted in the mid- to high-80% range, even though the copper(II) concentration was decreased sixtyfold. Recovery of copper(II) by means of pyrazolyl ligands **1–8** was generally achieved in decreasing order from ligand **1** to **8**. Once again, this was related to their individual abilities to hold on to copper(II). This trend was largely replicated in the case of nickel(II) recovery as well, with the exception of ligands **6–8** exhibiting nickel(II) releasing abilities of ~90%. In addition to these studies, the reader was introduced to time-dependent and pH isotherm studies as well, which provided valuable information regarding the extractive abilities of the pyrazolyl and imidazolyl ligands by altering time in the former and pH in the latter. A large portion of this chapter was dedicated to Job's plots (via UV/Vis) and slope analyses (via ICP-OES) to ascertain ligand-to-metal stoichiometric ratios in solution. Most ligands, with the exception of ligand **1**, revealed 1:1 (L:Cu²⁺) ratios in solution. Pyrazolyl ligand **2** and imidazolyl ligand **12** also displayed L:M²⁺ stoichiometric ratios of 2:1 when coordinated to Co²⁺, Ni²⁺, Zn²⁺ and Cd²⁺ (Pb²⁺, 1:1). Lastly, this chapter closes with synergistic-related studies. The optimum synergist-to-nickel(II) ratio experimentally determined to be 1:1 due to the formation of emulsions at higher concentrations. Pyrazolyl ligands **6–8**, in conjunction with DBSA, exhibited nickel(II) synergistic gains of >10%. This result prompted the investigation of synergistic studies by means of the model synergist, *p*TSA. This synergist, in conjunction with pyrazolyl ligand **7**, exhibited remarkable synergistic gains of ~17% (4:1 *p*TSA:Ni²⁺ ratio). No real gains were observed for imidazolyl ligand **12** in the presence of *p*TSA.

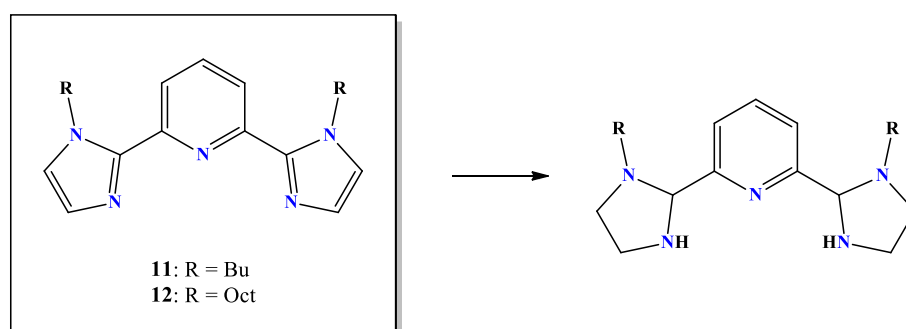
CHAPTER 4 presented and discussed the syntheses of eight base metal complexes. Ligands **2** (ethyl) and **9** (*tert*-butyl) were used as ligands due to their relatively short alkyl-pendant arms. Furthermore, crystal and molecular structures of two copper(II) complexes were prepared as well: [Cu(L**2**)₂](NO₃)₂ and [Cu(H₂O)₂(L**2**)]SO₄. Both complexes were prepared by reacting ligand **2** with the appropriate copper(II) salt in ethanol under refluxing conditions. Suitable crystals for X-ray diffraction analyses were obtained by means of slow evaporation and vapour diffusion. The octahedral [Cu(L**2**)₂](NO₃)₂ complex clearly showed two pyrazolyl molecules coordinated to the copper(II) centre, while the square pyramidal [Cu(H₂O)₂(L**2**)]SO₄ complex only revealed one pyrazolyl molecule coordinated to the metal centre. In both cases, hydrogen bonds appeared to be integral components in stabilising the overall complexes. These H-bonds operated through the pyrazolyl N–H moieties and might therefore explain why imidazolyl complexes were problematic to crystallise. Finally, three theoretical conjectures were put forward with regards to the “solution vs. solid state” debate swirling throughout the solvent extraction community.

CHAPTER 5 gave an account of nickel(II) extractions by means of aromatic oxime and bidentate pyrazolyl ligands in the presence of sulfonic-, carboxylic- and phosphinic acid synergists. The reader was walked through the syntheses of ligands **13** (oxime), **15** (pyrazole) and **16** (bispyrazole). Characterisation of ligand **16** was particularly challenging due to its poor solubility in most organic solvents. This was largely overcome by running ^1H and ^{13}C NMR analyses in DMSO-d_6 at 100°C . Ligands **13–16** and each of the three acid synergists' nickel(II) extractive abilities were individually determined. This was an essential necessity in order to ascertain the extractive abilities of the combined ligand-synergist systems. Only the sulfonic acid synergist, DNNSA, appeared to combine well in solution with ligands **13–16**, with nickel(II) extracted at $\sim 83\%$, $\sim 44\%$, $\sim 92\%$ and $\sim 80\%$, respectively. Additionally, pH isotherm studies were conducted as well. Unfortunately, the carboxylic- and phosphinic acid synergists performed poorly and was, in part, due to poor solubility in the toluene organic phase. This chapter was concluded with two crystal and molecular structures of free 5,5'-di-*tert*-butyl-1*H*,1'*H*-3,3'-bipyrazole (**16**) and the crystalline $[\text{Ni}_2(\text{H}_2\text{O})_2(\text{L15})_4(\text{SO}_4)(\text{naphth-SO}_3)_2]$ assembly. The free ligand structure clearly showed an extensive network of hydrogen bonds to neighbouring molecules, thereby supporting earlier assumptions made in this chapter. The $[\text{Ni}_2(\text{H}_2\text{O})_2(\text{L15})_4(\text{SO}_4)(\text{naphth-SO}_3)_2]$ assembly revealed an interesting sulfate-bridged complex with two distinct $\text{Ni}(\text{L15})_2$ centres stabilised via two peripheral naphtha- SO_3 molecules. This was a phenomenal finding that corroborated earlier postulations of SO_3 -type synergists merely acting as peripheral (outer coordination sphere) stabilisers via hydrogen bonds.

6.2 Suggested future work

6.2.1 Structural modifications to enhance metal ion extractability

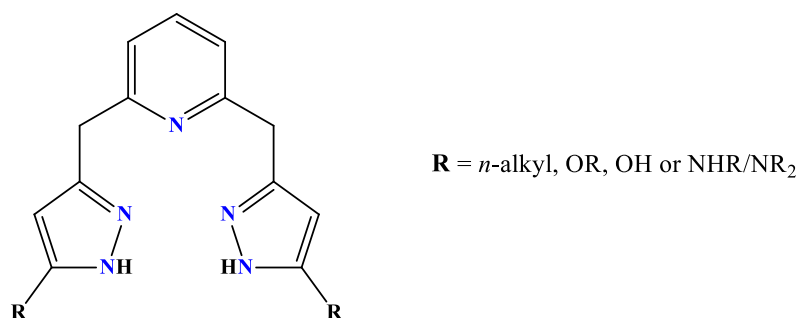
Upon observing the excellent copper(II) extraction results for pyrazolyl ligands **3–10**, structural modifications of imidazolyl ligands **11** and **12** are highly encouraged. Alterations should include the incorporation of an acidic/labile proton as this is likely to increase base metal extraction (**Scheme 6.1**). It must be taken into account, however, that the inclusion of such a N–H proton will strip the imidazolyl moieties of their aromaticity, resulting in the formation of non-flat sp^3 -hybridised imidazolidine moieties containing single bonds that allows the structure more flexibility. The loss of aromaticity might have a negative impact on the extractive ability of these ligands, yet still merits further investigation none the less.



Scheme 6.1: Modification of tridentate imidazolyl ligands **11** and **12** to include acidic protons to strengthen the overall coordination assembly in solution via hydrogen bonds.

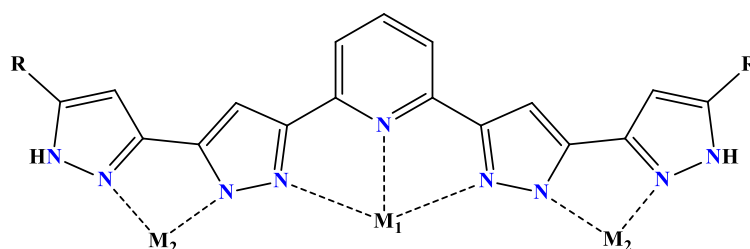
In general, pyrazolyl ligands **1–8** showed that an increase in the *n*-alkyl pendant arm length increases the percentage extraction (%*E*) of nickel(II), with the exception of ligands **6–8**. As purported in **CHAPTER 3**, this might be due to steric interference and therefore these *n*-alkyl arms should be substituted with branched alkyl pendant arms. This will shorten the pendant arms' reach while still retaining 6–8 carbons. Moreover, these hydrophobic alkyl arms may also be altered in terms of their position on the imidazolyl moieties in an attempt to determine the effect it might have on the extractive ability of these ligands.

In 2006, Bouabdallah *et al.*⁷ reported the extraction of copper(II) by means of tripodal *N*-donor pyrazolyl ligands. By following their lead, pyrazolyl ligands **1–8** can structurally be modified to incorporate methylene (–CH₂–) groups between the pyrazolyl and pyridinyl moieties (**Scheme 6.2**). This will grant much needed flexibility to the structure and possibly allow coordination to cobalt(II), zinc(II) or cadmium(II) as well. Strong alkyl electron donating moieties must be maintained, though, with possible expansion to alcohols (–OH), ethers (–OR) or perhaps 2°/3° amines (–NHR / –NR₂) being viable options too. These “exotic” electron donating moieties should be carefully selected, however, since they will inevitably decrease the hydrophobic nature of the overall ligand.



Scheme 6.2: Suggested methylpyrazolyl tripodal extractant with various electron donating R-groups.

Another interesting prospect is the extension of ligands **1–8** by the addition of two pyrazolyl moieties to the existing pyrazolyl moieties, thereby expanding the ligand to contain four pyrazolyl moieties in total (**Scheme 6.3**). This thought-provoking and exciting set of ligands will inherently contain three coordination “pockets”—one tridentate and two bidentates. This might allow coordination to two very different metal ions as a result. R-groups should ideally contain more than four carbons to promote solubility in the organic phase.

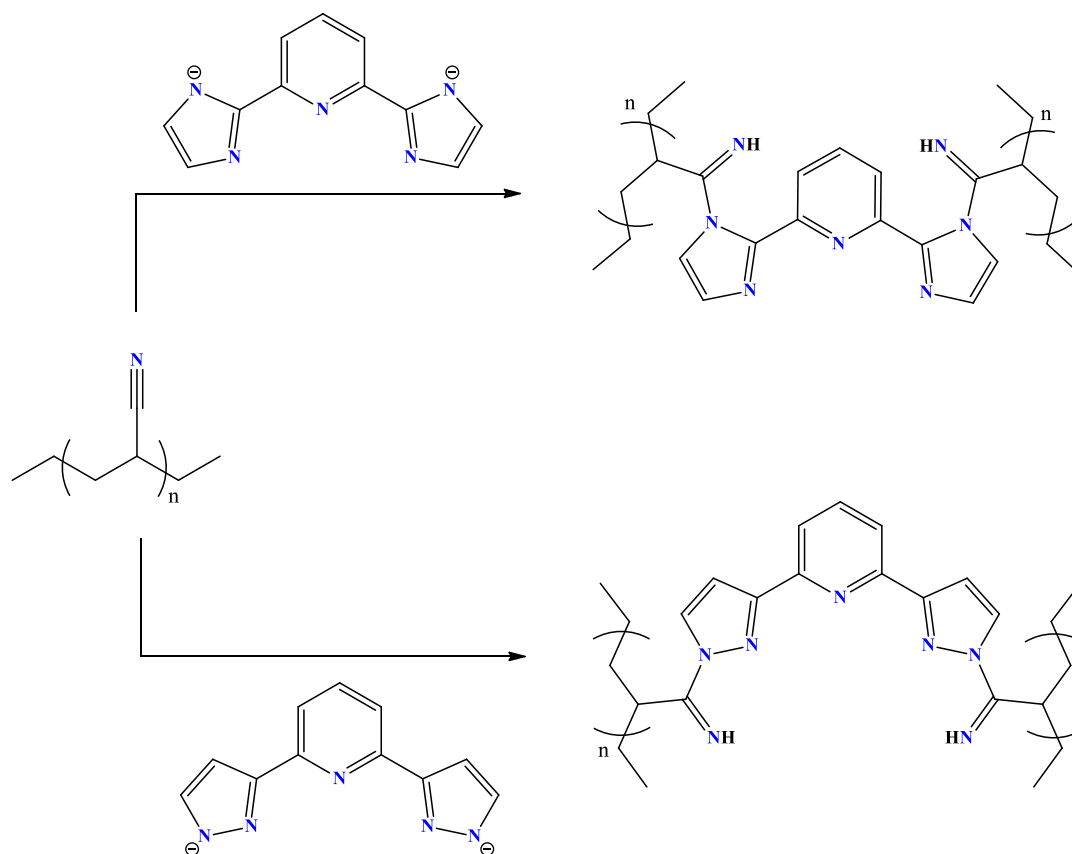


Scheme 6.3: Proposed “3-pocket” pyrazolyl ligands for the simultaneous extraction of three base metal ions.

6.2.2 Extraction of base metal ions using pyrazolyl- and imidazolyl ligands on resin, silica-based and nanofibrous polymeric supports.

The use of resin, silica-based and nanofibrous polymeric supports for the selective extraction of metal ions is a relatively new development in the arena of hydrometallurgy

The selective extraction of base metal ions by means of tridentate pyrazole- and imidazole-pyridinyl ligands tethered to nanofibrous polymeric backbones is a feasible modern hydrometallurgical novelty worth pursuing. The use of poly(acrylonitrile) (PAN) as scaffold is suggested due to its excellent stability at low pH. This is a vital property since PAN nanofibers must be able to maintain integrity under extreme acidic conditions during metal recovery studies. It is also important that PAN nanofibers be reusable and recyclable. To the best of our knowledge, only a single example in the literature, by Ndayambaje *et al.*,⁸ has reported the anchoring of 2-(2'-pyridyl)imidazole onto PAN nanofibers. By incorporating tridentate pyrazole- and imidazole-pyridinyl ligands onto PAN scaffolds, one could obtain material chemically equivalent to the products displayed in **Scheme 6.4**.



Scheme 6.4: Proposed anchoring of tridentate pyrazole- and imidazole-pyridinyl ligands onto poly(acrylonitrile) (PAN). [Adapted from Ndayambaje *et al.*⁸]

The extraction of copper(II) and nickel(II) by means of resin systems has not been fully explored either. Leinonen *et al.*⁹ and Zainol *et al.*¹⁰ did, however, use iminodiacid chelating resins, *Chelex 100* and *Amberlite IRC 748*, for the purification of aqueous streams containing base metal ions. For future work, these

examples should be consulted and studied in an attempt to synthesise novel resin systems for the selective extraction of base metal ions.

The use of silica-supported chelating adsorbents for the removal of heavy metals from aqueous solutions is somewhat of an under-researched discipline. Sirola *et al.*¹¹ studied the removal of copper(II) and nickel(II) from concentrated ZnSO₄ solutions using two different silica-supported chelating adsorbents: WP-1 and CuWRAM. The WP-1 adsorbent contained branched poly(ethyleneimine) anchored to silica, while CuWRAM had anchored polyamine that was further functionalised with 2-(aminomethyl)pyridine groups. Such systems must be regarded as blue-prints in order to develop novel systems that exhibit improved extraction of base metal ions, especially cobalt(II), zinc(II) and cadmium(II).

6.2.3 Computational modelling and calculations

To further probe metal-ligand and synergistic interactions, density functional theory (DFT) calculations should be carried out to determine, by means of quantum analyses, whether a metal-ligand and/or synergistic assembly is likely to form or not. This can be achieved by calculating binding energies (ΔU_b) of the assembly, which will allow insight into the strength of coordination bonds.¹² Thermodynamic considerations must be taken into account as well to ensure the results are accurate and reflective of “real world” conditions.

6.3 References

- (1) Geist, A.; Muellich, U.; Zevaco, T.; Karpov, A.; Mueller, T. Preparation of alkylated bis(pyrazolyl)pyridines for the selective extraction of actinides, DE102009003783, 21 October 2010.
- (2) Zheng, C.; Yin, Y.; Wei, W.; Liu, M.; Zhang, Y.; Deng, P. Composite corrosion inhibitor and its preparation method, CN105603436, 25 May 2016.
- (3) Flett, D. Solvent extraction in hydrometallurgy. *Chem. Ind.* **1977**, *17*, 706–712.
- (4) Okewole, A.; Magwa, N.; Tshentu, Z. The separation of nickel(II) from base metal ions using 1-octyl-2-(2'-pyridyl)imidazole as extractant in a highly acidic sulfate medium. *Hydrometallurgy* **2012**, *121–124*.
- (5) Osseo-Asare, K.; Keeney, M. Sulfonic acids: Catalysts for the liquid-liquid extraction of metals. *Sep. Sci. Technol.* **1980**, *15* (4), 999–1011.
- (6) Roebuck, J.; Bailey, P.; Doidge, E.; Fischmann, A.; Healy, M.; Nichol, G.; O'Toole, N.; Pelsler, M.; Sassi, T.; Sole, K.; *et al.* Strong and selective Ni(II) extractants based on synergistic mixtures of sulfonic acids and bidentate *N*-heterocycles. *Solvent Extr. Ion Exch.* **2018**, *36* (05), 1–22.
- (7) Bouabdallah, I.; Touzani, R.; Zidane, I.; Ramdani, A. Synthesis of new 1,1'-di(4-nitro or 2-nitrophenyl)-5,5'-disubstituted-3,3'-bipyrazoles under microwave irradiation and classical heating conditions. *Arkivok* **2006**, *XIV*, 46–52.

- (8) Ndayambaje, G.; Laatikainen, K.; Laatikainen, M.; Beukes, E.; Fatoba, O.; van der Walt, N.; Petrik, L.; Sainio, T. Adsorption of nickel(II) on polyacrylonitrile nanofiber modified with 2-(2'-pyridyl)imidazole. *Chem. Eng. J.* **2016**, *284*.
- (9) Leinonen, H.; Lehto, J. Ion-exchange of nickel by iminodiacetic acid chelating resin *Chelex 100*. *React. Funct. Polym.* **2000**, *43* (1), 1–6.
- (10) Zainol, Z.; Nicol, M. Ion-exchange equilibria of Ni²⁺, Co²⁺, Mn²⁺ and Mg²⁺ with iminodiacetic acid chelating resin *Amberlite IRC 748*. *Hydrometallurgy* **2009**, *99* (3), 175–180.
- (11) Sirola, K.; Laatikainen, M.; Lahtinen, M.; Paatero, E. Removal of copper and nickel from concentrated ZnSO₄ solutions with silica-supported chelating adsorbents. *Sep. Purif. Technol.* **2008**, *64* (1), 88–100.
- (12) Carson, I.; MacRuary, K.; Doidge, E.; Ellis, R.; Grant, R.; Gordon, R.; Love, J.; Morrison, C.; Nichol, G.; Tasker, P.; *et al.* Anion receptor design: Exploiting outer-sphere coordination chemistry to obtain high selectivity for chloridometalates over chloride. *Inorg. Chem.* **2015**, *54* (17), 8685–8692.